An investigation of

Human regulatory T cell metabolic pathways

Hisashi Hashimoto

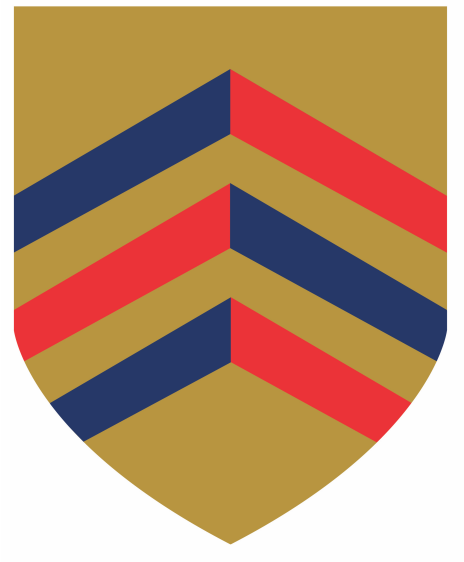

Merton college

Nuffield Department of Surgical Sciences

University of Oxford

Supervisors: Dr. Joanna Hester and Dr. Fadi Issa

Michaelmas term 2022

Abstract

Regulatory T cells (Tregs) are essential to homeostatic immune tolerance. Clinical trials of autologous Treg cell therapy have demonstrated promising preliminary results, but there remain challenges to overcome including the problem of recipient-dependent expansion variability. Enhancing the suppressive function of expanded Tregs to reduce the required Treg dose would present a potential solution to this problem.

Cellular metabolism regulates immune cells through two interacting aspects: bioenergic and biosynthetic activities, and non-canonical activities of metabolic enzymes and intermediates. Early *in vitro* work has revealed distinct metabolic profiles between mouse conventional T cells (Tconvs) and Tregs. However, it remains unclear how the metabolism of human Tregs is regulated. A better understanding of the contrasting metabolic demands and regulation of function between human Tconvs and Tregs may uncover routes to target Treg-specific metabolic pathways in order to tune their activity as desired.

In this work, the immunometabolism of human Treg is investigated and new strategies revealed to harness elements of their metabolism for therapeutic use. In *Chapters 3 and 4*, I show that Treg display the 'Warburg effect' after T cell receptor stimulation alongside CD28 co-stimulation via the mTOR signalling pathway. Subsequently, I show that only naïve and central memory Tregs preferentially utilise glucose; suggesting that human Treg metabolism may differ due to their anatomical location. In contrast, effector memory Tregs and Tconvs have distinct metabolic characteristics: whilst Tconvs negatively alter effector function through limiting glucose metabolism, Tregs positively regulate their suppressive function by limiting mitochondrial energy metabolism. Furthermore, this metabolic regulation allows Tregs to enhance their suppressive activity towards Treg-resistant Tconvs which are characterised by their low mitochondrial mass. In *Chapters 5 and 6*, I investigate the mechanism of this phenomenon, and show that Tregs generate immunosuppressive extracellular vesicles (exosomes) by mitochondrial ATP synthase inhibition. Metabolomics data suggests that epigenetic alteration in Tregs through a change in mitochondrial metabolism

intermediates. The donor-independent function of these small extracellular vesicles suggests a new potential therapeutic strategy in which Treg-derived extracellular vesicles could be used 'off-the-shelf'.

The immunometabolic experiments presented in this thesis shine new light on the differential metabolic regulation of human Tregs and Tconvs, and reveal novel and potent mode of Treg immunosuppresive action that can be induced by modulating metabolism. By defining these pathways, new therapeutic strategies to immune regulation may be potentially revealed.

Acknowledgements

First and foremost, I would like to thank my supervisors, Dr. Joanna Hester and Dr. Fadi Issa for their unfailing support, advice and mentorship during my D.Phil. course. My life in science started when I first met with Joanna who patiently taught me all lab techniques from pipetting to the way of thinking in science. Fadi continues to inspire the direction of my work with his broad perspectives. I am absolutely sure that I could not achieve this work without their support. I would also like to express my appreciation towards Dr. Oliver McCallion for his help in the *in vivo* experiments, his skills generating a comfortable working atmosphere and for proofreading. I am hugely grateful to Dr. Masateru Uchiyama for his enthusiasm in science. Our weekly discussions of immunology and his ignoble prize work during dinners remind me how important it is to enjoy science. I would also like to express my gratitude and respect towards Dr. George Adigbli, Dr. Kento Kawai, and Dr. Rebecca Hornero for their mentorship during the early stages of my DPhil course. Not only their scientific skills, but also their kind personalities allowed me to ask questions freely, which was fundamental to smoothly starting this course. I would also like to thank Dr. Amy Cross for our scientific discussions and her

broad experience, Mrs. Monica Dolton for her outstanding management skills and Mr. Joseph Beckett for his encouragement during late-night experiments. Needless to say, I received great help and precious advice from all other members of the Transplantation Research Immunology Group (TRIG) where I developed as a scientist. In addition, I would like to thank Dr. Kourosh Ebrahimi for his expertise in mass spectrometry and fruitful discussions. I would also like to thank my course director and former teacher, Professor Jonathan Austyn, who taught me the basics of immunology and the story of his precious experience with Professor Ralph Steinman which motivated my enthusiasm for science.

Lastly, I would like to thank my family for their faithful support and my partner Lucia who encouraged me throughout my entire student life—from the first year of medicine to the end of this Doctor of Philosophy.

Abbreviations

2-Deoxy-D-glucose	2-DG
2-Deoxy-2-[7-nitro-2,1,3-benzoxadiazol-4-yl)amino]-D-glucose	2-NBDG
7-Amino-actinomycin D	7-AAD
Adenosine diphosphate	ADP
Autoimmune regulator	AIRE
Autoimmune lymphoproliferative syndrome	ALPS
AMP-activated protein kinase	AMPK
Antigen presenting cells	APC
Autoimmune Polyendocrinopathy Candidiasis Ectodermal Dystrophy syndrome	APECED
Assay for transposase-accessible chromatin with high-throughput sequencing	ATACseq
Adenosine triphosphate	ATP
Adenylate-uridylate	AU
Cyclic adenosine monophosphate	cAMP
Chimeric antigen receptor	CAR
Central memory	CM
Conserved non-coding DNA sequence	CNS
Cytotoxic T-lymphocyte-associated protein 4	CTLA-4
Diacylglycerol	DAG
Dendritic cell	DC
Deionised	DI
Dimethylsulphodioxide	DMSO
Dynamin-related protein 1	Drp-1
Experimental autoimmune encephalomyelitis	EAE
Epstein-Barr-virus-induced gene 3	EBI3
Extracelular acidification rate	ECAR
Enzyme-linked immunosorbent assay	ELISA
Effector memory	EM
Electron transport chain	ETC

Extracellular vesicle	EV
in vitro-expanded Tconvs	expanded Tconvs
in vitro-expanded Tregs	Expanded Tregs
Fatty acid binding protein 5	FABP5
Fatty acid oxidation	FAO
Foetal bovine serum	FBS
Carbonyl cyanide-4-(trifluoromethoxy) phenylhydrazone	FCCP
FEZ family zinc finger 2	Fezf2
Forkhead box protein O1	Foxo1
Forkhead box P3	Foxp3
Glyceraldehyde 3-phosphate dehydrogenase	GAPDH
Glycoprotein-A repetitions predominant protein	GARP
GATA binding protein 3	GATA3
Glucokinase	GCK
Glucose transporter 8	Glut 8
Glucose transporter 1	Glut1
Good Manufacturing Practice	GMP
Histone deacetylase	HDAC
High endothelial venule	HEV
Hypoxia inducible factor	HIF
Human leukocyte antigen	HLA
3-Hydroxy-3-methylglutaryl coenzyme A	HMG-CoA
Human serum	HS
Inducible T-cell co-stimulator	ICOS
Indolamine 2,3-dioxygenase	IDO
ATPase inhitory factor 1	IF1
Interferon	IFN
Interleukin	IL
Immunodysregulation Polyendocrinopathy Enteropathy X-linked	IPEX
Interferon regulatory factor 4	IRF4
***in vitro*-induced Treg**	iTreg
Jumonji C domain-containing histone demethylase	JHDM

Knockout	KO
Lactate dehydrogenase A	LDHA
Liver kinase B	LKB1
Monoclonal antibody	mAb
Monocarboxylate transpoter	MCT
Mean fluorescent intensity	MFI
Major histocompatibility complex	MHC
Micro RNA	miRNA
Mitochondrial mass high	$Mito^{hi}$
Mitochondrial mass low	$Mito^{lo}$
Medullary thymic epithelial cell	mTEC
Mechanistic target of rapamycin	mTOR
Nuclear receptor coactivator 2	NCoA-2
Nuclear factor of activated T cells	NFAT
NF-kB-inducing kinase	NIK
Oxidative phosphorylation	OXPHOS
Phosphate buffered saline	PBS
Programmed cell death protein 1	PD-1
Pyruvate dehydrogenase complex	PDC
Pyruvate dehydrogenase kinase	PDK
Pyruvate dehydrogenase phosphatase	PDP
Phosphoenolpyruvate	PEP
Paraformaldehyde	PFA
Phosphofructokinase 1	PFK 1
Phosphofructokinase 2	PFK 2
Phosphoinositide 3-kinase	PI3K
Phorbol myristate acetate	PMA
Pentose phosphate pathway	PPP
Protein arginine methyltransferase 5	PRMT5
Phosphatidylcholine	PtdCho
Phosphatidylethanolamine	PtdEtn
Phosphatase and tensin homolog	PTEN

Peripherally derived Treg	pTreg
Reverse electron transport	RET
Reactive oxygen species	ROS
S-adenosyl-L-homocysteine	SAH
S-adenosyl methionine	SAM
Severe combined immunodeficiency	SCID
SUMO-specific protease 3	SENP3
Sarco/endoplasmic reticulum calcium-ATPase	SERCA
Spare respiratory capacity	SRC
T-box expressed in T cells	T-bet
t-distributed stochastic neighbor embedding	t-SNE
Tricarboxylic acid	TCA
Conventional T cell	Tconv
T cell receptor	TCR
Ten-eleven translocation	TET
Mitochondrial transcription factor A	Tfam
Transforming growth factor-β	TGF-β
Helper T cell type 1	Th1
Helper T cell type 17	Th17
Helper T cell type 2	Th2
T cell immunoreceptor with Ig and ITIM domains	TIGIT
Toll-like receptor	TLR
Tetramethylbenzidine	TMB
Tumor necrosis factor alpha	TNF-α
Regulatory T cell	Treg
Treg-specific demethylated regions	Treg-DRs
Treg-specific demethylated region	TSDR
Thymus-derived Treg	tTreg
Untranslated region	UTR
Violet proliferation dye	VPD

Summary of contents

Table of contents

Chapter 1: Introduction

1.1 Background

The immune system has evolved to eliminate pathogenic microbes (1, 2). The *innate immune system* evolved first to sense danger and discriminate self from non-self motifs without recognising specific pathogens. The *adaptive immune system* evolved later, first observed in jawless fish, and distinguished by its ability to recognise specific molecular targets by unique receptors. The adaptive immune system recognises, and crucially remembers in the form of immunological memory, specific pathogens which enables a more rapid response on subsequent encounters. However, the diversity of the receptors contained within the adaptive immune compartment generates a risk of self-recognition, and loss of *self tolerance* results in pathological immune responses and the development of autoimmune diseases (3-6). *Self tolerance* is maintained by both *recessive* (cell-intrinsic) and *dominant* (cell-extrinsic) mechanisms, which anatomically occur at *central* and *peripheral* sites. Recessive mechanisms include clonal deletion and anergy, defined as functional inactivation induced by inadequate stimulation (7, 8), whilst the main

dominant mechanism is mediated by specialised immune cells that actively prevent unwanted immune activation (5, 9, 10). Regulatory T cells (Tregs) are one of the most well-defined regulatory cell subsets and are crucial for maintaining immune homeostasis (11-13). Recently, significant attention has been focused to translate the therapeutic properties of Treg to treat autoimmune diseases and prevent transplant rejection (14). In our group, Treg cell therapy (adoptive transfusion of autologous Tregs) has been conducted to induce tolerance to transplanted organs (15, 16). This is particularly important considering that, whilst immunosuppressive drugs currently used to prevent transplant rejection do achieve high rates of 1-year graft survival, their non-specific nature causes broad immunosuppression resulting in an increased incidence of opportunistic infections and cancers, in addition to the drugs themselves being cardiotoxic and nephrotoxic (17-19). Moreover, current immunosuppressive drugs are unable to prevent chronic allograft dysfunction caused by chronic activation of immune system (20, 21). Treg cellular therapy is a promising strategy to reduce or even abolish the reliance on immunosuppressive drugs through achieving operational tolerance, defined as sustained donor-specific immune unresponsiveness.

The field of immunometabolism investigates the relationship between cellular metabolic pathways and altered immune cell functions (22, 23). For example, conventional T cells (Tconvs) switch their metabolism from oxidative phosphorylation (OXPHOS) to aerobic glycolysis upon stimulation (24-26), which ensures rapid energy availability and generates a pool of glucose-derived carbon for biosynthesis. In addition to both the catabolic and anabolic importance of glycolysis, it was revealed that metabolism controls Tconv effector functions by post-transcriptional modifications (27). Preliminary studies into Treg immunometabolism suggest a distinct relationship between metabolism and function compared with Tcovs. For example, studies from mice suggest that Treg metabolism is skewed towards OXPHOS (28, 29); highlighting how the extracellular environment may modulate the balance between tolerance and rejection by favouring either Tconv or Treg metabolic preferences. Describing immune tolerance in terms of the immunometabolism of discrete cellular compartments may reveal metabolic pathway targets that could be exploited to balance human immune responses. However, Treg immunometabolism remains poorly defined, particularly in humans. An understanding

of Treg immunometabolism may provide an insight into their mechanisms of function and reveal new therapeutic targets.

The aim of this thesis is to investigate Treg metabolism and to establish new therapeutic targets, capitalising on the unique aspects of their metabolism.

1.2 Immune tolerance and regulatory T cells

1.2.1 T cell tolerance

Burnet proposed, over half a century ago, that self-tolerance could be achieved by the clonal deletion of self-reactive lymphocytes (30). Later studies proved that both self-reactive B and T cell clones undergo programmed cell death in the bone marrow and thymus, respectively, in a process now termed clonal deletion (6, 31). During T cell development in the thymus, T cells receiving a strong T cell receptor (TCR) signal from either a high affinity and/or high avidity interaction with peptides presented on major histocompatibility complexes (MHC) of either medullary thymic epithelial cells (mTEC)

or thymic dendritic cells (DC) undergo apoptosis (32-35). mTECs have a specialised functional ability to express peripheral-tissue-specific antigens (promiscuous gene expression) regulated by autoimmune regulator (AIRE) and FEZ family zinc finger 2 (Fezf2) genes (34, 36). The importance of AIRE is well illustrated by the rare life-threatening genetic condition Autoimmune Polyendocrinopathy Candidiasis Ectodermal Dystrophy syndrome (APECED), resulting from mutations in *AIRE* (37).

In addition to clonal deletion, expression of self-antigen in the thymus is also important for Treg generation (38, 39). The significance of thymic Treg generation in tolerance development was first demonstrated in the now-classic experiments in which mice who underwent thymectomy at day 3 after birth developed spontaneous autoimmune disease (40, 41). Although the mechanism of this autoimmune phenotype was not known to result from failed Treg generation at the time, Sakaguchi *et al* revealed that a single injection of T cells from an untreated euthymic mice prevented the autoimmune phenotype, an observation that was subsequently refined to specifically implicate Tregs (42, 43). The incontrovertible evidence for the importance of Treg in immune tolerance

is displayed by scurfy mice (which characteristically develop fatal systemic autoimmunity) and the Immunodysregulation Polyendocrinopathy Enteropathy X-linked (IPEX) syndrome in humans, both of which are caused by mutations in the Treg master transcription factor, Forkhead box P3 (*FOXP3*) (44, 45). The fact that a single mutation of *FOXP3* causes lethal autoimmune disease independently of thymic clonal deletion indicates that mammalian immune tolerance is dependent on Treg function. Indeed, the thymus does not express some peripheral-tissue-specific antigens and tolerance towards these antigens is therefore mediated by Tregs (46). Importantly, the presence of Tregs may even compensate for complete failure of thymic clonal deletion. Conditional NF-κB-inducing kinase (NIK) deletion in mTEC causes lethal autoimmune disease from failed mTEC development (47). Transplantation of the NIK-ablated thymus into athymic mice similarly results in the development from autoimmune disease. However, co-transplantation of a NIK-ablated and healthy thymus prevents this phenotype despite autoreactive T cells maturing in the mTEC-deficient thymus. This proves that thymic generation of Treg can overcome the existence of autoreactive T cells permitted through failed clonal deletion. Direct evidence of Treg control of reactive

Tconvs can also be observed in models of organ transplantation where Tregs prevent Tconv-mediated allorejection as alloantigens are not expressed in the recipient thymus (48, 49). In these models, a single infusion of Tregs can prevent graft rejection without immunosuppressive drugs illustrating that Tregs alone may potentially induce tolerance.

1.2.2 The history of regulatory T cells

Although the concept of T cell subsets negatively regulating immune reactions dates back to the suppressor T cells proposed by Gershon and Kondo in 1970 (50), Sakaguchi *et al* provided the first evidence of $CD4^+$ T cells that possess immunoregulatory function in 1982 (42). Soon after, Bruce *et al* described an immunosuppressive $CD4^+$ T cell population using a cardiac transplantation model (51). In this model, adoptive transfer of $CD4^+$ T cells from rats that had previously achieved tolerance to a cardiac allograft prevented rejection of cardiac grafts in immunocompetent third-party rats without immunosuppressive treatment. Later they described that these $CD4^+$ T cells expressed the surface phenotype $OX22^+$ $CD25^+$ MHC class II^+ (52). However, it was not clear from

these experiments whether the immunoregulatory $CD4^+$ T cells were naturally occurring or appeared after tolerance induction. Sakaguchi *et al* and Powrie *et al* proved that removal of a specific subset of $CD4^+$ T cells disrupts immune tolerance (53, 54). In their experiments, infusion of partially-depleted $CD4^+$ T cells into athymic rodents spontaneously caused autoimmune disease: depletion of $CD5^{hi}$ $CD4^+$ T cells by Sakaguchi *et al* caused autoimmune diseases in stomach, thyroid, and gonads in mice; and depletion of $OX22^{lo}$ $CD4^+$ T cells by Powrie *et al* resulted in generalised weight loss and development of autoimmune peripheral tissue damage in the thyroid, pancreas and stomach. Powrie *et al* subsequently described similar findings in severe combined immunodeficiency (SCID) mice adoptively transferred with $OX22^{lo}$ depleted $CD4^+$ T cells which resulted in severe colitis (55). However, the markers demonstrated by Sakaguchi and Powrie were not identical, and importantly the autoimmune phenotypes developed in their models differed, likely because the markers they identified were not specific to Tregs. In 1995, Sakaguchi *et al* showed that depletion of $CD25^+$ $CD4^+$ cells (which constitute 5-10% of peripheral $CD4^+$ T cells) causes a more severe autoimmune phenotype to develop in mice involving several tissues including stomach, thyroid,

gonads, thyroid, pancreas and adrenal gland. This demonstrated that CD25 (the α-chain of the IL-2 receptor) is a specific marker of $CD4^+$ T cells with an immunoregulatory function. Today, these cells are called Tregs (11).

In 2001, it was demonstrated that mutation in *Foxp3* causes lethal autoimmunity in mice (scurfy mouse) and humans (IPEX) (44, 45). In 2003, the laboratories of Sakaguchi, Rudensky, and Ramsdell independently found that $CD25^+$ $CD4^+$ T cells specifically express FOXP3 (12, 13, 56). Importantly, retroviral transduction of *Foxp3* to $CD25^-$ $CD4^+$ T cells enabled immunosuppressive function with upregulation of CD25 along with the characteristic Treg molecules CTLA-4 and GITR, and down-regulation of IL-2 production. Thus, FOXP3 is now regarded as the 'master regulator' of Tregs.

1.2.3 Regulatory T cells stability and epigenetics

As mentioned above, Tregs are generated in the thymus during T cell maturation. However, $CD25^{+}$ CD4 T cells expressing FOXP3 can also be differentiated from peripheral Tconvs *in vitro* and *in vivo* (57-60). Tregs from these two origins—the thymus or differentiated from Tconvs—were historically termed 'natural Tregs' and 'induced Tregs', respectively. However, because the term 'natural Tregs' inferred that their counterpart 'induced Tregs' were somehow artificial despite accumulating evidence of this process occurring 'naturally' *in vivo*, Tregs are now classified into three subsets: 'thymus-derived Tregs (tTregs)' originating from the thymus during T cell maturation; 'peripherally derived Tregs (pTregs)' differentiated from Tconvs *in vivo*; and '*in vitro*-induced Tregs (iTregs)' differentiated from Tconvs *in vitro* (61). The main difference between tTregs and pTregs is their TCR repertoire: tTregs have TCRs specific to autoantigens, whilst pTregs have a higher proportion of TCRs specific to non-self antigens such as commensal microbiota found in gut (62-64). There are currently no known markers to distinguish tTregs and pTregs isolated from human peripheral blood.

The fundamental difference between natural Tregs (which throughout the remainder of this thesis will be used to designate both tTregs and pTregs) and iTregs is their linage stability (65, 66). Natural Tregs in mice stably express FOXP3 and possess suppressive properties even in inflammatory settings (67). In contrast, iTregs readily revert to pro-inflammatory Tconvs in the presence of inflammatory cytokines and do not demonstrate suppressive capacity *in vivo* on adoptive transfer (68-70). The lineage stability of natural Tregs is supported epigenetically by demethylation of the *FOXP3* conserved non-coding DNA sequence 2 (CNS2) region which is now known as Treg-specific demethylated region (TSDR) (71). Moreover, hypomethylated regions in linage-stable Tregs (tTregs and pTregs) are also observed in *Il2ra* (encoding CD25), *Ctla4*, *Ikzf2* (encoding Helios) and *Ikzf4* (encoding Eos) which are collectively termed Treg-specific demethylated regions (Treg-DRs) (72, 73). Importantly, hypomethylation of Treg-DRs occurs independently of FOXP3 expression (72, 74). This fact is supported by the observation that hypomethylation still occurs in Treg-DRs of $CD25^+$ $CD4^+$ T cells isolated from scurfy mouse where *Foxp3* is mutated even though Treg-DRs and Foxp3-biding sites do not overlap in the genome (75). Interestingly, Treg-DRs are associated more with upregulation of classical Treg defining

genes such as CD25 and CTLA-4, whilst *Foxp3* is associated more with downregulation of IL-2 and IFN-γ (76). Several other studies have demonstrated that a that small population of FOXP3 expressing cells *in vivo* convert to immunogenic T cells, although these cells do not exhibit a demethylated TSDR (77, 78). Thus, Tregs are not defined by *Foxp3* expression, but are instead defined by their epigenetic signature supporting stable expression of *Foxp3* and other Treg-specific markers such as CD25.

Compared with mouse Tregs which express *Foxp3* exclusively, human *FOXP3* is also unstably expressed by Tconvs upon activation (79-81). Similarly, CD25 is not a specific Treg marker in humans; however, despite this, Miyara *et al* were successfully able to isolate functionally stable human Tregs from peripheral blood using a combination of CD45RA and CD25 (79). Human $CD25^{+}$ $CD4^{+}$ cells can be divided into three groups: $CD45RA^{+}$ $CD25^{lo}$ ($FOXP3^{lo}$), $CD45RA^{-}$ $CD25^{lo}$ ($FOXP3^{lo}$) and $CD45RA^{-}$ $CD25^{hi}$ ($FOXP3^{hi}$) cells. Among these subsets, $CD45RA^{-}$ $CD25^{lo}$ (naïve Tregs) and $CD45RA^{-}$ $CD25^{hi}$ (activated Tregs) maintain stable *FOXP3* expression and suppressive function. CD127 (the α chain of the IL-7 receptor), in combination with CD4 and CD25, can also be used to identify

generalised human Tregs (82). Tregs defined as $CD25^{+}$ $CD127^{lo/-}$ $CD4^{+}$ express *FOXP3* and are functionally stable (82, 83). Importantly, human Tregs also demonstrate hypomethylated TSDR, including those isolated from patients with IPEX syndrome, indicating again that the Treg epigenetic signature is an important hallmark of human Tregs which is established independently of *FOXP3* (79, 84).

Taken together, Tregs can be divided into tTregs, pTregs and iTregs based on their origin. Stable FOXP3 expression and immunosuppressive function of tTregs and pTregs is supported by specific epigenetic signatures (demethylation of Treg-DRs) in both human and mice. Importantly, demethylation of Treg-DRs and *FOXP3* expression are independent mechanisms: whilst hypomethylation of Treg-DRs permits T cells to commit to stable expression of *FOXP3*, FOXP3 itself does not cause hypomethylation of Treg-DRs. Moreover, Treg signature genes are controlled by demethylation of Treg-DRs, and not *FOXP3*. Therefore, hypomethylation of Treg-DR defines Tregs by inducing stable *FOXP3* expression together with supporting the expression of Treg-specific molecules. That said, a single mutation in *FOXP3* causes deleterious autoimmune disease and therefore

hypomethylation patterns in Treg-DR determines Treg stability by supporting the expression of Treg-specific molecules including FOXP3 which is a key molecule required to enable Treg functionality.

1.2.4 Immune regulatory mechanisms utilised by regulatory T cells

Mechanisms of Treg suppression can be arbitrarily divided into contact-dependent and contact-independent (85-87). Contact-dependent mechanisms suppress target cell function by direct binding, whilst contact-independent mechanisms include production of immunosuppressive soluble factors and modulation of extracellular factors.

1.2.4.1 Contact-dependent mechanisms

Cytotoxic T-lymphocyte-associated protein 4 (CTLA-4) binds to CD80 and CD86 on antigen presenting cells (APC) with higher affinity than CD28, thereby inhibiting Tconv activation by depriving them of co-stimulatory signalling (88, 89). Additionally, Tregs

extract CD80/CD86 molecules from APCs through trans-endocytosis as a further mechanism depriving Tconvs of co-stimulation (90). T cells binding to target MHC complexes without co-stimulatory molecules (CD80 or CD86) undergo apoptosis or become anergic (91). This is illustrated by culturing activated DCs with Tregs and $CD8^+$ T cells—this induces anergy in the $CD8^+$ T cells (90). Moreover, CTLA-4 on Tregs enhances indolamine 2,3-dioxygenase (IDO) expression on DCs which catabolises tryptophan (the scarcest amino acid in the mammalian body) resulting in deprivation in peripheral tissues (92). The importance of CTLA-4 for Treg suppressive function is well illustrated by conditional *Ctla4* knockout (KO) in Treg, which causes a scurfy-like lethal autoimmune phenotype (93). However, whilst *Ctla4* deletion in adult mice using an inducible KO model resulted in lymphoproliferation and signs of peripheral autoimmunity, the phenotype was much milder compared with germ-line deletion (94, 95). In these *Ctla4* KO Tregs, however, expression of other immunomodulatory mechanisms such as IL-10 increased indicated a superior capacity to compensate for C*tla4* KO. However, it may also be that CTLA-4 has an important function modulating clonal deletion of Tconvs by altering antigen presentation in thymus. In humans, *CTLA4* mutation is known to cause

autoimmune lymphoproliferative syndrome (ALPS) (96, 97). Interestingly, *CTLA4* haploinsufficiency in humans results in clinically manifest disease, whilst *Ctla4* haploinsufficiency in mice does not result in an autoimmune phenotype (98, 99). Therefore, although it is not a direct comparison of Treg CTLA-4, the reliance on CTLA-4 to maintain immune tolerance seems to be greater in humans than mice.

Programmed cell death protein 1 (PD-1) is a cell-intrinsic inhibitor and PD-1 signalling inhibits T cell activation (100, 101). The role of PD-1 in tolerance is well illustrated by *Pd1* KO mice, which develop an autoimmune phenotype, and the success of anti-PD-1 monoclonal antibody therapy in cancer, although both observations could equally be explained by impaired auto-inhibition of Tconv, rather than impaired Treg suppression (102, 103). Interestingly, PD-1 inhibition induces Treg proliferation and increases Treg suppressive function indicating that PD-1 signalling also works to negatively regulate Tregs (104, 105). However, PD-1 expression on Treg may contribute to their immunosuppressive function via signalling to APCs. Although intrinsic signalling of PD-ligand 1 (PD-L1) in APCs is not well studied, macrophages treated with anti-PD-L1

antibodies upregulate mechanistic target of rapamycin (mTOR) pathway signalling and CD86 and MHC II (106). Therefore, PD-1 expression on Tregs may have a role in tolerance by mediating APC activation.

Recently several studies revealed that Tregs co-express *FOXP3* and other master transcription factors including T-bet, GATA3, and IRF4 to induce specific immunological reactions (107-112). In addition to expressing the same chemokine receptors as differentiated Tconvs required for peripheral tissue migration, these specialised Tregs express specific immunosuppressive molecules, for example T cell immunoreceptor with Ig and ITIM domains (TIGIT). TIGIT binds to CD155 on DCs to increase IL-10 and decrease IL-12 production (113). Importantly, $TIGIT^{+}$ Tregs are enriched in Tregs that also express the transcription factor T-bet; these specifically supress helper T cell type 1 (Th-1) and helper T cell type 17 (Th-17), but not helper T cell type 2 (Th-2), responses (108, 114). In contrast, inducible T-cell co-stimulator (ICOS) expression on Tregs is mediated by interferon regulatory factor 4 (IRF4) which is required to suppress Th2-type reactions (110).

1.2.4.2 Contact-independent mechanisms

Since FOXP3 directly supresses IL-2 gene expression, Tregs do not produce IL-2 despite exogeneous IL-2 being necessary for Treg survival (115, 116). CD25 (the α-chain of the IL-2 receptor) forms the trimeric IL-2 receptor together with the β- and γ-chains; the α chain however possesses a higher affinity for IL-2 compared with the β-chain and γ-chain dimeric receptor expressed by resting T cells (117). It was initially thought that a high consumption rate of IL-2 by Tregs expressing CD25 reduces the amount of available environmental IL-2 thereby preventing Tconv expansion. CD25-mediated Treg suppression can be observed *in vitro* through inhibiting both CD4 and CD8 T cell proliferation (118). However, whilst IL-2 receptor deficient Tregs have severely impaired immunosuppressive function and cannot prevent development of a scurfy-like phenotype, equipping IL-2 receptor deficient Tregs with a gain-of-function form of STAT5B (an IL-2 receptor downstream signalling molecule) prevents autoimmune phenotype development (although is associated with expansion of the memory CD8 compartment) (119). Therefore, the primary function of CD25 is Treg-intrinsic, rather than Treg-extrinsic. STAT5B mutation causes IPEX-like syndrome in human as well (120).

Anti-inflammatory cytokines such as transforming growth factor-β (TGF-β), IL-10 and IL-35 are produced by Tregs. TGF-β has a critical role in Treg differentiation (121, 122). Mechanistically, TGF-β recruits smad3 into CNS1 to induce *FOXP3* expression (123, 124). TGF-β is secreted in an inactive (latent) form from cells; in addition to secreting latent TGF-β, Tregs also convert it to its active form by glycoprotein-A repetitions predominant protein (GARP) and integrin αVβ8 (125-128). GARP works as a docking receptor for latent TGF-β whilst integrin αVβ8 interacts with the latent TGF-β/GARP complex to release the active form of TGF-β. IL-10 is produced from a variety of cells and is a classically immunosuppressive cytokine (129). Treg conditional IL-10 deletion results in specific inflammation of the colon and lung indicating that IL-10 is especially important to maintain tolerance in mucosal tissues (130). Similarly, IL-10 and IL-10 receptor defects in humans causes inflammatory bowel disease (IBD) in early life demonstrating a similar necessity in humans (131). IL-35 is a newly discovered anti-inflammatory cytokine produced by Tregs (132). IL-35 is encoded by Epstein-Barr-virus-induced gene 3 (*EBI3*) and forms a heterodimer with interleukin-12α (IL-12α). Interestingly, IL-35 not only suppresses T cell proliferation in mice and humans, but also converts Tconvs into IL-35

producing cells (132, 133). B cells with regulatory functions also produce IL-35 whilst IL-35 deletion in mice causes delayed recovery from experimental autoimmune encephalomyelitis (EAE) with a higher activation of T cells and APCs (134).

Adenosine is another immunosuppressive soluble factor which Tregs modulate by expressing the ectonucleotidases CD39 and CD73 (86). CD39 converts ATP and ADP into cAMP, which is then further converted by CD73 into the inhibitory molecule adenosine (135). CD39 is highly expressed on Tregs although, unlike mouse Tregs, CD73 expression is limited on human *ex vivo* Tregs (86, 136). However, this is context dependent as $CD73^{+}$ human Tregs have been identified in patients with certain cancers and following *in vitro* expansion of human Tregs (136, 137).

Recently immunomodulation via Treg-derived small extracellular vesicles (EVs), formerly known as exosomes, has been described (138, 139). Small EVs are endosomal-origin membrane-bound vesicles containing numerous substances such as protein, DNA, mRNA, and miRNA (140-143). Mouse Tregs produce a greater number of small EVs

compared with Tconvs (144). Treg-derived exosomes express several Tregs markers such as CD25, CTLA-4, CD39 and CD73 on their surface, which confer immunosuppressive function (145). For example, inhibition of CD73 reduces small EV suppressive capacity *in vitro* (145). However, blocking CTLA-4 with a neutralising antibody does not influence small EVs-mediated suppression of T cell proliferation, suggesting less of a role for CTLA-4 here (145). Others have demonstrated that Treg-derived small EVs express the IL-35 subunits Ebi3 and IL-12α which make the heterodimer (IL-35) on target cell surfaces which then suppress adjacent cells (146). miRNA contained in small EVs plays a significant role in immune suppression (144, 147). miRNA in Treg-derived small EVs directly acts on the target cell to suppress proliferation and cytokine production, whilst also skewing APCs towards a tolerogenic phenotype. The immunosuppressive capacity of Treg-derived small EVs *in vivo* is also observed in rodent transplantation models (148, 149). Importantly, human *in vitro* expanded Tregs produce small EVs with immunosuppressive properties sufficient to prevent allograft rejection in a humanised skin graft model through miRNA-mediated suppression of Tconv proliferation and cytokine production (150).

1.3 Regulatory T cell cellular therapy

1.3.1 Overview of Treg mediated suppression in Treg therapy

Adoptive transfer of human Tregs has been demonstrated as a new promising therapeutic strategy in many clinical settings such as autoimmune diseases and transplantation (14, 151). Tregs can regulate autoreactive Tconvs that escape from thymic clonal deletion (47). Importantly, tolerance to a specific antigen can be achieved even if the TCR clonotype is not expressed in the tTreg repertoire as the tolerance can be achieved without antigen expression in thymus (46). Likewise, adoptive transfer of Tregs can achieve peripheral tolerance even if the Treg TCR repertoires do not entirely cover the causative auto- or allo-antigens. This observation is mediated by *bystander suppression* and *infectious tolerance*.

Bystander suppression is defined as the suppression of immune activation in an antigen non-specific manner (152, 153). APCs present multiple antigens simultaneously whilst DCs can even present extracellular antigens on MHC I through the mechanism called cross-presentation (154, 155). Once a Treg binds to an antigen presented on the APC

surface, its CTLA-4 can either extract CD80/CD86 or modulate APCs to adopt a tolerogenic phenotype through IDO induction thereby inhibiting Tconv recognition of the other antigen presented by the same APCs (90, 92). In addition to other contact-dependent mechanisms modulating APCs towards a less immunogenic phenotype, Tregs can even kill the recognised APCs by through perforin and granzyme B (156). Moreover, contact independent Treg immunosuppressive mechanisms in general can suppress immune responses non-specifically.

Infectious tolerance is a phenomenon whereby a tolerant state achieved by one cell population transfers to a separate cell population, first described by Gershon and Kondo in 1971 (157, 158). Mechanistically, infectious tolerance involves the induction of many types of regulatory cells including IL-10 or TGF-β producing T cells, tolerogenic myeloid cells, and IL-35 producing cells; however, induction of pTregs is a key mechanism (122, 146, 159-162). The efficacy of Treg adoptive therapy is likely to depend on achieving infectious tolerance (163, 164).

1.3.2 Current and future Treg therapy

There are two main approaches to Treg cellular therapy at present: polyclonal Tregs and antigen-specific Tregs (14, 151). To produce both, Tregs are isolated from the patient, expanded *in vitro* for several weeks and subsequently re-infused to the donor. Polyclonal Tregs are generated from $CD25^+$ $CD4^+$ cells by stimulation with anti-CD3/CD28 magnetic beads in the presence of rapamycin which selectively suppresses proliferation of contaminating Tconvs and may even enhance Treg suppressive function (165-167). *In vitro* expanded Tregs possess a higher suppressive potency compared to *ex vivo* Tregs (136, 168). Thus, adoptive transfer of *in vitro* expanded Tregs boosts both Treg number and suppressive function. However, infusing polyclonal Tregs may theoretically risk generalised immunosuppression. Moreover, due to different Treg expansion potential between patients, laboratory manufacture of a Treg cell product may fail to achieve the required number of cells (15, 16).

Antigen-specific Tregs predominantly localise to target antigens and possess higher immunosuppressive potential, therefore using antigen-specific Tregs may be both safer

and more effective (169-171). In transplantation, allospecific Tregs are expanded *in vitro* using organ donor APCs which express alloantigens (172). However, the starting repertoire of Tregs possessing an alloantigen-reactive TCR is between 1 to 10% and the expansion of Tregs using donor APCs is much less effective than expansion with anti-CD3/CD28 magnetic beads (173, 174). Therefore, there is an even greater risk that alloantigen-specific Tregs will not expand in sufficient numbers for therapeutic use.

Chimeric antigen receptor (CAR) expressing Tregs (CAR-Tregs) have recently been introduced to generate antigen-specific Tregs with high post-expansion yield (175). The CAR construct is introduced by Good Manufacturing Practice (GMP)-grade lentiviral vector transfection during the expansion of polyclonal Tregs. The idea of CAR-Treg therapy was first investigated by expressing a CAR construct against the human leukocyte antigen (HLA) class I molecule A2 (176). A2-CAR Tregs have a CD28 CD3ζ intracellular domain, and demonstrate superior capacity than conventional polyclonal Tregs to suppress HLA-$A2^+$ T cells both *in vitro* and in a xenogeneic GvHD mouse model. Importantly A2-CAR Tregs did not exhibit cytotoxicity towards target cells indicating that

A2-CAR Tregs would be unlikely to damage a transplanted organ expressing HLA-A2. This was further supported by subsequent experiments demonstrating successful prevention of HLA-$A2^+$ human skin allograft rejection by the A2-CAR Treg in a humanised mouse model (177). Importantly, A2-CAR Tregs had better transmigration potential compared with conventional polyclonal Tregs. Thus, generation of antigen-specific Tregs by CAR technology represents a promising strategy. However, there remain unanswered questions including whether continuously-expressed target antigens *in vivo* would drive CAR-Treg exhaustion (178).

Whilst promising, there remain several problems preventing wider adoption of autologous adoptive Treg therapy, including:

1. Failure of expansion due to donor-dependent expansion capacity

2. Long preparation time for Treg expansion and quality control

3. Cost

A potential strategy to overcome these issues is the use of genetically modified third-

party Tregs (14). However, third-party Tregs must escape donor immune recognition, as third-party Tregs express alloantigens. Tregs with HLA deletion could be an idea. These Tregs may also additionally be arranged with transgenic expression of HLA-E to avoid NK cell mediated reaction (179). Using genetically modified third-party Tregs may allow the use of Treg therapy 'off-the-shelf'.

1.4 Overview of immunometabolism

1.4.1 The general concept of immunometabolism

Immunometabolism is the field of study at the intersection between immunology and metabolism (22, 23). Cellular metabolism is a fundamental process which balances the energy-producing mechanisms through the degradation of macromolecules (catabolism) with the energy-consuming macromolecular biosynthesis (anabolism). Catabolic processes can be divided into two main pathways: glycolysis, a fast but inefficient energy-producing process involving glucose consumption; and OXPHOS, in which metabolic intermediates derived from glucose, fatty acids and amino acids are

transported to the mitochondria for high-yield energy production by consuming oxygen in electron transport chain after the tricarboxylic acid (TCA) cycle. Although the glycolysis intermediate pyruvate can enter the TCA cycle, it can also be converted to lactate to maintain energy homeostasis without consuming oxygen, termed aerobic glycolysis. Despite inefficient energy production through aerobic glycolysis, Otto Warburg first described that oncologic cells preferentially utilise aerobic glycolysis under normoxic conditions, the so-called Warburg effect (180). Activated immunogenic cells also engage aerobic glycolysis (25, 181, 182). In exchange for consuming large quantities of glucose, a high rate of aerobic glycolysis mediates rapid energy synthesis and sufficient availability of carbon source for biosynthesis (183, 184).

However, the effect of cellular metabolism is not limited to meeting bioenergic and biosynthetic demands. For example, some metabolic intermediates work as cofactors or substrates for epigenetic and post-transcriptional modifications (185). Moreover, metabolic enzymes are multifunctional with non-canonical roles outside of metabolic pathways (186). One such non-canonical role is the regulation of immune cell function.

For example, macrophages accumulate the TCA intermediate succinate following Toll-like receptor (TLR) signalling, which in turn promotes stable hypoxia inducible factor (HIF)-1α expression and IL-1 production (187). Succinate functions as a competitive inhibitor of α-ketoglutarate in HIF degradation through prolyl hydroxylase (PHD). In this manner, activation-induced accumulation of succinate modulates macrophage effector function through stabilising the HIF-1α signalling pathway.

Recent studies of iTregs have demonstrated their preferential utilisation of OXPHOS, in intriguing contrast to Tconvs which preferentially utilise aerobic glycolysis (28, 188, 189). Furthermore, in mice glucose transporter 1 (Glut1) deletion selectively inhibits Tconv effector function but not natural Treg (tTreg and pTreg) suppressive function. This suggests that Tconvs and Tregs have different metabolic requirements for their functions (190). In short, cellular metabolism regulates immune cells through two interacting aspects: firstly, through regulating bioenergic and biosynthetic activities; and secondly, through modulation of non-canonical activities by metabolic intermediates and metabolic enzymes. Differing metabolic requirements of Tconvs and Tregs suggests that

immune tolerance may be modulated through targeting metabolic pathways.

1.4.2 T cell immunometabolism

Tconvs enhance their metabolism by preferentially shifting to aerobic glycolysis upon TCR stimulation alongside CD28 co-stimulation via the PI3K-Akt-mTORC1 pathway (24, 25). mTORC1 enhances expression of glycolysis enzyme genes at least partially through HIF-1α signalling (26, 191-193), but also mediates post-transcriptional effects by trafficking Glut1 to the cell surface (194). In the early phase following stimulation, the Myc signalling pathway induced by TCR signalling plays an important role to activate T cells (26). Alongside the bioenergic and biosynthetic requirement for glucose, a high rate of aerobic glycolysis must be maintained for Tconv effector function (27). Glyceraldehyde 3-phosphate dehydrogenase (GAPDH) is a glycolysis enzyme that also binds to adenylate-uridylate (AU) rich elements within the IFN-γ mRNA 3' untranslated region (UTR). Under the condition of high glycolytic flow in activated Tconvs, GAPDH preferentially engages in the glycolysis pathway. However, in a glucose-deprived

environment GAPDH binds to IFN-γ mRNA and blocks translation. Because mRNAs of other effector cytokines including IL-4 and IL-17A also contain AU-rich elements, this post-transcriptional control may play a general role in regulating effector cytokine production (195). The glycolysis intermediate phosphoenolpyruvate (PEP) also controls Tconv function by regulating nuclear factor of activated T cells (NFAT) signalling (196). In glucose-sufficient conditions, intracellular PEP represses sarco/endoplasmic reticulum calcium-ATPase (SERCA), which maintains cytosolic calcium level for sustained activation of NFAT. NFAT is required for T cell activation along with transcription of Tconv master genes such as T-bet (197). Thus, in glucose-deprived conditions, low intracellular PEP no longer supress SERCA, inhibiting Tconv effector function through low calcium-NFAT signalling. Moreover, Tconv reliance on aerobic glycolysis prevents consumption of TCA cycle intermediates by ATP-linked OXPHOS, allowing citrate to be exported out from mitochondria (198). Following mitochondrial export, citrate is converted into cytosolic acetyl-CoA which modulates histone acetylation of genes including IFN-γ (198, 199). Whilst these mechanisms have not yet been reported in human Tconvs, human Tconvs also change their metabolism to aerobic glycolysis following activation, and glycolysis

inhibition completely prevents cytokine production (200). Taken together, aerobic glycolysis is required for Tconv energy production, biosynthesis, in addition to gene expression and post-transcriptional control of effector cytokine production.

Mitochondrial energy production (ATP-linked OXPHOS) supports Tconv proliferation by maintaining maximum energy production but, unlike aerobic glycolysis, does not modulate Tconv effector cytokine production (27, 199). Nevertheless, the mitochondria itself still plays a role in Tconv function. As mentioned, the TCA cycle intermediate citrate epigenetically regulates cytokine production (198, 199). Mitochondrial reactive oxygen species (ROS) are generated by mitochondrial complexes I and III (201). Mitochondrial complex III deletion in Tconvs significantly inhibits mitochondrial ROS generation, required for Tconv activation (202). In agreement with this, both pan-antioxidants and mitochondria-specific antioxidants inhibit Tconv activation (202, 203). In this way, mitochondria still regulate T cell effector function in their role as a signalling organelle.

In summary, cellular metabolism regulates T cell function through both modulation of

bioenergetics and biosynthetic rates, and through non-canonical functions of metabolic enzymes and metabolites. Tconvs switch their metabolism toward aerobic glycolysis, required to maintain their effector function. The importance of aerobic glycolysis is extensive including energy production, biosynthesis, and epigenetic and genetic controls. Mitochondrial energy production is required to maintain energy homeostasis for maximum proliferation rate, but does not modulate cytokine production. However, through glycolysis, mitochondria have an important role in maintaining Tconv function via citrate provision. Furthermore, mitochondrial ROS production is required for Tconv activation, highlighting their role as a signalling organelle in Tconv effector function.

1.5 Immunometabolism in regulatory T cells

Early work comparing iTreg metabolism with that of differentiated effector CD4 Tconvs demonstrated that iTregs utilise OXPHOS as their preferred fuel source (28, 29, 188). This conclusion was supported by Seahorse XF experiments revealing a high oxygen consumption rate (OCR) and low aerobic glycolysis rate in iTregs. In agreement with this result, *Foxp3* was implicated in Treg metabolism by suppressing glycolysis and enhancing OXPHOS (204, 205). However, as iTregs and natural Tregs (tTregs and pTregs) significantly differ in their epigenetic signature, iTregs and natural Tregs may have completely different in metabolic characteristics. Moreover, how human Tregs change their metabolism upon activation has not yet been reported. Many studies of Treg immunometabolism have treated natural and induced Treg synonymously, which likely obscures the true metabolic differences between subsets; in the following discussion, we have carefully selected studies that specifically investigate natural Tregs (tTregs and pTregs).

1.5.1 Glycolysis in Treg function

An interesting contrast between Tconvs and Tregs is that Tregs do not require Glut1 for their suppressive function (190). Another remarkable aspect is that enhanced glycolysis from transgenic expression of Glut1 significantly decreases Treg suppressive function (206). Similarly, increased aerobic glycolysis from enhancing mTORC1-HIF1α signalling pathway also abolishes Treg suppressive function (206-209). mTORC2 signalling also enhances Treg aerobic glycolysis (210). Treg-specific deletion of phosphatase and tensin homolog (PTEN), a negative regulator of mTORC2, induces spontaneous autoimmune disease (211). mTORC2 inhibits forkhead box protein O1 (Foxo1) and Treg-specific Foxo1 deletion causes a scurfy-like phenotype to develop (212). These studies suggest that enhancing aerobic glycolysis through increased mTORC2 signalling negatively regulates Treg function. Interestingly, conditional *Foxo1* KO in $CD4^+$ lymphocytes cause mice to develop spontaneous autoimmunity indicating that mTORC2 enhancement selectively inhibits Treg, but not Tconv, function (213). FOXP3 itself represses glycolysis (204, 205). Interestingly, Tregs isolated from *Foxp3* mutated mice exhibit over-activated mTORC2 signalling, and mTORC2 deletion in these Tregs rescues their suppressive function (210).

Both *Foxo1* deletion and, more importantly, glycolysis inhibition also rescues suppressive function. Taken together, FOXP3 suppresses mTORC2-Foxo1 mediated glycolysis to maintain Treg suppressive function. Additionally, human Tregs isolated from patients with IPEX syndrome also demonstrate mTORC2 over-activation with high aerobic glycolysis rate; importantly, mTOR inhibition also restores suppressive function in these Treg (210). Moreover, mTORC1 inhibition with low-dose rapamycin increases human Treg suppressive function (167). As such, enhancing aerobic glycolysis via mTOR signalling is likely to negatively control human Treg suppressive function. However, the mechanism underpinning this remains to be established.

Although FOXP3 represses Treg glycolysis to maintain Treg suppressive function, Glycolysis plays an important role in Treg tissue migration. Although HIF1α overexpression impairs Treg suppressive function as mentioned, HIF1α deletion also reduces Treg-mediated immunosuppressive capacity *in vivo* by impairing their ability to migrate into peripheral tissues (214, 215). This phenomenon has also been seen with mTORC2-Foxo1 modulation (216). Foxo1 over-activation (thus glycolysis is inhibited)

impairs Treg capacity to migrate into peripheral tissues resulting in Treg accumulation in secondary lymphoid organs. Mechanistically, glycolysis is an important energy source for cytoskeleton remodelling (217). Interestingly, glycolysis is mediated by mTORC2-mediated expression of glucokinase (GCK) which directly binds to actin in Tregs (217). Importantly, human Tregs isolated from carriers of a loss-of-function mutation in the GCK regulatory protein (causing high GCK activity) exhibited high migratory capacity *in vitro* (217). Interestingly, the migratory capacity of Tconvs isolated from these patients remained unchanged. Thus, GCK-mediated migration is a specific feature of Tregs.

1.5.2 Mitochondria in Treg function

Limiting mitochondrial energy production may reduce Treg suppressive function by increasing aerobic glycolysis to compensate. However, direct evidence of how mitochondrial energy inhibition alters Treg suppressive function has not been reported yet. The TCA cycle intermediate citrate is an important source of acetyl-CoA required for Tconv effector function via histone acetylation (198, 199). However, acetyl-CoA is also an

important source for lipid synthesis (218). As previously mentioned, mTORC1 signalling reduces Treg suppressive function, whilst Treg-specific mTORC1 deletion causes a scurfy-like phenotype to develop, characterised by an impaired mevalonate (cholesterol synthesis) pathway (219). Similarly, Treg-specific liver kinase B1 (*Lkb1*) deletion causes low cholesterol synthesis and a scurfy-like phenotype (220-222). Importantly, mevalonate supplementation ameliorates the scurfy-like phenotype of Treg-specific *Lkb1* mutation (222). HMG-CoA is an enzyme required in a rate limiting step of the mevalonate pathway, and both genetic deletion and pharmacological inhibition of HMG-CoA supress Treg function *in vitro* and *in vivo* (219, 222, 223). Maintaining cholesterol synthesis therefore has an important role in Treg function. However, because lipid synthesis is a key process to maintain cell homeostasis, this may not be a Treg-specific feature. In contrast, cytosolic acetyl-CoA sources may demonstrate interesting differences. Cytosolic acetyl-CoA in Tconvs is maintained by glycolysis (198), whilst recently it was found that Tregs express the monocarboxylate transporter 1 (MCT1) which imports extracellular lactate that is subsequently converted into pyruvate and cytosolic acetyl-CoA through mitochondria (224). Together with a greater reliance on

OXPHOS for energy, therefore, lactate may allow Tregs to effectively synthesise lipids without relying on glycolysis.

α-ketoglutarate is another TCA cycle intermediate mainly derived from glutamine, that functions in metabolic pathways either as a cofactor of ten-eleven translocation (TET) or as the Jumonji C domain-containing histone demethylase (JHDMs) in DNA demethylation (225-227). This DNA demethylation is inhibited by other metabolites with structural homology to α-ketoglutarate: succinate and fumarate (other TCA cycle intermediates) and 2-hydroxyglutarate (a derivative of α-ketoglutarate). Thus, the balance between α-ketoglutarate and its homologous intermediates regulates DNA and histone methylation. Mouse Tregs with mitochondrial complex III deletion exhibit impaired function with accumulation of succinate and 2-hydroxyglutarate (228). Importantly, this is associated with hypermethylation of DNA coding neuropirin-1, PD-1, CD73 and TIGIT without *FOXP3* expression disturbance. In this manner, mitochondrial intermediates alter Treg epigenetics.

Tregs accumulate ROS upon activation, which in turn causes accumulation of SUMO-specific protease 3 (SENP3) required for stable *FOXP3* expression (229). Mitochondrial complex III deletion in Tconvs ameliorates mitochondrial ROS production, leading to failed Tconv activation (202). However, Tregs with mitochondrial complex III deletion do not exhibit impaired *Foxp3* expression (228). This may be because production of ROS in Treg does not originate from mitochondria complex III, but further investigation is required to prove this. In any case, mitochondrial complex III is required for both Tconv and Treg functions, although the mechanism appears to be different.

Lastly, a recent study has demonstrated that mitochondrial disruption increases the suppressive function of Treg by releasing mitochondrial DNA into the cytoplasm, which in turn induces IL-10 production via the IFN type 1 signalling pathway (230). Mitochondrial disruption here is caused by inhibition of fatty acid binding protein 5 (FABP5) which binds fatty acids for extracellular fatty acid uptake and intracellular trafficking. However, given that maintaining the lipid pool has a significant effect on maintaining Treg function and that mitochondria themselves are required for lipid

synthesis, this enhancement may be temporal. Indeed, deletion of CD36 (a receptor for fatty acid uptake) supresses the available lipid pool within Treg and disrupts Treg-mediated suppression of tumour tissue *in vivo* (231).

In summary, studies from mice demonstrate that natural Tregs (tTregs and pTregs) exhibit key metabolic distinctions from Tconv, particularly how glycolysis negatively regulates Treg suppressive function. However, the mechanism underpinning the relationship between glycolysis and suppression remains unclear. Treg immunometabolism has also been linked to several key functions including migration—dependent on glycolysis—and suppression which requires an intact lipid pool and may be modulated by TCA-cycle mediated epigenetic alterations. However, whether these mitochondrial studies are reproducible in human Tregs remains unknown.

1.6 Conclusion

Regulatory T cells are required to maintain immune tolerance. Their antigen non-specific effector function (bystander suppression) and potential to promote infectious tolerance renders them attractive therapeutic targets to treat autoimmune diseases and prevent transplantation rejection. Clinical trials of autologous Treg therapy have demonstrated early successes, but improvements will be required to overcome several key issues including recipient-dependent expansion variability, the duration required to expand Treg, the manufacturing costs and the risk of non-specific suppression by polyclonal Tregs. Generation of non-autologous antigen-specific CAR Tregs may be a solution, but remains largely unexplored. Enhancement of expanded Treg suppressive function may provide a strategy to reduce the required dose of Treg therapy, which can overcome the issue of recipient-dependent expansion variability and the costs of expansion.

Cellular metabolism regulates immune cells through two interacting aspects: bioenergic and biosynthetic activities, and non-canonical activities of metabolic enzymes and intermediates. In terms energy metabolism, iTregs and Tconvs have characteristics, with

iTregs favouring OXPHOS and Tconvs favouring aerobic glycolysis. However, given that natural Tregs (tTregs and pTregs) and iTregs are epigenetically different, the energy metabolism of natural Tregs may also be different from iTregs. Nevertheless, the relationship between their metabolism and function is distinctly different between natural Tregs (tTregs and pTregs) and Tconvs: Tconvs are dependent on glycolysis, whilst glycolysis impairs Treg suppressive function. However, glycolysis is still necessary for Treg tissue migration highlighting the context dependence of immunometabolic effects. Mitochondria also play several important roles outside of their primary metabolic function including as a signalling organelle including ROS production and synthesiser of cellular lipid in both Tconvs and Tregs. However, in several aspects Tconvs and Tregs differentially utilise mitochondria (for example, mouse Tregs import extracellular lactate whilst Tconv do not); the precise differences therefore remain unclear and require further investigation.

Understanding the contrasting metabolic demands and regulation of function between Tconvs and Tregs indicates fundamental differences in cellular activity. This raises the

possibility of targeting metabolic pathways to modulate human immune responses and enhance Treg cellular therapy.

1.7 Thesis aim

The aims of this thesis are:

1. To understand the metabolic characteristics of human Tregs (***Chapter 3 and 4***), and:
2. To understand how metabolism regulates human Treg function as a route to developing a translational therapeutic strategy based on harnessing specific pathways of Treg immunometabolism (***Chapter 5 and 6***)

Chapter 2: Materials and methods

2.1 Cell isolation and culture

All *in vitro* techniques were performed with aseptic precautions in a laminar flow cabinet.

2.1.1 PBMC isolation

Peripheral blood mononuclear cells (PBMC) from blood cones obtained from healthy donors (NHS Blood and Transplant UK) were isolated by density gradient centrifugation. Blood was layered onto lymphocyte separation medium (Corning, 25-072-CV) and then centrifuged for 30 minutes at 2200 RPM at room temperature. PBMC isolated from the buffy coat were pelleted and red cells were lysed with Pharmlyse buffer (BD Biosciences, 555899). PBMC were then washed by phosphate buffered saline (PBS) and either cryopreserved (cryopreserved PBMC) for future use or directly used (freshly-isolated PBMC) in downstream applications.

2.1.2 Cell cryopreservation

Cells were first pelleted by centrifugation and resuspended in freezing medium: 45% foetal bovine serum (FBS) (Gibco, 10270-098), 45% pure RPMI (see section 2.1.6) and 10% dimethylsulphodioxide (DMSO), to a final concentration up to 10^8 cells per 500µl. Cells were frozen at -80°C for 12 -24 hours and then transferred into vapour phase liquid nitrogen.

2.1.3 $CD4^+$ T cells isolation

$CD4^+$ T cells were isolated from PBMC using the $CD4^+$ T cell isolation kit, human (Miltenyi 130-096-533). Freshly-isolated or thawed PBMC were first incubated with $CD4^+$ T cell Biotin-Antibody Cocktail followed by incubation with $CD4^+$ T cell MicroBead cocktail in MACS buffer solution (PBS + 1mM EDTA + 0.5% FBS) at 4°C. The mixture was then applied onto a LS MACS column (Miltenyi, 130-042-401) placed on a magnetic MACS separator (Miltenyi, 130-091-51) according to the manufacturer's protocol.

2.1.4 Treg and Tconv isolation

Freshly-isolated PBMC were first incubated with anti-human CD25 MicroBeads (Miltenyi, 130-092-983) and then magnetically isolated to obtain CD25-enriched and CD25-depleted cells. $CD4^+$ $CD25^+$ $CD127^{lo/-}$ cells (Tregs) were sorted from $CD25^+$-enriched cells by BD FACSAria II (BD Biosciences), using CD4 PE-eFluor 610, CD25 PE-Cy7 and CD127 PE antibodies (see section 2.2.3) and 7-amino-actinomycin D (7-AAD) viability dye (eBioscience, 00-6993). $CD4^+$ $CD25^-$ cells (Tconvs) were flow sorted from CD25-depleted cells in parallel to Treg isolation. $CD45RA^+$ $CCR7^+$ (naïve), $CD45RA^-$ $CCR7^+$ (central memory: CM) and $CD45RA^-$ $CCR7^-$ (effector memory: EM) cells were isolated from either CD25-enriched cells (Treg compartment) or CD25-depleted cells (Tconv compartment) by BD FACSAria II cell sorter, using CD4 PE-eFluor 610, CD25 PE-Cy7, CD127 PE, CD45RA APC-eFluor 480, and CCR7 APC antibodies and 7-AAD.

2.1.5 Mitochondrial mass high ($Mito^{hi}$) and low ($Mito^{lo}$) EM Tconv isolation

Freshly-isolated PBMC were first incubated with anti-human CD45RA MicroBeads

(Miltenyi, 130-045-901). $CD45RA^+$ cells were depleted using LS MACS columns on magnetic MACS separator. EM T cells were then isolated from CD45RA-depleted cells using an anti-human CD4+ effector memory T cell isolation kit (Miltenyi UK, 130-094-125). CD45RA-depleted cells were first incubated with $CD4^+$ EM T cell Biotin-Antibody Cocktail followed by incubation with $CD4^+$ EM T cell MicroBead cocktail in MACS buffer solution. EM T cells were isolated through an LS MACS column and magnetic MACS separator. EM CD4 T cells were placed into pre-warmed RPMI containing 2% human AB pooled serum (HS) (see section 2.1.6) and stained with 7.5nM MitoTracker Deep Red FM (Thermo Fisher, M22426) for 15 minutes at 37°C. Mitotracker stained cells were pelleted and washed in MACS buffer, followed by staining with CD4 PE-eFluor 610, CD25 PE-Cy7, CD127 PE, CD45RA FITC, and CCR7 BV 421 antibodies. $Mito^{hi}$ and $Mito^{lo}$ EM Tconvs were sorted using a BD FACSAria II cell sorter based on the intensity of MitoTracker Deep Red FM signal (***Figure 4.9.a***).

2.1.6 Table of culture medium

All media used in cell cultivation are listed below. Cells were incubated at 37°C with 5% CO_2 supplementation.

Name	Base	Supplementation
10% HS RPMI (Treg culture)	RPMI-1640, no glutamine (Sigma-Aldrich, R0883)	1) 2mM L-glutamine (Sigma-Aldrich, G7531) 2) 10% human AB pooled serum (HS) (Life Science Production, S-101) 3) 100 U/ml penicillin and 100µg/ml streptomycin (Sigma-Aldrich, P4333) 4) 200 U/ml recombinant human IL-2 (rhIL-2)

		(Chiron, HZ-1015)
10% HS RPMI (Tconv culture)	RPMI-1640, no glutamine	1) 2mM L-glutamine 2) 10% human AB pooled serum (HS) 3) 100 U/ml penicillin and 100μg/ml streptomycin
10% FBS RPMI (PBMC culture)	RPMI-1640, no glutamine	1) 2mM L-glutamine 2) 10% FBS 3) 100 U/ml penicillin and 100μg/ml streptomycin
2% HS RPMI	RPMI-1640, no glutamine	1) 2mM L-glutamine 2) 2% HS 3) 100 U/ml penicillin and 100μg/ml

		streptomycin
10% HS RPMI (for Treg expansion)	RPMI-1640, no glutamine	1) 2mM L-glutamine 2) 500μM sodium pyruvate (Gibco, 11360-070) 3) 10% HS 4) 1000 U/ml rhIL-2 (or 250 U/ml rhIL-2 during resting phase)
5% HS X-VIVO 15 (for Treg expansion)	X-VIVO 15 with Gentamycin and PR (Lonza, LZBE02-060F)	1) 5% HS 2) 1000 U/ml rhIL-2 (or 250 U/ml rhIL-2 during resting phase)
Seahorse medium	Seahorse XF RPMI medium, pH 7.4 (Agilent, 103576-100)	1) 10mM glucose (Agilent, 103577-100) 2) 2mM Glutamine

		(Agilent, 103579-100) 3) 2% HS 4) 100 U/ml rhIL-2
Small EV-depleted medium	X-VIVO 15 with Gentamycin and PR	1) 200 U/ml rhIL-2
No glucose medium	RPMI-1640, no glucose (Gibco, 11879020)	1) 100 U/ml penicillin and 100µg/ml streptomycin 2) 200 U/ml rhIL-2
Very low glucose medium	RPMI-1640, no glucose	1) 100 U/ml penicillin and 100µg/ml streptomycin 2) 10% HS 3) 200 U/ml rhIL-2
Control medium (used only in	RPMI-1640, no glucose	1) 100 U/ml penicillin and 100µg/ml

Figure 6.9)		streptomycin 2) 10% HS 3) 200 U/ml rhIL-2 4) 10 mM glucose
Pure RPMI (cryopreservation)	RPMI-1640, no glutamine	

2.1.7 *in vitro* T cell stimulation

Both Tregs and Tconvs were stimulated with Dynabeads Human T-Activator CD3/CD28 (anti-CD3/CD28 beads) (Gibco, 11132D) at a 5:1 cell to bead ratio for 60h. Cells were seeded at a density of 10^5 cells per well into a round-bottom 96-well plate.

2.1.8 Treg *in vitro* expansion

Freshly-isolated Tregs ($CD4^+$ $CD25^+$ $CD127^{lo/-}$ cells) were cultured for 16-17 days in either 10% HS RPMI or 5% HS X-VIVO15, both of which were supplemented with 1000 U/ml rhIL-2 during the two week expansion phase and then with 250 U/ml during the 2-3 days resting phase. For expansion, Tregs were seeded at a density of 0.5 x 10^6 cells per well into a round-bottom 96-well plate with anti-CD3/CD28 beads at a 1:3 cell to bead ratio for the first seven days, followed by restimulation with anti-CD3/CD28 beads at a 1:1 cell to bead ratio in a flat-bottom 24-well plate at a density of 10^6 cells per well for the next seven days. During the expansion, cultures were split and new media was added as required. After expansion, Tregs were rested for 2-3 days without stimulation in the presence of 250 U/ml rhIL-2.

2.1.9 Table of inhibitors

All inhibitors used in this thesis were aliquoted in stock solution and stored at -20°C. After thawing, inhibitors were diluted with PBS before use.

Name	Target	Stock solution (% in final concentration)	Final concentration
Rapamycin (MACS GMP) (Miltenyi, 170-076-308)	mTOR	DMSO (0.05%)	100 nM
2-Deoxy-D-glucose (2-DG) (Sigma-Aldrich, 154-17-6)	Glucose structural analogue	Deionised water	2mM
Oligomycin (Sigma-Aldrich, 1404-19-9)	Mitochondrial ATP synthase (mitochondrial complex V)	DMSO (0.2%)	2µM
PFK15	6-Phosphofructo-2-	DMSO	10µM

(Cayman, 4382-63-2)	kinase/fructose-2,6-bisphosphatase 3 (PFKB3)	(0.15%)	
GSK 2837808A (Cayman, 1445879-21-9)	Lactate dehydrogenase A (LDHA)	DMSO (0.1%)	20µM
FX 11 (Sigma-Aldrich, 213971-34-7)	LDHA	DMSO (0.05%)	25µM
UK 5099 (Sigma-Aldrich, 56396-35-1)	Mitochondrial pyruvate carrier	DMSO (0.1%)	10µM
6-aminonicotinamide (6-AN) (Cayman, 329-89-5)	6-phosphogluconate dehydrogenase	DMSO (0.0725 %)	5µM
Carbonyl cyanide-4-	Mitochondrial ATP	DMSO	2µM

(trifluoromethoxy) phenylhydrazone (FCCP) (Sigma-Aldrich, 370-86-5)	synthesis (Mitochondrial uncoupler)	(0.133%)	
Rotenone (Sigma-Aldrich, 83-79-4)	Mitochondrial complex I	DMSO (0.05%)	1 uM
Antimycin A (Sigma-Aldrich, 1397-94-0)	Mitochondrial complex III	Ethanol (0.02%)	4 uM

2.2 Flow-cytometry based assays

Flow cytometric data were acquired using a BD FACSAria II, BD Canto II BD (Biosciences), or Attune NxT flow cytometer (Thermo Fisher), and analysed using FlowJo software (BD

Bioscience). All fluorochrome-coupled monoclonal antibodies (mAbs) are listed in section 2.2.3.

2.2.1 Cell surface staining

Cells were first washed in PBS, resuspended in either PBS or MACS buffer and then incubated with fluorochrome-coupled mAb for 30 minutes at 4°C in the dark. CCR7 antibody staining was performed at 37°C for 30 minutes. Cells were then washed by adding PBS, centrifuging at 500g for 5 minutes, and then decanting the supernatant. Cell pellets were fixed in 1% paraformaldehyde (PFA) before analysis, except for flow-cytometry based metabolic assays in which cells were resuspended in ice-cold PBS and analysed by flow cytometry immediately.

2.2.2 Intracellular staining

Following cell-surface staining, cells were permeabilised in eBioscience FOXP3 transcription factor staining buffer (Invitrogen, 00-5523-00). Briefly, cells were kept in

Fixation/Permeabilization buffer for 1 hour (or overnight). Cells were then washed by adding permeabilization buffer, centrifuging at 500g for 5 minutes and then decanting the supernatant. Cell pellets were then resuspended in permeabilization buffer containing 5% mouse or rat serum and incubated for 15 minutes at 4°C in the dark, followed by staining with fluorochrome-coupled mAb. Cells were washed in permeabilization buffer and then resuspended in PBS before analysis.

2.2.3 Table of fluorochrome-coupled monoclonal antibodies

Specificity	Conjugation	Clone	Cat number
CCR7	BV 421	G043H7	353208
CCR7	APC	G043H7	353214
CD3	APC-eFluor 780	OKT3	47-0037-42
CD3	PE	OKT3	317308
CD39	PE	eBioA1	12-0399-42

CD4	PE eFluor 610	RPA-T4	61-0049-42
CD45RA	FITC	HI100	11-0458-42
CD45RA	APC-eFluor 780	47-0458-42	47-0458-42
CD62L	APC-eFluor 780	DRED56	47-0629-42
CD73	APC-eFluor 780	AD2	47-0739-42
CD8a	FITC	SK1	11-0087-42
CTLA-4	PE	L3D10	349906
FOXP3	eFluor 450	PCH101	48-4776-42
FOXP3	FITC	PCH101	11-4776-42
FOXP3	APC	PCH101	17-4776-42
Human CD45	APC-eFluor 780	HI30	47-0459-42
IFN-g	FITC	4S.B3	11-7319-82
IL-17A	PE	eBio64CAP17	12-7178-42
PD-1	FITC	EH12.2H7	329904
TNF-a	BV 650	MAb11	563418

2.2.4 Live/dead cell staining

All flow-cytometric data were acquired by exclusion of dead cells except within the viability assay. Dead cells were detected by staining with either 7-AAD or the Zombie NIR fixable viability kit. Cells were stained with 7-AAD during cell surface staining when used, whilst cells were stained with Zombie NIR fixable viability dye prior to cell-surface staining. Zombie NIR fixable viability dye stock solution was made by adding 100µl DMSO and was stored at -20°C before use. Prior to staining, cells were first washed in PBS, and were then stained with 8000-times diluted (PBS) Zombie NIR stock solution for 15 minutes in the dark. The cells were washed in PBS before cell surface staining.

2.2.5 Violet proliferation dye staining

For staining with Violet Proliferation Dye 450 (VPD) (BD Bioscience, 562158), cells were first washed in PBS, resuspended in 1µM VPD diluted in PBS for staining, and then incubated for 10 minutes at 37°C. After staining, FBS was immediately added to stop staining, then cells were washed twice in PBS.

2.2.6 Proliferation assay

Cells were first stained with VPD, and stimulated by anti-CD3/CD28 beads at a 5:1 cell to bead ratio for 84h, following live/dead staining and cell fixation as described. Cells were seeded at a density of 0.5x 10^5 cells per well into a round-bottom 96-well plate. For Treg proliferation assays, metabolic inhibitors were added (see section 2.1.9). To quantify cell proliferation rate, the division index (defined as the average number of divisions that cells have undergone) was calculated as $(\sum_{k=0}^{n} nd_n/2^n)$ / $(\sum_{k=0}^{n} d_n/2^n)$, where d represents the number of cells in a group and n represents the maximum number of divisions that cells have undergone. (Undivided cells: n = 0).

2.2.7 Intracellular cytokine production assay

Cells were first stimulated with ImmunoCult Human CD3/CD28 T cell activator (anti-CD3/CD28 activating mAb) (Stemcell, 10971) at a 2.5% concentration for 15h, followed by 100ng/ml phorbol myristate acetate (PMA) (Sigma Aldrich, P1585), 1µg/ml ionomycin (Sigma Aldrich, 10634) and 2µM monensin (eBioscience, 00-4505-51). Cells were seeded

at a density of 1.0 x 10^5 cells per well into a round-bottom 96-well plate. After stimulation, cell surfaces were stained followed by intracellular cytokine staining using IFN-γ FITC, IL-17A PE and TNF-α BV 650 mAbs.

2.2.8 LEGENDplex cytokine bead-based immunoassay

LEGENDPlex HU Th Cytokine Panel (Biolegend, 741027) was used to quantify cytokines within EM Tconv culture supernatants. The culture supernatants were either diluted 19 times (culture supernatant from 84h cell culture) or used directly (18h cell culture) prior to the assay. The procedure was done as per the manufacturer's protocol. Briefly, culture supernatants were placed into a V-bottom 96-well plate and mixed with antibody-immobilised beads, and then incubated for 2h on a plate shaker at 300rpm. The beads were washed, and then bead-captured cytokines were stained by detection antibodies for 1h on a plate shaker at 300rpm in the dark. Bead-captured cytokines were washed twice and then analysed immediately by flow cytometry.

2.2.9 MACSPlex small extracellular vesicle bead-based immunoassay

MACSPlex Exosome Kit, human (Miltenyi, 130-108-813) was used to both quantify and characterise small EVs produced by Tregs. Tregs were cultured in small EV-depleted medium for 48h in the presence of anti-CD3/CD28 beads. Culture supernatants were isolated by centrifugation at 500g for 5min. Culture supernatants were then centrifuged at 2000g for 30 minutes to remove cell debris and then were passed through a Vivaspin 0.2µm (Sartorius, VS0172) filter to remove large extracellular vesicle. Filtered culture supernatants were concentrated 4 times using a 100kDa Amicon Ultra-0.5 Centrifugal Filter (Millipore, UFC10024). The assay was performed as per the manufacturer's protocol. Briefly, concentrated culture supernatants were plated onto the provided assay plate, mixed with MACSPlex Exosome capture, and incubated overnight on a plate shaker at 300rpm. Bead-captured small EVs were stained with detection antibodies and incubated for 1h on a plate shaker at 300rpm in the dark. The bead-captured small EVs were then washed twice and analysed immediately by flow cytometry.

2.2.10 CD81^{+} extracellular vesicle bead-based immunoassay

Exosome-Human CD81 Flow Detection Reagent (Invitrogen, 100622D) was used to quantify CD81^{+} small EVs produced by Tregs. Treg culture supernatants were prepared and concentrated in a same way as for the MACSPlex small EV bead-based assay (see section 2.2.9). CD81 Flow detection regent (CD81 capture bead) was first washed in a 2ml vial in washing buffer (PBS containing 1% Exosome-depleted FBS (Gibco, A2720803)), before being placed in magnetic field where the washing buffer was then removed by pipetting. The concentrated Treg culture supernatants were mixed with the CD81 capture bead and incubated overnight on a plate shaker at 300rpm. The bead-captured small EVs were then briefly centrifuged at 1000rpm for 1 minute, and then washed in washing buffer. The bead-captured small EVs were stained either by CD81 PE (BD Bioscience, 555676) or isotype control (BD bioscience, 559320) for 1 hour on a shaker at 300rpm in the dark, and then washed twice in washing buffer. Bead-captured small EVs were resuspended in washing buffer and detected by flow cytometry immediately.

2.3 Flow cytometry-based metabolic assays

2.3.1 2-NBDG glucose uptake rate assay

Glucose uptake rate of stimulated cells (see section 2.1.7) was analysed using 2-NBDG (Cayman, 186689-07-6). Cells were first centrifuged to remove cell culture medium, then were resuspended in 200µM 2-NBDG in no-glucose medium and incubated for 30 minutes at 37°C with 5% CO_2 supplementation for staining. After 2-NBDG staining, cells were centrifuged and washed twice in cold PBS before live/dead staining. Cells were then washed by PBS and immediately detected by flow cytometry.

2.3.2 Glucose transporter 1 expression assay

The expression of glucose transporter 1 (Glut1) on stimulated cells (see section 2.1.7) was analysed using Anti-Glut1.RBD.GFP (Metafora, Glut1-M25). Cells were first centrifuged to remove cell culture and then resuspended in 10% HS RPMI containing Anti-Glut1.RBD.GFP and 1mM EDTA before incubation for 25 minutes at 37°C with 5%

CO_2 supplementation for staining. Following this, cells were centrifuged and washed twice in cold PBS containing 2% FBS and 1mM EDTA before live/dead staining. Cells were then washed by PBS and immediately detected by flow cytometry.

2.3.3 MITO-ID membrane potential detection assay

The MITO-ID membrane potential detection kit (MITO-ID) (Enzo, ENZ-510018-0025) was used to investigate freshly-isolated (unstimulated) Treg and Tconv mitochondrial membrane potential. CD25-enriched (Treg compartment) and CD25-depleted cells (Tconv compartment) were first incubated in 2% HS RPMI for 2 hours at 37^{o}C with 5% CO_2 supplementation with or without addition of carbonyl cyanide-4-(trifluoromethoxy) phenylhydrazone (FCCP) for the last 30 minutes, followed by MITO-ID staining as per the manufacturer's protocol. Briefly, cells were washed in the provided assay solution, resuspended in staining solution, incubated for 15 minutes for staining, and then washed twice in the provided assay solution. After washing, cells were stained with CD4 PE-eFluor 610, CD25 PE-Cy7, CD127 APC, CD45RA APC-eFluor 780, and CCR7 BV421

antibodies and 7-AAD for 30 minutes in the provided assay solution. Cells were then washed by PBS and immediately detected by flow cytometry.

2.3.4 MitoTracker co-staining assay

MitoTracker Green FM (Invitrogen, M7514) and MitoTracker Deep Red FM were used to detect mitochondrial mass and membrane potential of Tregs and Tconvs. CD25-enriched cells (Treg compartment) and CD25-depleted cells (Tconv compartment) were first incubated in 2% HS RPMI for 2 hours. During the last 15 minutes of incubation, 80nM of MitoTracker Green FM and 10nM of MitoTracker Deep Red FM were added. Cells were centrifuged and washed twice in PBS before staining with CD4 PE-eFluor 610, CD25 PE-Cy7, CD127 PE, CD45RA eFluor, and CCR7 BV421 antibodies and 7-AAD for 15 minutes at 4°C in the dark. Cells were then washed by PBS and immediately detected by flow cytometry.

2.3.5 MitoTracker Green FM mono staining assay

To investigate mitochondrial mass of Mito^{hi} EM Tconvs, Mito^{lo} EM Tconvs and EM Tregs after stimulation, MitoTracker Green FM was used. Stimulated cells were first centrifuged to remove culture supernatant, resuspended in 80nM of MitoTracker Green FM and incubated for 15 minutes at 37^{o}C with 5% CO_2 supplementation. Cells were then centrifuged and washed twice in PBS, before live/dead staining for 15 minutes at 4°C in the dark. Cells were then washed by PBS and immediately detected by flow cytometry.

2.4 Treg functional assays

Treg suppressive function was estimated by percentage suppression (% suppression) defined as: [(Positive control) – (Responders + Tregs)] / (Positive control) x 100. This yielded either division index, % of cytokine producing cells or absolute amount of cytokines produced. Responders were either PBMC, CD4^{+} T cells, Mito^{hi} EM Tconvs or Mito^{lo} EM Tconvs. For surface staining, PBMC were stained with CD3 APC-eFluor 780, CD4 eFluor 610, and CD8a FITC antibodies whilst CD4^{+} T cells, Mito^{hi} EM Tconvs and

Mito^{lo} EM Tconvs were mono stained with live/dead dye prior to flow cytometry assays.

2.4.1 *in vitro* suppression assay

VPD-stained responders were co-incubated with Tregs at different ratios along with Dynabeads Human T-Activator CD3/CD28 (Gibco, 11132D) at a 5:1 cell to bead ratio for 84h. Responders alone with beads (positive control) or without beads (negative control) were used as controls. After incubation, cells were stained by the surface staining procedure described above and analysed by flow cytometry. Culture supernatants were stored at -20°C before subsequent quantification by LEGENDPlex.

2.4.2 *in vitro* T cell cytokine production suppression assay

VPD-stained responders were co-incubated with Treg at a 1:1 ratio in the presence of Human CD3/CD28 T cell activator (Stemcell, 10971) at a 2.5% concentration for 15h, following by addition of 100ng/ml PMA, 1µg/ml ionomycin and 2µM monensin for 3h.

Responders alone with activating antibiodies (positive control) or without activating antibiodies (negative control) were used as controls. Responders were seeded at a density of 1.0x 10^5 cells per well into a round-bottom 96-well plate. After stimulation, cells underwent surface and intracellular staining as described above and were analysed by flow cytometry. For intracellular cytokine staining, PBMC were stained with IFN-γ FITC and IL-17A PE, whilst Mito^{hi} EM Tconvs and Mito^{lo} EM Tconvs were stained with IFN-γ, IL-17A and TNF-α. Culture supernatants were stored in -20°C before subsequent quantification by LEGENDPlex.

2.4.3 Treg metabolic inhibitors pre-treatment

Tregs were first incubated in 2% HS RPMI containing 100 U/ml rhIL-2 for 2 hours in the presence or absence of metabolic inhibitors (see section 2.1.9) at 37°C with 5% CO_2 supplementation. After pre-treatment, Tregs were collected into 15ml Falcon tubes, topped up by PBS to 14 ml and then centrifuged. After decanting the supernatant, Treg pellets were resuspended in 14 ml of PBS containing 2% FBS. The washing step was

repeated twice. Following this, Tregs were resuspended in fresh medium for further assays.

2.4.4 Isolation of Treg culture supernatant

Treg culture supernatants were collected to analyse their suppressive function. Tregs were first incubated with anti-CD3/CD28 beads in 10% HS RPMI at a density of 10^6 cells/ml. 10% HS RPMI without cells was incubated in parallel as a medium control. After 48h stimulation, cells were harvested and centrifuged at 500g for 5 minutes. Culture supernatants were gently aspirated and centrifuged again to ensure complete removal of Tregs.

2.4.5 Size fractionation of Treg supernatants using ultracentrifugal filters

100kDa molecules from Treg supernatants and medium control were first isolated using 100kDa Amicon Ultra-0.5 Centrifugal Filters. Molecules >100kDa isolated from Treg

supernatants were mixed with the <100kDa fraction of medium control to be used as the >100kDa Treg supernatants. Following this, the <100kDa fractions of Treg supernatants and new medium controls were fractioned using 3kDa Amicon Ultra-0.5 Centrifugal Filters (Millipore, UFC500324). The >3kDa fraction of Treg culture supernatant (between 100kDa and 3kDa) was mixed with >100kDa of medium control and < 3kDa of medium control to be used as the 3-100kDa Treg supernatants. Lastly the <3kDa fraction of Treg culture supernatant and the > 3kDa fraction of medium control were mixed to be used as the <3kDa Treg supernatants. The fractionated Treg supernatants were added to T cell proliferation assays to investigate their suppressive function.

2.4.6 Proteinase K treatment of Treg supernatant

Treg culture supernatants were treated with 100µg/ml proteinase K (APExBIO, K1307) for 1h at 37°C. The treated culture supernatants were then heat inactivated at 95°C for 10 minutes, followed by centrifugation at 10,000g for 10 minutes to remove debris. Controls underwent the same treatment without addition of proteinase K. The

proteinase K treated Treg supernatants were applied to T cell proliferation assays to investigate their suppressive function.

2.4.7 Serial centrifugations to isolate apoptotic bodies and large EVs

Treg culture supernatants were first centrifuged at 2,000 g for 30 minutes to isolate apoptotic bodies as a pellet. Supernatants were then centrifuged at 10,000 g for 45 minutes to isolate large extracellular vesicles (large EVs) as a pellet. Pellets of apoptotic bodies and large EVs were reconstituted to their original volume by parallelly-centrifuged medium control.

2.4.8 Small EV depletion: Norgen method

The FBS Exosome depletion kit (Slurry format) (Norgen, 61100) was used to deplete small EVs from Treg culture supernatants. The sensitivity to human small EVs was confirmed by a Norgen technical advisor. Samples were processed as per the

manufacturer's instructions. Briefly, Treg culture supernatants were treated with Exo C buffer and Slurry E solution for 10 minutes at room temperature. Slurry E was then removed by centrifugation and the small EV-depleted supernatants were collected and used for the T cell proliferation assay.

2.4.9 Small EV removal: bead method

Small EVs were removed from Treg culture supernatants using the human Exosome Isolation Kit Pan (Miltenyi, 130-110-912) with a modified protocol. Treg culture supernatants were first filtered by serial centrifugation to remove apoptotic bodies and large EVs (see section 2.4.7), following addition of 50µl of Exosome Isolation Microbeads per 1 ml of culture supernatant and incubation for 1h at room temperature. A column was placed into magnetic field and primed with 100µl equilibration buffer. The column was washed with PBS three times, before addition of the microbead-treated supernatant. The first half (500µl) of the culture supernatant passing through the column was discarded and only the second half was collected and used for the T cell proliferation assay.

2.5 Seahorse XF assay

Real time bioenergetics analysis of extracellular acidification rates (ECAR) and oxygen consumption rate (OCR) of T cells was undertaken by Seahorse XF assay using XFe96 sensor cartridges, XFe96 cell culture plates, and Seahorse XF Calibrant solution (contained with the Seahorse XFe96 FluxPak (Agilent, 102416-100)). A day before assay, the XFe96 cell culture plate was treated with 100µg/ml Poly-D-lysine hydromide (P6407) for 1 hour in room temperature, followed by two washes with deionised (DI) water. The treated plate was kept at 4°C and pre-warmed to room temperature one hour before use. The sensor cartridge was hydrated with DI water a day before assay and kept at 37°C without CO_2 supplementation; DI water was replaced with Calibrant solution 1h before assay. On the day of assay, the culture plate was pre-warmed to room temperature one hour before seeding cells. Cells were seeded onto the XFe96 cell culture plate at a cell density of 3.0×10^5 for unstimulated Tregs and Tconvs, 2.0×10^5 for stimulated Tregs and Tconvs (see section 2.1.7), 2.0×10^5 for expanded Tregs, and 2.0×10^5 for EM T cells. During the assays, 2µM oligomycin, 1.5µM FCCP, 1µM rotenone, 4µM antimycin A, or 5% ImmunoCult Human CD3/CD28 T cell activator was injected. Experiments on the

seahorse system were done under the following assay conditions: three minutes mixture; two minutes wait and three minutes measurement. All assays were analysed using the Seahorse XFe96 analyzer (Agilent) and Wave software (Agilent).

2.6 Enzyme-linked immunosorbent assay (ELISA)

ELISA was performed to determine the IL-10 concentration of Treg culture supernatants using the IL-10 Human Uncoated ELISA Kit (eBioscience, 88-7106-88) based on the manufacturer's protocol. Briefly, the NUNC Maxisorp ELISA plate (Invitrogen, 44-2404) was first coated with an IL-10 capture antibody at 4°C overnight. After washing, the Treg culture supernatant was added onto the capture antibody-coated plate which was incubated at 4°C overnight to achieve maximum accuracy. The plate was washed the following day and incubated with the detection antibody for 1h, followed by washing and incubation with Avidin-HRP for 30 minutes. After washing intensively, tetramethylbenzidine (TMB) solution was added, and 15 minutes later stop solution was added. The ELISA plate was analysed with a spectrophotometer at 450 nm.

2.7 NanoString nCounter assay

Cells were incubated for 40h with anti-CD3/CD28 beads at a 5:1 cell to bead ratio. RNA from the activated cells was isolated using the RNeasy Plus Micro kit (QIAGEN, 74034) according to the manufacturer's protocol. The quantity of isolated RNA was measured by Quant-IT RNA Assay Kit (Invitrogen, Q33140) using Qubit 4 Fluorometer (Invitrogen). T cell gene profiles were detected using the nCounter Human Metabolic Pathway Panel (NanoString, XT-CSO-HMP1-12) and nCounter Human CAR-T Characterisation panel (NanoString, XT-CSO-HCART1-12). RNA was first incubated with the Reporter CodeSet and Capture ProbeSet for 20h at 65°C for RNA hybridisation. The hybridised RNA was then applied to the nCounter SPRINT Catridge and analysed by nCounter SPRINT. Data were analysed by nSolver software (NanoString).

2.8 Mass-spectrometry based metabolomics

100 x 10^6 expanded Tregs and Tconvs were first pre-treated with DMSO (0.2%) or 2 µM oligomycin for 2h (see section 2.4.3). Pre-treated cells (50 x 100^6 in each condition) were incubated with anti-CD3/CD28 beads at a 5:1 cell to bead ratio for 48h on a 12 well plates

seeded at density of 2.0 x 10^6 cells per well in 2ml of 10% HS RPMI. After stimulation, cells were collected into 15 ml Falcon tubes (5 wells per tube) and centrifuged at 500g for 5 minutes. After removing the supernatants, cells were washed by adding ice-cold PBS, centrifuged at 500g for 5 minutes complete removal of the supernatant. The cell pellet was then resuspended by ice-cold methanol (Sigma-Aldrich, 900688) to isolate metabolites. Isolated metabolites were first centrifuged at 13,000g for 30 minutes to remove cell debris precipitated as a pellet, followed by DNA measurement for standardisation using NanoDrop. Standardisation was achieved by adding additional methanol to dilute all samples to the lowest measured concentration. The standardised metabolites were then filtered through a 10 kDa Amicon ultracentrifugation filter. The metabolites (< 10kDa) were further analysed by Dr. Ebrahimi in the McCullagh lab by mass spectrometry. Each condition had 5 technical repeats. The immunosuppressive capacity of the culture supernatants were checked as a quality control.

2.9 *in vivo* suppression assay using mouse peritoneal lavage model

Pre-treated expanded Tregs (DMSO or oligomycin) were incubated with anti-CD3/CD28 beads at a 5:1 cell to bead ratio for 48h on 12 well plates seeded at a density of 2.0 x 10^6 cells per well in 2ml of 10% HS RPMI. Culture supernatants were gently removed and filtered through a 0.22µm Millex-GP Syringe Filter Unit (Merck, SLG033R) to remove cell debris and large EVs. The filtered culture supernatants were then concentrated 20 times using >100 kDa MilliporeSigma Amicon Ultra-15 Centrifugal Filter Units (Fisher Scientific UFC910024). With the kind help of Dr. Oliver McCallion, 250µl of concentrated culture supernatant derived from 5.0 x 10^5 expanded Tregs was injected into the peritoneal cavity of BALB/c $RAG^{-/-}c\gamma c^{-/-}$ mice along with 5.0 x 10^6 PBMCs suspended in 250µl of pure RPMI. VPD-stained PBMC were then harvested by peritoneal lavage, stained with CD3 PE, CD4 PE eFluor 610, CD8a FITC, human CD45 APC-eFluor 780 antibodies and 7-AAD, then analysed by flow cytometry.

2.10 Statistical analysis

Except for data generated from NanoString nCounter experiments, nonparametric paired and unpaired t-tests or one-way ANOVA tests were applied to data to determine statistical significance using GraphPad Prism software (GraphPad). P values less than 0.05 were taken to be significant. Data generated from NanoString nCounter experiments were analysed on the nSolver platform (NanoString) by applying the Benjamini-Yakutieli test. Adjusted p-values less than 0.05 were taken to be significant

Chapter 3: Characteristics of human *ex vivo* Treg metabolism

3.1 Introduction

The immunometabolism of Tconvs has been the focus of much study. It is well established that Tconvs activated by TCR binding alongside CD28 co-stimulation switch their metabolism away from oxidative phosphorylation (OXPHOS) towards aerobic glycolysis (24-26, 232). This ensures rapid availability of adenosine triphosphate (ATP) and a pool of carbon for biosynthesis. In addition to both the catabolic and anabolic importance of glycolysis, a high glycolytic rate is required to maintain Tconvs effector function (27, 196, 198).

The study of Treg immunometabolism, in comparison, has been less extensive with early work comparing iTreg metabolism with that of differentiated effector CD4 Tconvs (28, 29, 188, 189). These studies revealed lower glycolysis and higher OXPHOS rates in iTregs compared to differentiated Tconvs. FOXP3 (the master transcription factor of Tregs) was

implicated in Treg metabolism, suppressing glycolysis and enhancing OXPHOS (204, 205). These data suggested that OXPHOS was the more dominant fuel in iTregs, compared with glycolysis in differentiated Tconv, and indicated that Tregs and Tconvs may have different preferred extracellular environments based on their metabolic preferences. The possibility of describing immune tolerance in terms of the immunometabolism of discrete cellular compartments raised the possibility of targeting metabolic pathways to balance human immune responses.

However, iTregs and natural Tregs (tTregs and pTregs) have several fundamental differences. For example, natural Tregs stably express FOXP3 and maintain a regulatory immune phenotype. FOXP3 expression has been suggested to be stabilised by demethylation of Treg-specific demethylation region (TSDR). This is in contrast to iTregs which demonstrate transient FOXP3 expression and regulatory function associated with a methylated TSDR. Thus, iTregs and natural Tregs are different in origin and phenotype. It is therefore possible that the cellular metabolism of natural Tregs and iTregs also differs. iTregs are differentiated from naïve Tconvs in the presence of several factors including

TGF-β. Therefore, the study of iTreg metabolism often cannot reliably exclude the influence of extrinsic factors. For example, Priyadharshini *et al* report that TGF-β represses glycolysis and reprograms cellular metabolism to favour OXPHOS in mice CD4 T cells (233). As such, previous studies comparing the metabolism of iTregs and differentiated effector Tconvs must be carefully revisited to assess whether their results were due to intrinsic differences in Treg immunometabolism or were an artifact of the cytokines employed during the differentiation process.

Moreover, early Treg immunometabolism studies did not directly answer whether Tregs maintain OXPHOS as a preferential energy source following TCR stimulation. As a part of adaptive immunity, which responds to specific antigens, T cells are functional only when they are activated through their TCR binding a specific peptide within an HLA molecule alongside co-stimulation signals. A direct comparison of metabolism between activated Tregs and Tconvs must be assessed to elucidate their actual metabolic preferences in functional states.

Clonal expansion is a fundamental property of activated T cells. This proliferation requires not only energy but also significant biosynthesis, which is supported by aerobic glycolysis (234). Glucose is an important carbon source for biomass synthesis. Alongside rapid ATP synthesis, the advantage of aerobic glycolysis is that high glycolytic flow maintains a large quantity of glycolysis intermediates consumed as branches of the anabolic process. If Tregs did not increase their aerobic glycolysis, they would need to utilise carbon from different pathways such as gluconeogenesis. The importance of glucose in Treg clonal expansion has not yet been investigated.

A final limitation of early Treg metabolism studies is that the majority were conducted using Tregs from mice. This potentially limits therapeutic translation of results into the clinic and as such investigation of human Treg immunometabolism is critical.

In summary, the previously reported concept of 'OXPHOS-dependent Treg metabolism' has four outstanding questions:

1. Do natural Tregs have similar metabolic phenotype to iTregs?

2. Are Tregs still dependent on OXPHOS in their activated state?

3. Is glucose required for Treg clonal expansion?

4. Do human Tregs have same metabolic phenotype as mouse Tregs?

Although it is possible to utilise other substances including glutamine and fat as a source of carbon, these mechanisms are lesser efficient from glycolysis. Therefore, we hypothesise that human Tregs change their metabolism towards aerobic glycolysis to support their clonal expansion upon activation.

3.1.1 Chapter aim

The aim of this chapter is to investigate how human *ex vivo* Tregs modulate their metabolism following TCR and CD28 stimulation and how Tregs maintain their clonal expansion. The results of this chapter provide the background to further analysis of Treg metabolism within different subsets (chapter 4) with an exploration of the relationship between Tregs metabolism and function, and an exploration of possible strategies of

clinical translation (chapter 5).

3.2 T cell receptor signalling alongside CD28 co-stimulation increases human *ex vivo* Treg metabolism which is dependent on aerobic glycolysis.

Human Tconvs are known to be dependent upon aerobic glycolysis following TCR (or CD3) stimulation alongside CD28 co-stimulation. However, how human Tregs change their metabolism upon activation has not yet been reported. To investigate this, human Tregs were freshly isolated from healthy human donors as $CD4^+$ $CD25^+$ $CD127^{lo}$ cells and cultivated immediately without cryopreservation. Isolated Tregs were stimulated by anti-CD3/28 beads to provide TCR stimulation and co-stimulatory signal. The impact of activation on Tregs in glucose uptake rate was investigated using the fluorescently labelled glucose analogue 2-NBDG. We found a significantly higher 2-NBDG signal from stimulated Tregs compared to the unstimulated controls, indicating that human Tregs dramatically increase their glucose uptake rate upon stimulation (***Figure 3.1***).

Glucose is used as an energy fuel both in aerobic glycolysis and OXPHOS. Thus, the high rate of glucose uptake does not directly prove the high rate of aerobic glycolysis in stimulated Tregs. To investigate this further, we used Seahorse XF to directly measure the extracellular acidification rate (ECAR) and oxygen consumption rate (OCR) of live cells. The final product of aerobic glycolysis is lactate, which is the major acidic substance produced by cells, and ECAR can therefore be used as a proxy measure of aerobic glycolysis. Stimulated Tregs showed a higher glucose uptake rate and a remarkably higher ECAR, demonstrating that stimulation strongly increases the rate of aerobic glycolysis in Tregs (***Figure 3.2a***).

We then questioned whether stimulation increases the rate of aerobic glycolysis in isolation or in parallel to the rate of OXPHOS. Stimulated Tregs showed notably higher basal OCR (which is the initial OCR value), suggesting a higher OXPHOS rate in their activated state (***Figure 3.2.b Left***). Oxygen is used not only during OXPHOS but also by other processes such as cellular oxidation. To directly investigate the OCR used for energy production by OXPHOS, oligomycin was injected during Seahorse XF

measurement. Oligomycin is an inhibitor of mitochondrial ATP synthase (mitochondrial complex V), and so the difference before and after oligomycin treatment represents the energy-linked OXPHOS rate (known as the ATP-linked OCR). Significantly higher ATP-linked OCR indicated that stimulation also increases the rate of energy production through OXPHOS (***Figure 3.2.b Right***).

Anti-CD3/CD28 stimulation therefore dramatically increases both aerobic glycolysis and OXPHOS rates, and these results demonstrate high catabolic metabolism on Treg activation. Although the basal metabolic level is generally higher in the activated state, there may also be differences in their preferred energy source. To investigate this, we calculated the basal ECAR to OCR ratio which shows the degree of dependency on aerobic glycolysis as an energy source. A significantly higher ECAR/OCR ratio in stimulated Tregs illustrates that Tregs switch their metabolic preference from OXPHOS to aerobic glycolysis upon stimulation (***Figure 3.2.c***).

Next we wondered if this shift in preference from OXPHOS to aerobic glycolysis was

driven at the transcriptomic level. To examine this, we compared the expression of 768 genes involved in metabolism between unstimulated and stimulated Tregs using the NanoString nCounter Human metabolic pathways panel. Stimulation significantly altered the expression of metabolic gene characteristics upon activation in Tregs (***Figure 3.3a***). As expected most of genes relating to energy metabolism (catabolic process) were upregulated in stimulated Treg, and interestingly genes involved in anabolic pathways such as amino acid and nucleotide synthesis were also upregulated (***Figure 3.3b***). Expression of glycolysis genes including *HK1*, *ALDOA*, *PGK1*, *ENO1* and *LDHA* was significantly higher in stimulated Tregs, suggesting that stimulation skews the Treg transcriptomic signature toward glycolysis (***Figure 3.3c***). Furthermore, a variety of genes relating to mitochondrial respiration were downregulated by stimulation, except for genes including *CS* and *IDH3A* in TCA cycle (***Figure 3.3d***). Thus, the transcriptomic signature of Treg metabolism shifts from OXPHOS to aerobic glycolysis upon activation. Although stimulation downregulates mitochondrial respiratory genes in Tregs, stimulated Tregs possess higher actual OCR than unstimulated cells (***Figure 3.2b***). This result suggests that unstimulated Tregs already express sufficient mitochondrial

respiration genes at baseline to fulfil a high OCR during an activated state. On the other hand, Tregs still upregulate genes involved in pathways to supply the fuels of OXPHOS such as glutamine metabolism and fatty acid oxidation in addition to glycolysis (***Figure 3.3b***).

We concluded that TCR stimulation alongside CD28 co-stimulation dramatically increases the metabolic rate of Treg which are highly dependent on aerobic glycolysis. This dependence on aerobic glycolysis is also seen at the transcriptomic level in the upregulation of glycolysis genes and the down regulation of mitochondrial respiration genes. However, although mitochondrial respiration genes were downregulated at the transcriptomic level, stimulated Tregs actually increase their OXPHOS rate to fulfil their high energy requirements and this is at least partially mediated by upregulating the expression of genes implicated in catabolic pathways such as glutamine and fatty acid oxidation.

3.3 Human CD4 Tconvs have a higher metabolic rate compared to Tregs, although Tregs and Tconvs are dependent on similar energy sources in their activated states.

Whilst Tregs demonstrated a glycolytic phenotype in my preliminary experiments and the results suggest that both Tregs and Tconvs have similar metabolic phenotype, we hypothesised that there may be a difference in the degree to which each depended on glycolysis. To examine this, we isolated Tconvs as $CD4^+$ $CD25^-$ cells and compared their metabolism to Tregs isolated from same donor. We stimulated the isolated Tregs and Tconvs with anti-CD3 and CD28 beads and first examined their glucose uptake rate. The significantly higher glucose uptake rate demonstrated that stimulated Tconvs have a higher glucose consumption rate (***Figure 3.4.a***). In agreement with this, the percentage of Glut1 (glucose transporter 1) positive cells was higher in Tconvs (***Figure 3.4.b***).

To examine the aerobic glycolysis rate of Tconvs, we utilised the Seahorse XF. Higher basal ECAR in stimulated Tconvs indicated that Tconvs have a higher aerobic glycolysis rate compared to Tregs (***Figure 3.5.a***). Next, we questioned if this result indicated that

Tconvs have an increased dependency on aerobic glycolysis compared to Tregs or whether it is an artifact of a high metabolic rate within Tconvs. For this reason, we analysed the OCR of stimulated Tconvs and Tregs by Seahorse XF. Tconvs showed a significantly higher OCR (***Figure 3.4.b***) echoing our ECAR data described above. We therefore conclude that in their active state Tconvs have a higher energy metabolic rate compared to Tregs.

We next investigated the glycolytic reserve and spare respiratory capacity (SRC) of stimulated Tregs and Tconvs. Glycolytic reserve and SRC quantify the spare capacity for cells to respond in situations of acute energy demand by increasing their aerobic glycolysis and respiration. Glycolytic reserve is calculated as the difference between basal ECAR and the highest ECAR value achieved after blocking ATP-linked OXPHOS with oligomycin. Aerobic glycolysis was slightly higher following oligomycin injection in both Tregs and Tconvs (***Figure 3.5.a left***). Although the absolute increase was not significantly different between Tregs and Tconvs, the percentage increase compared to basal state was higher in Tregs, indicating that Tregs have more capacity to increase their aerobic

glycolysis rate in situations of acute energy demand (***Figure 3.5.c***). SRC is calculated as the difference between basal OCR and the highest OCR value achieved after injection of FCCP (trifluoromethoxy carbonylcyanide phenylhydrazone). FCCP is an uncoupler of OXPHOS and interferes with the proton gradient, which induces maximal respiratory capacity. Whilst the absolute SRC value appears higher in Tconvs, the percentage increase is not significantly different between Tregs and Tconvs (***Figure 3.5.b Left and Figure 3.5.d***). Most importantly, the percentage increase of SRC is notably higher than the glycolytic reserve in both Tconvs and Tregs (***Figure 3.5.e***). Therefore, even though the glycolytic reserve is slightly higher in Tregs, OXPHOS is the primary energy source that meets the acute energy demands of both Tconvs and Tregs in activated state.

Stimulated Tconvs have higher rates of both aerobic glycolysis and OXPHOS compared with Tregs. However, there may be differences in their preference towards different energy sources. To investigate this, we calculated the ratio of basal ECAR and OCR. As previously reported, stimulation changed Tconvs metabolic dependency from OXPHOS to aerobic glycolysis (***Figure 3.5.f***). Importantly, the degree of the shift is not different

between stimulated Tregs and Tconvs, revealing that there is no difference in their metabolic preference in their activated state.

Lastly we checked the difference in metabolic gene signatures between stimulated Tregs and Tconvs using the NanoString nCounter human metabolic pathways panel. Some metabolic genes were differentially expressed between Tconvs and Tregs (***Figure 3.6.a Left).*** For example, *GLRX* encoding the glutathione cofactor glutaredoxin which maintains the cellular redox state is highly expressed in Tregs. On the other hand, *PSAT1* encoding phosphoserine aminotransferase and *GART,* encoding trifunctional purine biosynthetic protein 3, were highly expressed in Tconvs. PSAT1 and GART are involved in serine synthesis and purine synthesis, respectively. However, the majority of metabolic genes including glycolysis genes were not differentially expressed between Tregs and Tconvs (***Figure 3.6.a Right***). We observed that stimulated Tconvs and Tregs have similar metabolic genes signature compared to the unstimulated Tregs (***Figure 3.6.b***).

Taken together these data indicate that Tregs and Tconvs have no significant difference

in their metabolic dependencies in their activated states and that both populations naturally reach close to their maximum glycolytic capacity by stimulation and use mainly OXPHOS to meet acute energy demands. Although the metabolic gene signatures were similar between Tregs and Tconvs in their activated state, the actual consumption rates of both glucose and oxygen were significantly higher in Tconvs, revealing that Tconvs have a generally higher metabolic rate than Tregs which is regulated post-transcriptionally.

3.4 Human Tregs require mTOR signalling to increase their metabolism after anti-CD3/CD28 stimulation.

Mechanistic target of rapamycin complex (mTOR) is a serine/threonine kinase involved in TCR signalling pathways. It is well known that the mTOR signalling pathway is key to changing Tconv metabolism toward aerobic glycolysis on activation and that mTOR signalling is required for Tconv function (25, 235, 236). mTOR signalling in Tregs is also vitally important, but complex. Although inhibition of mTOR with rapamycin enhances

Treg suppressive function and hyperactivation of mTOR decreases Treg suppressive function (167, 206, 207), mice studies also demonstrate that Tregs seem to require mTOR signalling to maintain their metabolic homeostasis (219, 237, 238). In these mice studies, Tregs with genetic mTOR signalling disruption have distinct metabolic gene signatures with low ECAR and OCR rates, which translates to a scurfy-like phenotype. However, this metabolic alteration of mice Tregs could be due to perturbations of Treg maturation by disruption of lipid synthesis.

Direct assessment of the metabolic impact of mTOR signalling in activated human Treg has not yet been reported. We demonstrated above that Tregs increase their metabolism on activation in a similar pattern to Tconvs. Here, we will examine if metabolic changes in human Tregs are also triggered by mTOR signalling akin to that seen in Tconvs. To investigate this we used the mTOR inhibitor rapamycin. Freshly-isolated human Tregs were stimulated by anti-CD3/CD28 beads in the presence of 100 nM of rapamycin or 0.05% of vehicle (DMSO) as a control. Firstly we examined the viability of Tregs to check that blocking mTOR signalling did not cause catastrophic

effects in stimulated Tregs. We observed high viability in rapamycin-treated Tregs indicating that rapamycin does not induce cell death in stimulated Tregs (***Figure 3.7.a***).

Next, we investigated how glucose uptake rate is changed by blocking mTOR signalling using 2-NBDG. Rapamycin-treated Tregs showed significantly lower glucose uptake rate compared to control, revealing that enhanced glucose consumption upon stimulation is regulated by mTOR signalling in Tregs (***Figure 3.7.b***). To investigate the actual metabolic rates, we used Seahorse XF. We observed significantly lower ECAR in rapamycin-treated Tregs demonstrating that the high aerobic glycolysis rate in stimulated Tregs is induced by mTOR signalling (***Figure 3.7.c Left***). Furthermore, mTOR signalling is also required to achieve high OXPHOS rate in Tregs upon stimulation (***Figure 3.7.c Right***).

T cells first undergo clonal expansion after stimulation, which is a metabolically intensive process. Because inhibition of mTOR signalling significantly impaired dynamic increase of Treg metabolic rate, we hypothesised that mTOR signalling would be required for Treg proliferation. To examine this, freshly-isolated human Tregs were stained with violet

proliferation dye (VPD) prior to incubation. VPD is cleaved by esterases within viable cells which then becomes fluorescent and binds to protein. VPD-stained proteins are distributed uniformly between daughter cells during proliferation, so one may identify proliferating cells as VPD^{lo} cells and calculate the average number of times an individual cell proliferates as the division index. VPD-stained Tregs were incubated with anti-CD3/CD28 microbeads in the presence or absence of rapamycin. Treg proliferation was dramatically reduced by rapamycin treatment indicating that the TCR-mTOR signalling axis is important for the capacity of Tregs to clonally expand (***Figure 3.7.d***).

Taken together the metabolic switch in human Tregs is triggered by mTOR signalling, which is similar to the previously reported metabolic switch in Tconvs, and the mTOR signalling pathway is also important for Treg clonal expansion following stimulation.

3.5 Human Tregs require glucose during proliferation for anabolic reasons, but not for ATP synthesis.

We have so far demonstrated that human Tregs significantly increase their metabolism via upregulation of aerobic glycolysis after TCR engagement with CD28 co-stimulation through the mTOR signalling pathway. However, we have also showed that stimulated human Tregs also dramatically increases OCR and importantly possess high SRC, indicating that they preferentially use aerobic glycolysis in their activated state even though they have the capacity to generate energy through respiration. The advantage of a high aerobic glycolysis rate is not only that ATP is rapidly generated, but also that high glycolysis flow maintains the large quantity of glycolysis intermediates to fuel cellular anabolic processes (234). For example, the pentose phosphate pathway (PPP) branches upstream of glycolysis initiation and PPP intermediaries are used in nucleotide synthesis. Therefore, we hypothesised that the high glycolysis rate in human stimulated Tregs was not to fulfil their energy demands, but to fulfil their anabolic needs.

Alongside energy, proliferation requires de novo synthesis of macromolecules. Therefore,

proliferating Tregs may have higher glucose demands for biosynthesis. To examine this, freshly-isolated human Tregs were stained with VPD prior to stimulation with anti-CD3/CD28 beads, followed by incubation with 2-NBDG. Proliferating Tregs uniformly showed a high rate of glucose uptake (***Figure 3.8.a and 3.8.b***). My previous experiments demonstrated that stimulated Tconvs showed a higher metabolic rate with dramatically increased glucose metabolism compared with Tregs (***Figure 3.4.a***). Therefore, we wondered if proliferating Tconvs also have a higher glucose consumption rate than Tregs. To investigate this, we examined VPD-stained Tconvs. Like Tregs, proliferating Tconvs uniformly showed high glucose uptake rate (***Figure 3.8.a***). Surprisingly, however, there was no significant difference between the glucose consumption rate of proliferating Tregs and Tconvs, indicating that proliferation equally skews Treg and Tconv metabolic phenotype towards high glucose consumption (***Figure 3.8.b***). Concordant with high glucose uptake, proliferating Tregs also expressed high levels of Glut1 similarly to Tconvs (***Figure 3.8.c***). Thus, proliferation increases the glucose demands of both Tregs and Tconvs, and there is no difference between proliferating Tregs and Tconvs in their glucose consumption rate and the Glut1 expression.

Next, we investigated if Tregs require glucose for their proliferation and if the high glucose demands of proliferating Tregs were due to their anabolic requirements over their energy needs. VPD-stained Tregs were cultured with anti-CD3/CD28 beads in the presence of metabolic inhibitors (2-DG and oligomycin). 2-deoxyribo glucose (2-DG) is a structural glucose analogue which cannot undergo glycolysis and so accumulates within the cell and disrupts upstream glycolysis enzymes such as hexokinase. Although both 2-DG and oligomycin (ATP-linked OXPHOS inhibitor) dramatically reduce cellular metabolism by inhibiting glycolysis and OXPHOS respectively, cellular viability does not decrease significantly indicating that stimulated Tregs can switch their energy metabolism to survive (***Figure 3.9.a***). Whilst the division index (which indicates the average number of times the cells proliferate) of oligomycin-treated Tregs is effectively reduced, it nevertheless demonstrates that they retain some proliferative capacity (***Figure 3.9.b and c***). On the other hand, 2-DG almost completely blocks Treg proliferation, although we found that stimulated Treg possess a high SRC compared to glycolytic reserve to compensate for increased energy demand (***Figure 3.5.e***). These data demonstrate that Tregs require glucose for their proliferation and support the idea that

high glucose consumption in proliferating Tregs is required for anabolic reasons.

To investigate the purpose of high glucose consumption during Treg proliferation directly, VPD-stained Tregs were stimulated with anti-CD3/CD28 and exposed to different glycolysis inhibitors (***Figure 3.9.d***). PFK15 prevents PFKB3 from producing PFK2 (Phosphofructokinase 2) which would normally allosterically activate PFK1 (Phosphofructokinase 1). PFK1 normally functions as a first irreversible glycolysis step downstream of some glycolysis branches including PPP. GSK2837808A and FX11 are lactate dehydrogenase A (LDHA) inhibitors which block the last reaction of aerobic glycolysis. Therefore, LDHA inhibitors selectively inhibit energy metabolism via glycolysis, but maintain the function of other pathways including PPP and the TCA cycle. UK5099 is a mitochondrial pyruvate carrier inhibitor which blocks pyruvate transportation into mitochondria and inhibits glucose energy production from mitochondrial respiration. 6-AN is a PPP inhibitor, which inhibits one of the glucose anabolic pathways which functions to generate nucleotides. In the same way that 2-DG does not significantly impact cellular viability in stimulated Tregs, Tregs exposed to other glucose inhibitors

also maintain their viability except for PFK15 (***Figure 3.9.e***). This may be due to off-target effects of PFK15 or indicate that PFKB3 has other important roles in cell survival. Next, we examined the division index of Tregs treated with glycolysis inhibitors. Although 2-DG clearly blocked Treg proliferation, LDHA inhibitors did not, indicating that ATP synthesis through aerobic glycolysis is easily compensated by OXPHOS (***Figure 3.9.f***). Furthermore, UK5099 did not reduce Treg proliferation strongly. Although we did not simultaneously block aerobic glycolysis and the mitochondrial pyruvate carrier to investigate if Tregs can proliferate under complete lack of energy derived from glucose, these results strongly indicate that glucose is neither required as an energy source in aerobic glycolysis nor mitochondrial respiration to maintain their high proliferation rate. However, 6-AN strongly inhibited Treg proliferation indicating that glucose is an important carbon source for nucleotide production required to maintain their high proliferation rate.

Overall, proliferation increases Treg glucose metabolism and the glucose consumption rate between proliferating Tregs and Tconvs is not distinct. However, inhibiting energy

production from aerobic glycolysis with a LDHA inhibitor does not reduce Treg proliferation rate indicating that ATP synthesis through aerobic glycolysis can be easily compensated for by OXPHOS due to the high SRC of Treg. Moreover, inhibition of glucose usage by UK5099 also did not reduce Treg proliferation. Therefore, the energy production from glucose can easily be compensated. On the other hand, the low glycolytic reserve of Tregs is not able to fully compensate for the high rate of Tregs proliferation when energy production through OXPHOS is inhibited indicating that ATP synthesis through mitochondrial respiration still has a key role in maintaining high energy expenditure during Treg proliferation. However, anabolism fuelled by glycolysis intermediates is absolutely necessary to maintain Treg proliferation. Indeed, inhibition of the PPP dramatically reduces Treg proliferation rate unlike other inhibitors related to energy production by glycolysis. Thus, glucose is required for Treg clonal expansion and one of the main reasons why proliferating Tregs demonstrate such a high glycolysis rate is not to meet their energy requirement, but to maintain the supply to anabolic pathways from glycolysis intermediates.

3.6 Discussion

In this chapter, we have investigated how human Tregs change their metabolism upon TCR stimulation. Although previous studies suggested the concept of 'OXPHOS-dependent metabolism in Tregs', a recent publication revealed that TGF-β (a key cytokine added during Treg differentiation from naïve Tconvs) skews T cell metabolism towards OXPHOS (233, 239). Prior to these studies there had been a lack of data describing Treg metabolism during activation. Our data reveals that human *ex vivo* Treg shift their metabolism toward aerobic glycolysis on activation (***Figure 3.2.c***). Fundamentally, the genetic signature and the preferences of energy metabolism between Tregs and Tconvs are not clearly distinct (***Figure 3.3.b and 3.5.f***).

The shifting dependence toward aerobic glycoslysis does not automatically mean that the OXPHOS rate is downregulated. In the same way that Tconvs also increase their glutaminolysis and OXPHOS rate upon activation (240), the actual OXPHOS rate of Tregs is dramatically increased by stimulation (***Figure 3.2.b***). As oligomycin—an ATP-linked OXPHOS inhibitor—reduces Treg proliferation, energy production through mitochondrial

respiration is clearly still important to meet the high energy demand experienced by Treg during activation, at least during the clonal expansion phase (***Figure 3.9.b***). However, at the genetic level, mitochondrial respiration genes are downregulated by activation in both Tregs and Tconvs (***Figure 3.6.b***) whilst catabolic pathways fuelling OXPHOS, for example glutaminolysis, are upregulated by activation. Therefore, the elevated OXPHOS rate during stimulation is not regulated by mitochondrial respiration genes, but by the cellular processing of OXPHOS fuels. It has been shown that chronic stimulation induces exhaustion with mitochondrial dysfunction in tumour infiltrating lymphocytes (241, 242). Whilst these studies focused on CD8 T cells, my data also demonstrate downregulation of respiration genes after stimulation suggesting that not only CD4 Tconvs but also Tregs may become exhausted by chronic stimulation secondary to mitochondrial dysfunction.

mTOR signalling is a key regulator of Tconvs metabolic change during activation (24, 25, 194). We showed that rapamycin dramatically reduces the metabolic rate within stimulated Tregs indicating that mTOR signalling is key to increasing both aerobic glycolysis and OXPHOS in Tregs after activation (***Figure 3.7.c***). Although in our

experimental setting Treg proliferation was strongly (but not completely) inhibited by rapamycin (***Figure 3.7.d***), the same dose of rapamycin is used in the Treg expansion protocol of cellular therapy products (166). One of the reasons why rapamycin is added in this protocol is that it has been shown to selectively inhibit Tconvs (165, 166). However, in this clinical expansion protocol the ratio of stimulation beads to cells is 20 times higher than in our experiments. Therefore, in Tregs strong TCR signalling seems to compensate for the mTOR signalling blockage induced by this rapamycin dose either by simply overpowering the mTOR inhibition or through signalling via a distinct TCR axis. mTOR exists as two complexes, mTOR complex 1 (mTORC1) and mTOR complex 2 (mTORC2). Both Tregs and Tconvs require glycolysis for cell migration, but glycolysis appears to be maintained by different mTOR complexes between the two populations with Tconvs utilising mTORC1 signalling whilst mTORC2 plays a critical role in Tregs (217, 243). Low-dose rapamycin strongly and specifically inhibits only mTORC1, whilst high-dose rapamycin inhibits both mTORC1 and mTORC2 in cancer cells (244, 245). Although 100 nM of rapamycin can be categorised as a low dose which selectively inhibits mTORC1 in cancer cells, we did not directly prove rapamycin specificity in human Tregs. Therefore,

the disruption of Treg metabolism in our experimental model could be caused by inhibition of both mTOR complexes. In this context, strong TCR stimulation in the clinical expansion protocol may selectively overcome the weaker inhibition of mTORC2 by low dose rapamycin, resulting in a preferential benefit for Tregs over Tconvs.

Metabolic rates are generally higher in stimulated Tconvs than Tregs when they are compared in bulk (***Figure 3.5.a and b***). However, Tregs and Tconvs have a uniformly high glucose consumption rate and Glut1 expression level when they are proliferating (***Figure 3.8.***). A high SRC in Tregs and Tconvs suggests that proliferating T cells can easily compensate for reduced energy production by aerobic glycolysis through enhancing OXPHOS (***Figure 3.5.e***). Indeed, LDHA inhibitors (aerobic glycolysis inhibitors) do not prevent Treg proliferation. However, blocking an anabolic pathway driven by glycolysis intermediates strongly reduces Treg proliferation (***Figure 3.9.f***). Therefore, in the same way that other proliferating cells have a high glycolysis rate to maintain their rapid proliferation (234), Tregs also have high glucose consumption rate to maintain their elevated demand for biosynthesis during clonal expansion.

In this chapter, we conclude that human *ex vivo* Tregs increase their metabolism upon TCR stimulation alongside CD28 co-stimulation via mTOR signalling pathway. Treg metabolism shifts to be more dependent on aerobic glycolysis, which is not distinct from Tconvs. We also found that proliferation equally changes Tregs and Tconvs metabolism with higher glucose needed for cells to meet their anabolic requirements. Therefore, it seems that the phenotype of high aerobic glycolysis is a general feature of T cells in clonal expansion. We investigated Tregs isolated from human blood in bulk throughout this chapter. However, T cells in peripheral circulation can be divided into three subtypes: naïve, central memory (CM) and effector memory (EM) according to their phenotype. After stimulation, naïve and CM T cells first undergo clonal expansion in lymphoid organs, whilst EM T cells immediately start functioning in tissue. As Tregs require glucose to proliferate, we assume that naïve and CM Tregs will show high glycolytic dependency. However, the metabolism of EM Tregs remains poorly defined. In chapter 4, we will investigate the metabolism of Tregs across different subsets and consider the relationship between Treg function and metabolism.

3.7 Figures and legends

Figure 3.1

(a)

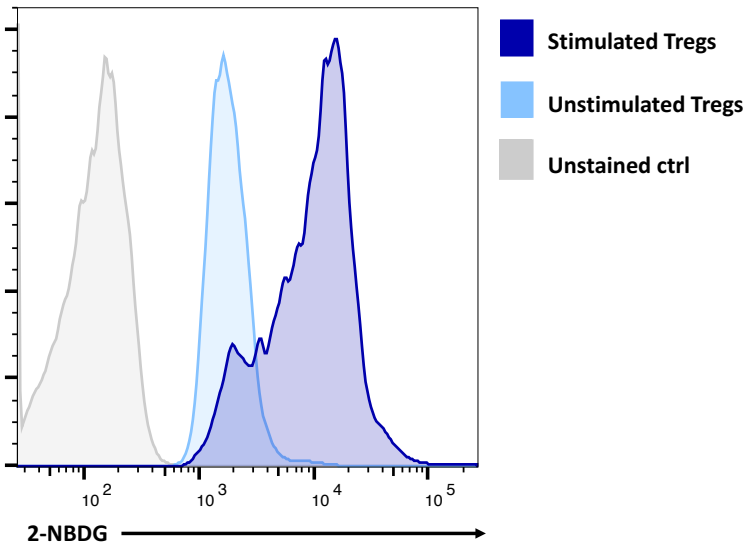

(b)

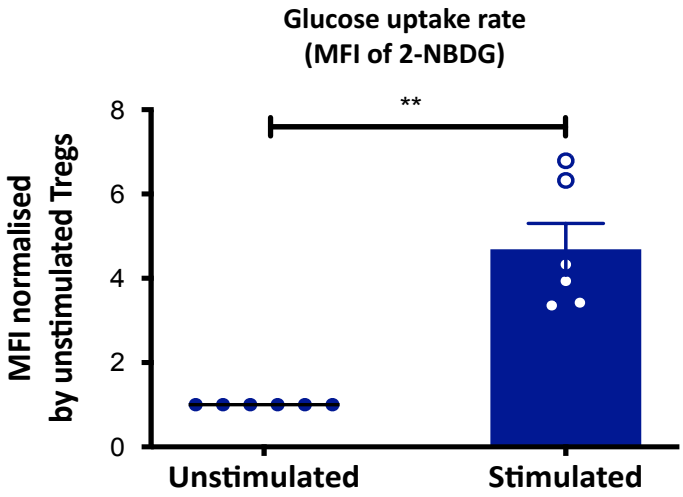

Figure 3.1. Human *ex vivo* Tregs dramatically increase their glucose uptake rate upon activation.

Freshly isolated human Tregs from healthy donors (*ex vivo* Tregs) were incubated for 60h with or without anti-CD3/CD28 beads, followed by 20 min incubation with the fluorescently labelled glucose analogue 2-NBDG to determine glucose uptake rate of unstimulated and stimulated Tregs. (a) a representative histogram from 6 independent donors. (b) A graph of mean fluorescent intensity (MFI) of 2-NBDG. The values of stimulated Tregs are normalised by unstimulated Tregs from the same donor. Each dot represents an individual donor. Columns represent mean ± SD. **p<0.01, by paired t test.

Figure 3.2

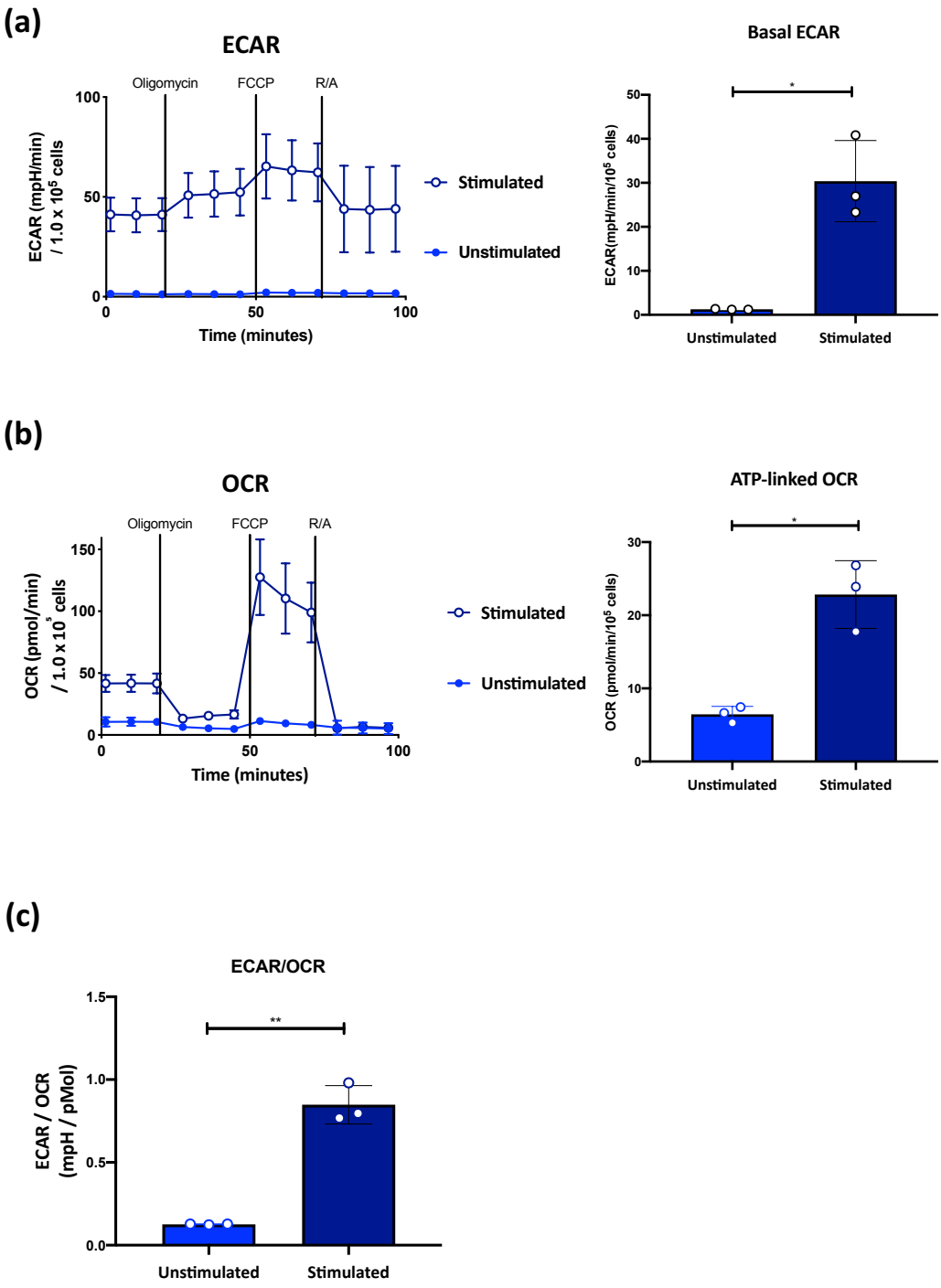
(a)
ECAR
Oligomycin
FCCP
R/A
ECAR (mpH/min) / 1.0 x 10^5 cells
Time (minutes)
Stimulated
Unstimulated
Basal ECAR
ECAR(mpH/min/10^5 cells)
Unstimulated
Stimulated
(b)
OCR
OCR (pmol/min) / 1.0 x 10^5 cells
ATP-linked OCR
OCR (pmol/min/10^5 cells)
(c)
ECAR/OCR
ECAR / OCR (mpH / pMol)

Figure 3.2. Human ex vivo Tregs switch their metabolism from OXPHOS to aerobic glycolysis on activation.

Metabolic measurement flux using Seahorse XF Mito stress test. Human *ex vivo* Tregs were applied into the Seahorse XFe either directly after sorting (unstimulated) or after 60h stimulation with anti-CD3/CD28 beads. (a) Left, a representative Extracellular acidification rate (ECAR) figure from 3 independent donors. Right, a graph of initial ECAR values indicating basic ECAR. (b) Left, a representative OCR (oxygen consumption rate) figure from 3 independent donors. Right, a graph of ATP-linked OCR. ATP-linked OCR is calculated as the difference between initial OCR (basal OCR) and the lowest OCR values achieved after oligomycin injection. (c) Ratio of basal ECAR and basal OCR, indicating aerobic glycolysis dependency. R/A indicates rotenone + antimycin A. Each dot represents an individual donor. Columns represent mean ± SD. *$p<0.05$, **$p<0.01$, by paired t test.

Figure 3.3

(a)

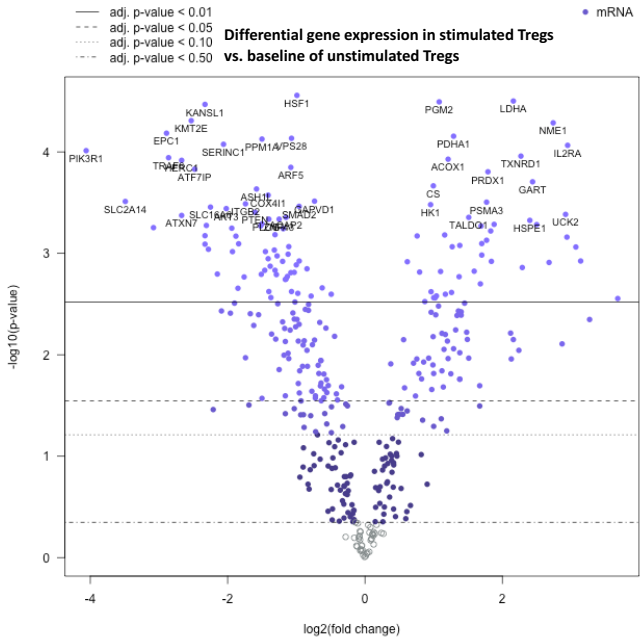
adj. p-value < 0.01
adj. p-value < 0.05
adj. p-value < 0.10
adj. p-value < 0.50
mRNA
Differential gene expression in stimulated Tregs
vs. baseline of unstimulated Tregs
HSF1
KANSL1
KMT2E
EPC1
SERINC1
PPM1A
PSS28
PIK3R1
ATF7IP
ARF5
SLC2A14
ATXN7
PGM2
LDHA
NME1
PDHA1
IL2RA
ACOX1
TXNRD1
PRDX1
GART
CS
HK1
PSMA3
TALDO1
HSPE1
UCK2
-log10(p-value)
log2(fold change)

(b)

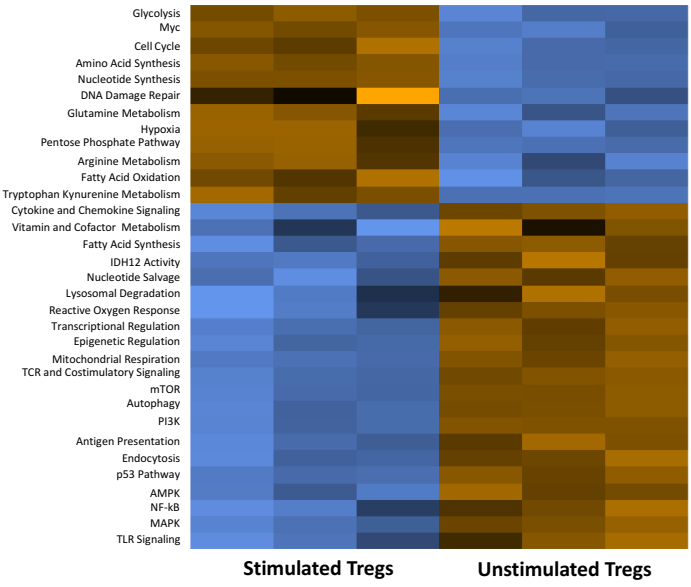
Glycolysis
Myc
Cell Cycle
Amino Acid Synthesis
Nucleotide Synthesis
DNA Damage Repair
Glutamine Metabolism
Hypoxia
Pentose Phosphate Pathway
Arginine Metabolism
Fatty Acid Oxidation
Tryptophan Kynurenine Metabolism
Cytokine and Chemokine Signaling
Vitamin and Cofactor Metabolism
Fatty Acid Synthesis
IDH12 Activity
Nucleotide Salvage
Lysosomal Degradation
Reactive Oxygen Response
Transcriptional Regulation
Epigenetic Regulation
Mitochondrial Respiration
TCR and Costimulatory Signaling
mTOR
Autophagy
PI3K
Antigen Presentation
Endocytosis
p53 Pathway
AMPK
NF-kB
MAPK
TLR Signaling
Stimulated Tregs
Unstimulated Tregs

Figure 3.3 (cont.)

(c)

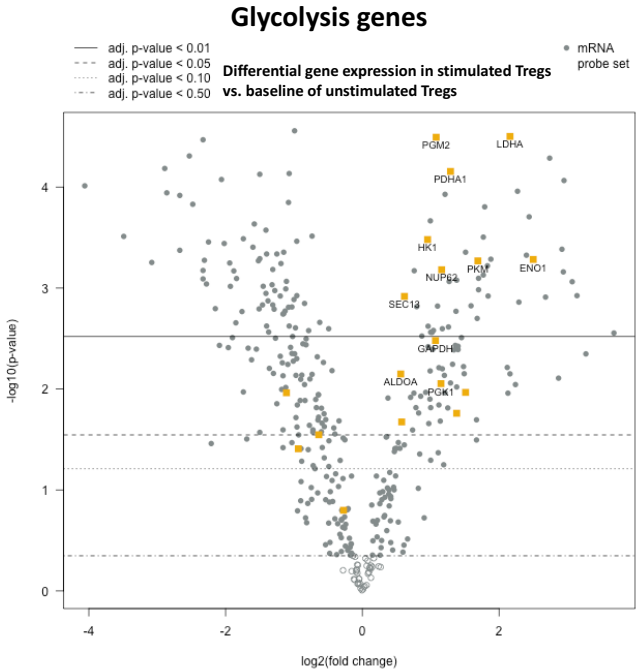

(d)

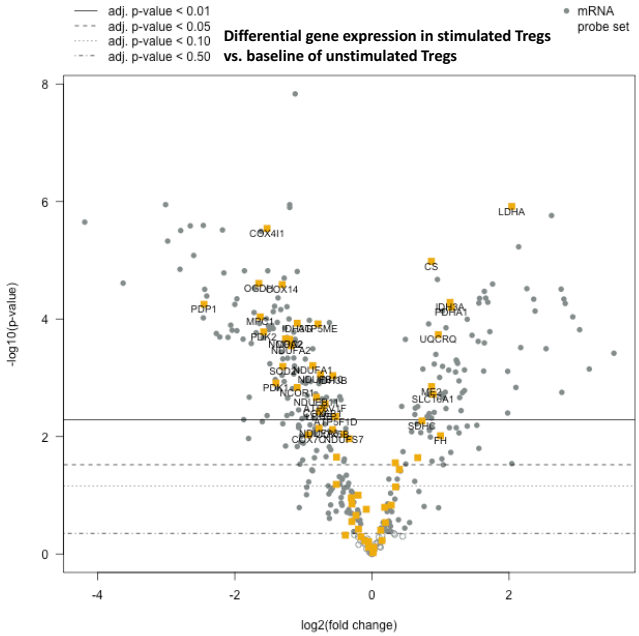

Figure 3.3. Stimulation increases glycolysis genes and downregulate mitochondrial respiration genes in *ex vivo* Tregs.

NanoString nCounter Sprint gene expression analysis using Human Metabolic Pathways panel. RNA was isolated from human *ex vivo* Tregs either directly after sorting (unstimulated) or after 40h stimulation with anti-CD3/28 beads. (a) A volcano plot revealing the most differentially expressed genes, relative to a baseline of unstimulated Tregs. (b) A heatmap revealing the differentially expressed specific groups of metabolic genes. (c) A volcano plot revealing the most differentially expressed glycolysis genes, highlighted in orange. (d) A volcano plot revealing the most differentially expressed mitochondrial respiration genes, highlighted in orange.

Figure 3.4

(a)

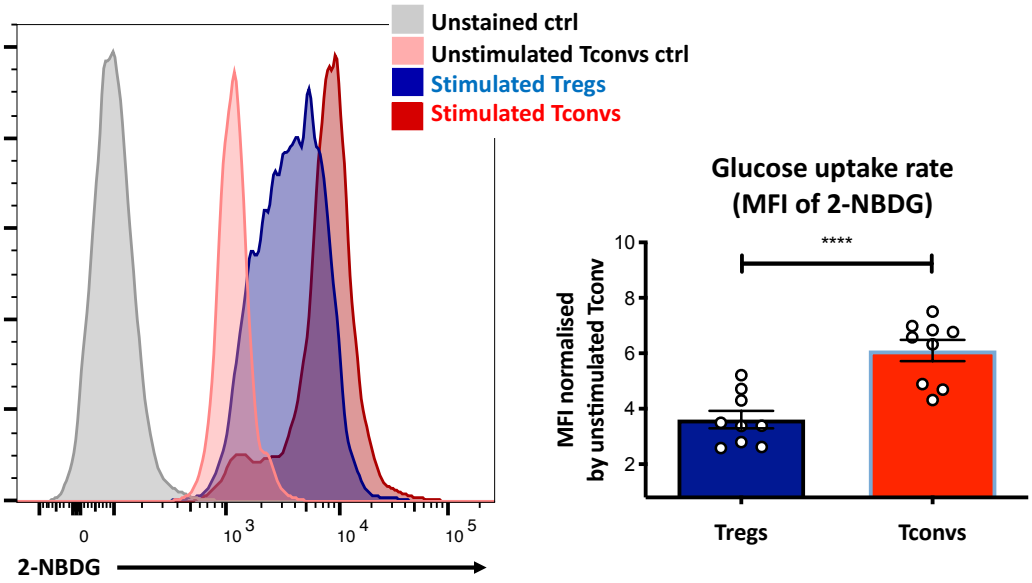
Unstained ctrl
Unstimulated Tconvs ctrl
Stimulated Tregs
Stimulated Tconvs
0
10 3
10 4
10 5
2-NBDG
Glucose uptake rate
(MFI of 2-NBDG)
****
MFI normalised
by unstimulated Tconv
10
8
6
4
2
Tregs
Tconvs

(b)

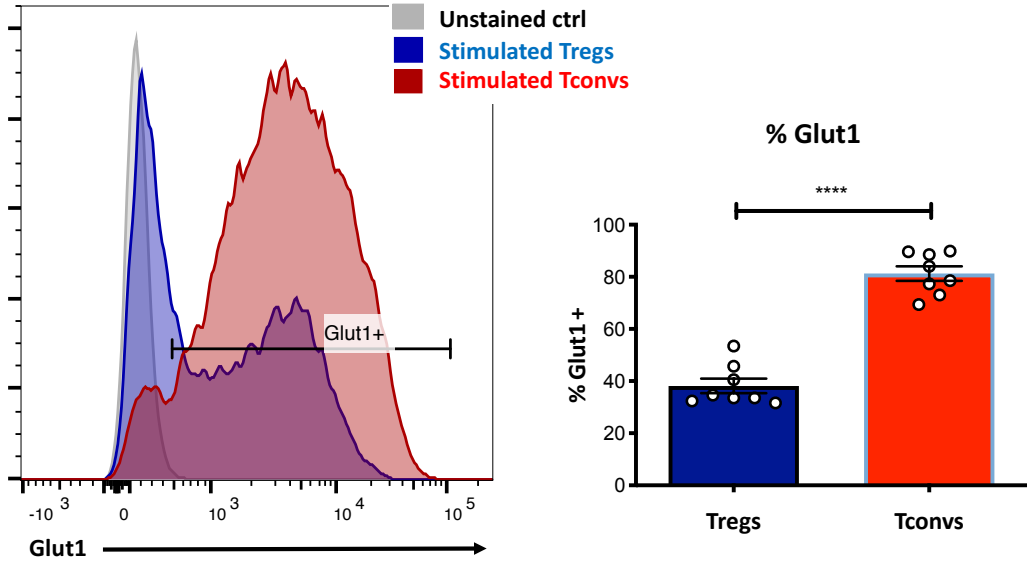
Unstained ctrl
Stimulated Tregs
Stimulated Tconvs
Glut1+
-10 3
0
10 3
10 4
10 5
Glut1
% Glut1
****
% Glut1 +
100
80
60
40
20
0
Tregs
Tconvs

Figure 3.4. Stimulated CD4 Tconvs have a higher rate of glucose uptake and Glut1 expression than Tregs.

Freshly isolated $CD4^+$ $CD25^-$ T cells (Tconvs) and Tregs were incubated for 60h in the presence of anti-CD3/CD28 beads. (a) Glucose uptake rate data. Left, a representative histogram from 9 independent donors. Right, a graph of MFI. Values were normalised with unstimulated Tconvs from the same donor. (b) Glut 1 expression data. Left, a representative histogram from 6 independent donors. Right, a graph of % Glut1+ cells. Each dot represents an individual donor. Columns represent mean ± SD. ****$p<0.0001$ by paired t test.

Figure 3.5

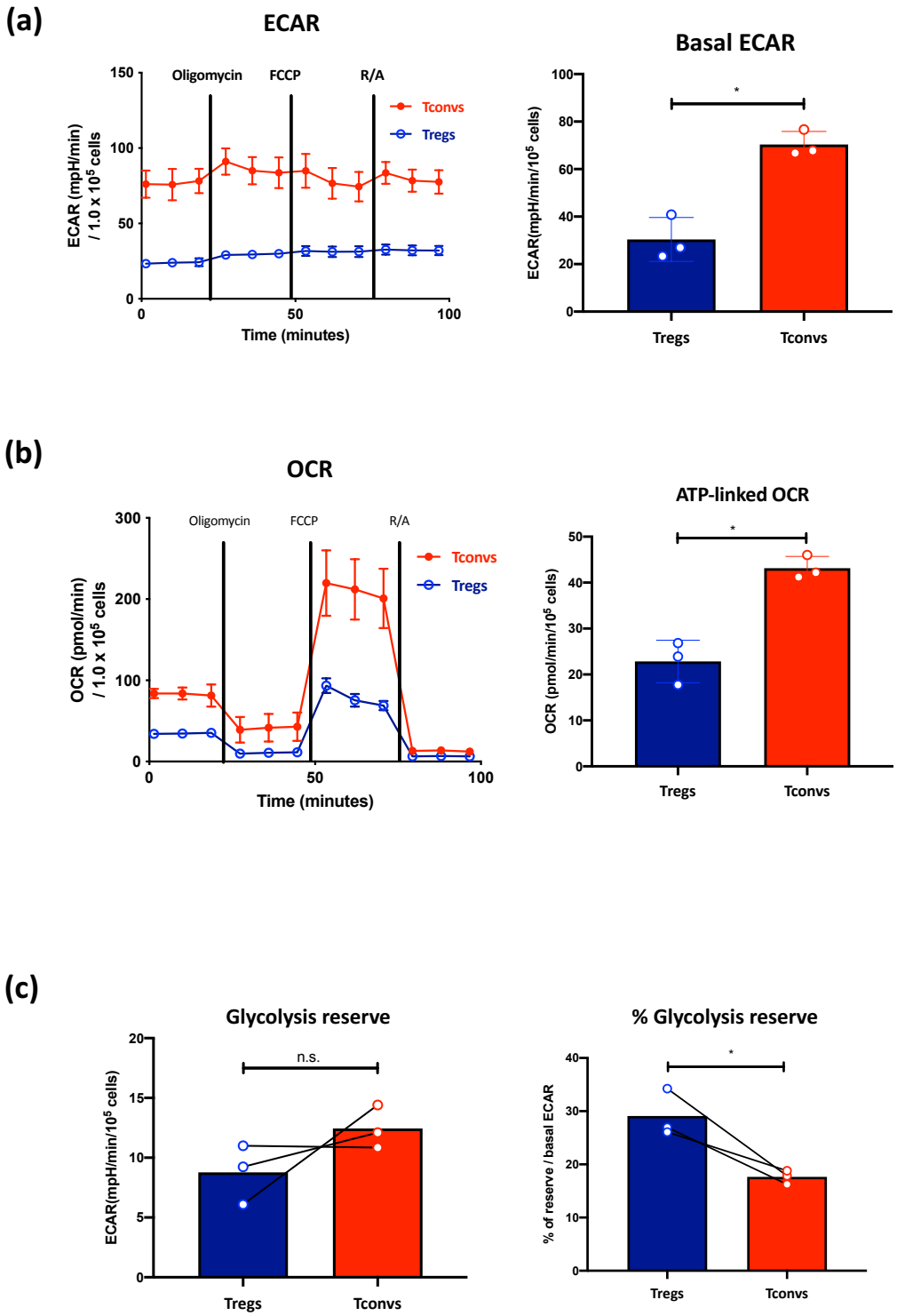
(a)
ECAR
Oligomycin
FCCP
R/A
Tconvs
Tregs
ECAR (mpH/min) / 1.0 x 10^5 cells
Time (minutes)
Basal ECAR
ECAR(mpH/min/10^5 cells)
Tregs
Tconvs
(b)
OCR
OCR (pmol/min) / 1.0 x 10^5 cells
ATP-linked OCR
OCR (pmol/min/10^5 cells)
(c)
Glycolysis reserve
n.s.
ECAR(mpH/min/10^5 cells)
% Glycolysis reserve
% of reserve / basal ECAR

Figure 3.5 (cont.)

(d)

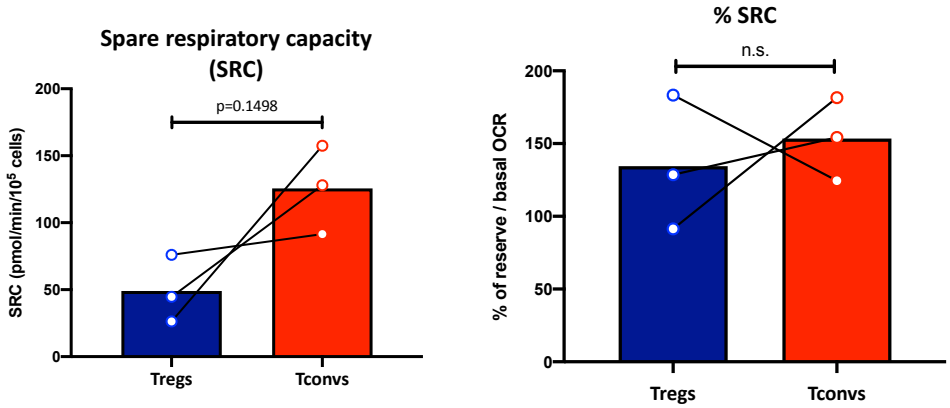

(e)

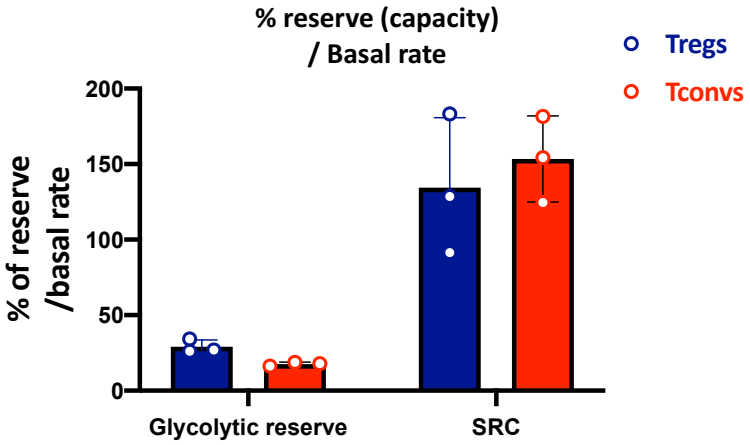

(f)

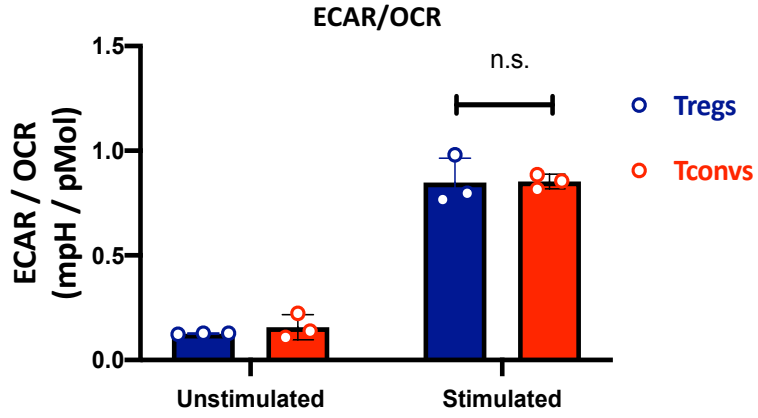

Figure 3.5. Activated Tconvs have a higher metabolic rate in both aerobic glycolysis and mitochondrial respiration, although activated Tregs and Tconvs have similar characteristics in energy fuels dependency.

Metabolic measurement flux using Seahorse XF Mito stress test. Human *ex vivo* Tregs and Tconvs were applied into the Seahorse XFe after 60h stimulation with anti-CD3/CD28 beads. (a) Left, representative ECAR figure from 3 independent donors. Right, A graph of basal ECAR. (b) Left, a representative OCR figure from 3 independent donors. Right, a graph of ATP-linked OCR. ATP-linked OCR is calculated as the difference between basal OCR and the lowest OCR values achieved after oligomycin injection. (c) Left, a graph of glycolysis reserve. Glycolysis reserve is calculated as the difference between basal ECAR and the highest ECAR value achieved after oligomycin injection. Right, the percentage increase of glycolysis reserve based on basal ECAR. (d) Left, A graph of spare respiratory capacity (SRC). SRC is calculated as the difference between basal OCR and the highest OCR value achieved after FCCP injection. Right, the percentage increase of SRC based on basal OCR. (d) Ratio of basal ECAR and basal OCR, indicating aerobic glycolysis dependency. Unstimulated Tregs and Tconvs values were obtained by the same method

as activated cells, but without 60h stimulation. Columns represent mean ± SD, dots represent individual blood donors. *p<0.05, by paired t test.

Figure 3.6

(a)

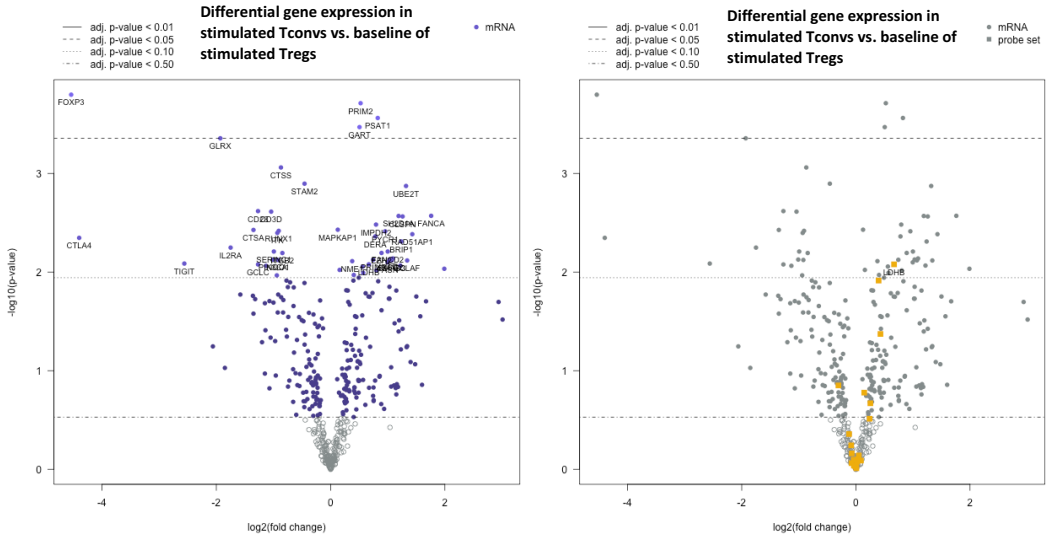
Glycolysis genes
Differential gene expression in stimulated Tconvs vs. baseline of stimulated Tregs
adj. p-value < 0.01
adj. p-value < 0.05
adj. p-value < 0.10
adj. p-value < 0.50
mRNA
probe set
-log10(p-value)
log2(fold change)
FOXP3
PRIM2
PSAT1
GART
GLRX
CTSS
STAM2
UBE2T
CTLA4
IL2RA
TIGIT
MAPKAP1
LDHB

(b)

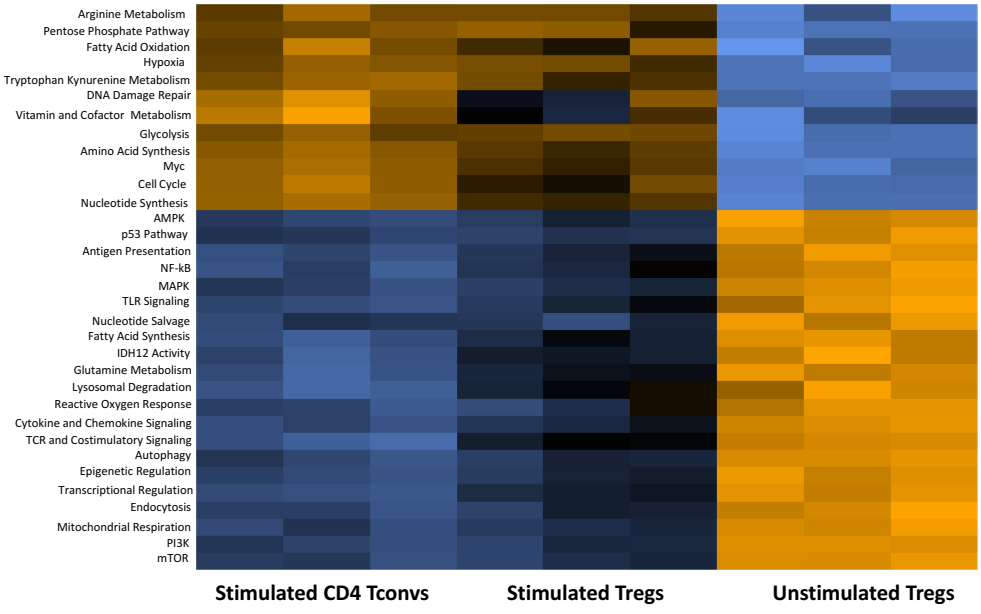
Arginine Metabolism
Pentose Phosphate Pathway
Fatty Acid Oxidation
Hypoxia
Tryptophan Kynurenine Metabolism
DNA Damage Repair
Vitamin and Cofactor Metabolism
Glycolysis
Amino Acid Synthesis
Myc
Cell Cycle
Nucleotide Synthesis
AMPK
p53 Pathway
Antigen Presentation
NF-kB
MAPK
TLR Signaling
Nucleotide Salvage
Fatty Acid Synthesis
IDH12 Activity
Glutamine Metabolism
Lysosomal Degradation
Reactive Oxygen Response
Cytokine and Chemokine Signaling
TCR and Costimulatory Signaling
Autophagy
Epigenetic Regulation
Transcriptional Regulation
Endocytosis
Mitochondrial Respiration
PI3K
mTOR
Stimulated CD4 Tconvs
Stimulated Tregs
Unstimulated Tregs

Figure 3.6. Human Tregs and Tconvs have a similar metabolic genes signature after activation.

Nanostring nCounter Sprint gene expression analysis using Human Metabolic Pathways panel. RNA was isolated from human *ex vivo* Tregs and Tconvs after 40h stimulation with anti-CD3/28 beads. (a) Left, a volcano plot revealing the most differentially expressed genes relative to Treg baseline. Right, a volcano plot revealing the most differentially expressed glycolysis genes, highlighted in orange. (b) A heatmap revealing the differentially expressed specific groups of metabolic genes comparing stimulated Tconvs, stimulated Tregs and unstimulated Tregs from which RNA was isolated directly after sorting.

Figure 3.7

(a)

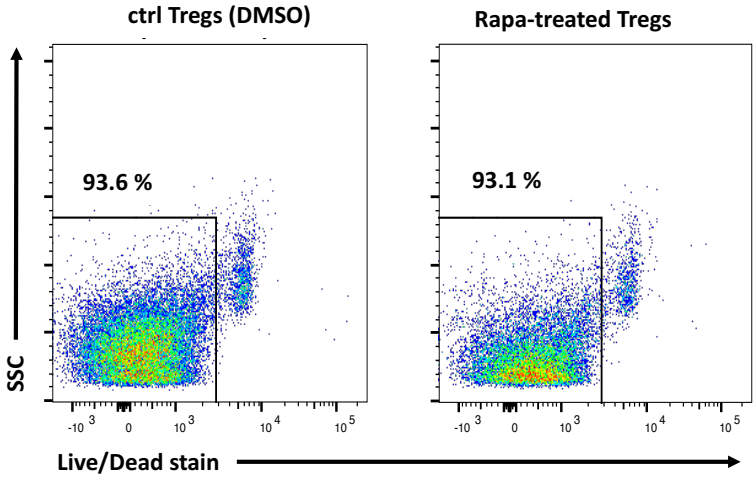

(b)

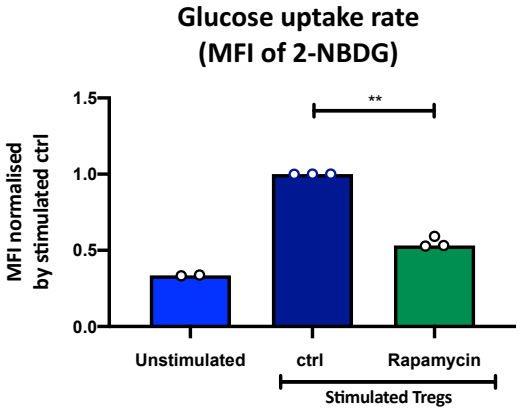

(c)

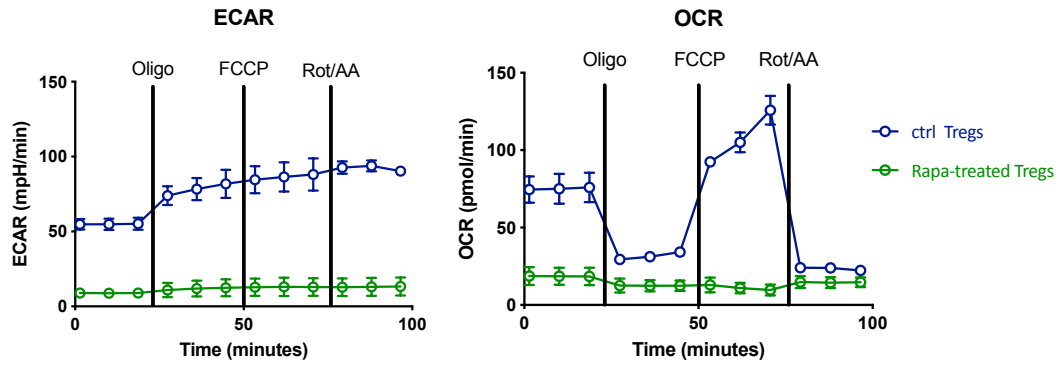

(d)

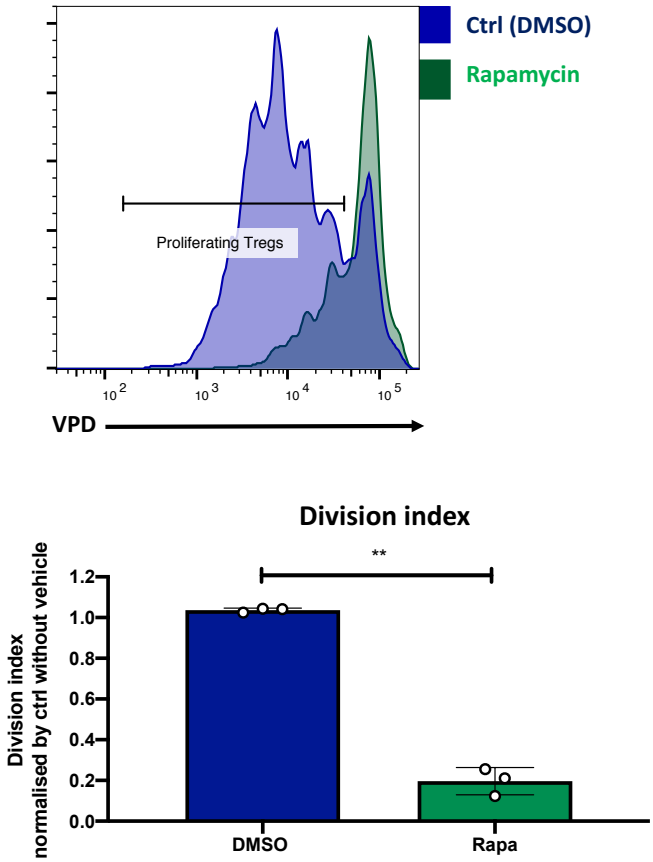
Ctrl (DMSO)
Rapamycin
Proliferating Tregs
10^2
10^3
10^4
10^5
VPD
Division index
**
Division index normalised by ctrl without vehicle
1.2
1.0
0.8
0.6
0.4
0.2
0.0
DMSO
Rapa

Figure 3.7. Human Tregs require mTOR signalling to increase their metabolism after anti-CD3/CD28 stimulation.

Freshly isolated Tregs were stimulated by anti-CD3/CD28 beads for 60h in the presence of 100 nM rapamycin (Rapa-treated Tregs) or 0.05% of DMSO (ctrl). (a) A representative FACS plot from 3 independent donors, revealing viability of cells after 60h incubation. (b) 2-NBDG glucose uptake ratio. The values were normalised by stimulated control Tregs from same donor. Unstimulated Tregs were incubated under the same conditions as control Tregs but without bead stimulation. (c) Metabolic measurement flux using the Seahorse XF Mito stress test. Left, a representative ECAR. Right, a representative OCR from 2 independent donors. (d) Freshly isolated Tregs were first stained by violet proliferation dye (VPD) prior to stimulation with anti-CD3/CD28 beads for 84h in the presence of 100 nM rapamycin or DMSO (DMSO control). Top, a representative histogram from 3 independent donors. Bottom, a graph of division index indicating the average number of cell divisions in each condition. The values of are normalised to control without vehicle. Columns represent mean ± SD. *p<0.05, **p<0.01, ***p<0.001 ****p<0.0001 by paired t test.

Figure 3.8

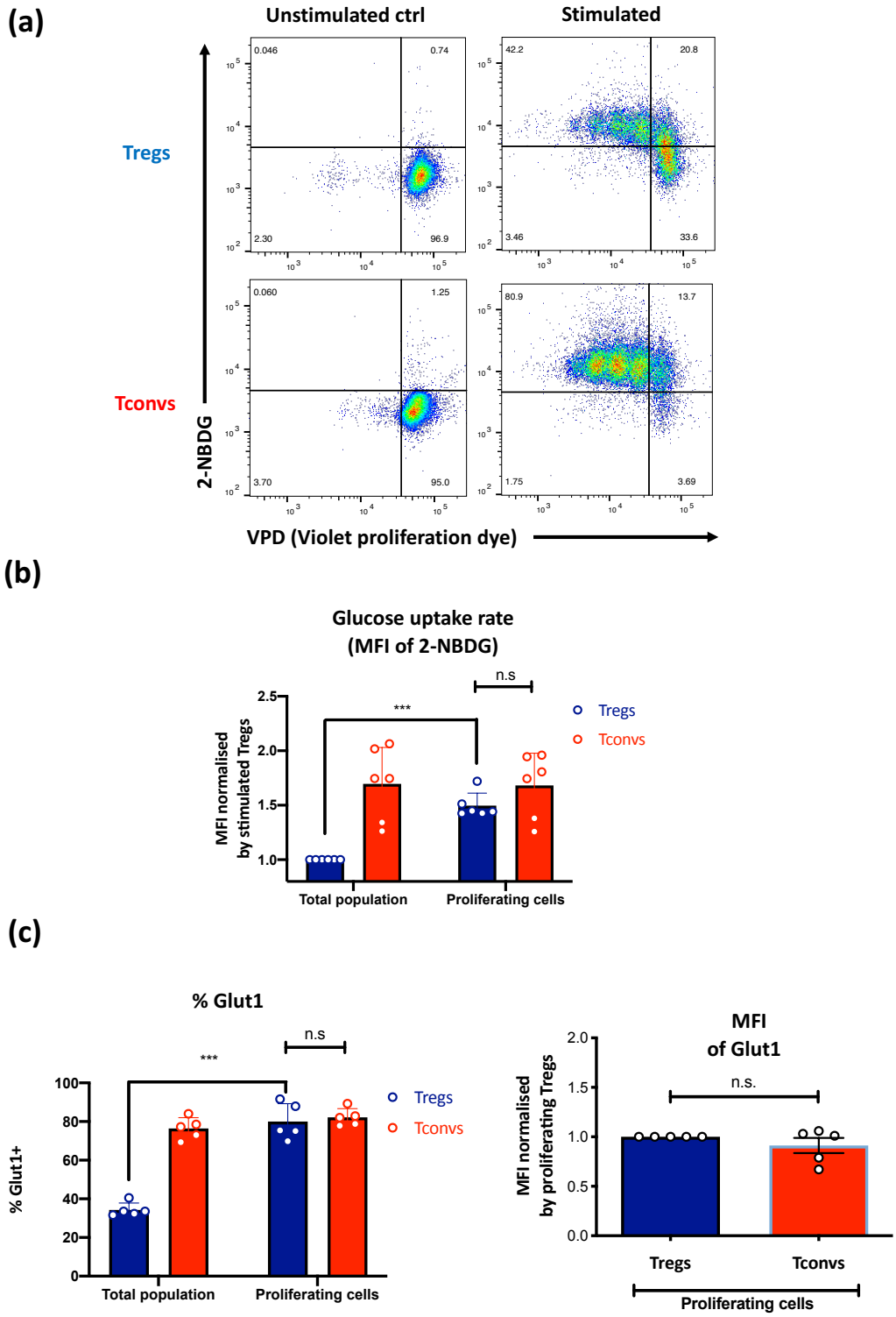
(a)
Unstimulated ctrl
Stimulated
Tregs
Tconvs
2-NBDG
VPD (Violet proliferation dye)
0.046
0.74
2.30
96.9
42.2
20.8
3.46
33.6
0.060
1.25
3.70
95.0
80.9
13.7
1.75
3.69
(b)
Glucose uptake rate
(MFI of 2-NBDG)
MFI normalised
by stimulated Tregs
n.s
***
Tregs
Tconvs
Total population
Proliferating cells
(c)
% Glut1
% Glut1+
n.s
***
Tregs
Tconvs
Total population
Proliferating cells
MFI
of Glut1
MFI normalised
by proliferating Tregs
n.s.
Tregs
Tconvs
Proliferating cells

Figure 3.8. Tregs and Tconvs increase their glucose metabolism rate during proliferation.

Freshly isolated Tregs and Tconvs were first stained by violet proliferation dye (VPD) prior to stimulation with anti-CD3/CD28 beads for 60h. (a) A representative FACS plot from 6 independent donors, revealing VPD^{lo} cells have high 2-NBDG signal. Unstimulated controls were incubated under the same conditions but without beads. (b) A graph comparing the glucose uptake rate between the total population and VPD^{lo} population (representing proliferating cells). (c) Glut1 expression data. Each dot represents an individual donor. Columns represents mean ± SD. *p<0.05, **p<0.01, ***p<0.001 ****p<0.0001 by paired t test.

Figure 3.9

(a)

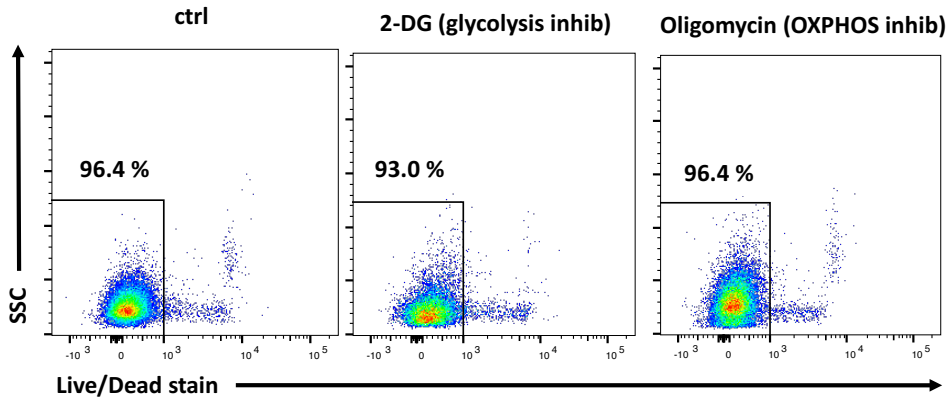

(b)

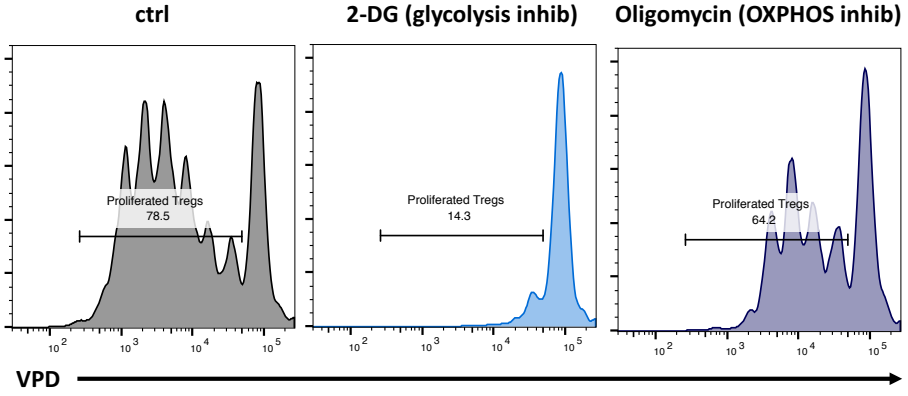

(c)

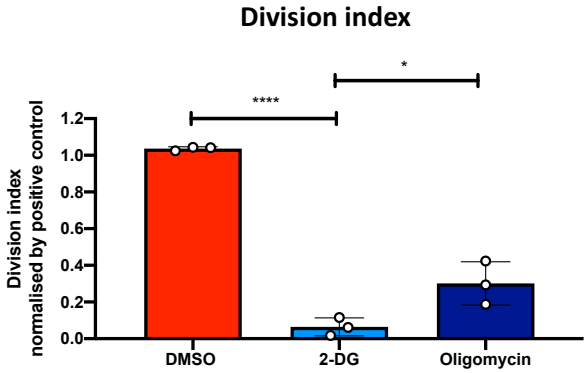

Figure 3.9 (cont.)

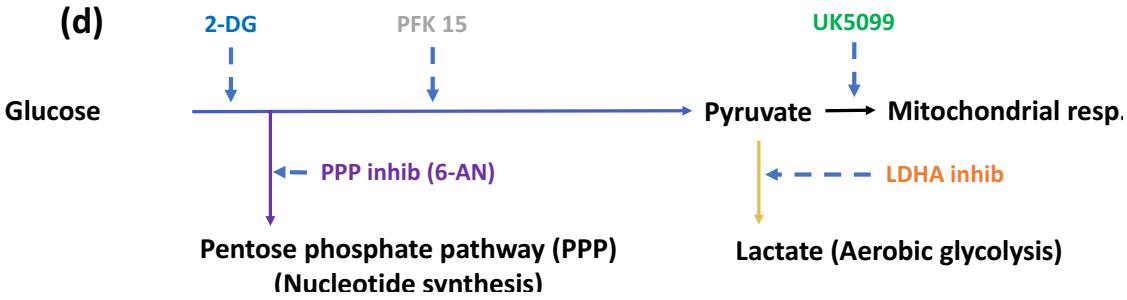

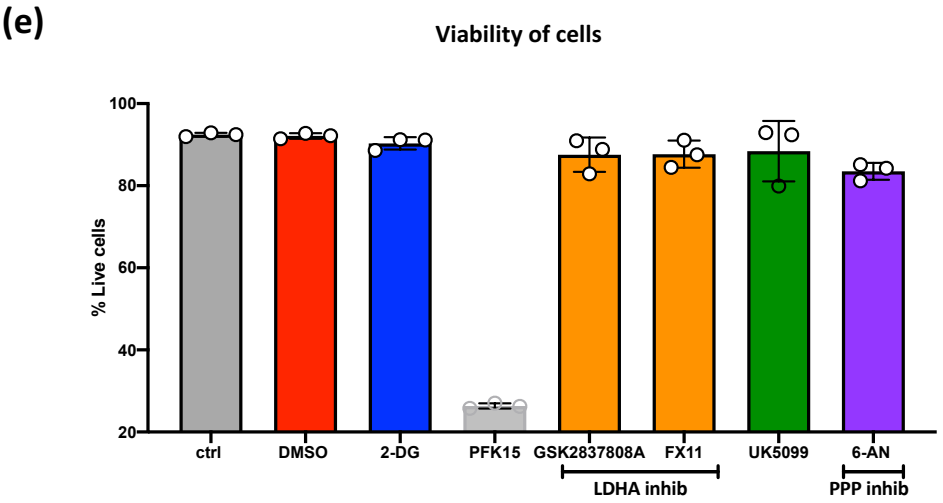

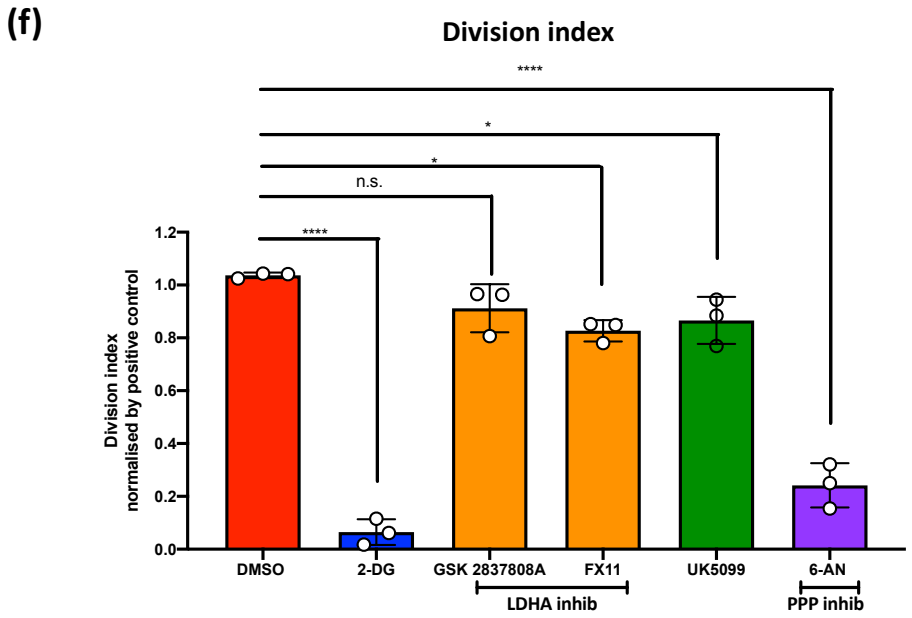

Figure 3.9. Tregs require glucose during proliferation for anabolic reasons, but not for the energy.

VPD-stained *ex vivo* Tregs were incubated for 86h with anti-CD3/CD28 beads in the presence of inhibitors. (a,b,c) Incubation with energy metabolism inhibitors: 2mM 2-DG (a glycolysis inhibitor), 0.2µM Oligomcyin (an OXPHOS inhibitor), 0.02% DMSO control or without an inhibitor (control). (a) A representative FACS plot from 3 independent donors, revealing viability of cells after 86h incubation in the presence of inhibitors. (b) A representative histogram from independent donors, revealing the percentage of proliferated cells. (c) A graph of division index indicating the average number of cell divisions in each condition. (d,e,f) Incubation with glycolysis inhibitors: 2mM 2-DG, 10µM PFK15, 20µM GSK 2837808A, 25µM FX11, 10µM UK5099, 5µM 6-AN, 0.2% DMSO and without inhibitor (control). (d) A schematic summarising the target of inhibitors. (e) A graph revealing the viability of cells. (f) A graph of division index. Columns represent mean ± SD. *p<0.05, **p<0.01, ***p<0.001 ****p<0.0001 by one-way ANOVA.

Chapter 4: Characteristics of human naïve, central memory and effector memory CD4 T cells metabolism

4.1 Introduction

In *chapter 3*, We examined the metabolism of bulk Tregs and Tconvs in human peripheral blood. However, T cells in circulation are heterogeneous and consist of two distinct populations based on their experience of antigen exposure: naïve T cells, which have not encountered their cognate antigen; and memory T cells, which are generated during the primary antigen encounter and retain the ability to respond immediately if the same antigen is subsequently re-encountered (246). Memory T cells can also be divided into two subsets according to their location: central memory (CM), which reside in secondary lymphoid organs (SLO) alongside naïve T cells; and effector memory (EM), which continuously circulate between blood and peripheral tissues. Whilst both naïve and CM T cells undergo clonal expansion after stimulation in secondary lymphoid organs, EM T cells immediately exhibit powerful effector functions in the peripheral tissues (246, 247). Our research presented in *chapter 3* revealed that human *ex vivo* Tregs change their

metabolism towards aerobic glycolysis on stimulation, and that glycolysis is fundamentally required for their clonal expansion. However, whether Tregs require aerobic glycolysis for their suppressive function in a similar fashion to Tconvs is not completely known (27, 198). In fact, several studies demonstrated that glycolysis negatively correlates with Treg suppressive function (28, 206, 215). As my study of Treg metabolism in previous chapter was undertaken with bulk Tregs, it is likely that the results were skewed by particular Treg subpopulations (naïve and CM versus EM) undergoing differential clonal expansion due to their differential proliferative glucose requirements. Therefore, revealing the metabolism of EM subsets of Tconvs and Tregs which are both characterised by their rapid and vigorous activation, will reveal new insight in Treg immunometabolism and will begin to reveal the relationship between Treg function and metabolism.

CD8 memory T cells have been widely studied. CD8 T cells distal to antigen presenting cells (APCs) are more likely to differentiate into a memory phenotype rather than effector cells due to lower TCR and mTOR signalling activity (248-250). Memory CD8 T

cells are metabolically distinct from their effector counterparts due to their reduced aerobic glycolysis and enhanced mitochondrial metabolism (250-252). Interestingly, direct inhibition of glycolysis by 2-DG increases memory differentiation (253). Although the enhanced mitochondrial metabolism in memory T cells relies on fatty acid oxidation (FAO), FAO inhibition itself does not perturb memory cell formation (254-256). Instead, the dynamic mitochondrial state between fission and fusion seems to be the key determinant of memory T cell formation (256). Mitochondrial fragmentation from dynamin-related protein 1 (Drp1)-dependent fission increases glycolysis and induces an effector phenotype in CD8 T cells. Moreover, both pharmacological inhibition of fission and promotion of fusion increases memory T cell formation. Thus, the mitochondrial state following primary antigen encounter determines the memory or effector fate of T cells.

However, the majority of CD8 memory T cells studies have focused on the CM subset. The formation of the EM subset may have a different mechanism. Human CAR CD8 T cells containing the CD137 signalling domain have an enhanced mitochondrial

biogenesis with high FAO reliance, whilst CAR T cells containing the CD28 signalling domain have a higher rate of aerobic glycolysis rate with lower mitochondrial biogenesis (257). Importantly, CAR T cells with high mitochondrial biogenesis have a more CM phenotype, whilst an EM phenotype is more common in the case of low mitochondrial biogenesis. In agreement with this finding, enforced aerobic glycolysis in T cells with a low OXPHOS rate through HIF activation demonstrate a high proportion of EM CD8 T cell formation (258). Taken together, during memory T cell formation, CM and EM generation have different metabolic processes. Whilst inhibition of aerobic glycolysis and mitochondrial biogenesis are important for CM T cell formation, aerobic glycolysis enhances the production of EM T cells. However, it remains unknown what the key factor determining the fate of T cells into either short-lived effector T cells or EM T cells is, both of which prefer aerobic glycolysis during differentiation.

Although there is accumulating evidence for the importance of mitochondrial biogenesis and, to a lesser extent glycolytic characterisation during CM differentiation of CD8 T cells, the metabolism of CM T cells following second antigen exposure should not be assumed

to be identical. As proliferating cells generally require Drp1-dependent mitochondrial fission, which induces aerobic glycolysis dependent metabolism (259), CM T cells may also show an aerobic glycolysis-dependent phenotype for proliferation on subsequent antigen exposure. Indeed, both CM and EM CD8 T cells equally enhance aerobic glycolysis upon activation (260). Interestingly, in contrast to naïve T cells the aerobic glycolytic switch in both CM and EM CD8 T cells occurs immediately after activation, which may indicate that the rapid response of memory T cells on re-exposure are underpinned by similarly rapid metabolic adaptation.

Compared to CD8 T cells, memory subsets of CD4 T cells are less well studied due to the technical difficulties of isolating them including their lower proliferation potential and the diversity of the Th subsets (e.g. Th1, Th17 and Tregs) (247, 261). In particular, the diversity of CD4 T cell subsets makes it difficult to reveal the nature of CM and EM differentiation. For example, a weak TCR signal seems to induce a CM phenotype in CD4 T cells (247), recapitulating CD8 CM formation following weak TCR and mTOR signalling; however, other studies have demonstrated that weak TCR signalling and mTOR inhibition

induces Tregs from naïve Tconvs (262-264). Although the precise relationship between mitochondrial dynamics and CD4 T cell memory formation has not yet been established, EM and CM CD4 T cells do have different metabolic characteristics. Whilst CM CD4 T cells have lower viability and reduced proliferative capacity upon stimulation under hypoxic conditions, EM CD4 T cells both maintain their viability and function and may even enhance their proliferative capacity under hypoxia (265, 266). Whilst EM Tconvs are insensitive to OXPHOS inhibition due to hypoxia, aerobic glycolysis seems to be key to maintaining their effector function (27, 198). Thus, even though the metabolic conditions required for memory CD4 generation remain unclear, EM CD4 T cells appear more dependent on aerobic glycolysis compared to the CM subset.

The study of memory Tregs is even more challenging than Tconvs. Because of their specificity for self-antigen which is constitutively expressed *in vivo*, it is difficult to differentiate Tregs as short-lived effectors (recently activated cells) or long-lived memory cells (persistent cells without antigens) (267). Nevertheless, several mice studies have focussed on memory Tregs. For example, using a genetically-modified inducible self-

antigen mouse model, it is possible to observe both Treg accumulation within tissue following induction, and enhanced Treg suppressive capacity on second antigen induction (268). Maternal-foetal tolerance has also been associated with the presence of memory Tregs in peripheral blood. During a first pregnancy, foetal-specific maternal Tregs expand and form a memory subtype, which prevents foetal resorption during a second pregnancy (269). Importantly, circulating maternal Tregs are also significantly expanded during a pregnancy in adoptively transferred mice, which directly proves the existence of memory Tregs at a systemic level.

Human Tregs in peripheral circulation consist of two phenotypically different subsets based on their expression of CD45RA (known as a naïve Tconv marker), CD25 and FOXP3: the $CD45RA^{+}$ $CD25^{lo}$ $FOXP3^{lo}$ 'resting' Treg subset and the $CD45RA^{-}$ $CD25^{hi}$ $FOXP3^{hi}$ 'activated' Treg subset (79). Resting $CD45RA^{+}$ Tregs highly express CD31 which indicates recent emigration from thymus. Resting Tregs switch expression of CD45RA to CD45RO upon stimulation; as people age, the proportion of 'resting' Tregs decrease, whilst the proportion of $CD45RA^{-}$ 'activated 'Treg increase (79, 270, 271). The fact that 'resting'

Tregs are recently emigrated from the thymus which then transition to a separate 'activated' subset upon stimulation suggests that CD45RA^{+} Tregs are the counterpart of naïve Tconvs. Although it is technically difficult to distinguish recently activated Tregs and long-lived memory Tregs within human CD45RA^{-} Tregs from blood, it is more natural to consider that the majority of CD45RA^{-} cells in healthy adult blood are memory Tregs, as the number of naïve Tregs reduces and converts into CD45RA^{-} cells over time.

CM and EM CD4 Tconvs can be defined by expression of surface markers required for migration to SLO: CD62L^{+} CCR7^{+} distinguishes CM Tconv from their CD62L^{-} CCR7^{-} EM Tconv counterpart (246, 247). CD62L is a cell adhesion molecule that interacts with its ligands expressed by high endothelial venules (HEV) in SLO whilst CCR7 is a chemokine receptor that recognises the CCL19 and CCL21 produced in SLO. Similarly, mice memory Tregs also comprise CM and EM subsets; and CCR7 also has a key role in Tregs ability to home to SLO as Tregs without CCR7 migrate directly to peripheral tissue (272, 273). Therefore, the expression of CCR7 may be used to separate human memory Tregs into a CM subset, which reside in SLO, and a EM subset, which directly migrate to tissues.

Human Tregs in peripheral circulation dramatically change their metabolism toward aerobic glycolysis upon activation and we demonstrated that aerobic glycolysis is required for Treg clonal expansion (*Chapter 3*). However, others have demonstrated that glycolysis negatively influences Treg suppressive function, which may suggest that human Tregs have different metabolic demands during their clonal expansion and functional phases. On the other hand, glycolysis is a still key metabolic pathway to maintain Tconv effector function. Moreover, the EM subset of Tconvs is highly dependent on glycolysis compared to their naïve and CM counterparts. Therefore, we hypothesised that Tregs and Tconvs have differ in their metabolism during the effector phase.

4.1.1 Chapter aim

The aim of this chapter is to investigate differences between human *ex vivo* Treg metabolism within naïve, CM and EM subsets and to investigate whether EM Treg metabolism differs from their Tconv counterpart. The results of this chapter provide the

background to exploring the relationship between Tregs metabolism and function and possible clinical translation strategies in *chapter 5*.

4.2 CCR7 divides human memory Tregs into two population with CCR7$^-$ memory Tregs having effector memory properties.

CD62L and CCR7 surface markers are classically used to distinguish CM and EM subsets within Tconvs, as both CD62L and CCR7 are required for Tconvs to reside in SLO (274, 275). Therefore, we first investigated whether we can use CD62L and CCR7 expression levels by FACS to distinguish distinct subsets of human *ex vivo* memory Tregs. Surprisingly CD62L was highly expressed uniformly across FOXP3$^+$ Tregs (***Figure 4.1.a***). In contrast, CCR7 expression varied across FOXP3$^+$ cells and correlated with CD45RA expression. Importantly, the expression level of CCR7 was also different amongst the CD45RA$^-$ population, indicating that memory Tregs comprise different populations based on their CCR7 expression level. Because FOXP3 is an intracellular protein it cannot be used as a marker for cell sorting, and we therefore sorted Tregs using surface markers

CD25 and CD127. We next confirmed whether CCR7 can classify distinct populations of memory Tregs defined as CD45RA$^-$ CD25$^+$ CD127$^{lo/-}$ cells. As observed within FOXP3$^+$ cells, most memory Tregs expressed CD62L, whilst CCR7 clearly differentiated two distinct populations (***Figure 4.1.b Left***). Because CCR7 has a key role in Treg migratory capacity to SLO, we hypothesised that CCR7$^+$ (and CD62L$^+$) Tregs have a CM-like property which facilitate migration to SLO, whilst CCR7$^-$ (but CD62L$^+$) Tregs would migrate directly to the peripheral tissue (272, 273). On the other hand, memory CD4 Tconvs have three population defined as CD62L$^+$ CCR7$^+$ (CM Tconvs), CD62L$^-$ CCR7$^+$, or CD62L$^-$ CCR7$^-$ (EM Tconvs) (***Figure 4.1.b Right***) (246, 247). Thus, most of the CCR7$^-$ population is comprised of EM Tconvs. These results indicated that we can use CCR7 as a marker to sort two distinct Treg memory subsets and also to sort EM CD4 Tconvs as CD45RA$^-$ CCR7$^-$ cells from memory Tconvs.

Next we checked the phenotype of CD45RA$^+$ CCR7$^+$ (naïve), CD45RA$^-$ CCR7$^+$ (CM) and CD45RA$^-$ CCR7$^-$ (EM) Tregs. Although all three subsets maintain the expression of FOXP3, the expression level varied, with highest level shown by EM Tregs (***Figure 4.2.a***). *FOXP3*

is the master Treg gene and controls Treg suppressive functions (12, 13, 276). Similar to FOXP3 expression level, EM Tregs also expressed the highest level of CD25 (***Figure 4.2.b***). CD39 is another important mechanism of Treg immunosuppression (135). CD39 is an ectonucleotidase which converts ATP and ADP into cAMP, which is then further converted by CD73 (another cell surface ectonucleotidase) into adenosine, which inhibits effector cells. Unexpectedly, most naïve Treg do not express CD39, whilst the majority of EM Tregs do (***Figure 4.2.c***). These data indicate that EM Tregs have the highest immunosuppressive function compared to other subsets.

To examine the suppressive function of EM Treg directly, we ran an *in vitro* suppression assay in which VPD-stained PBMC were co-incubated with Tregs or CD4 Tconvs (as a control) in the presence of anti-CD3/CD28 beads. As expected, co-incubation with CD4 Tconvs did not suppress proliferation of T cells, whilst all Treg subsets suppressed proliferation of both CD4 (***Figure 4.2.d***) and CD8 T cells (***Figure 4.2.e***). Although the suppression between EM and CM Tregs was not clearly different, EM Tregs were Tregs with the highest suppressive function.

Lastly, we examined the proliferation capacity of EM Tregs as a hallmark of the EM subset is their reduced expansion potential. Concordantly, naïve Tregs proliferated robustly whilst EM Tregs proliferation was strongly diminished, having the lowest expansion potential amongst all Tregs subsets (***Figure 4.2.f***).

Taken together, CD45RA and CCR7 divide human *ex vivo* Tregs into three subsets: $CD45RA^{+}$ $CCR7^{+}$, $CD45RA^{-}$ $CCR7^{+}$ and $CD45RA^{-}$ $CCR7^{-}$ Tregs. As CCR7 has a key role in the migration of Treg to SLO, $CD45RA^{-}$ $CCR7^{-}$ Tregs may represent a subset that continuously circulates between blood and peripheral tissues. Phenotypically, $CD45RA^{-}$ $CCR7^{-}$ Tregs have the highest suppressive and the lowest proliferation capacities. Due to technical limitations, however, we cannot assess the behaviour of human $CD45RA^{-}$ $CCR7^{-}$ Tregs *in vivo*; however, our *in vitro* data strongly suggest that $CD45RA^{-}$ $CCR7^{-}$ Tregs have an EM-like property which is defined by a lower proliferation capacity, a strong effector capacity, and an ability to migrate to peripheral tissues (246, 277). Although memory Tconvs have three subsets based on CD62L and CCR7 expression, most of the $CCR7^{-}$ population is comprised of EM Tconv ($CD62L^{-}CCR7^{-}$). Therefore, we concluded that CCR7 can divide

Tregs into CM and EM subsets like $CD4^+$ Tconvs, and that sorting memory Tregs and Tconvs based on CCR7 expression was a reasonable strategy to facilitate investigation of EM Treg and EM Tconv immunometabolism.

4.3 EM Tregs have a lower glucose consumption rate than other Treg subsets.

Investigation of bulk Tregs demonstrated an increased glucose uptake rate upon activation, that proliferating Tregs uniformly required a high amount of glucose, and that a large Treg population maintained a low glucose consumption rate within non-proliferating cells (***Figure 3.8.a Top***). Because proliferation capacity is extremely low in EM Tregs ($CD45RA^-$ $CCR7^-$ Tregs) (***Figure 4.2.f***), we hypothesised that the non-proliferating Tregs with low glucose uptake rate represented EM Tregs. Prior to examining the Treg subsets directly, we first investigated if CCR7 expression correlates with the level of glucose uptake rate amongst activated bulk Tregs using 2-NBDG. 2-NBDG and CCR7 co-staining demonstrated two distinct populations in activated bulk

Tregs: 2-NBDG^{hi} CCR7^{+} Tregs and 2-NBDG^{lo} CCR7^{-} Tregs (***Figure 4.3.a***). This indicated that CCR7 partitions activated Tregs into two populations which consume different levels of glucose: CCR7^{+} Tregs which have a high glucose consumption rate, and CCR7^{-} Tregs which have a low glucose consumption rate. We then examined directly whether these Treg subsets (naïve, CM and EM Tregs) had different glucose uptake rates by sorting the subsets prior to stimulation. As expected, EM Tregs showed a dramatically lower glucose uptake rate (***Figure 4.3.b***). Thus, naïve and CM Tregs expressing CCR7 robustly increase their glucose uptake rate upon activation, whilst EM Tregs do not.

Next, we investigated whether the three activated Tregs subsets were also different at the transcriptional level using the NanoString nCounter Human Metabolic Pathways panel. Transcriptionally, naïve and EM Tregs were significantly different (***Figure 4.4.a***). Genes relating to chemokine signalling, autophagy and the reactive oxygen species response were highly expressed in EM Tregs (***Figure 4.4.b***). For example, EM Tregs highly expressed *CXCR6* which ligand CXCL16 plays an important role in the migration of cells into peripheral tissues including liver, airway, colon, and certain tumours, highlighting

the tissue-migration potential of EM Tregs (278-281). However, most of the metabolic genes were more highly expressed in naïve Tregs (***Figure 4.4.b***). As naïve Tregs uptake more glucose, glycolysis genes including *HK2*, *PKM* and *LDHA* were highly expressed within the naïve subset (***Figure 4.4.c Left***). This supports a high proliferation rate of naïve Tregs mirrored by a high expression of cell cycle genes (***Figure 4.4.c Right***). Although both glucose uptake rate and glycolysis genes were highly expressed in naïve Tregs, *SLC2A8*, which encodes the glucose transporter 8 (Glut 8), was expressed more in EM Tregs (***Figure 4.4.a***). Glut 8 has been demonstrated to transport trehalose (disaccharide) which induces cellular autophagy (282), which is paralleled by a higher expression of autophagy genes in the EM Treg subset (***Figure 4.4.d***).

Whilst this comparison of naïve Tregs and EM Tregs demonstrated clear differences in metabolic genes expression, there were no significant differences between the CM and EM Treg subsets (***Figure 4.5.a***). This indicates that metabolic genes expression is not necessarily different amongst all memory Tregs subsets. However, whilst there were no statistically significant differences (N = 3 independent donors), the expression level of

certain genes between CM and EM Tregs did appear to vary. For example, the chemokine receptor *CXCR6* was highly expressed in EM Tregs, which may explain the different migration pattern of EM Treg to peripheral tissues compared to CM Treg migration to SLO. Importantly, the majority of genes with high fold change in CM Tregs were involved in cell cycle, whilst expression levels of genes associated with glycolysis was not distinguishable (***Figure 4.5.b***). Therefore, the higher proliferation rate in CM Tregs was supported transcriptionally, but the different glucose uptake rate between CM and EM Tregs is likely determined by post-transcriptional mechanisms.

Taken together, CCR7 expression level differentiates two subsets of activated human Tregs based on their glucose consumption rate: high glucose demanding $CCR7^+$ Tregs and low glucose demanding $CCR7^-$ Tregs. In agreement with this, activated EM Tregs characterised as $CD45RA^-$ $CCR7^-$ Tregs have the lowest glucose consumption rate amongst the Tregs subsets. Naïve and EM Tregs have a distinct metabolic genetic signature, whilst CM Tregs and EM Tregs do not. Therefore, the observed differences in metabolic genes signature between naïve and EM Tregs is driven by differences between

the naïve and memory subsets. Nevertheless, CM Tregs consume more glucose than EM Tregs which indicates that the regulation of glucose metabolism is controlled post-transcriptionally in memory Tregs.

4.4 EM Tregs but not naïve and CM Tregs show low glucose consumption compared to their Tconvs counterparts. However, the different rates of glucose metabolism between EM Tregs and EM Tconvs are controlled post-transcriptionally.

We showed that EM Tregs are the Treg subset with the lowest glucose requirement, whilst others have demonstrated that EM Tconvs are more dependent on glycolysis (265, 266). Therefore, we hypothesised that Tregs and Tconvs may show a different metabolic signature between EM subsets. To investigate this, we first isolated naïve, CM and EM Tconvs as $CD45RA^{+}$ $CCR7^{+}$, $CD45RA^{-}$ $CCR7^{-}$ and $CD45RA^{-}$ $CCR7^{-}$ cells together with their Tregs counterparts and compared the glucose uptake rate after stimulation. As expected, EM Tconvs demonstrated a notably higher glucose consumption rate compared to EM

Tregs (***Figure 4.6.a***). We observed no difference between proliferating Tconvs and Tregs in glucose uptake rate (***Figure 3.8.b***), and therefore a comparison of Tconvs and Tregs within naïve and CM subsets also did not demonstrate a significant difference (***Figure 4.6.b***). These data indicate that both Tregs and Tconvs similarly require glucose in SLO for clonal expansion, but that they have distinct glucose demands in peripheral tissues.

Next we investigated transcriptional differences between EM Tregs and Tconvs using the NanoString nCounter Human Metabolic Pathways panel. Compared to our earlier molecular investigation of bulk Tregs and Tconvs (***Figure 3.6.a***), more genes were differentially expressed amongst EM subsets indicating that EM subsets of Tregs and Tconvs do indeed have a distinct molecular signature (***Figure 4.7.a***). However, glycolysis genes were not differentially expressed between EM Tregs and EM Tconvs, despite their distinct glucose uptake rates. This indicates that their different glucose metabolism rates are due to post-transcriptional regulation (***Figure 4.7.b Left***).

Because autophagy genes were highly expressed in EM Tregs compared to naïve Tregs,

we next compared the expression of autophagy genes between EM Tregs and EM Tconvs. However, these genes were not differentially expressed between EM Tregs and EM Tconvs (***Figure 4.7.b***).

We next compared the expression of genes involved in mitochondrial respiration, noting differential expression between EM Tregs and EM Tconvs (***Figure 4.7.c***). Interestingly four out of five significant differentially-expressed mitochondrial respiration genes in EM Tregs were related to pyruvate metabolism. *SLC16A1* and *SLC16A3* encode monocarboxylate transporter 1 (MCT1) and monocarboxylate transporter 4 (MCT4), respectively. MCT1 and MCT4 exhibit proton-coupled symport of monocarboxylic acids including lactate (224, 283). MCT1 is associated with the import of lactate, whilst MCT4 is associated with its export. Thus, pyruvate derived from glycolysis is converted into lactate which is then exported through MCT4, whilst extracellular lactate is transported into cells through MCT1 and converted into pyruvate for metabolic use. EM Tregs demonstrate elevated expression of *MCT1* and *MCT4*, and *MCT1* in particular. This indicates that lactate transport is more tightly regulated in EM Tregs with a possible

preference in lactate import. Similarly, *PDP1* and *PDK1* are highly expressed in EM Tregs. *PDP1* and *PDK1* encode pyruvate dehydrogenase phosphatase (PDP) and pyruvate dehydrogenase kinase (PDK), respectively. PDP activates and PDK inhibits the pyruvate dehydrogenase complex (PDC) which converts pyruvate into acetyl-CoA which enters the TCA cycle. Thus, this transcriptomic study indicates that the fate of pyruvate derived from glycolysis or extracellular lactate is tightly regulated in EM Tregs compared with EM Tconvs.

NCOA2 encodes the transcriptional coactivator Nuclear receptor coactivator 2 (NCoA-2, also known as a steroid receptor coactivator-2). *NCOA2* expression was slightly but significantly upregulated in EM Tregs (***Figure 4.7.c***). Interestingly the expression level of NCOA2 in EM Tregs was also higher when compared to naïve and CM Tregs (***Figure 4.4.a and 4.5.a***). Therefore, elevated expression levels of *NCOA2* is unique to the EM Treg subset. NCoA-2 is known to limit fatty acid oxidation and reduces energy expenditure in adipose tissues and skeletal muscles (284, 285). However, the importance of NCoA-2 in Tregs is still unknown. Our data reveals that the expression level of fatty acid oxidation

associated genes is not significantly different between EM Tregs and EM Tconvs indicating that the transcriptional inhibition of fatty acids oxidation by NCoA-2 in EM Tregs is not significant (***Figure 4.7.d***).

We conclude that the glucose demand of Tregs and Tconvs is equally high amongst their naïve and CM subsets, but that there are interesting differences between Treg and Tconv EM subsets. EM Tconvs maintain high glucose demand, whilst EM Tregs do not. A high glucose uptake rate in EM Tconvs is not due to increased expression of glycolysis genes which indicates that their different glucose consumption rates are regulated by post-transcriptional mechanisms. Although EM Tconvs use more glucose, EM Tregs highly express genes of proteins regulating PDC activity and those of intra- and extra-cellular lactate transportation indicating that the regulation of the amount of pyruvate and acetyl-CoA is more tightly regulated in EM Tregs compared with EM Tconvs.

4.5 EM Tregs have high mitochondrial mass with low metabolic rate, whilst EM Tconvs have mitochondrial mass high and low populations with high metabolic rate.

We revealed that EM Tregs have a dramatically lower glucose demand compared with EM Tconvs. Nevertheless, EM Tregs still highly express genes responsible for the regulation of pyruvate-Acetyl CoA conversion and expression of lactate transporters. This indicates that EM Tregs require tight regulation of pyruvate for TCA cycle in mitochondria. CD8 EM T cells are known to demonstrate low mitochondrial biogenesis (257, 258) and we therefore hypothesised whether EM Tregs and CD4 EM Tconvs may have a different mitochondrial state. First we investigated the mitochondrial membrane potential (MMP) of Tregs and Tconvs using the MITO-ID membrane potential detection kit. The MITO-ID membrane potential detection kit regent is a dual-emission dye fluorescing either green or orange which can be detected by FACS. The green monomer accumulates on the mitochondrial membrane; with altered membrane potential this changes colour to orange. MMP is produced by the proton gradient across the mitochondrial inner membrane which result from mitochondrial activity including ATP

synthesis. We freshly isolated PBMCs from healthy donors and examined the MMP of Tregs and Tconvs, distinguishing between CM and EM subsets by staining for CD45RA and CCR7. Whilst Tconvs gradually lost the high Mito-orange population from naïve to EM, all subset of Tregs uniformly maintained the high Mito-orange population. This indicates that Tregs can maintain their mitochondria with high MMP even within the EM subset (***Figure 4.8.a***). Surprisingly, memory Tconvs demonstrated two distinct populations by skewing to double Mito-Orange^{lo} Mito-Green^{lo}, which was more noticeable within the EM population (***Figure 4.8.a and b***). This suggests that the loss of the high MMP population within memory Tconvs may not simply be due to reduced MMP but may instead be due to a reduced MITO-ID signal itself, which could be caused by a low number of mitochondria (***Figure 4.8.b***). Incubation with FCCP, which is known to interfere with the proton gradient, reduced only the Mito-Orange signal but not the Mito-green signal in EM Tregs, supporting this idea that double Mito-Orange^{lo} Mito-Green^{lo} cells in Tconvs are cells with a low quantity of mitochondria (***Figure 4.8.c***).

These MITO-ID experiments revealed two distinct MITO-ID^{hi} and MITO-ID^{lo} populations

in EM Tconvs; however, the MITO-ID green monomer is not specifically located in mitochondria and may remain in the cytosol. Therefore, we next used MitoTracker dyes which localise specifically to mitochondria. MitoTracker Green FM is a green-fluorescent mitochondrial stain which is used to detect mitochondrial mass, whilst MitoTracker Deep Red FM is a membrane potential-dependent probe equivalent to the MITO-ID orange described in the last experiment (286, 287). Co-staining of MitoTracker green FM and MitoTracker Deep Red FM revealed cells in three populations: MitoTracker^{hi} (Mito hi), MitoTracker^{lo} (Mito lo) and MitoTracker Deep Red^{lo} but MitoTracker Green^{hi} (MMP^{lo}). MMP^{lo} cells maintain a high mitochondrial mass but lose their membrane potential indicating early apoptosis of these cells. As we observed in the MITO-ID experiment, all subsets of Tregs maintain a high number of MitoTracker^{hi} cells whilst the memory subsets of Tconvs, especially EM Tconvs, have two distinct MitoTracker^{hi} and Mitotracker^{lo} populations (***Figure 4.8.d and e***). This indicates that in memory Tconvs (especially EM Tconvs) there is a distinct population with a low quantity of mitochondria.

EM Tregs and EM Tconvs demonstrated interesting differences in their glucose uptake

rates; however, we also revealed that EM Tconvs are comprised of a mixture of cells either with a high quantity of mitochondria (Mito^{hi}), comparably to EM Tregs, and a low quantity of mitochondria (Mito^{lo}). We hypothesised that the metabolism of Mito^{hi} and Mito^{lo} EM Tconvs may be different and therefore investigated the metabolism of Mito^{hi} and Mito^{lo} EM Tconv metabolism in comparison to EM Tregs. To investigate the metabolic differences between these three subsets, we sorted EM Tregs, Mito^{hi} EM Tconvs, and Mito^{lo} EM Tconvs based on their MitoTracker Deep Red FM signal (***Figure 4.9.a***). First we investigated whether CD3/CD28 stimulation changed their mitochondrial mass by staining with MitoTracker Green FM after stimulation. This revealed that, even after stimulation, Mito^{hi} EM Tconvs and Tregs maintain their higher quantity of mitochondria compared to Mito^{lo} EM Tconvs, indicating that their mitochondrial mass does not change after activation (***Figure 4.9.b***).

Next we investigated the glucose uptake rate of these three subsets in their activated state using 2-NBDG. Both Mito^{hi} and Mito^{lo} EM Tconvs dramatically increased their glucose uptake rate compared to EM Tregs upon activation, and Mito^{lo} EM Tconvs take

up more glucose than Mito^{hi} EM Tconvs (***Figure 4.9.c***). To investigate the aerobic glycolysis and OXPHOS rates of these cells directly, we used the Seahorse XF. Because memory T cells are characterised by their ability to quickly respond to stimulation, we applied *ex vivo* EM T cells onto the Seahorse XF directly after sorting and stimulated them *in situ* to observe dynamic metabolic changes. Both Mito^{hi} and Mito^{lo} EM Tconvs immediately increased their aerobic glycolysis rate upon activation (***Figure 4.9.d***). As Mito^{lo} EM Tconvs take up more glucose than Mito^{hi} EM Tconvs, the aerobic glycolysis rate was higher in Mito^{lo} EM Tconvs. Moreover, injection of oligomycin (an ATP-linked OXPHOS inhibitor) strongly increased the aerobic glycolysis rate with a remarkable jump in Mito^{lo} EM Tconvs. This indicates that both Mito^{lo} and Mito^{hi} EM Tconvs have pronounced energy compensation mechanisms under hypoxic condition and that these mechanisms are especially pronounced in the Mito^{lo} EM Tconv subset. In contrast, aerobic glycolysis of EM Tregs remained quiescent even after stimulation. Thus, EM Tregs can be characterised as cells that have a low glucose requirement and that do not exhibit an immediate aerobic switch upon activation. Surprisingly, Mito^{lo} EM Tconvs also showed the highest OXPHOS rate, even though they have lower mitochondrial mass (***Figure***

4.9.e). This result suggested that the mitochondrial mass does not directly correlate with the OXPHOS rate. Importantly, EM Tregs that exhibited a significantly lower glucose metabolism also exhibited the lowest OXPHOS rate indicating that EM Tregs are metabolically quiescent despite their high immunosuppressive function.

Taken together, CD4 EM T cells consist of three metabolically-distinct populations: Mito^{hi} EM Tconvs, Mito^{lo} EM Tconvs and EM Tregs. Whilst Mito^{lo} EM Tconvs possess a lower quantity of mitochondria, they demonstrate the highest OXPHOS rate together with a high glucose uptake and aerobic glycolysis rate. This indicates that Mito^{lo} EM Tconvs are the most metabolically active cells. In contrast, Mito^{hi} EM Tconvs maintain a high mitochondrial mass but exhibit lower metabolic rates compared to Mito^{lo} EM Tconvs. Finally, EM Tregs are metabolically quiescent with remarkably lower OXPHOS and aerobic glycolysis rates and a missing aerobic switch upon activation.

4.6 Mitochondrial mass differentiates EM CD4 effector subsets into Th2-type Mito^{hi} and Th1 and 17-types Mito^{lo} cells, and both require glycolysis for their effector functions.

EM Tconvs comprise two metabolically-distinct populations: EM Tconvs with a lower mitochondrial mass but higher metabolism (Mito^{lo} EM Tconvs) and EM Tconvs with a higher mitochondrial mass (Mito^{hi} EM Tconvs). We wondered whether these populations represented functionally-distinct populations. To answer this question, we started with a transcriptomic analysis using the NanoString nCounter Human CAR-T Characterisation panel. Mito^{hi} and Mito^{lo} EM Tconvs have significantly different gene signatures (***Figure 4.10***). Notably Mito^{hi} EM Tconvs have a more Th2-related gene signature with remarkably higher expression of *CCR4*, *CCR8*, *PTGDR2* and *IL-10*, whilst Mito^{lo} EM Tconvs expressed Th17 related with high expression of *RORC* (master gene of Th17) and *CCL20*. These results indicate functional differences between Mito^{hi} and Mito^{lo} EM Tconvs.

To investigate the functional difference between Mito^{hi} and Mito^{lo} EM Tconvs directly, we measured the actual cytokine production levels. Freshly isolated Mito^{hi} and Mito^{lo}

EM Tconvs were incubated for 3/4 days in the presence of anti-CD3/CD28 beads before quantification of the amount of cytokines in the culture supernatant. As expected, Mito^{hi} EM Tconvs produced more Th2-type cytokines, whilst Mito^{lo} EM Tconvs produced more Th1-type cytokines (***Figure 4.11.a***). Although Mito^{hi} EM Tconvs did produce a certain amount of Th1-type cytokines such as IL-2, IFN-γ and TNF-α, the magnitude of production by Mito^{lo} EM Tconvs was remarkably higher (***Figure 4.11.b***). When it comes to Th2-type cytokines, Mito^{lo} EM Tconvs completely lost the potential to produce IL-4, IL-5 and IL-9 (***Figure 4.11.c***). On the other hand, Th17-type cytokine production was not noticeably different between Mito ^{hi} and Mito^{lo} EM Tconvs, in opposition to their transcriptional signature, apart from higher production of IL-17F by Mito^{lo} EM Tconvs.

It has been reported that glycolysis, but not OXPHOS, is a key metabolic process required to maintain Tconv effector function (27, 198). Therefore, we next wondered if this concept could be applied to both Mito^{hi} and Mito^{lo} EM Tconvs as well. Moreover, these previous reports have shown only the relationship between IFN-γ production and glycolysis. Therefore, we also investigated if the same concept can be applied to other

cytokines. To study this, we added the metabolic inhibitors: 2-DG (a glycolysis inhibitor) or oligomycin (an ATP-linked OXPHOS inhibitor) into $Mito^{hi}$ and $Mito^{lo}$ EM Tconv cell cultures. In order to observe the direct impact of these metabolic inhibitors on EM Tconv effector function, we shortened the incubation period to 15 hours to avoid unwanted secondary effects of the metabolic inhibitors. For example, 2-DG is known to completely block T cell proliferation and therefore the measurement of cytokine concentration within the supernatant would be largely influenced by the cell number and not by a direct effect of 2-DG on cytokine production. We first investigated how the proportion of IFN-γ and IL-17A producing cells changed when cultured with either 2-DG or oligomycin using FACS. 2-DG strongly limited the IFN-γ and IL-17A production of both $Mito^{hi}$ and $Mito^{lo}$ EM Tconvs (***Figure 4.12.a***). Oligomycin reduced percentage of IFN-γ producing cells, but the magnitude of this reduction was notably smaller than that observed under inhibition by 2-DG. Moreover, IL-17A was not influenced by oligomycin. To confirm that cytokine production exhibited a reduced sensitivity to OXPHOS inhibition, we used rotenone, a second OXPHOS inhibitor that acts at mitochondria complex I. As observed under the oligomycin condition, rotenone did not reduce the percentage of

cytokine producing cells to the same degree as 2-DG (***Figure 4.12.b***). However, because FACS analysis detects only the percentage of cytokine producing cells and does not check the actual amount of the cytokine released, we measured absolute amount of cytokines within the culture supernatants using the LEGENDplex Human Th Cytokine Panel. 2-DG robustly blocked both Th1 and Th2-type cytokine production, whilst OXPHOS inhibitors did not (***Figure 4.12.c and d***). Due to the short incubation time, we could not detect Th17-type cytokines which were under the threshold of detection; however, previous FACS data strongly indicated that 2-DG but not oligomycin reduced Th17-type cytokine production (***Figure 4.12.a and b***). Thus, these results demonstrate that glycolysis, but not OXPHOS is a key metabolic process required to maintain both $Mito^{hi}$ and $Mito^{lo}$ EM Tconv cytokine production.

Taken together, $Mito^{hi}$ and $Mito^{lo}$ EM Tconvs are functionally distinct populations as demonstrated by their transcriptomic signatures. $Mito^{hi}$ EM Tconvs are more Th2-type CD4 T cells, whilst $Mito^{lo}$ EM Tconvs are more Th1- and 17-type CD4 T cells. Although $Mito^{hi}$ and $Mito^{lo}$ EM Tconvs are metabolically distinct, they both require glycolysis for

their effector function and OXPHOS inhibition influences this to a markedly lesser degree than glycolysis inhibition.

4.7 Mito^{hi} EM Tconvs are sensitive to Treg suppression whilst mito^{lo} EM Tconvs are not.

Although mitochondrial mass divided EM Tconvs into two functionally distinct subsets, they both require glucose for their effector function indicating that a glucose-deprived condition in peripheral tissues would limit EM Tconv function. Tregs also play a key role in suppressing Tconv function. Therefore, we next wondered whether EM Tregs suppress both Mito^{hi} and Mito^{lo} EM Tconvs. To investigate this, we ran an *in vitro* suppression assay. We stained Mito^{lo} and Mito^{hi} EM Tconvs with VPD and co-incubated them with EM Tregs in the presence of anti-CD3/CD28 beads. Unlike EM Tregs which strongly lack proliferative capacity (***Figure 4.2.f***), both Mito^{hi} and Mito^{lo} EM Tconvs can still effectively proliferate (***Figure 4.13.a TOP***). Surprisingly EM Tregs strongly suppressed Mito^{hi} EM Tconv proliferation, whilst Mito^{lo} EM Tconvs were more resistant to EM Tregs (***Figure***

4.13.a and b) indicating that the mitochondrial mass also divides EM Tconvs into Treg-sensitive (Mito^{hi}) and Treg-resistant (Mito^{lo}) EM Tconv populations.

The primary function of CD4 EM Tconvs is to produce effector cytokines. Thus, we next checked whether the capacity for cytokine production by Mito^{hi} and Mito^{lo} EM Tconvs also have different sensitivity to Treg suppression. We investigated this by examining the quantity of cytokines within the supernatants from our *in vitro* suppression assay. IL-2 production by both Mito^{hi} and Mito^{lo} EM Tconvs appeared to be reduced by co-incubation with EM Tregs, which was more pronounced in Mito^{hi} EM Tconvs (***Figure 4.13.c***). IFN-γ production showed a remarkable difference between Mito^{hi} and Mito^{lo} EM Tconvs. Whilst IFN-γ production from Mito^{hi} EM Tconvs dramatically reduced after co-incubation with EM Tregs, Mito^{lo} EM Tconv were strongly resistant to Treg suppression (***Figure 4.13.d***). Similarly, EM Tregs did not effectively suppress production of TNF-α by Mito^{lo} EM Tconv (***Figure 4.13.e***). The suppression of TNF-α production from Mito^{hi} EM Tconvs was also not observed; however, TNF-α production was already generally low compared to the production from Mito^{lo} EM Tconvs. Th2-type cytokine production from

Mito^{hi} EM Tconvs was also strongly sensitive to Treg-mediated suppression (***Figure 4.13.f and g***). Mito^{lo} EM Tconvs were resistant to Treg-mediated suppression of Th17-type cytokine production (***Figure 4.13.h***), in a similar pattern to the intransigent production of Th1-type cytokines described above. However, EM Tregs significantly suppressed IL-17A cytokine production from Mito^{hi} EM Tconvs. Thus, EM Tregs strongly supress Th2-type cytokine production from Mito^{hi} EM Tconvs, whilst Th1-type and Th17-type cytokine production by Mito^{lo} EM Tconvs was strongly resistant to EM Treg suppression (***Figure 4.13.i***). Importantly, because EM Tregs also strongly suppress IFN-γ and IL-17A production from Mito^{hi} EM Tconvs, the suppressive capacity of EM Tregs is not confined to the Th-subsets spectrum.

We conclude that Mito^{hi} and Mito^{lo} EM Tconvs have different susceptibilities to Treg-mediated suppression: Mito^{hi} EM Tconvs are sensitive to EM Treg suppression whilst Mito^{lo} EM Tconvs are resistant. Mito^{hi} and Mito^{lo} EM Tconvs are functionally different with Mito^{hi} being more Th2-like and Mito^{lo} being either Th1- or Th17-like. However, this Treg susceptibility is not due to the distribution of different Th subsets as IFN-γ and IL-

17A production from Mito^{hi} EM Tconvs is also remarkably suppressed.

4.8 EM Tregs gain the ability to suppress Mito^{lo} EM Tconvs under OXPHOS inhibited conditions.

We revealed that a specific population of EM CD4 Tconvs with lower mitochondrial mass (Mito^{lo} EM Tconvs) have a strong resistance to EM Treg-mediated suppression. During inflammation, peripheral tissues become metabolically harsh environments due to the infiltration and expansion of immune cells. For example, glucose, glutamine, and oxygen availability is reduced which causes negative regulation of EM Tconv effector function and limits mitochondrial energy production. Because neither OXPHOS inhibition nor Treg-mediated suppression strongly impact Mito^{lo} EM Tconv function individually, it seems that only glucose deprivation may be able to regulate Mito^{lo} EM Tconv function. However, within-tissue conditions impairing OXPHOS may indirectly impact Mito^{lo} EM Tconvs due to a skew in the balance of Mito^{lo} EM Tconvs and EM Tregs or through potentiated EM Treg function.

To investigate this, we isolated Mito^{lo} EM Tconvs and EM Tregs from healthy donors. We stained Mito^{lo} EM Tconvs with VPD and stimulated these in culture with EM Tregs in the presence of the OXPHOS inhibitor oligomycin. We first investigated whether OXPHOS inhibition differentially effects Mito^{lo} EM Tconv and EM Treg viability. Surprisingly, adding oligomycin did not change the ratio of EM Tregs and Mito^{lo} EM Tconvs compared to control conditions (***Figure 4.14.a***). Thus, the viability of cells upon OXPHOS inhibition was not different between EM Tregs and Mito^{lo} EM Tconvs. Next, we investigated whether the OXPHOS inhibition impacted suppression of Mito^{lo} EM Tconvs effector function, measured as IFN-γ and TNF-α production. As described before, EM Tregs did not noticeably suppress Mito^{lo} EM Tconvs ability to produce IFN-γ and TNF-α (***Figure 4.14.b***). However, EM Tregs strongly gained suppressive function in the presence of oligomycin, which is illustrated by the larger IFN-γ and TNF-α double-negative population compared to the oligomycin condition without EM Tregs.

Taken together, Mito^{lo} EM Tconvs are resistant to Treg-mediated suppression under

physiological conditions, whilst Tregs in OXPHOS inhibited conditions gain the ability suppress Mito^{lo} EM Tconvs.

4.9 Discussion

Here we first showed that CCR7 differentiates phenotypically and metabolically distinct subsets within human memory Tregs. CCR7$^-$ memory Tregs are the most immunosuppressive Tregs with the lowest proliferative capacity and glucose uptake rate (***Figure 4.2 and Figure 4.3.b***). Although we did not prove directly that human CCR7$^-$ memory Tregs are cells directly emigrating to peripheral tissues *in vivo*, transcriptional analysis revealed that CCR7$^-$ memory Tregs expressed a higher level of CXCR6 compared to both naïve and CCR7$^+$ memory Tregs indicating their tissue emigration potential (278-281). The low proliferation capacity and high suppressive function, together with the chemokine receptor status (specifically the lack of CCR7 expression), is highly indicative that CCR7$^-$ memory Tregs have EM-like properties that develop as T cells migrate to peripheral tissues and acquire strong effector function. This contrasts with CM T cells

which migrate to SLO and undergo clonal expansion as their primary function (246, 277). CCR4 and CCR8 are known chemokine receptors expressed on Tregs residing in peripheral tissues (288, 289). Unfortunately, as the NanoString nCounter Human Metabolic Pathways panel does not contain genes encoding these chemokine receptors, we were not able to reveal if EM Tregs also express these highly. Therefore, additional investigation of the expression of these chemokine receptors may support the hypothesis that EM Tregs have tissue migratory properties.

Expression of CD62L, the ligand for receptors on HEV, showed an interesting contrast between EM Tregs ($CCR7^-$ $CD62L^+$) and EM Tconvs ($CCR7^-$ $CD62L^-$) (***Figure 4.1.b***). HEV are expressed not only in SLO, but also in tertiary lymphoid organs (TLO) which may be found in peripheral tissues at sites of chronic inflammation such as transplanted organs and tumours (290, 291). Although the necessity for CCR7 to migrate to TLO remains controversial, the T cells infiltration into TLO in CCR7 knockout mice demonstrates that T cells maintain their migratory capacity into TLO independently of CCR7 expression (292-294). Interestingly, TLO have dual functions in driving and suppressing immunity

(295). TLO have important roles of potential therapeutic relevance in suppressing cancer immunity and inducing tolerance to transplanted organs by recruiting Tregs (296-299). Therefore, CD62L expression on only EM Tregs but not EM Tconvs suggests that one function of EM Tregs may be to emigrate to TLO in chronically-inflammed peripheral tissues; this may indicate anatomic and temporal differences in EM Treg and EM Tconv infiltration. However, further studies are required to reveal the physiological meaning of this difference.

Whilst naïve and CM Tregs and Tconvs revealed high glucose consumption rates, EM Tregs showed a lower glucose demand which is significantly different from EM Tconvs. This indicates that Tregs and Tconvs have a different metabolic signature only in peripheral tissues (***Figure 4.6 a and b***). Interestingly, analysis of glycolysis genes, including glucose transporter genes, showed no significant differences between EM Tregs and EM Tconvs despite their remarkably different glycolysis rates, indicating that this is due to post-transcriptional regulation (***Figure 4.7.b and Figure 4.9.d***). Glut1 is the

key glucose transporter that maintains human CD4 Tconv effector function and its expression is also known to be regulated through post-transcriptional mechanisms (190, 194, 300). Although we did not show Glut1 expression on EM Tregs directly, activated Tregs demonstrated a Glut1^{-} population amongst non-proliferating Tregs (***Figure 3.8.c***) suggesting that EM Tregs have a post-transcriptional defect in expression of Glut1. Glut1 trafficking to the cell surface is regulated by the Akt-mTOR signalling pathway in T cells (25, 190). As bulk Tregs required the mTOR signalling pathway to increase their glucose metabolism rate (most likely naïve and CM Tregs), the metabolic quiescence of EM Tregs may be due to suppressed mTOR activity (***Figure 3.7.b***). Therefore, the different metabolic characteristics between EM Tregs and EM Tconvs may result from differential mTOR signalling after activation.

We revealed that EM CD4 T cells have two metabolically and functionally distinct population based on mitochondrial mass. EM Tconvs with a high mitochondrial mass (Mito^{hi} EM Tconvs) are metabolically less active compared to EM Tconvs with a low mitochondrial mass (Mito^{lo} EM Tconvs). Both MITO-ID and MitoTracker Deep Red FM

staining revealed that Mito^{hi} Tconvs have a higher MMP, which seems to contradict their lower OXPHOS rate as MMP indicates mitochondrial activity. However, oligomycin (a mitochondrial ATP synthase inhibitor) decreases OXPHOS but increases MMP, whilst FCCP (an uncoupler transporting protons across cell membranes) increases OXPHOS but decreases MMP; indicating that MMP cannot be used directly as a measure of OXPHOS rate (301, 302). Thus, the low MMP with high OXPHOS rate observed in Mito^{lo} EM Tconvs may simply arise from effective mitochondrial activity despite of low mitochondrial quantity compared to Mito^{hi} EM Tconvs. Dynamics within the mitochondrial compartment are determined by mitochondrial fusion and fission which is essential for mitochondrial function (303). Therefore, morphological studies of mitochondria using electron microscopy may be an option to reveal another difference between Mito^{hi} and Mito^{lo} EM Tconvs.

Mito^{hi} and Mito^{lo} EM Tconvs are functionally distinct populations with Mito^{hi} EM Tconvs being more Th2-like whilst Mito^{lo} EM Tconvs are more Th1- and Th17-like (***Figure 4.10.b and 4.11.a***). Although Th2-type cytokine production was strictly limited to Mito^{hi} EM

Tconvs, Mito^{hi} cells can still produce both Th1 and Th17 cytokines, albeit to a lesser degree (***Figure 4.11.***). Thus, it could be that Mito^{hi} EM Tconvs comprise a mixture of Th subsets, whilst Mito^{lo} cells comprise more specifically Th1- and Th17-skewed cells with high effector function. The mitochondrial transcription factor A (Tfam) controls mtDNA copy number in cells and CD4-specific genetic deletion of Tfam causes high mitochondrial mass, but with disorganised cristae and a low OXPHOS rate (304, 305). Unlike the Mito^{hi} cells here, Tfam KO T cells with a high mitochondrial mass increased their IFN-γ production and RORγ expression, whilst dramatically reducing their IL-4 production. Thus, Tfam KO cells a have high mitochondrial mass with disorganised function, similar functional characteristics to Mito^{lo} EM Tconvs in our investigations. Tfam deletion is known to impair mitochondrial complex formation although complex II remains intact in genetic Tfam ablation (304). In contrast, the pharmacological and genetic deletion of mitochondrial complex II significantly decreases IFN-γ and IL-17 production whilst preserving IL-4 production (306). Both mitochondrial complex I and II deliver electrons into the coenzyme Q and eventually mitochondrial complex III and IV (307). Whilst complex I accepts electrons from the TCA cycle in form of NADH, complex

II is a TCA cycle enzyme which oxidises succinate and reduces coenzyme Q. Thus, functional differences between $Mito^{hi}$ and $Mito^{lo}$ EM Tconvs may not be due to a different degree of mitochondrial activity, but may result from a robust electron transport chain through mitochondrial complex II in $Mito^{lo}$ EM Tconvs. Iron deficiency also increases mitochondrial size and results in disorganised cristae (201, 308). Interestingly, although iron deficiency in humans remarkably disrupts our immune system, it does not significantly impact allergic reactions (309, 310). Indeed, pharmacological iron chelation reduces Th1-type cytokine production but not Th2-type cytokine production (311, 312). Although complex II is one of the many iron-containing enzymes, iron deficiency strongly associates with high ROS production which is mainly driven by complex I and III (201). Both high environmental levels and an increased mitochondrial production of ROS increase Th2-mediated immune responses (313, 314). By contrast, reduced ROS levels increase Th1- and Th17-type cytokine production (313, 315-317). Therefore, investigation of mitochondrial iron together with ROS status may shed new light on the difference between $Mito^{hi}$ and $Mito^{lo}$ EM Tconvs. Taken together, current studies of $CD4^+$ T cells subsets indicate that either reduced complex II respiration

or low iron status selectively inhibit Th1 and Th17, but not Th2, responses. As cells with reduced complex II electron respiratory chain rely more on mitochondrial complex I for electron delivery, and as complex I is the location of ROS production, both low complex II and reduced iron conditions cause high mitochondrial ROS production. Although mitochondrial ROS is required for Tconvs activation (202), other reports directly investigating ROS influence on Th subsets demonstrate a dual function of ROS in $CD4^+$ T cell effector function reducing Th1 and Th17 function whilst increasing Th2 response. Thus, $Mito^{lo}$ EM Tconvs have enhanced Th1- and Th17-type effector functions whilst losing the capacity to produce Th2-type cytokines. This may be due to their organised mitochondrial state, which supports effective mitochondrial respiration with high energy production but dramatically reduces ROS production. Together with the study of mitochondrial morphology mentioned above, the investigation of ROS production and the effector function employing other mitochondrial complex inhibitors with anti-oxidant agents may be an option to reveal this mechanism.

$Mito^{hi}$ and $Mito^{lo}$ EM Tconvs have different sensitivities to EM Treg-mediated

suppression (***Figure 4.13***). Both proliferation and effector function of Mito^{hi} EM Tconvs are strongly suppressed by EM Tregs, whilst Mito^{lo} EM Tconvs are Treg resistant. Importantly, both IFN-γ and IL-17A production from Mito^{hi} EM Tconvs is suppressed by EM Tregs indicating that differences in Treg sensitivity is not due to compositional differences between the Th subsets amongst EM Tconvs. Additional studies including RNA sequencing of Mito^{hi} and Mito^{lo} EM Tconvs together with epigenetic studies will be required to reveal precise phenotypic differences and what directly influences the Treg sensitivity. Moreover, it remains unclear if the different mitochondrial status directly defines Tregs sensitivity, or if other factors determine both Tregs sensitivity and mitochondrial difference. We also showed that EM Tregs strongly suppress Mito^{lo} Tconvs in the presence of oligomycin (an OXPHOS inhibitor) (***Figure 4.14 b***). This may suggest that mitochondrial activities modulate Treg sensitivity in EM Tconvs; however, our studies in the next chapter (*Chapter 5*) suggest that oligomycin directly affect EM Tregs to gain stronger suppressive function. Therefore, whether oligomycin also alters the Treg sensitivity of Mito^{lo} EM Tconvs directly remains to be established.

Others showed that enhanced glycolysis rate either by Toll-like receptor (TLR) signalling or genetically increased Glut1 expression strongly reduced mouse Tregs suppressive function (28, 206). However, the maximum glycolysis rate induced in human EM Tregs by oligomycin increased suppressive function (***Figure 4.14***). Mouse Tregs likely behave differently from human Tregs, but it can be said the effect of OXPHOS inhibition in Treg suppressive function overcomes the influence of increased glycolysis at least in human EM Tregs. Unlike glucose deprivation which directly regulates Tconv effector function, OXPHOS limitation does not directly influence Tconvs strongly but suppresses their effector functions through enhancing Treg function. However, how Treg function is influenced under hypoxic condition may be controversial due to HIF expression. HIF-1α is overexpressed in hypoxic conditions and works as a sensor of environmental oxygen availability (318). HIF-1α expression negatively regulates Treg function by enhancing glycolysis (208, 209, 215). In these studies, Tregs isolated from mice with hyperactivation of HIF-1α—resulting from deletion of genes responsible for HIF-1α degradation—completely abolished Treg function, whilst mice Tregs increased suppressive function by deletion of HIF-1α. Although it is clear that HIF-1α signalling has a negative impact on

Treg suppressive function, the hypoxic condition also dramatically reduced OXPHOS due to low oxygen availability and these mouse studies did not directly answer whether Tregs reduce their suppressive function under hypoxic conditions compared with their function under normoxic conditions. Indeed, a direct comparison of Treg suppressive function under normoxic and hypoxic conditions reveals that Treg suppression is increased under hypoxia (319). In this study, however, the authors investigated bulk CD4 T cells which are known to dramatically reduce their proliferation under hypoxic conditions. Therefore, the enhanced suppressive function by Treg under hypoxic condition is not so clear in this work. Others have reported that EM CD4 Tconvs specifically increase their proliferation capacity and maintain their effector functions under hypoxic condition (265, 266). Therefore, a direct comparison of the suppressive capacity of human EM Tregs against the effector capacity of EM Tconvs under normoxic and hypoxic conditions may clearly answer the question of how hypoxic peripheral tissues modulate Tregs suppression. Whilst the question of how hypoxic condition effect Treg function is not entirely resolved, we showed here that EM subsets of Tconvs and Tregs have contrasting metabolic regulatory mechanisms: Tconv effector function is

controlled by glycolysis and glycolysis deprivation negatively influences their function, whilst Treg function is controlled by OXPHOS and OXPHOS limitation increases Treg function.

We also reveal that EM Tregs highly express genes relating to the regulation of pyruvate metabolism, of which *MCT1* is most highly expressed compared to EM Tconvs (***Figure 4.7.c***). MCT1 is used to import lactate into Tregs and this mechanism appears to be important for increasing Treg function in lactate-enriched tissues (224). MCT1 deleted Tregs do not spontaneously induce an autoimmune phenotype, but do show less suppressive activity in colitis model indicating that Tregs do not absolutely require lactate, but that they gain additional function through MCT1-imported lactate. Others have demonstrated that Tregs have an advantage in lactate-enriched environments compared to Tconvs (204). NAD^+ is consumed during glycolysis and produces NADH which is either used in OXPHOS or lactate production from pyruvate. It is known that Tregs have high NAD^+ compared to Tconvs due to their supressed glycolysis rate. To maintain OXPHOS, Tregs consume excess NAD^+ by importing lactate and converting it to

pyruvate. It has been argued that Tregs may have an advantage under lactate-enriched conditions because aerobic glycolysis in Tconvs is disturbed due to high concentrations of end-products whilst Tregs may still generate energy through OXPHOS. This would suggest high viability of Tregs under lactate-enriched conditions. However, we revealed that Tregs have higher suppressive function when cultured with oligomycin. This indicates that the maintenance of energy production through lactate uptake is not important for EM Treg suppressive function (***Figure 4.14.b***). As such, lactate may have another important role to control Treg suppressive function rather than simply energy production through OXPHOS.

In summary, naïve and CM Tregs and Tconvs demonstrate similar metabolic characteristics with a high glucose consumption rate, whilst EM subsets demonstrate differences between the EM Tconv and EM Treg compartment. Although there are functionally and phenotypically distinct populations amongst EM Tconvs based on different mitochondrial mass, glycolysis and OXPHOS rates are higher in both EM Tconvs subsets compared with EM Tregs. These functional differences may be explained in

metabolic terms: whilst EM Tconvs require glucose for their effector functions, EM Tregs enhance their suppressive function under OXPHOS-inhibited conditions. In next chapter, we will investigate the details of Treg suppressive function resulting from OXPHOS inhibition and explore possible strategies for clinical translation.

4.10 Figures and legends

Figure 4.1

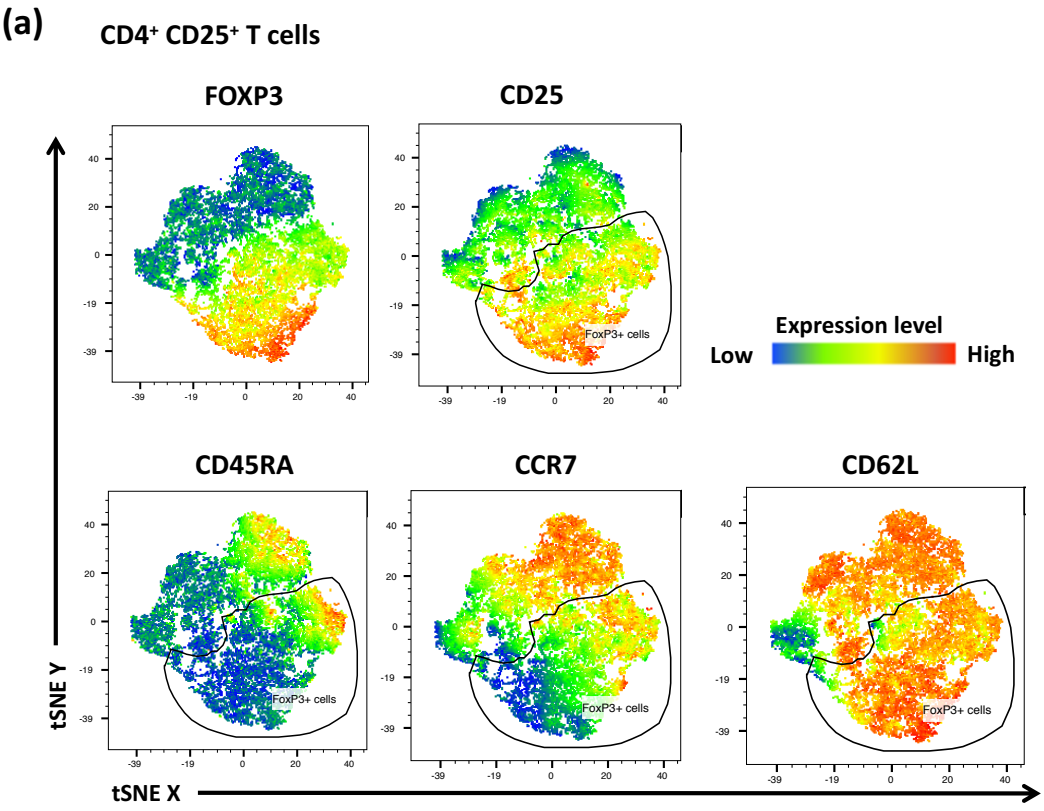

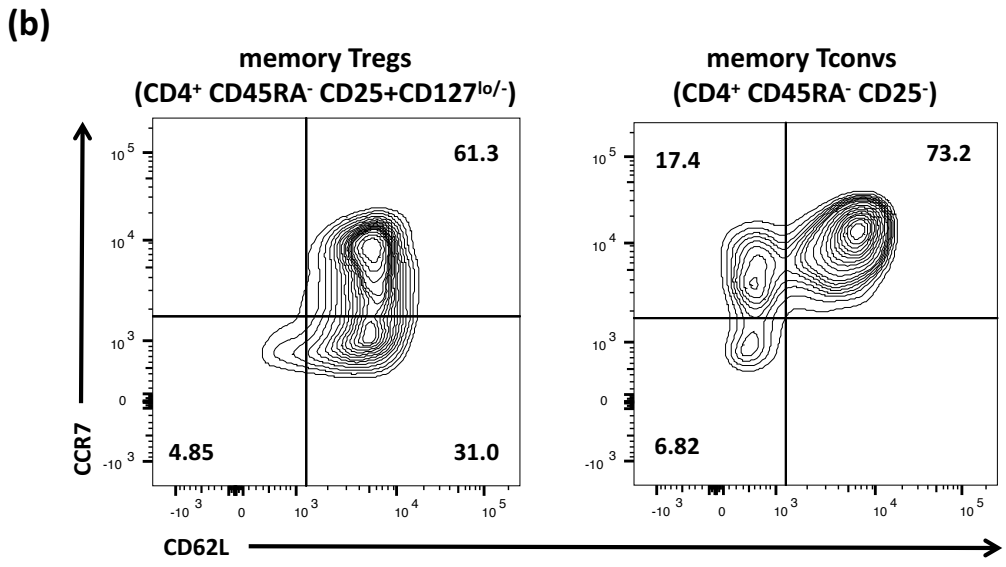

Figure 4.1. CCR7, but not CD62L divides human memory Tregs into two subsets.

Freshly isolated human $CD4^+$ T cells were stained with monoclonal antibodies and the phenotype was examined by FACS. (a) A representative t-SNE plot from 6 independent donors. These data were generated by Flow Jo gating on $CD4^+$ $CD25^+$ T cells. (b) A representative FACS plot from 1 of 6 donors, revealing CD62L and CCR7 expression amongst memory cells. Memory Tregs were gated as $CD4^+$ $CD25^+$ $CD127^{lo/-}$ $CD45RA^-$ cells. Memory Tconvs were gated as $CD4^+$ $CD25^-$ $CD45RA^-$ cells.

Figure 4.2

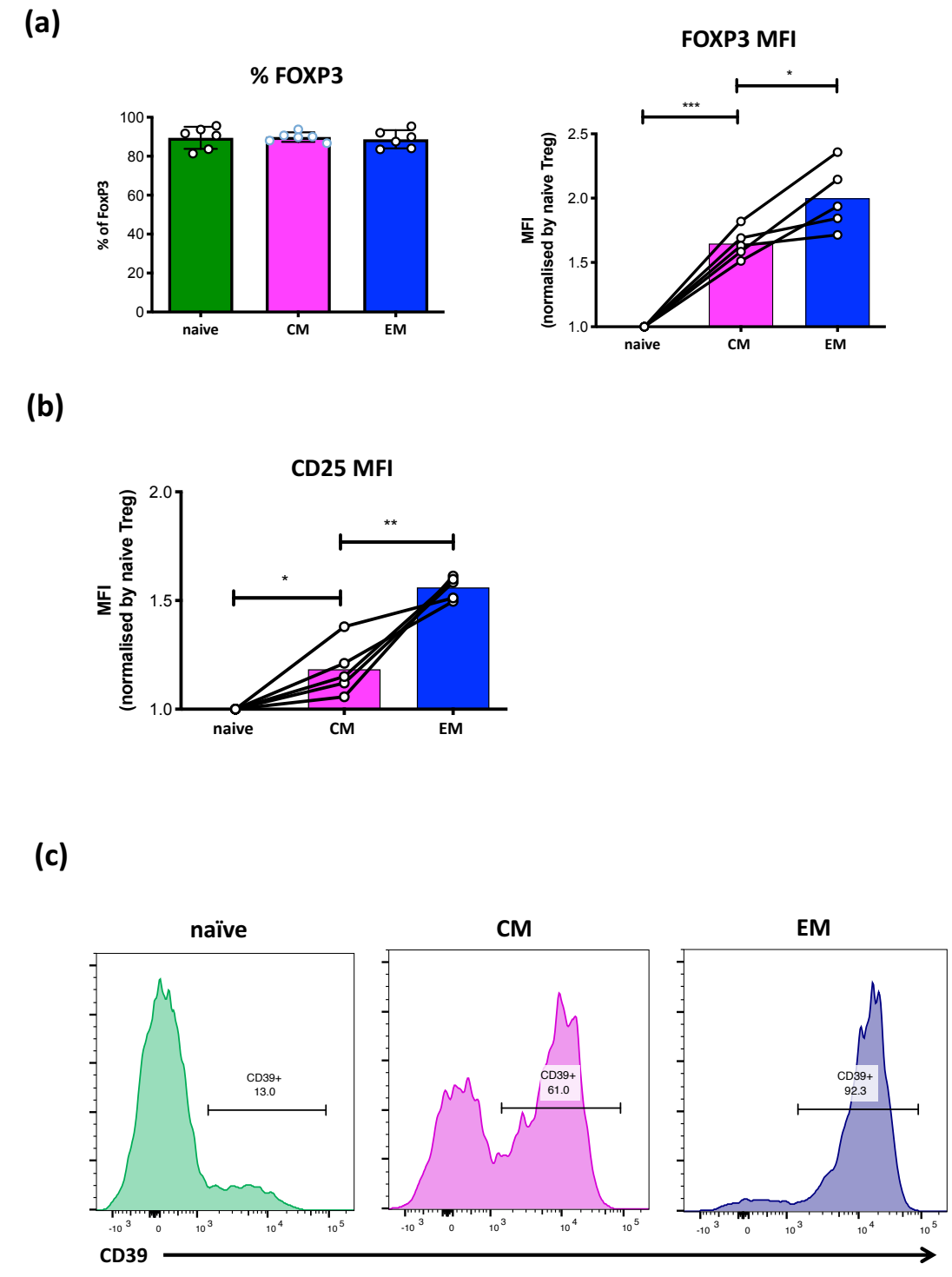
(a)
% FOXP3
% of FoxP3
100
80
60
40
20
0
naive
CM
EM
FOXP3 MFI
MFI
(normalised by naive Treg)
2.5
2.0
1.5
1.0
***
*
naive
CM
EM
(b)
CD25 MFI
MFI
(normalised by naive Treg)
2.0
1.5
1.0
**
*
naive
CM
EM
(c)
naïve
CM
EM
CD39+
13.0
CD39+
61.0
CD39+
92.3
CD39

Figure 4.2 (cont.)

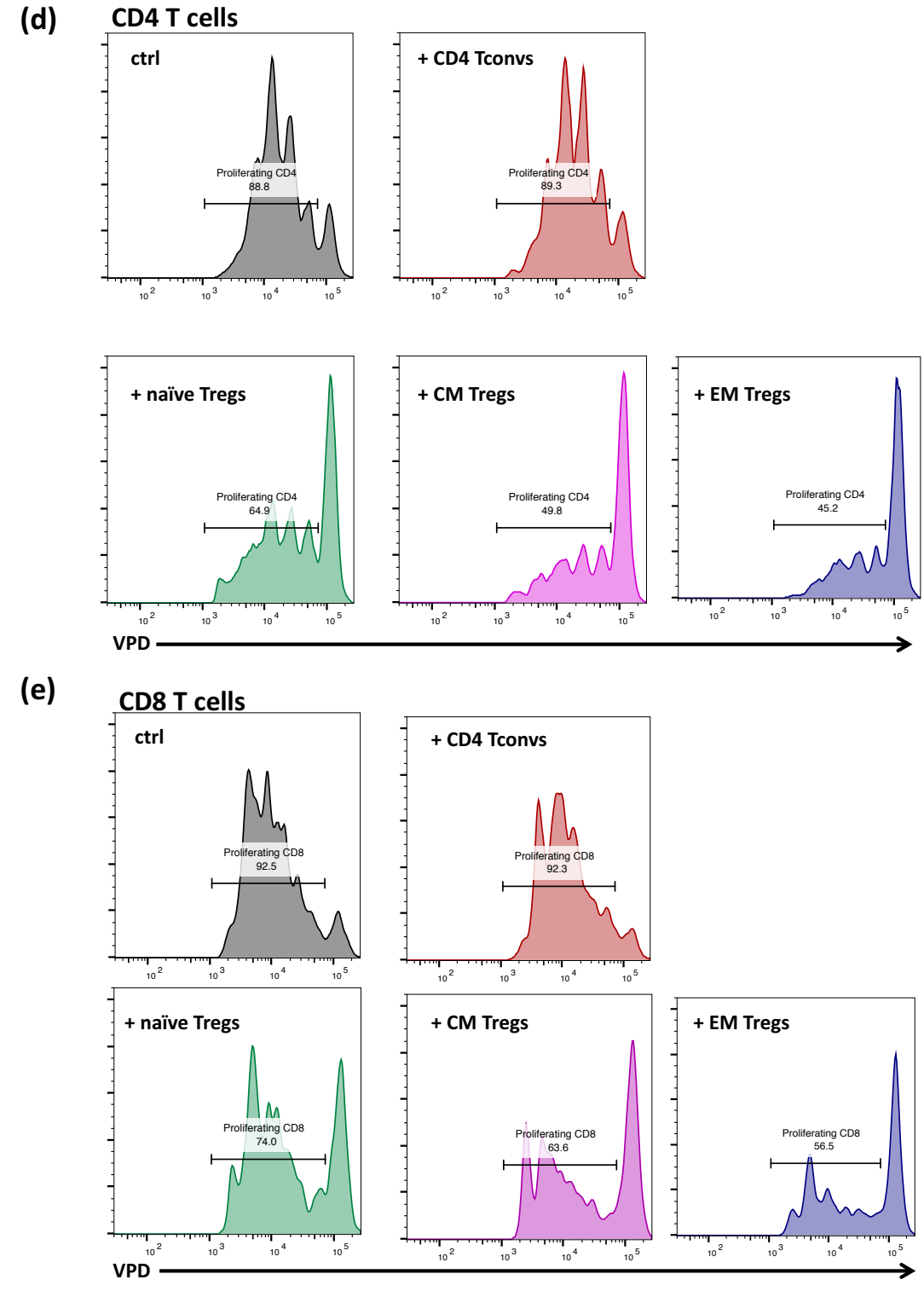

Figure 4.2 (cont.)

(f)

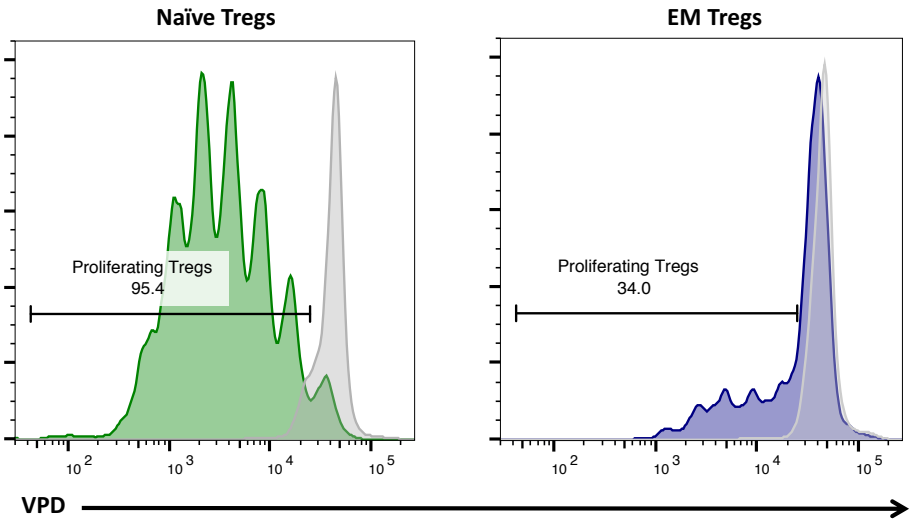

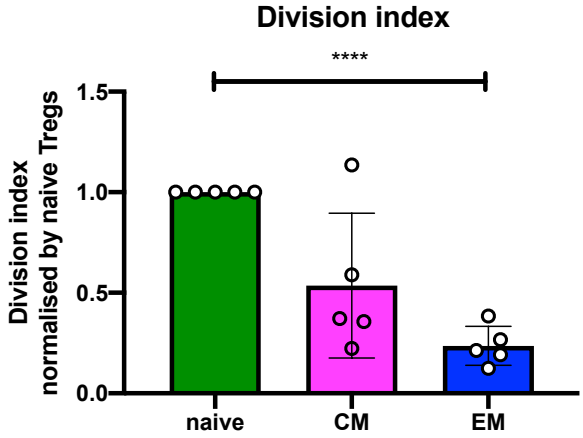

Figure 4.2. Phenotype of naïve, central memory, and effector memory human Tregs.

(a-c) Freshly isolated human $CD4^+$ T cells were examined by FACS to identify the phenotype of human Tregs subsets. Human Tregs were first gated as $CD4^+$ $CD25^+$ $CD127^{lo/-}$ and further gated into three subsets: naïve ($CD45RA^+$ $CCR7^+$), central memory ($CD45^-$ $CCR7^+$) and effector memory ($CD45RA^-$ $CCR7^-$). (a) Left, a graph revealing the percentage of FOXP3 positive cells. Right, a graph of MFI of FOXP3 indicating the expression level of FOXP3. (b) A graph of MFI of CD25. (c) A representative histogram of 2 independent donors, revealing the percentage of CD39 positive cells. (d and e) Data generated from an *in vitro* suppression assay. $CD4^+$ Tconvs and each subset of human Tregs were freshly isolated, followed by co-incubation with VPD-stained PBMCs at a 1:5 (Tregs to PBMC) ratio in the presence of anti-CD3/CD28 beads. (d) A representative histogram from 2 independent donors showing the proliferation of CD4 T cells. (e) A representative histogram from 2 independent donors showing the proliferation of CD8 T cells. (f) Data generated from a Treg proliferation assay. Each subset of human Tregs was freshly isolated, stained with VPD, and incubated for 84h with anti-CD3/CD28 beads. Top, a representative histogram of naïve and EM Treg proliferation from 5 independent

donors. Bottom, a graph of division index. The values were normalised to naïve Tregs. Each dot represents an individual donor. Columns represent mean ± SD. *p<0.05, **p<0.01, ***p<0.001 ****p<0.0001 by paired t test.

Figure 4.3

(a)

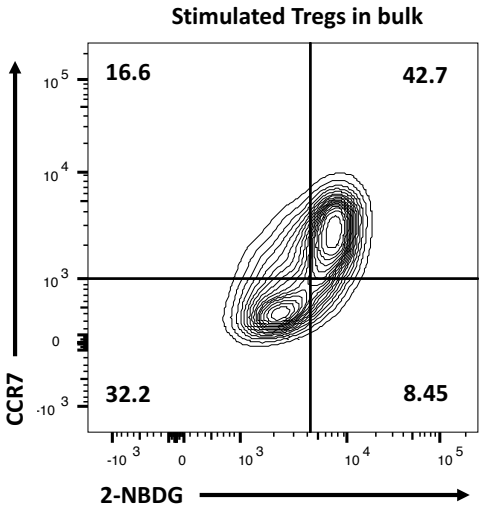
Stimulated Tregs in bulk
16.6
42.7
32.2
8.45
CCR7
2-NBDG
10^5
10^4
10^3
0
-10^3

(b)

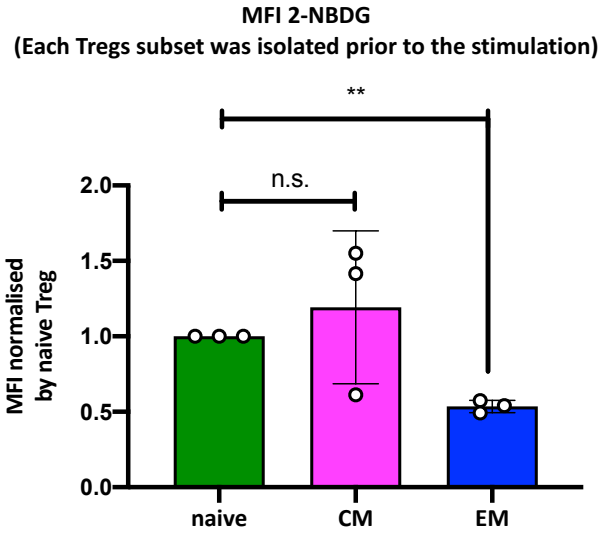
MFI 2-NBDG
(Each Tregs subset was isolated prior to the stimulation)
**
n.s.
MFI normalised by naive Treg
2.0
1.5
1.0
0.5
0.0
naive
CM
EM

Figure 4.3. Each subset of stimulated Tregs shows different glucose uptake rate.

(a) Freshly isolated human Tregs were incubated for 60h with anti-CD3/CD28 beads, followed by incubation with 2-NBDG, and anti-CCR7 antibody staining. A representative FACS plot from one of three independent donors. (b) Each Treg subset was freshly isolated, stimulated for 60h, and then briefly incubated with 2-NBDG. A graph of MFI of 2-NBDG. The values were normalised to naïve Tregs from the same donor. Each dot represents an individual donor. Columns represent mean ± SD. **p<0.01 by paired t test.

Figure 4.4

(a)

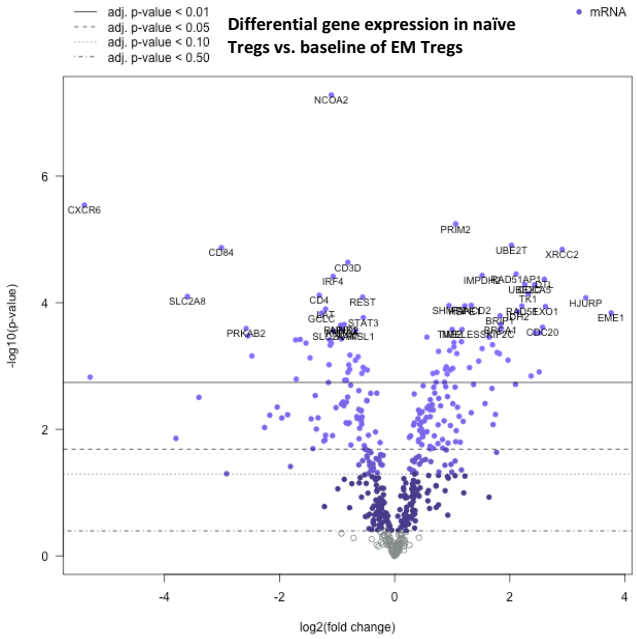
adj. p-value < 0.01
adj. p-value < 0.05
adj. p-value < 0.10
adj. p-value < 0.50
Differential gene expression in naïve Tregs vs. baseline of EM Tregs
mRNA
NCOA2
CXCR6
PRIM2
CD84
UBE2T
XRCC2
CD3D
IRF4
SLC2A8
CD4
REST
HJURP
EME1
PRKAB2
STAT3
CDC20
-log10(p-value)
log2(fold change)

(b)

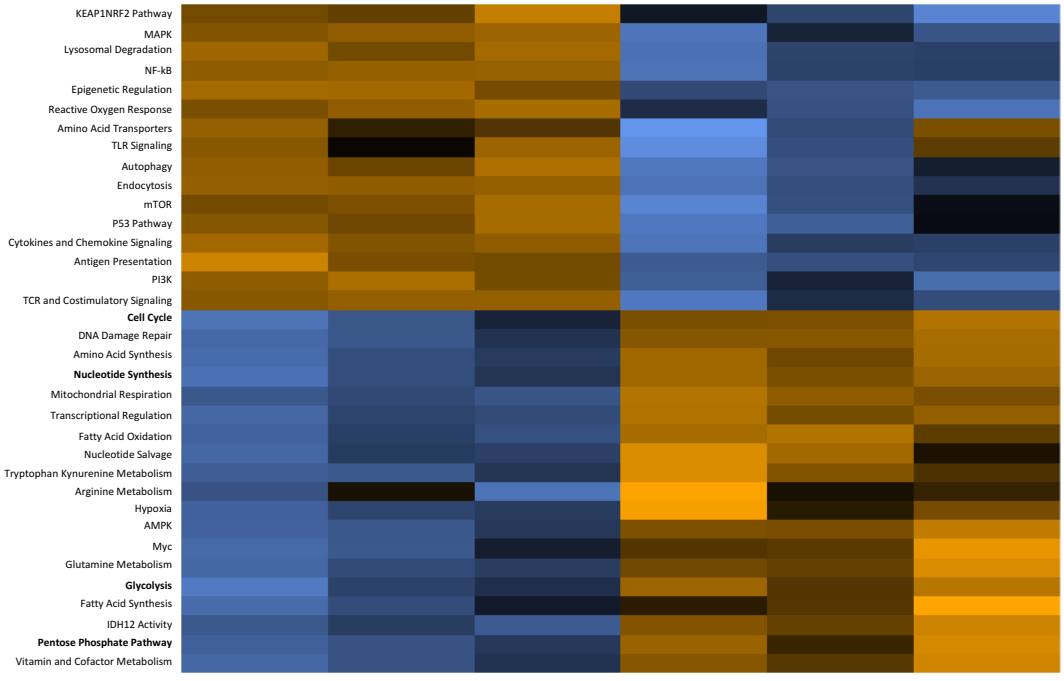
KEAP1NRF2 Pathway
MAPK
Lysosomal Degradation
NF-kB
Epigenetic Regulation
Reactive Oxygen Response
Amino Acid Transporters
TLR Signaling
Autophagy
Endocytosis
mTOR
P53 Pathway
Cytokines and Chemokine Signaling
Antigen Presentation
PI3K
TCR and Costimulatory Signaling
Cell Cycle
DNA Damage Repair
Amino Acid Synthesis
Nucleotide Synthesis
Mitochondrial Respiration
Transcriptional Regulation
Fatty Acid Oxidation
Nucleotide Salvage
Tryptophan Kynurenine Metabolism
Arginine Metabolism
Hypoxia
AMPK
Myc
Glutamine Metabolism
Glycolysis
Fatty Acid Synthesis
IDH12 Activity
Pentose Phosphate Pathway
Vitamin and Cofactor Metabolism
EM Tregs
Naïve Tregs

Figure 4.4 (cont.)

(c)

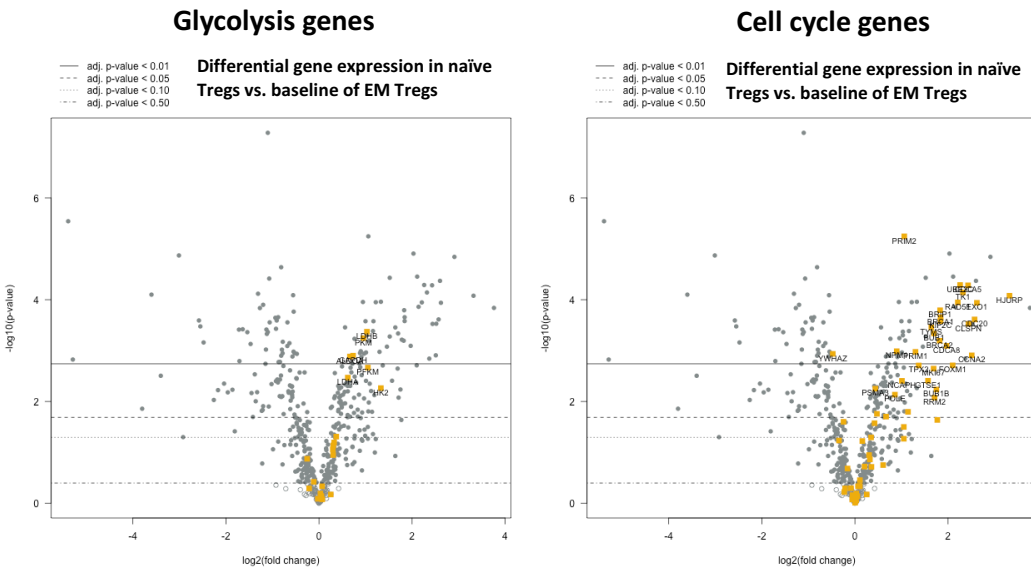

(d)

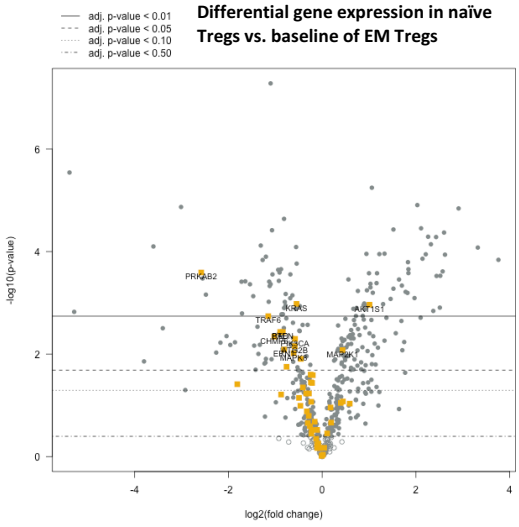

Figure 4.4. Naïve Tregs possess higher expression of glycolysis and cell cycle genes than EM Tregs.

NanoString nCounter Sprint gene expression analysis using the Human Metabolic Pathways panel. RNA was isolated from naïve and effector memory (EM) Tregs after 40h stimulation with anti-CD3/CD28 beads. (a) A volcano plot revealing the most differentially expressed genes, relative to a baseline of EM Tregs. (b) A heatmap revealing the differentially expressed specific groups of metabolic genes. (c and d) A volcano plot revealing the most differentially expressed glycolysis genes (c, left panel), cell cycle genes (c, right panel) and autophagy genes (d), highlighted in orange.

Figure 4.5

(a)

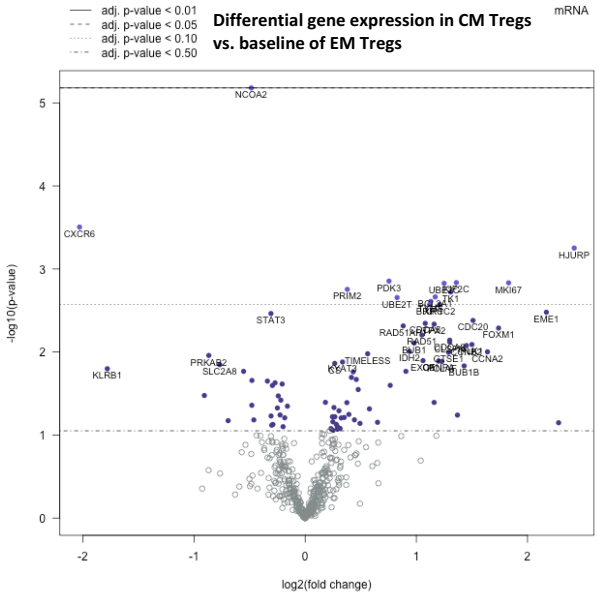
adj. p-value < 0.01
adj. p-value < 0.05
adj. p-value < 0.10
adj. p-value < 0.50
Differential gene expression in CM Tregs vs. baseline of EM Tregs
mRNA
-log10(p-value)
log2(fold change)
NCOA2
CXCR6
HJURP
PDK3
PRIM2
MKI67
UBE2T
TK1
STAT3
EME1
CDC20
FOXM1
RAD51
PRKAB2
SLC2A8
KLRB1
TIMELESS
IDH2
CCNA2
BUB1B

(b)

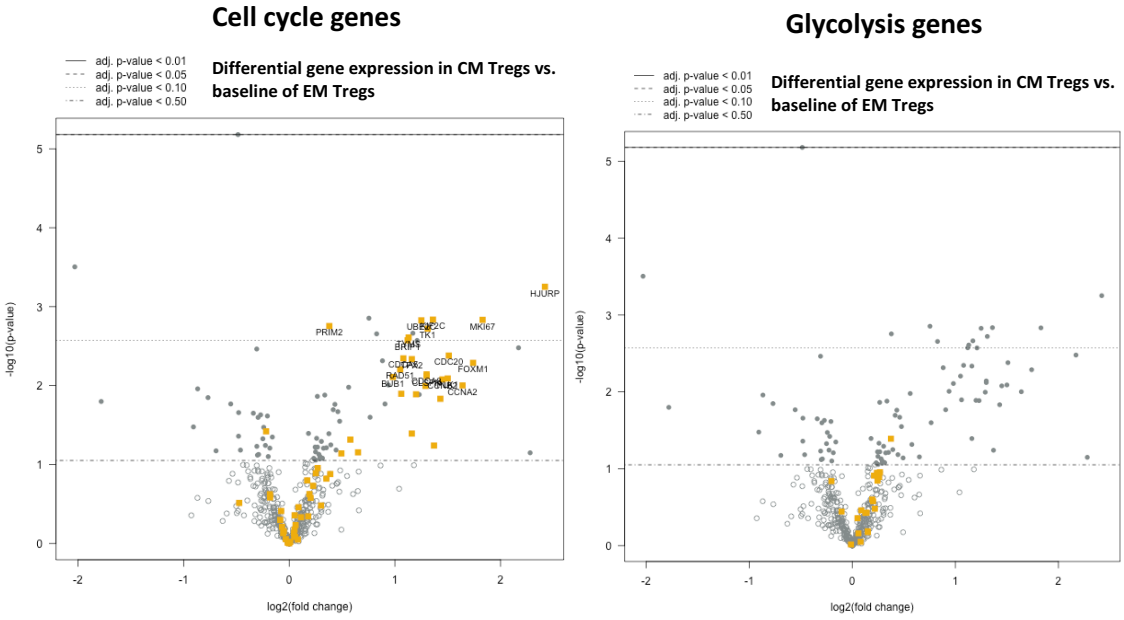
Cell cycle genes
adj. p-value < 0.01
adj. p-value < 0.05
adj. p-value < 0.10
adj. p-value < 0.50
Differential gene expression in CM Tregs vs. baseline of EM Tregs
-log10(p-value)
log2(fold change)
HJURP
PRIM2
MKI67
TK1
CDC20
FOXM1
CCNA2
Glycolysis genes
adj. p-value < 0.01
adj. p-value < 0.05
adj. p-value < 0.10
adj. p-value < 0.50
Differential gene expression in CM Tregs vs. baseline of EM Tregs
-log10(p-value)
log2(fold change)

Figure 4.5. CM Tregs and EM Tregs do not have a distinct metabolic gene signature, except for genes relating to cell cycle.

NanoString nCounter Sprint gene expression analysis using the Human Metabolic Pathways panel. RNA was isolated from central memory (CM) and EM Tregs after 40h stimulation with anti-CD3/CD28 beads. (a) A volcano plot revealing the most differentially expressed genes, relative to a baseline of EM Tregs. (b) A volcano plot revealing the most differentially expressed cell cycle genes (left) and glycolysis genes (right), highlighted in orange.

Figure 4.6

(a)

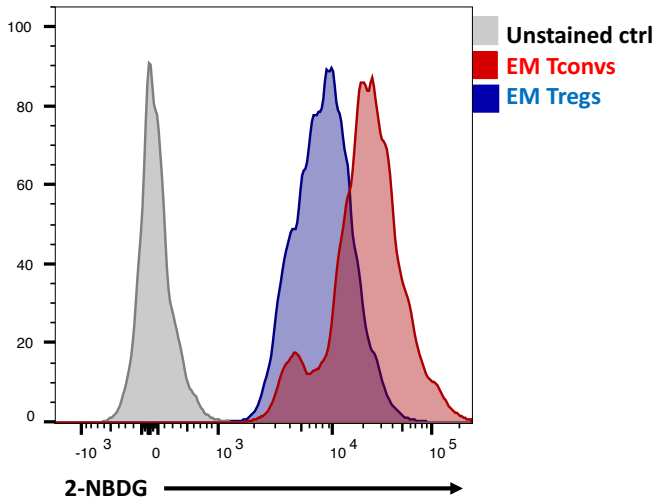
100
80
60
40
20
0
-10 3
0
10 3
10 4
10 5
2-NBDG
Unstained ctrl
EM Tconvs
EM Tregs

(b)

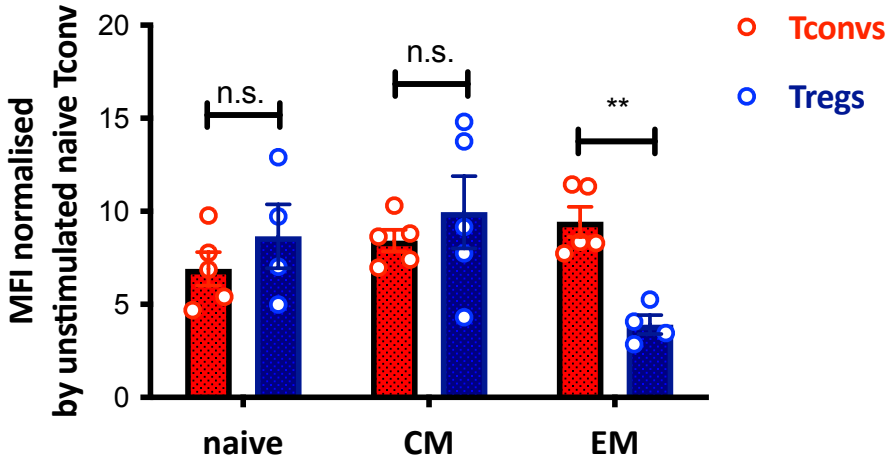
MFI normalised by unstimulated naive Tconv
20
15
10
5
0
n.s.
n.s.
**
naive
CM
EM
Tconvs
Tregs

Figure 4.6. Only the EM subset shows a distinct glucose uptake rate between Tregs and Tconvs after stimulation.

Each Treg and Tconv subset was freshly isolated as naïve (CD45RA+ CCR7+), CM (CD45RA-, CCR7+) and EM (CD45RA-, CCR7-) cells, followed by stimulation for 60h with anti-CD3/CD28 beads and 2-NBDG incubation. (a) A representative histogram from one of four independent donors, revealing EM Tregs and EM Tconvs 2-NBDG level. (b) A graph of MFI of 2-NBDG. Values are normalised to unstimulated naïve Tconvs from same donor. One of five donors had a reduced proportion of naïve Tregs and another had a reduced proportion of EM Tregs and respective populations were not possible to sort in a required amount. Each dot represents an individual donor. Columns represent mean ± SD. **p<0.01 by paired t test.

Figure 4.7

(a)

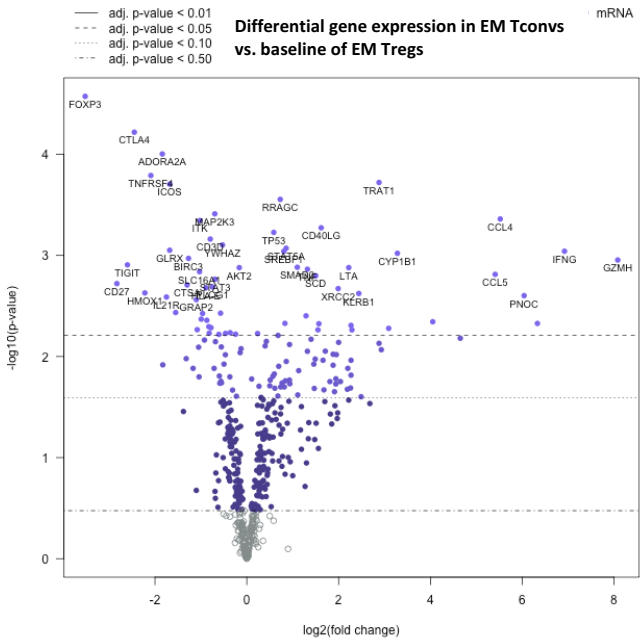
adj. p-value < 0.01
adj. p-value < 0.05
adj. p-value < 0.10
adj. p-value < 0.50
Differential gene expression in EM Tconvs vs. baseline of EM Tregs
mRNA
FOXP3
CTLA4
ADORA2A
TNFRSF4
ICOS
TRAT1
RRAGC
MAP2K3
ITK
TP53
CD40LG
CCL4
IFNG
GZMH
GLRX
BIRC3
YWHAZ
CYP1B1
TIGIT
AKT2
SCD
LTA
CCL5
PNOC
CD27
HMOX1
IL21R
GRAP2
XRCC2
KLRB1
-log10(p-value)
log2(fold change)

(b)

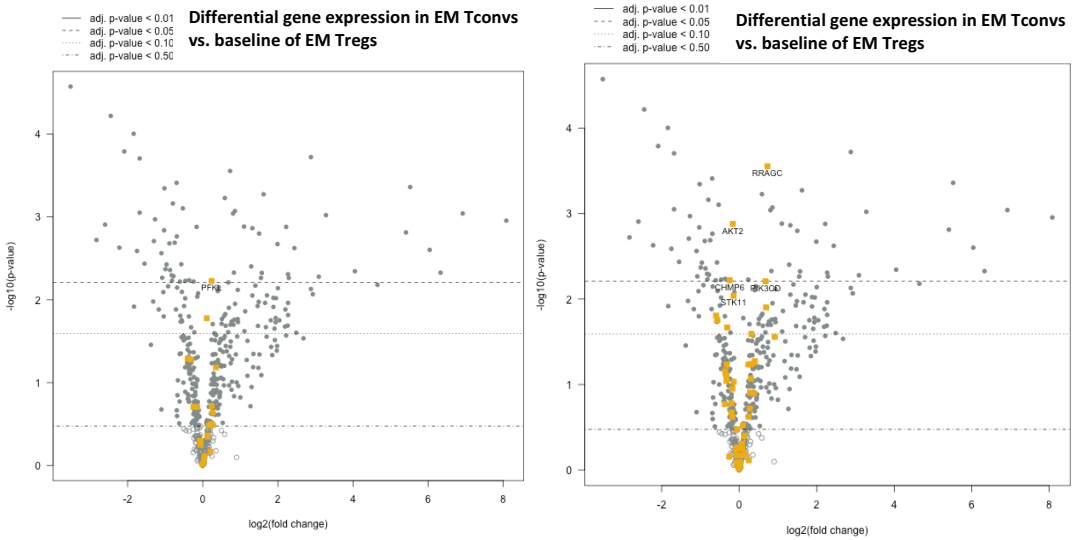
Glycolysis genes
Autophagy
adj. p-value < 0.01
adj. p-value < 0.05
adj. p-value < 0.10
adj. p-value < 0.50
Differential gene expression in EM Tconvs vs. baseline of EM Tregs
PFKL
RRAGC
AKT2
CHMP6
STK11
-log10(p-value)
log2(fold change)

Figure 4.7 (cont.)

(c)

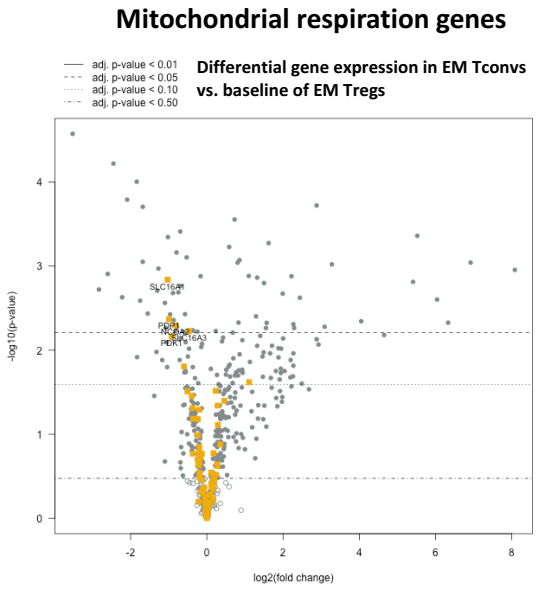

(d)

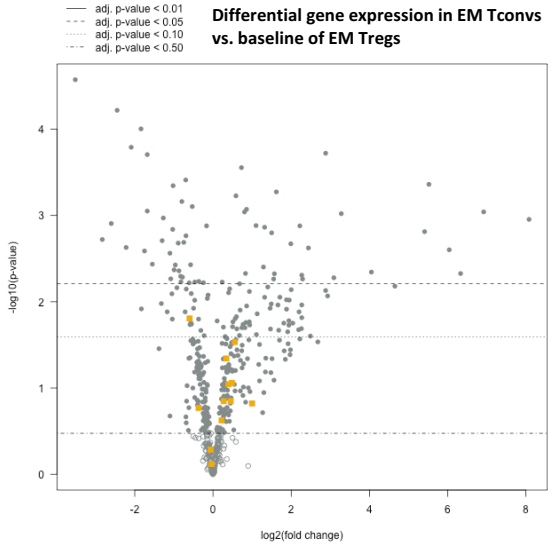

Figure 4.7. EM Tregs and EM Tconvs have a similar glycolysis genes signature but different in mitochondrial respiration genes.

Nanostring nCounter Sprint gene expression analysis using the Human Metabolic Pathways panel. RNA was isolated from EM Tregs and EM Tconvs after 40h stimulation with anti-CD3/CD28 beads. (a) A volcano plot revealing the most differentially expressed genes, relative to a baseline of EM Tregs. (b-d) A volcano plot revealing the most differentially expressed glycolysis genes (b, left panel), autophage genes (b, right panel), mitochondrial respiration genes (c), and fatty acid oxidation genes (d), highlighted in orange.

Figure 4.8

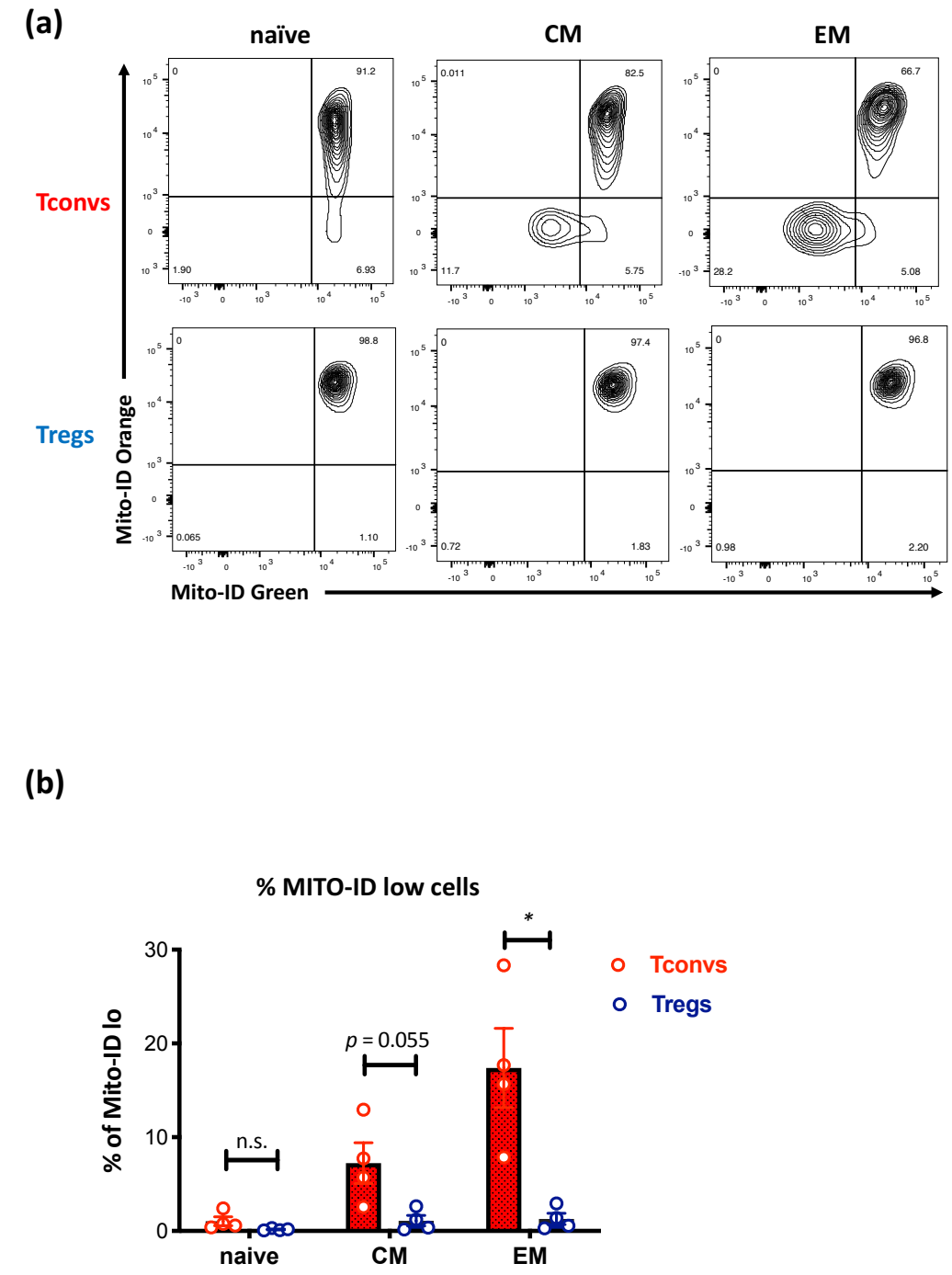
(a)
naïve
CM
EM
Tconvs
Tregs
Mito-ID Orange
Mito-ID Green
91.2
1.90
6.93
0.011
82.5
11.7
5.75
66.7
28.2
5.08
98.8
0.065
1.10
97.4
0.72
1.83
96.8
0.98
2.20
(b)
% MITO-ID low cells
% of Mito-ID lo
30
20
10
0
n.s.
p = 0.055
*
naive
CM
EM
Tconvs
Tregs

Figure 4.8 (cont.)

(c)

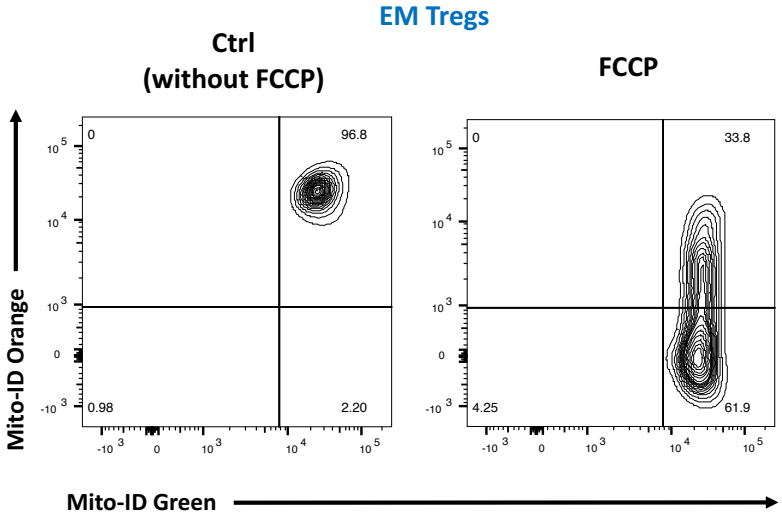

Figure 4.8 (cont.)

(d)

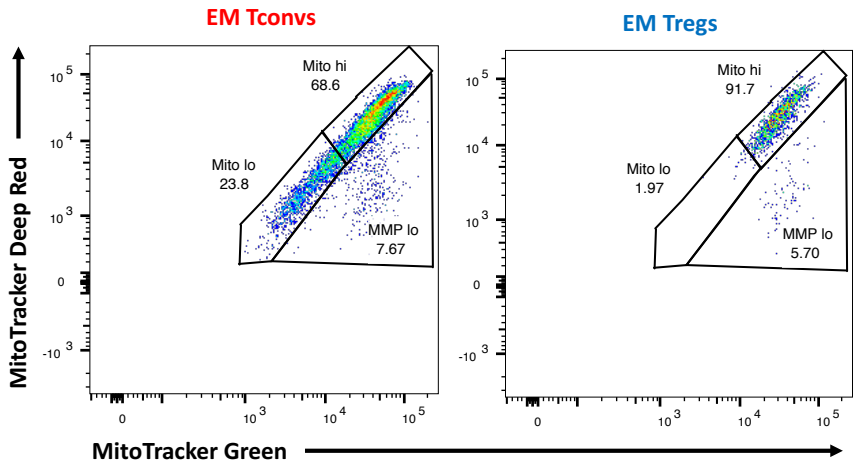

(e)

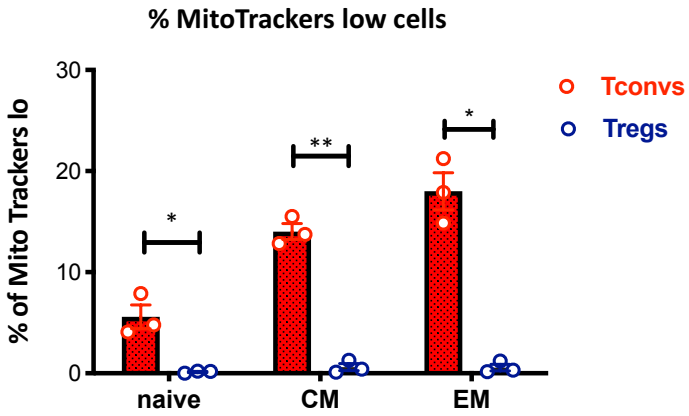

Figure 4.8. Human memory Tconvs but not Tregs downregulate mitochondria.

The mitochondrial mass and membrane potential of each subset of Tregs and Tconvs were examined by FACS using the Mito-ID membrane potential detection kit or MitoTrackers. The cells were incubated for 2 hours prior to the assays. (a-c) Mito-ID membrane potential detection kit data. (a) Representative FACS plots from one of four independent donors. (b) A graph revealing a percentage of cells gated as Mito-ID green low and Mito-ID orange low cells. (c) Representative FACS plots from one of two independent donors. Carbonyl cyanide-4-(trifluoromethoxy) phenylhydrazone (FCCP) was added for 30 min at the end of the cultivation. (d and e) MitoTracker Green FM and MitoTracker Deep Red FM co-staining data. (d) A representative FACS plots from one of three independent donors. (e) A graph revealing the percentage of cells gated as MitoTracker green FM low, MitoTracker DeepRed low cells.

Figure 4.9

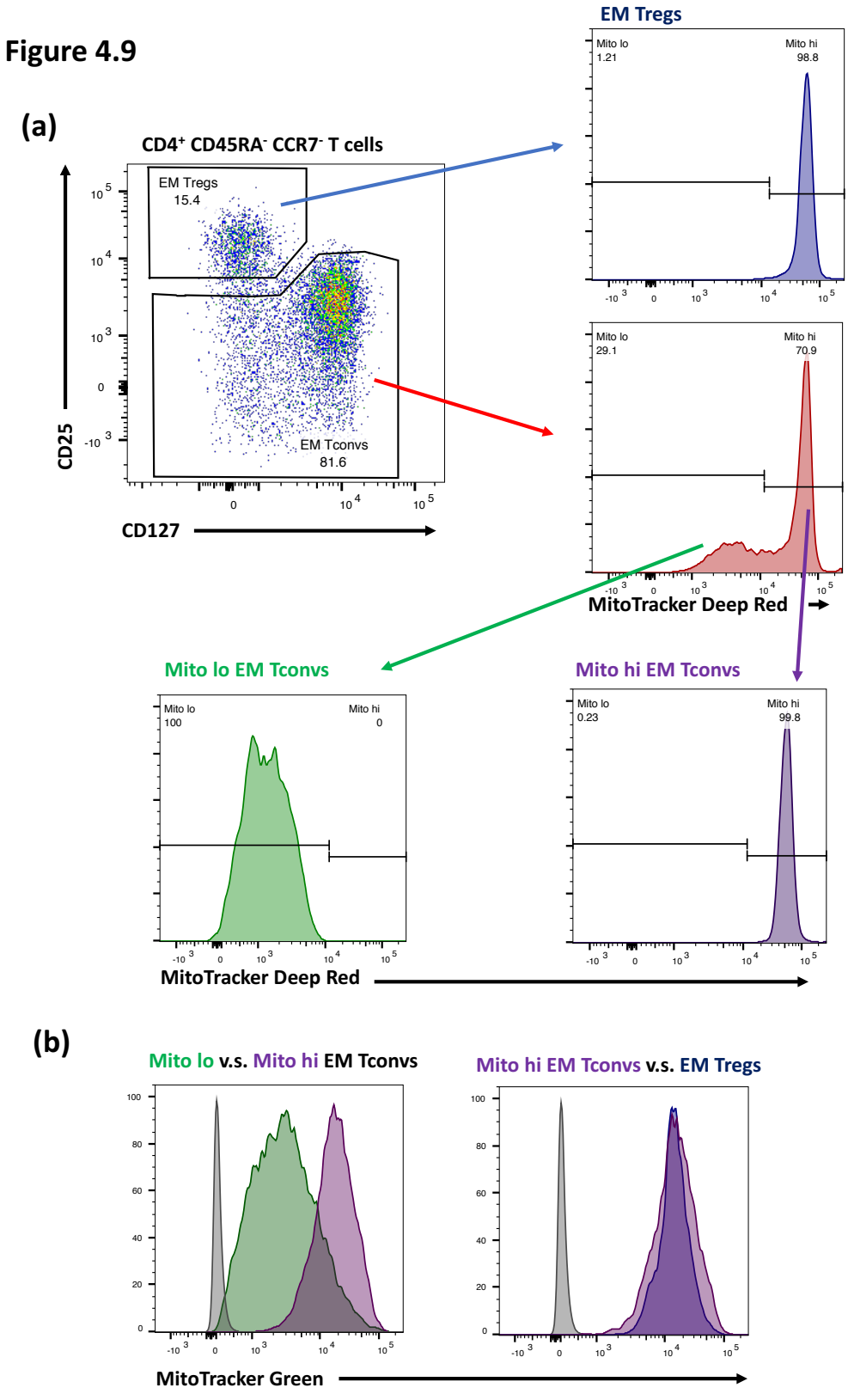
(a)
CD4+ CD45RA- CCR7- T cells
EM Tregs
15.4
EM Tconvs
81.6
CD25
CD127
EM Tregs
Mito lo
1.21
Mito hi
98.8
Mito lo
29.1
Mito hi
70.9
MitoTracker Deep Red
Mito lo EM Tconvs
Mito lo
100
Mito hi
0
Mito hi EM Tconvs
Mito lo
0.23
Mito hi
99.8
MitoTracker Deep Red
(b)
Mito lo v.s. Mito hi EM Tconvs
Mito hi EM Tconvs v.s. EM Tregs
MitoTracker Green

Figure 4.9 (cont.)

(c)

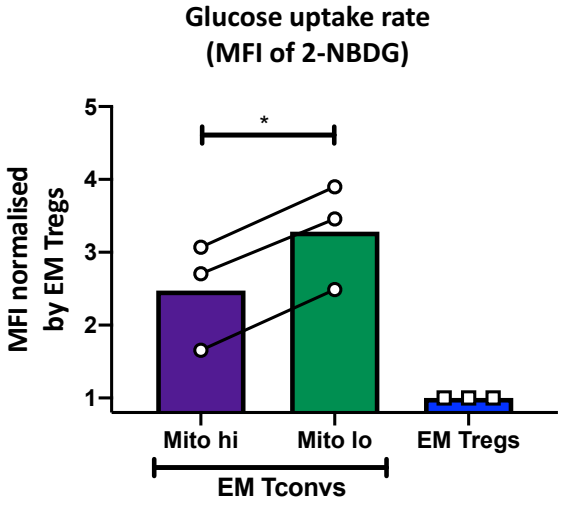

(d)

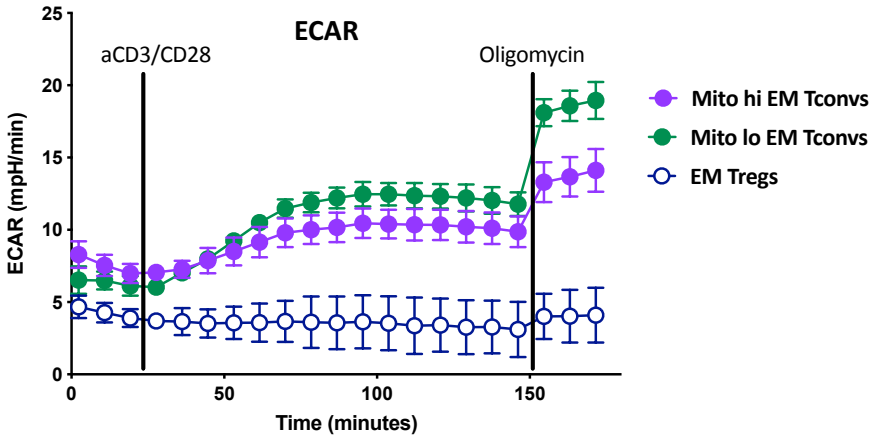

(e)

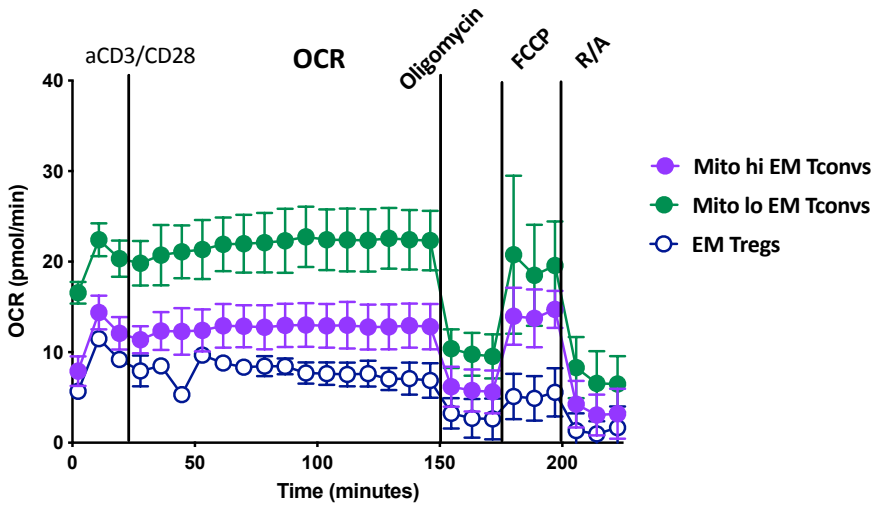

Figure 4.9. EM $CD4^+$ T cells have three metabolically distinct subsets: EM Tregs, EM Tconvs with high mitochondrial mass and EM Tconvs with low mitochondrial mass.

Freshly isolated EM Tregs, EM Tconvs with high mitochondrial mass ($Mito^{hi}$ EM Tconvs) and EM Tconvs with low mitochondrial mass ($Mito^{lo}$ EM Tconvs) were sorted to investigate their metabolism. (a) Gating strategy for cell sorting. EM Tregs were gated as $CD25^+$ $CD127^{lo/-}$ amongst $CD45RA^-$ $CCR7^-$ EM CD4 T cells. EM Tconvs were gated by the inverse gate of EM Tregs and further gated into $Mito^{hi}$ and $Mito^{lo}$ cells based on the intensity of MitoTracker Deep Red FM signal. (b and c) Each subset of EM T cells was stimulated for 60h with anti-CD3/CD28 beads after sorting, followed by Mitotracker Green FM or 2-NBDG staining. (b) A representative histogram from one of two independent donors, revealing the intensity of Mito Green FM. (c) A graph revealing the MFI of 2-NBDG. The values were normalised to EM Tregs. Each dot represents an individual donor. Columns represent mean ± SD. *$p<0.05$ by paired t test. (d and e) Metabolic measurement flux using Seahorse XF. Each subset of EM CD4 T cells was applied to the Seahorse XF directly after sorting. Anti-CD3/CD28 activating monoclonal antibodies were injected during the experiment followed by oligomycin, FCCP and

rotenone and antimycin A (R/A) injections. (d) A representative ECAR plot from one of two independent donors. (e) A representative OCR plot from one of two independent donors.

Figure 4.10

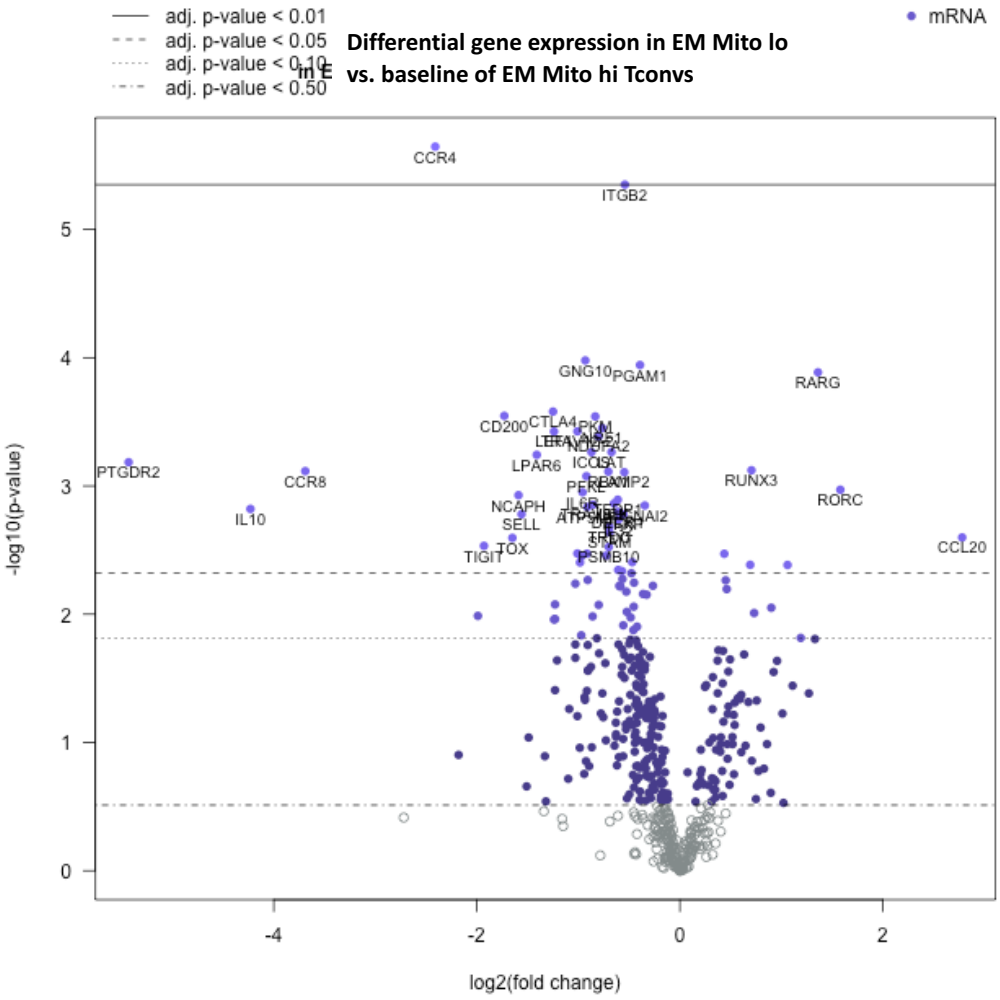
adj. p-value < 0.01
adj. p-value < 0.05
adj. p-value < 0.10
adj. p-value < 0.50
mRNA
Differential gene expression in EM Mito lo
vs. baseline of EM Mito hi Tconvs
CCR4
ITGB2
GNG10
PGAM1
RARG
CD200
CTLA4
PKM
LPAR6
PTGDR2
CCR8
IL10
RUNX3
RORC
NCAPH
SELL
TIGIT
TOX
PSMB10
CCL20
-log10(p-value)
log2(fold change)
5
4
3
2
1
0
-4
-2
0
2

Figure 4.10. Mito^{hi} and Mito^{lo} EM Tconvs express distinct T helper subset genes.

Nanostring nCounter Sprint gene expression analysis using the CAR-T characterization panel. RNA was isolated from Mito^{hi} and Mito^{lo} EM Tconvs immediately following sorting. A volcano plot revealing the most differentially expressed genes, relative to a baseline of Mito^{hi} EM Tconvs.

Figure 4.11

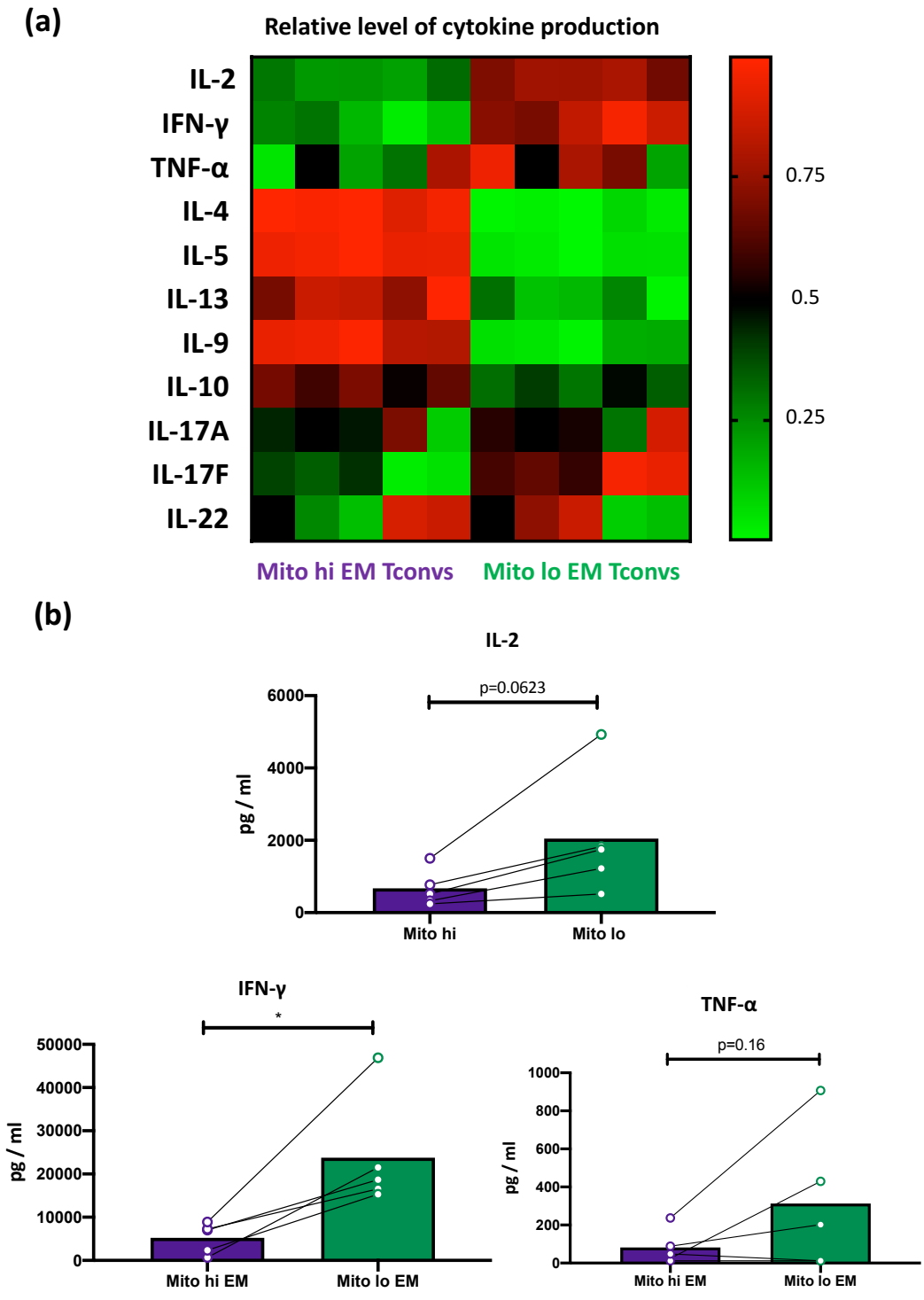
(a)
Relative level of cytokine production
IL-2
IFN-γ
TNF-α
IL-4
IL-5
IL-13
IL-9
IL-10
IL-17A
IL-17F
IL-22
0.75
0.5
0.25
Mito hi EM Tconvs
Mito lo EM Tconvs
(b)
IL-2
p=0.0623
6000
4000
2000
0
pg / ml
Mito hi
Mito lo
IFN-γ
*
50000
40000
30000
20000
10000
0
pg / ml
Mito hi EM
Mito lo EM
TNF-α
p=0.16
1000
800
600
400
200
0
pg / ml
Mito hi EM
Mito lo EM

Figure 4.11 (cont.)

(c)

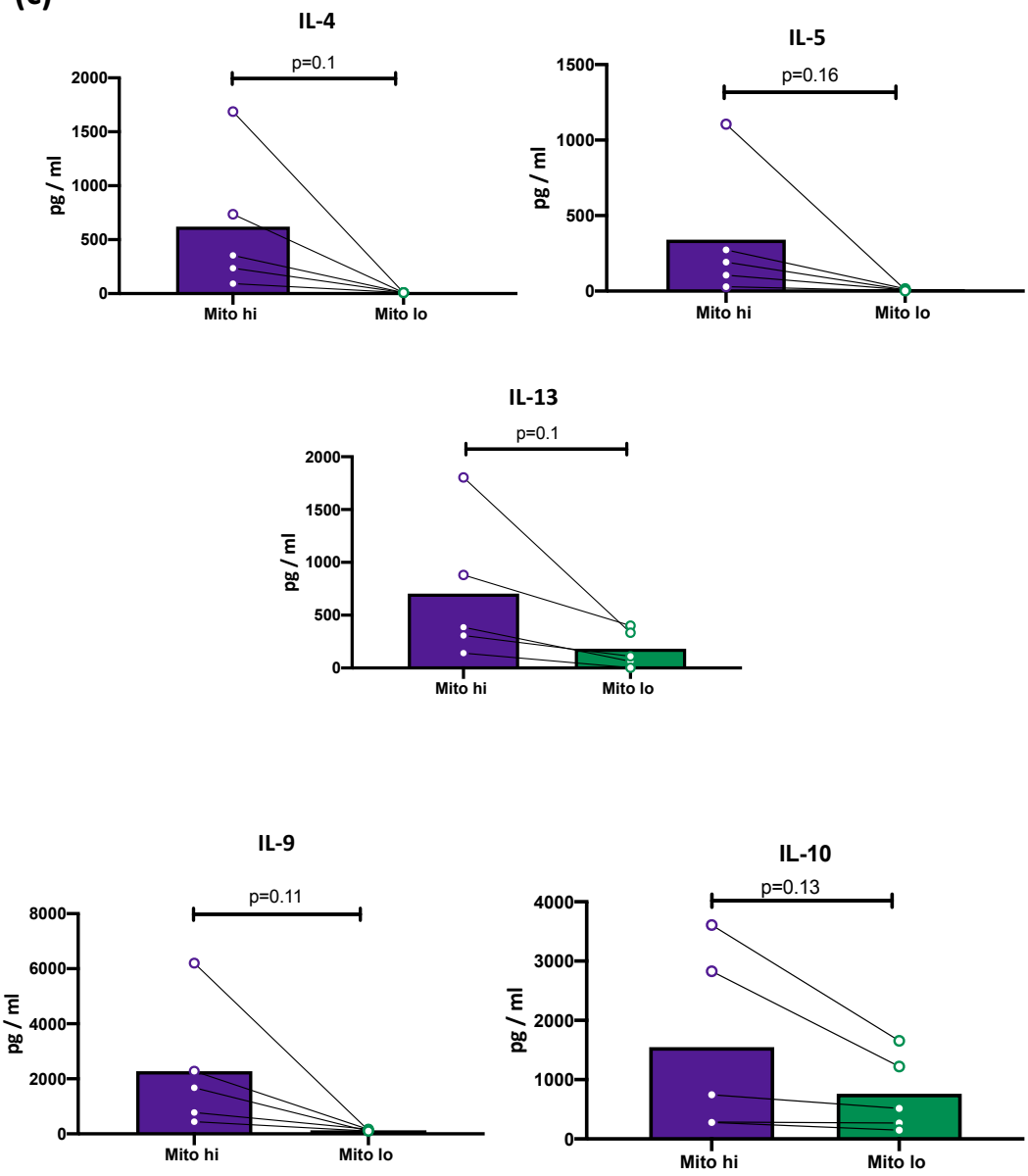

Figure 4.11 (cont.)

(d)

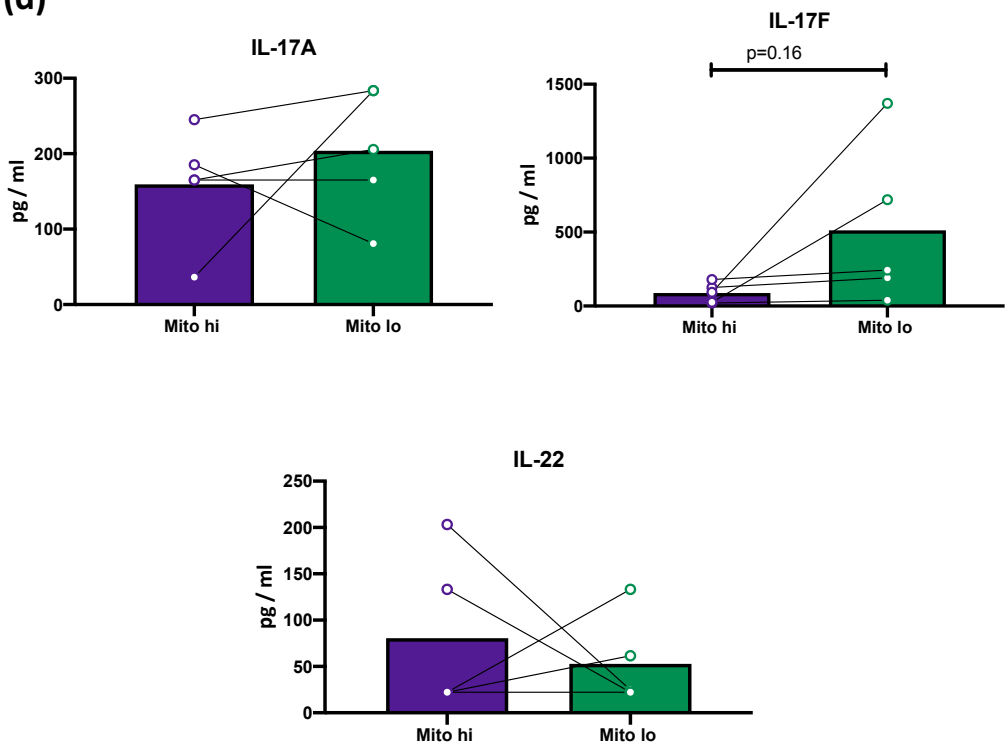

Figure 4.11. Mito^{hi} EM Tconvs produce Th2-type cytokines whilst Mito^{lo} EM Tconvs produce more Th1 and Th17-type cytokines.

Freshly isolated subsets of EM Tconvs were stimulated with anti-CD3/CD28 beads for 84h. Culture supernatants were gently removed and the concentrations of cytokines were examined by FACS using the LEGENDplex Human Th Cytokine Panel. (a) A heatmap of cytokine production level. Values represent the relative level of cytokine production between Mito^{hi} and Mito^{lo} within donors. (b) Absolute concentrations of Th1-type cytokines. (c) Absolute concentrations of Th2-type cytokines. (d) Absolute concentrations of Th17-type cytokines. Each dot represents an individual donor. Columns represent mean ± SD. *$p<0.05$ by paired t test.

Figure 4.12

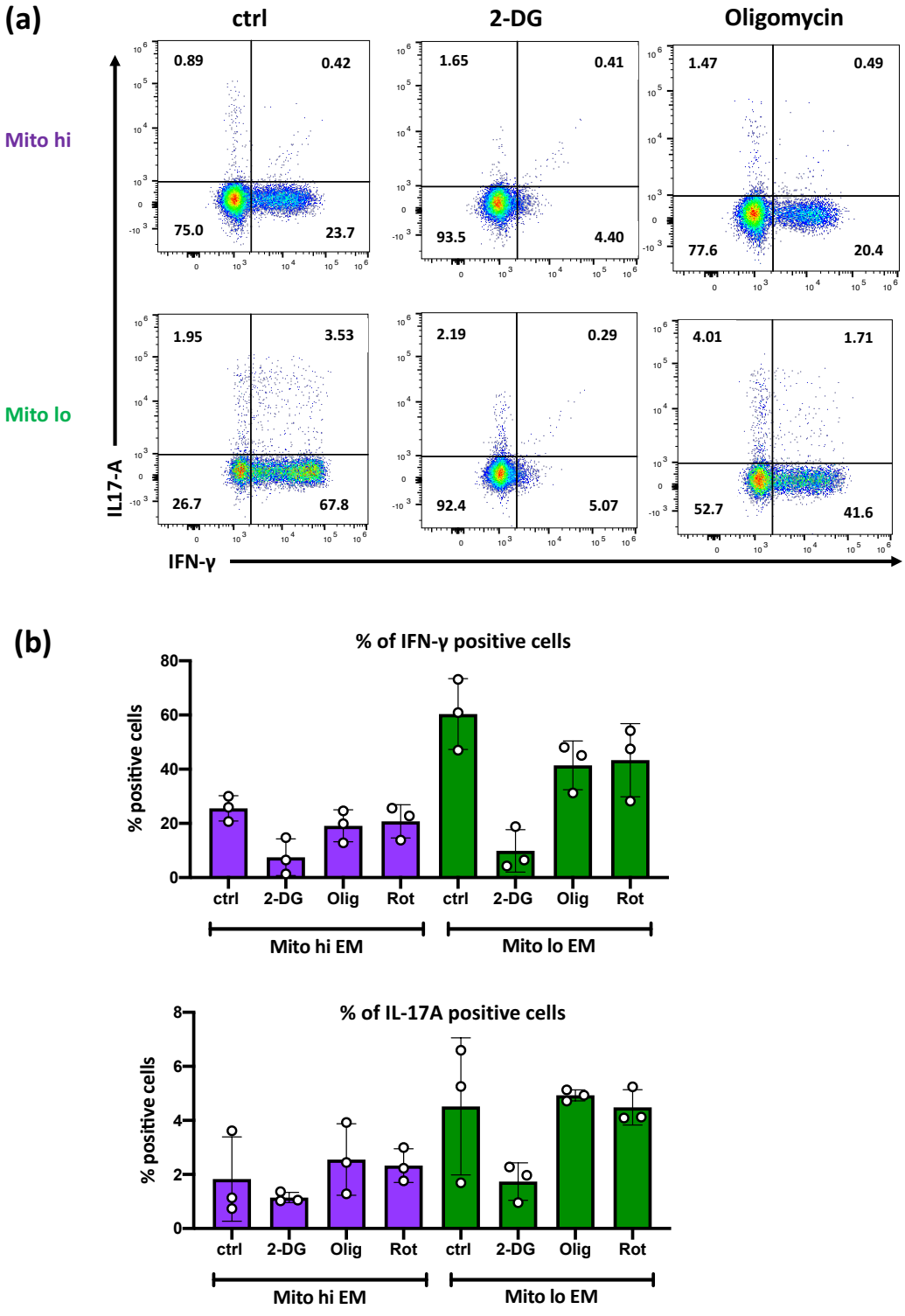
(a)
ctrl
2-DG
Oligomycin
Mito hi
Mito lo
0.89
0.42
75.0
23.7
1.65
0.41
93.5
4.40
1.47
0.49
77.6
20.4
1.95
3.53
26.7
67.8
2.19
0.29
92.4
5.07
4.01
1.71
52.7
41.6
IL17-A
IFN-γ
(b)
% of IFN-γ positive cells
% positive cells
ctrl
2-DG
Olig
Rot
Mito hi EM
Mito lo EM
% of IL-17A positive cells

Figure 4.12 (cont.)

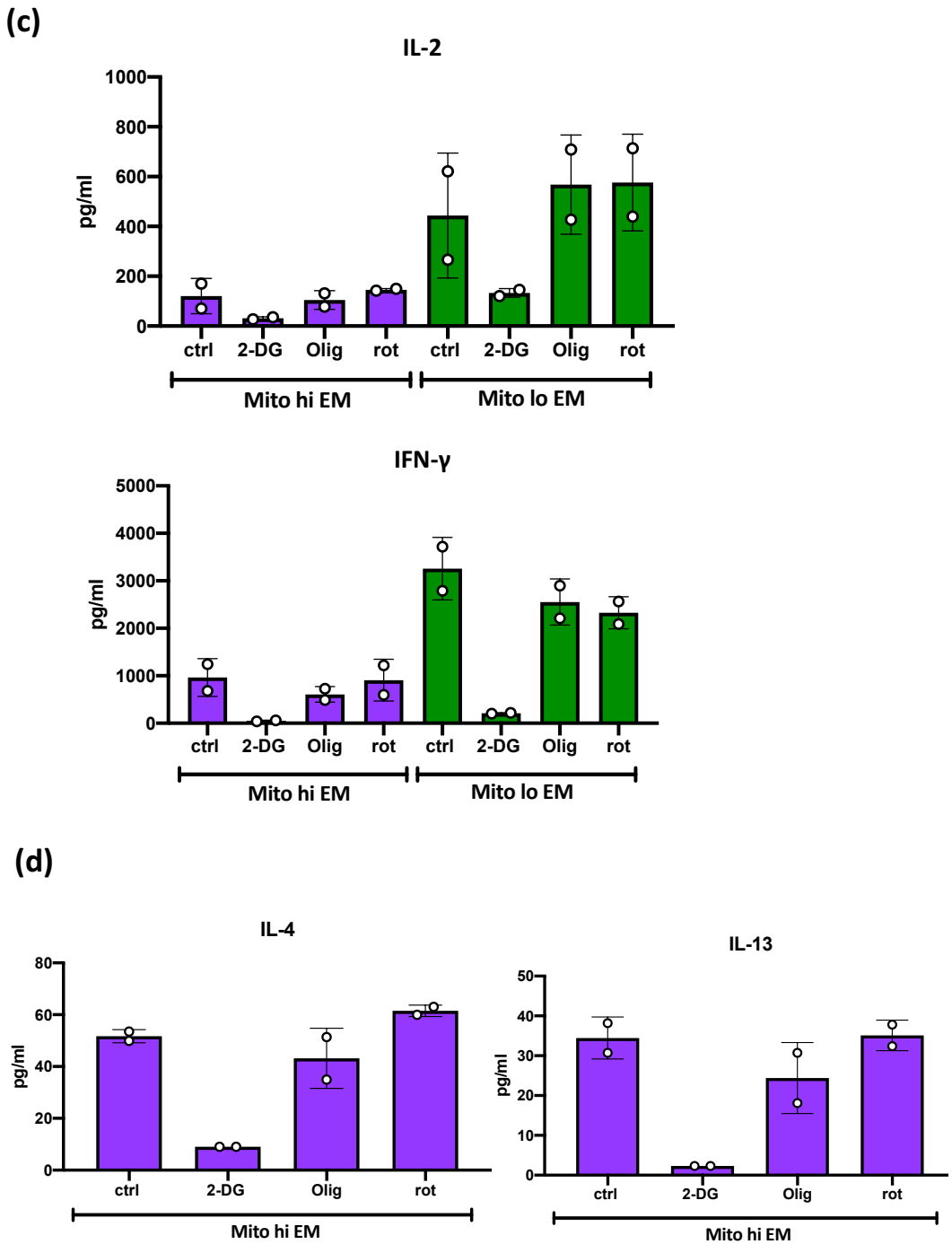

Figure 4.12. Glycolysis is required for both Mito^{hi} and Mito^{lo} cytokine production.

Freshly isolated subsets of EM Tconvs were briefly stimulated for 15h with anti-CD3/28 activating monoclonal antibody in the presence of inhibitors: 10 mM 2-DG, 2 uM oligomycin (Olig), 1 uM rotenone (Rot) or without (control), followed by PMA/ionomycin stimulation for 3h with monensin. (a and b) The cytokine production from EM Tconvs was examined by FACS. (a) A representative FACS plot from one of three independent donors. (b) A graph revealing the percentage of IFN-γ (top panel) and IL-17A (bottom panel) cells. (c and d) The quantities of cytokines were investigated using LEGENDplex Human Th Cytokine Panel. (c) A graph revealing the cytokines concentrations of the culture supernatants. IL-2 (top panel) and IFN-γ (bottom panel). (d) A graph revealing the concentration of Th-2 cytokines within the Mito^{hi} cell culture supernatant. IL-4 (left panel) and IL-13 (right panel). Each dot represents an individual donor. Columns represent mean ± SD.

Figure 4.13

(a)

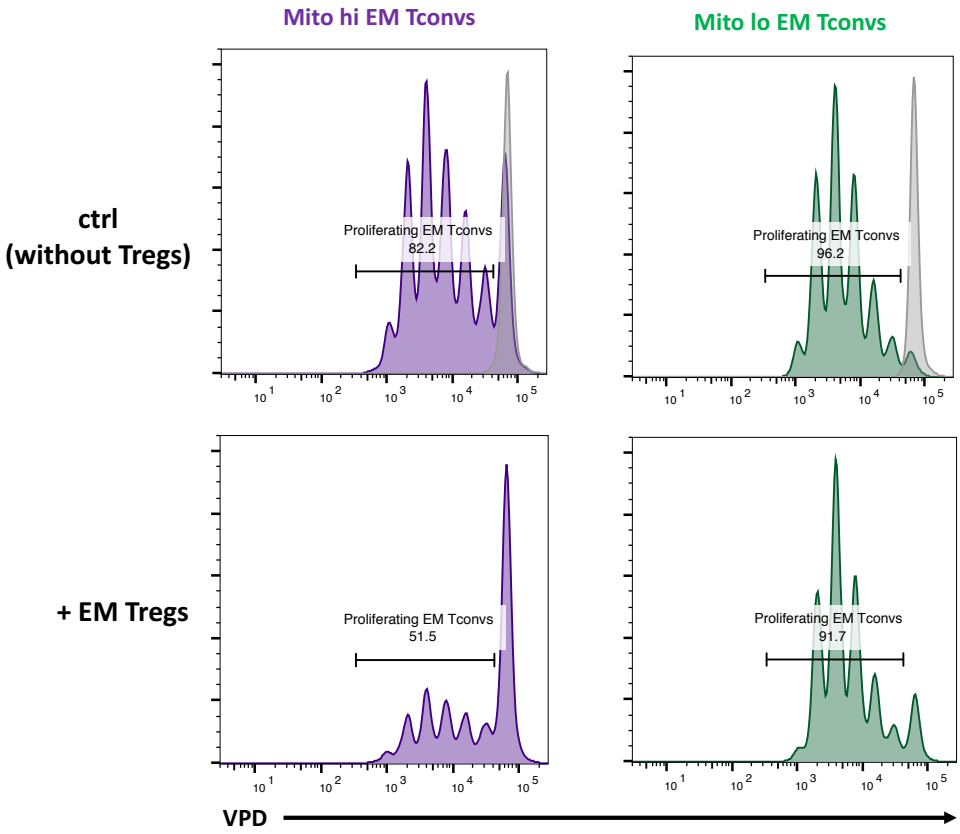

(b)

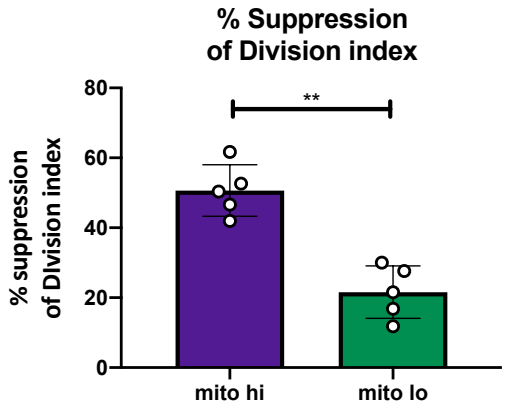

Figure 4.13

(c)

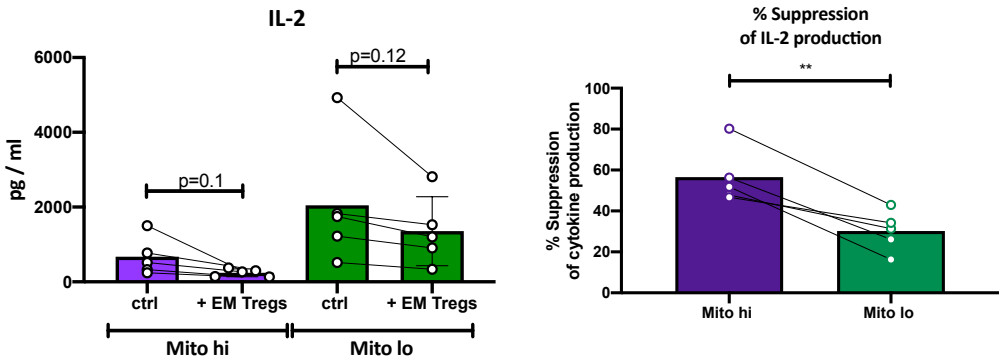

(d)

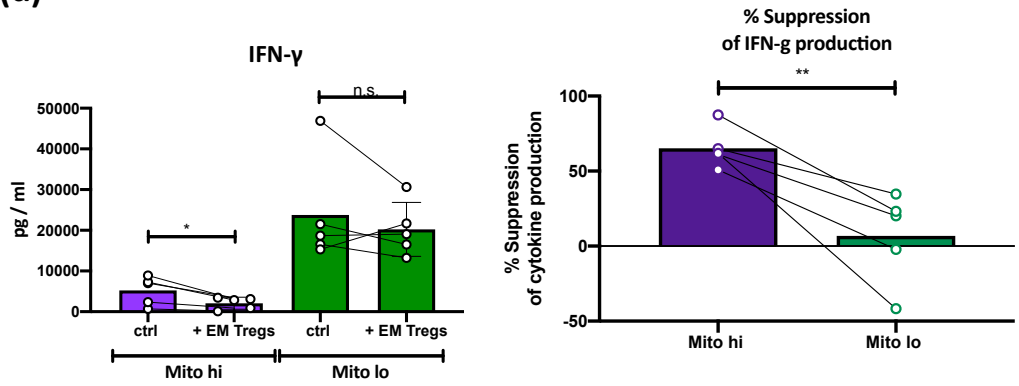

(e)

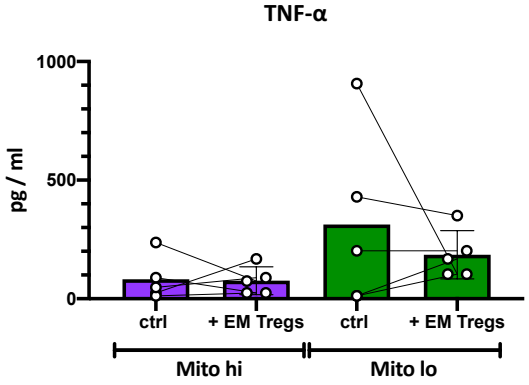

Figure 4.13 (cont.)

(f)

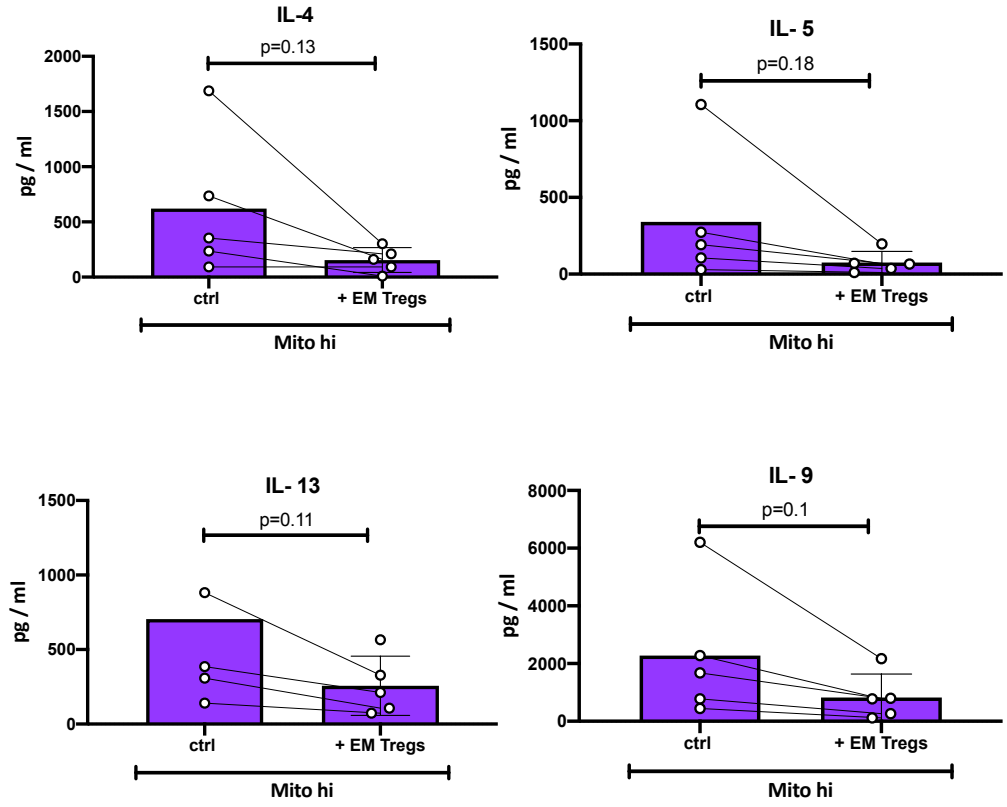

(g)

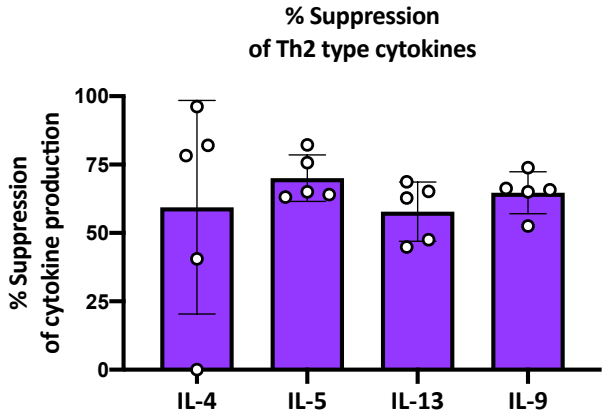

Figure 4.13 (cont.)

(h)

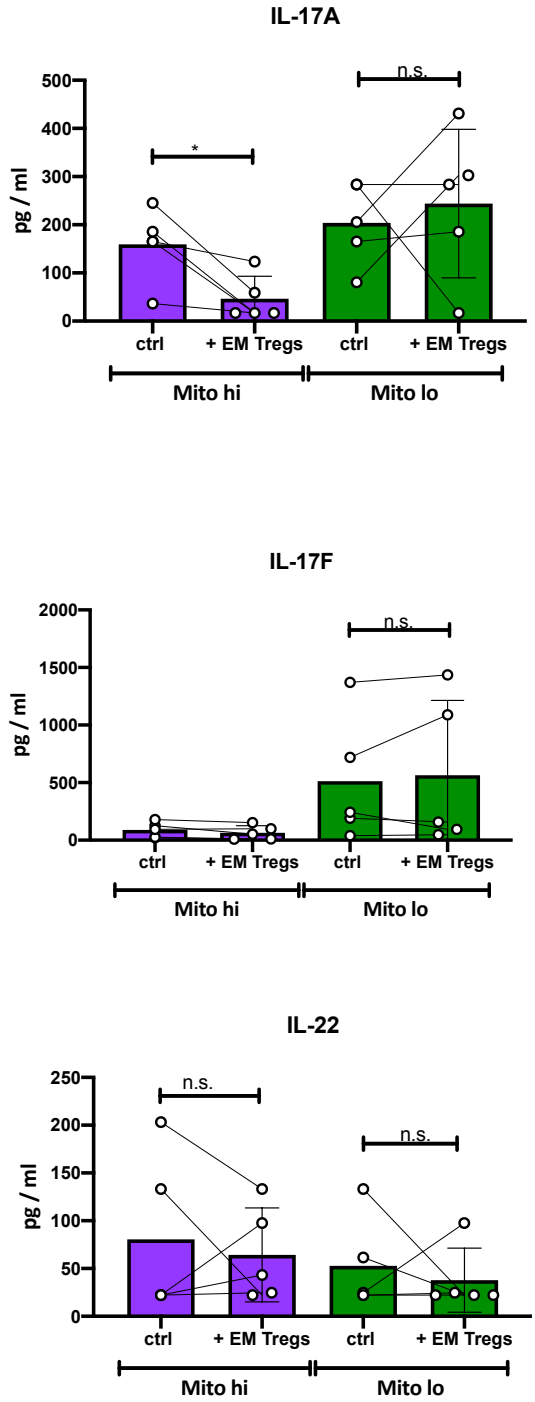

Figure 4.13 (cont.)

(i)

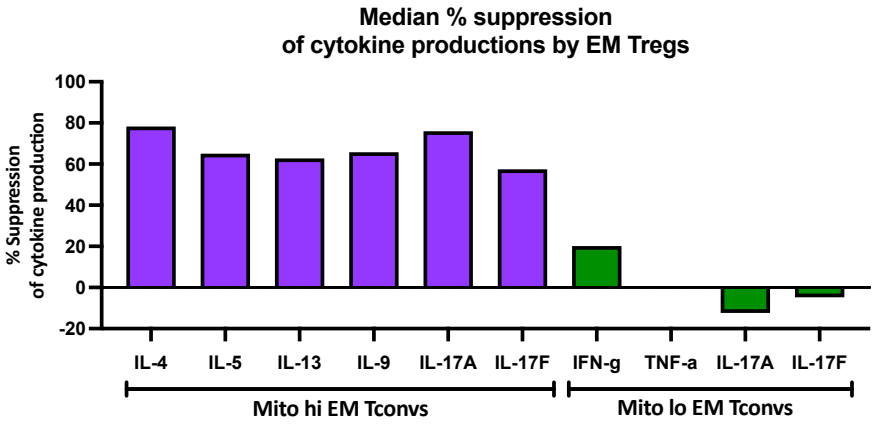

Figure 4.13. EM Tregs supress Mito^{hi}, but not Mito^{lo}, EM Tconv proliferation and cytokine production.

In vitro Treg suppression assay. VPD-stained Mito^{hi} and Mito^{lo} EM Tconvs were co-cultures for 84h with EM Tregs at a 1:1 ratio (Tconvs to Tregs) in the presence of anti-CD3/CD28 beads. (a and b) Investigation of EM Treg suppressive function by EM Tconv proliferation rate. (a) A representative histogram from one of 5 independent donors. (b) A graph revealing the percentage of suppression of division index by the presence of EM Tregs. (c and i) Quantification of the percentage suppression of EM Tconv cytokine production by EM Treg. The concentrations of culture supernatant cytokines were examined by FACS using the LEGENDplex HU Th cytokine panel. (c) Graphs revealing the absolute values of IL-2 concentration (Left) and the percentage suppression by co-culture with EM Tregs (right). (d) Graphs revealing the absolute values of IFN-γ concentration (left panel) and the percentage suppression by co-culture with EM Tregs (right panel). (e) A graph revealing the absolute concentration of TNF-α . (f) Graphs revealing the absolute concentrations of Th-2 cytokines in Mito^{hi} EM Tconv culture supernatant. (g) A graph revealing the percentage suppression of Th-2 cytokine

production from Mito^{hi} Tconvs by co-culture with EM Tregs. (h) Graphs revealing the absolute concentrations of Th-17 cytokines. (b-h) Each dot represents an individual donor. Columns represent mean ± SD. *$p<0.05$ by paired t test. (i) A summary graph showing the percentage suppression of cytokine production by co-culture with EM Tregs. Columns represent the median value of each cytokine.

Figure 4.14

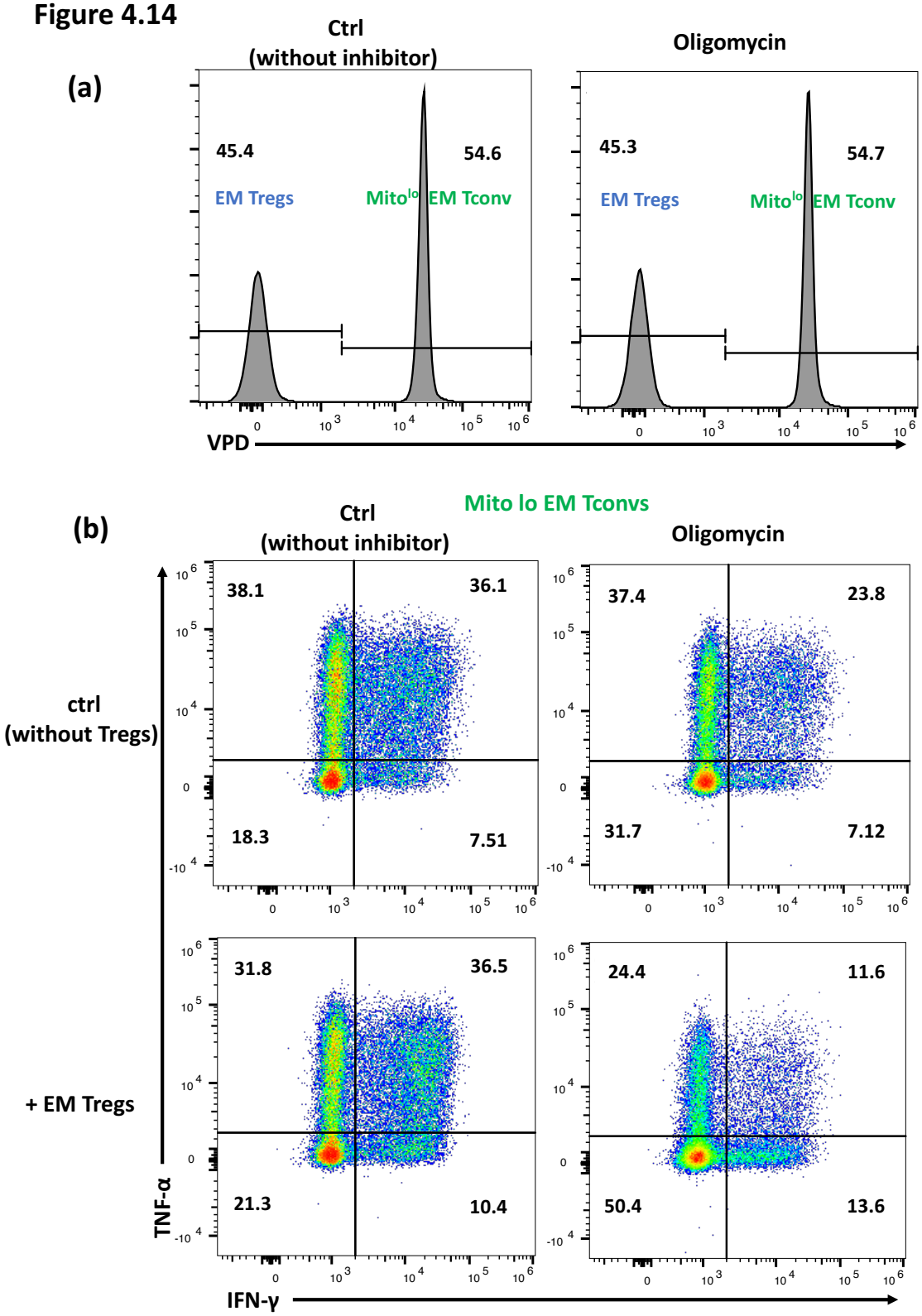
(a)
Ctrl
(without inhibitor)
Oligomycin
45.4
54.6
EM Tregs
Mito lo EM Tconv
45.3
54.7
EM Tregs
Mito lo EM Tconv
VPD
(b)
Mito lo EM Tconvs
Ctrl
(without inhibitor)
Oligomycin
ctrl
(without Tregs)
38.1
36.1
18.3
7.51
37.4
23.8
31.7
7.12
+ EM Tregs
31.8
36.5
21.3
10.4
24.4
11.6
50.4
13.6
TNF-α
IFN-γ

Figure 4.14. EM Tregs suppress Mito^{lo} EM Tconvs under OXPHOS inhibited condition.

(a and b) VPD-stained Mito^{lo} EM Tconvs were briefly stimulated by anti-CD3/28 activating monoclonal antibodies for 15h in the presence of 2 uM oligomycin or 0.02% DMSO (ctrl) with EM Tregs at a 1:1 ratio, followed by PMA/ionomycin stimulation for 3h with monensin. (a) Representative histograms illustrating the percentage of EM Tregs (VPD^{-}) and Mito^{lo} EM Tconvs (VPD^{+}) from one of two independent donors. (b) Representative FACS plots illustrating the percentage of IFN-γ and TNF-α positive cells amongst Mito^{lo} EM Tconvs from one of two independent donors.

Chapter 5: Translational strategies for enhancing human Treg suppressive function by targeting immunometabolic pathways.

5.1 Introduction

In previous chapters we revealed that activated human *ex vivo* Tregs and Tconvs in bulk have similar metabolic preferences and that Tregs require glucose to clonally expand. In agreement with these results, naïve and CM Tregs demonstrate high rates of glucose consumption, which is not distinguishable to their Tconv counterparts. On the other hand, EM Tregs show dramatically lower glucose demands compared to EM Tconvs. Thus, Tregs and Tconvs have similar metabolic demands for clonal expansion but may have different metabolic needs for their function. Importantly, both the aerobic glycolysis and OXPHOS rates were lower in EM Tregs compared to EM Tconvs demonstrating that EM Tregs are metabolically quiescent compared to EM Tconvs. Nevertheless, EM Tregs uniformly maintain a high mitochondrial mass and exhibit higher expression of pyruvate metabolism regulatory genes which fuel OXPHOS. This indicates that mitochondria may

have another important role in EM Tregs aside from their classical function as the 'powerhouse of the cell'. Unlike EM Tregs, EM Tconvs have two functionally distinct subsets based on their mitochondrial mass: Mito^{hi} and Mito^{lo} EM Tconvs. Despite these differences in mitochondrial mass, however, their effector functions are strongly reliant on glycolysis metabolism as inhibition of OXPHOS energy production through the mitochondrial ATP synthase inhibitor (oligomycin) or mitochondrial complex I inhibitor (rotenone) does not strongly supress EM Tconv cytokine production. Surprisingly, however, EM Tregs strongly enhance their suppression of Mito^{lo} EM Tconvs (demonstrated in *chapter 4* to be Treg-resistant EM Tconvs) under oligomycin-mediated OXPHOS inhibition. Thus, our previous experiments illuminate a new aspect of human T cell immunometabolism. Glucose metabolism is necessary for EM Tconv effector function, whilst the limitation of mitochondrial energy production enhances EM Treg suppression. Although data in *chapter 4* specifically examined the EM Tregs subset, this feature of OXPHOS-modulation of suppressive function may be generalisable across all Treg subsets.

The mTOR signalling pathway is key to modulating Tconv metabolism and function upon TCR-mediated activation (25, 235, 236). Importantly, we have demonstrated that mTOR signalling has a key role in Treg metabolism and that mTOR inhibition by low dose rapamycin strongly reduces both aerobic glycolysis and OXPHOS rates, and Treg proliferation (***Figure 3.7***). Low dose rapamycin selectively inhibits mTORC1 and increases Treg suppressive function (167, 244), despite of the strong reduction of metabolic rates. On the other hand, hyperactivation of mTORC1 decreases Treg suppressive function (206, 207), putatively by increasing rate of aerobic glycolysis. Indeed, Tregs with high Glut1 expression also lose their suppressive function (206). Similarly, hyperactivation of mTORC2 abolishes Tregs suppressive function with a high rate of aerobic glycolysis (211). Interestingly, selective deletion of mTORC2 in the scurfy mouse model (carrying a *foxp3* mutation) ameliorates the autoimmune phenotype (210). FOXP3 is implicated in Treg metabolism by suppressing glycolysis (204, 205), and mTORC2 deletion may restore suppressive function of Foxp3-mutated Tregs by normalising their metabolic signature. Indeed, direct glycolysis inhibition by genetic perturbation or pharmacological inhibition of glycolysis enzymes also restores the suppressive function of Foxp3-mutated Tregs

(210). Thus, it is clear that mTOR signalling decreases Treg suppressive function at least partially by enhancing Treg glycolysis. Although the mechanism(s) impairing Treg suppressive function by high rates of aerobic glycolysis remain unknown, a compensatory reduction in the rate of OXPHOS resulting from high energy production via aerobic glycolysis may at least be ruled out: firstly, we demonstrated that mTOR inhibition reduces the rates of both aerobic glycolysis and OXPHOS in human Tregs; and secondly mTORC2 deletion in Foxp3 mutated Tregs also reduces aerobic glycolysis and OXPHOS (210). This same study also reports that human Tregs isolated from patients with IPEX syndrome possess even a high OXPHOS rate. On the other hand, we have demonstrated that EM Tregs enhance their suppressive capacity under OXPHOS inhibition by oligomycin (***Figure 4.14.***). Although our data did not reveal that OXPHOS inhibition directly enhances Treg suppressive function (possibly because Tconvs became more sensitive to Treg-mediated suppression as a secondary effect of the oligomycin), others have recently reported that mitochondrial disruption in Tregs, either by pharmacological and genetic inhibition of fatty acid binding protein 5 (FABP5), increases their suppressive function (230). Taken all together, although mTOR signalling is

important to enhance Treg metabolism at least for their clonal expansion by upregulating glycolysis and OXPHOS rates, an enhanced glycolysis rate has a negative impact on Treg function. The relationship between upregulation of OXPHOS and Treg suppressive function remains unclear although inhibition of OXPHOS seems to increase Treg function.

Although enhancement of glycolysis reduces Treg suppressive function, glycolysis may nevertheless be required to maintain Treg suppressive function (320). The glycolytic enzyme enolase 1 induces an alternative non-functional FOXP3 splicing variant. Therefore, strong inhibition of glycolysis makes enolase 1 away from the glycolysis pathway, which may induce non-functional FOXP3 variant. However, this was reported in human iTreg, so this must be carefully assessed in natural Tregs (tTregs and pTregs). We previously demonstrated that glycolysis is necessary for Treg clonal expansion (***Figure 3.9.***). Moreover, Tregs require glycolysis for their emigration from SLO to peripheral tissues (217). Indeed, suppression of glycolysis within Tregs either via deletion of HIF-1α (downstream of mTORC1. mTORC1 signalling activates HIF-1α) or via

overexpression of Foxo1 (downstream of mTORC2. mTORC2 signalling inhibits Foxo1) results in the development of mice with a scurfy-like phenotype (214, 215, 321). Therefore, glycolysis has a dual role in Tregs: required both for Treg clonal expansion and migration into tissues, whilst high glycolysis rates negatively regulate Treg function.

Treg cellular therapy holds significant promise to achieve clinical tolerance, reducing or even abolishing the reliance on immunosuppressive drugs to treat autoimmune disease or prevent transplant rejection (9, 15, 16, 151). In Treg therapy to prevent allograft rejection, Tregs are expanded *in vitro* (expanded Tregs) and infused into transplant recipients. Treg cellular therapy in transplantation is a promising method, but the clinical trial revealed that the laboratory manufacture of Treg expansion can fail to achieve enough number of Tregs during the *in vitro* expansion in some patients (15, 16). Therefore, additional strategies to reduce the required Treg dose would be beneficial in Treg cellular therapy. This may potentially be achieved by targeting immunometabolism. However clearly direct administration of primary metabolic modulators directly to patient is not possible as it will affect other organs including the brain. This has been

demonstrated in animal models where pharmacological glycolysis inhibition cannot prevent mouse transplantation rejection, although glycolysis is key to maintaining T cell effector function, as the required dose could not be reached (322). On the other hand, it may be possible to reduce the Treg dose required for cellular therapy by enhancing the function of *in vitro* expanded Treg through targeting their metabolism before infusing into recipients. Reducing Treg glycolysis could potentially be one strategy as enhanced glycolysis negatively regulates Treg suppressive function, although it is also reported that Treg may require glycolysis to maintain their expression of the functional FOXP3 splice variant. Furthermore, glycolysis is required for Treg clonal expansion and tissue emigration suggesting that glycolysis-inhibited Tregs may have impaired suppressive and migratory capacity. However, our data suggests that the mitochondrial ATP synthase inhibitor oligomycin may be a good candidate to increase Treg suppressive function whilst minimising the impact on clonal expansion and tissue emigration.

The enhancement of EM Treg suppression under condition of OXPHOS inhibition suggests a new role for mitochondrial respiration in Treg suppressive function. This

observation may be translated to benefit clinical Treg cellular therapy by treating expanded Tregs with oligomycin. However, there are four outstanding questions:

1. Does the mitochondrial ATP synthase inhibitor oligomycin directly enhance bulk Treg suppressive function?
2. If so, can *in vitro* expanded Tregs also be more suppressive after oligomycin treatment?
3. Why do oligomycin-treated Tregs have a higher suppressive function?
4. Can superior immunosuppressive function after oligomycin treatment be observed *in vivo*?

5.1.1 Chapter aim

The aim of this chapter is to investigate how mitochondrial ATP synthase inhibition alters human Treg suppressive function and to analyse potential translational strategies in expanded Tregs for cell therapy.

5.2 Mitochondrial ATP synthase inhibition enhances human *ex vivo* Treg immunosuppressive function.

We revealed that EM Tregs gain the ability to suppress Treg-resistant Mito^{lo} EM Tconvs when treated with oligomycin (***Figure 4.14***). However, it is not clear whether this resulted from Tregs gaining a higher suppressive function or from Mito^{lo} EM Tconvs becoming more sensitive to Treg suppression. Moreover, it is also unclear whether the suppressive function of Tregs can be generally potentiated, or specifically potentiated against certain cell subsets. To investigate these questions, we extended our experiments investigating suppression of *ex vivo* bulk Tregs against bulk CD4 and CD8 Tconvs, utilising oligomycin pre-treated Tregs. We first pre-treated freshly isolated human Tregs (*ex vivo* Tregs) with the irreversible mitochondrial ATP synthase inhibitor oligomycin or 0.2% DMSO (control) for 2 hours, washed cells intensively, and co-incubated the oligomycin-treated Tregs or control Tregs with VPD-stained PBMC in fresh medium containing anti-CD3/CD28 beads for 84h to assess the ability for Treg to suppress CD4 and CD8 T cell proliferation. Control Tregs not strongly but clearly suppressed both CD4 and CD8 T cells proliferation (***Figure 5.1.a***). The weaker

immunosuppressive function of *ex vivo* Tregs compared to *in vitro* expanded Tregs has been previously reported by our group and others (136, 168). However, oligomycin-treated Tregs strongly suppressed both CD4 and CD8 T cells proliferation indicating that oligomycin pre-treatment dramatically increased the suppressive function of freshly-isolated Treg against both CD4 and CD8 T cells (***Figure 5.1.a***). To investigate whether oligomycin-treated Tregs also suppress T cell cytokine production from both CD4 and CD8 T cells, we shortened the incubation time and checked the percentage of IFN-γ and IL-17A producing cells using FACS. The percentages of both IFN-γ and IL-17A producing CD4 T cells were dramatically reduced by co-incubation with oligomycin-treated Tregs compared to control Tregs (***Figure 5.1.b).*** Similarly, the percentage of IFN-γ CD8 T cells was also significantly reduced (***Figure 5.1.c)***. Thus, oligomycin pre-treatment dramatically increases human Tregs suppressive function against both CD4 and CD8 T cells.

Next we wondered if the suppressive function gained by oligomycin-treated Treg was a direct effect on T cells or an indirect effect mediated by, for example, myeloid cells

present within PBMCs. To investigate this, we co-incubated the pre-treated Tregs with VPD-stained purified CD4 Tconvs in the presence of anti-CD3/CD28 beads. Oligomycin-treated Tregs showed significantly higher suppressive function compared to control Tregs indicating that the gained suppressive function was a direct effect (***Figure 5.2 a and b***).

We concluded that OXPHOS inhibition by the mitochondrial ATP synthase inhibitor oligomycin directly increases the suppressive function of bulk human *ex vivo* Treg. This potentiated suppressive function works equally on CD4 and CD8 T cells. The suppression of CD4 Tconvs was mediated directly and not by an intermediate cell population.

5.3 Mitochondrial ATP synthase inhibition induces production of soluble immunosuppressive factors from human *ex vivo* Tregs.

We revealed that mitochondrial ATP synthase inhibition directly increased human Treg suppressive function. Next, we wondered by which suppression mechanisms Tregs

gained this potentiated inhibition. First we analysed Treg phenotype examining canonical Treg functional markers including FOXP3, CD25, CTLA-4 and PD-1 by FACS (85, 86). Oligomycin-treated Tregs and control Tregs were first incubated for 40h in the presence of anti-CD3/CD28 beads so that their phenotype was assessed during an activated state. Both Treg groups maintained a high percentage of FOXP3 and CD25 double positive cells indicating oligomycin does not change Treg stability (***Figure 5.3.a***). Unexpectedly, however, the MFIs of both markers in the oligomycin-treated Tregs were significantly lower than control Tregs demonstrating that the expression levels of FOXP3 and CD25 were reduced by mitochondrial ATP synthase inhibition (***Figure 5.3.a***). Similarly, both CTLA-4 and PD-1 expression levels were also reduced after OXPHOS blockade. Thus, suppressive function gained by Treg after oligomycin treatment is not dependent on FOXP3 and neither relates to IL-2 depletion through CD25 nor relates to known contact-dependent mechanisms of suppression such as CTLA-4 and PD-1.

Mechanisms of Treg suppression are classically divided into contact-dependent and contact-independent (85-87). Contact-dependent mechanisms include CTLA-4 and PD-1

which suppress target cell function by directly binding to their respective receptors, whilst contact-independent mechanisms include production of immunosuppressive soluble factors such as cytokines and modulation of extracellular factors such as adenosine or IL-2. Although we did not investigate all Treg markers relating to contact-dependent suppressive mechanisms, lower expression of FOXP3, CTLA-4 and PD-1 in oligomycin-treated Tregs prompted us to examine soluble factors produced by oligomycin-treated Tregs. To investigate this, we first incubated oligomycin-treated or control Tregs for 48h in fresh medium with anti-CD3/CD28 beads before gently removing Treg culture supernatants (***Figure 5.4.a***). The Treg culture supernatants were then mixed with VPD-stained CD4 T cells suspended in the same volume of fresh RPMI along with anti-CD3/CD28 beads for 84h to assess the function of immunosuppressive soluble factors produced by Tregs. The supernatant from control Treg culture did not show any suppression (***Figure 5.4.b***) confirming the previously-reported finding that Treg *in vitro* suppression is contact dependent (83, 152). However, the culture supernatant from oligomycin-treated Tregs strongly reduced CD4 T cells division index indicating that OXPHOS inhibition at mitochondrial ATP synthase blockage induces the production of

immunosuppressive soluble factors from Tregs.

We then sought to identify which soluble factor oligomycin-treated Tregs generated. FABP5-inhibited Tregs have significantly lower OXPHOS due to mitochondrial disruption but possess stronger immunosuppressive function from potentiated IL-10 production (230). We therefore first checked the amount of IL-10 in the Treg culture supernatant using ELISA. As expected, oligomycin-treated Tregs produced a significantly higher amount of IL-10 compared to control (***Figure 5.4.c Left***). However, the absolute concentration of IL-10 in the culture supernatant remained low and importantly, the variability between donors was larger than the variability between pre-treatment conditions (***Figure 5.4.c Right***). As the incubation with Treg supernatants did not show notable donor dependent difference (***Figure 5.4.b***), we concluded that its effect was unlikely to be mediated by IL-10.

Next, we investigated adenosine which is another known soluble immunosuppressive factor. Extracellular ATP and ADP are converted by the cell surface expressed

ectonucleotidase CD39 into cAMP which is then converted by CD73 into adenosine (135). CD39 is highly expressed on Tregs although CD73 expression is limited on human *ex vivo* Tregs (86, 136). To investigate the adenosine production capacity of oligomycin-treated Tregs, we quantified the surface expression of CD39 and CD73 on Tregs by FACS. The expression of CD39 is not distinguishable between control and oligomycin-treated Tregs, and more importantly CD73 expression was strongly limited in both conditions (***Figure 5.4.c***). Therefore, we concluded that the potentiated Treg immunosuppression was not due to adenosine.

Taken together, the strong immunosuppressive capacity of Tregs observed after mitochondrial ATP synthase inhibition is due to the production of FOXP3-independent soluble factors. Although oligomycin-treated Tregs produced higher amounts of IL-10, the absolute amount of IL-10 production remains low. Oligomycin treatment did also not change CD39 and CD73 expression levels. Therefore, neither IL-10 nor adenosine are the immunosuppressive soluble factors. Thus, mitochondrial ATP synthase inhibition by oligomycin induces Tregs to produce strong immunosuppressive soluble factors other

than IL-10 and adenosine.

5.4 Mitochondrial ATP synthase inhibition induces the production of immunosuppressive small extracellular vesicles (EVs) from human *ex vivo* Tregs.

Human Tregs gained potentiated immunosuppressive function due to the production of soluble factors other than IL-10 and adenosine after pharmacological mitochondrial ATP synthase inhibition. To investigate the responsible soluble factors we first fractioned the Treg culture supernatant based on the size of factors. Tregs culture supernatants were fractionated using 100 kDa Amicon ultra centrifugal filter into over 100 kDa and under 100 kDa fractions. The supernatants containing the molecules lower than 100 kDa fraction were further fractionated by 3 kDa filter. Thus, we divided the culture supernatants into three fractions: supernatants containing the substances over 100 kDa, between 100 kDa and 3 kDa and lower than 3 kDa (***Figure 5.5.a***). The contents of interest in the fraction between 100 kDa and 3 kDa were immunosuppressive cytokines such as

IL-10, IL-33 and IL-35, whilst the fraction over 100 kDa contained proteins larger than cytokines and extracellular vesicles (EVs) (323, 324). Adenosine is a smaller molecule than cytokines with a size under 3 kDa (325). Although we intensively washed Tregs after oligomycin pre-treatment, it is possible that intracellular oligomycin leaked out from Tregs during the 48h cultivation. As such oligomycin may also be present under the 3 kDa fraction (326). The fractionated supernatants were mixed with VPD-stained CD4 T cells in fresh RPMI in a ratio of one part supernatant to three parts cells to investigate the potency of T cell suppression. Surprisingly, only the >100 kDa fraction strongly suppressed CD4 T cell division index, whilst fractions containing molecules between 100 kDa and 3 kDa and <3 kDa did not show any suppression (***Figure 5.5.b***). These data completely exclude the involvement of either cytokines or small molecules such as adenosine in the strong immunosuppression observed in oligomycin-treated Tregs, instead revealing that macromolecule(s) over 100 kDa are responsible.

Next we investigated whether the macromolecules are proteins or other molecules such as EVs. We treated the Treg culture supernatants with proteinase K which was then heat

inactivated prior to the addition of CD4 T cells in the ratio of one part supernatant to three parts cells. Although treatment of the supernatant from control Treg with proteinase K reduced the T cell division index, this was most likely due to the digestion of other important substances required by T cells such as a growth factors (***Figure 5.5 c***). Importantly, the oligomycin-treated Treg culture supernatant still possessed a significantly higher immunosuppressive effect compared to control Treg culture supernatant after proteinase K treatment indicating that the immunosuppressive soluble factors are not proteins.

We have so far demonstrated that mitochondrial ATP synthase inhibition induces the production of immunosuppressive soluble factor(s) from human Tregs which is over 100 kDa and not a protein. These results strongly suggest that EVs may be responsible for their potentiated immunosuppression. EVs are membrane-bound vesicles containing numerous substances such as protein, DNA, mRNA and miRNA, and may be classified into three categories based on their size: 1) apoptotic bodies, 2) large extracellular vesicles and 3) small extracellular vesicles (formerly known as exosomes) (140-142, 327).

Apoptotic bodies are the largest vesicles up to 5,000 nm in diameter and are produced from cells undergoing apoptosis. There are no specific cut-off values distinguishing large from small EVs although most researchers arbitrarily define a value between 100 and 200 nm (140). The main constituent of large EVs fraction is microvesicle, which is now characterised as one of ectosomes (141, 143). Ectosomes and exosomes are generated separately: whilst ectosomes are vesicles pinched off from the plasma membrane, exosomes are derived from endosomal compartments. Apoptotic bodies, large EVs and small EVs are conventionally isolated using differential centrifugation (142, 327). To investigate which EVs are responsible for the strong immunosuppressive function of oligomycin-treated Treg, we isolated apoptotic bodies and large EVs from culture supernatants using differential centrifugation methods (***Figure 5.5.d***), and then combined these with VPD-stained CD4 T cells in a proliferation assay. Apoptotic bodies and large EVs isolated from the oligomycin-treated Treg culture supernatant did not reduce CD4 T cells division index. However, the remaining components of the culture supernatants which include small EVs still demonstrated strong immunosuppressive function implicating small EVs in the strong immunosuppressive property of oligomycin-

treated Tregs (***Figure 5.5.e***).

We demonstrate that strongly immunosuppressive soluble factors produced by mitochondrial ATP synthase inhibited Tregs were large particles but not proteins suggesting instead that they may be EVs. Our differential centrifugation experiments excluded apoptotic bodies and large EVs strongly suggesting that immunosuppressive small EVs (formerly known as exosomes) are instead responsible. To investigate the role of small EVs directly, we depleted small EVs from Treg culture supernatants using the Norgen Exosome depletion kit. After small EV depletion, the culture supernatants were mixed with VPD-stained CD4 T cells in a proliferation assay. As expected, depletion of small EVs completely abolished the immunosuppressive properties of oligomycin-treated Treg culture supernatant. This directly proves that the mitochondrial ATP synthase inhibitor induces immunosuppressive small EVs production by human Tregs (***Figure 5.6 a and b***). Therefore, we concluded that human *ex vivo* Tregs start producing immunosuppressive small EVs when their mitochondrial ATP synthase is inhibited.

5.5 Mitochondrial ATP synthase inhibited Tregs do not produce a higher quantity of small EVs but instead synthesise a different type of small EVs.

We revealed that human Tregs with mitochondrial ATP synthase inhibition by oligomycin begin producing robust immunosuppressive small EVs. Several researchers have reported the immunosuppressive function of Treg-derived small EVs (138, 144, 146, 148). However, Treg culture supernatant without oligomycin treatment (control Tregs) do not demonstrate any strong suppressive effect indicating that the small EVs do not have a key role in (control) Treg suppressive function in our *in vitro* setting. This is most likely due to a lower quantity of small EVs compared with other researchers' reports. However, Tregs with mitochondrial ATP synthase inhibition produced strongly immunosuppressive small EVs in our *in vitro* setting. We next wondered if the strong immunosuppression we observed was due to production of a higher quantity of small EVs or was due to qualitatively different small EVs with a higher immunosuppressive function. We used the MACSPlex exosome kit to quantitate the production of small EVs by oligomycin-treated Treg (***Figure 5.7.a***). Treg culture supernatants were first mixed with MACSPlex Capture beads which recognise specific surface markers of small EVs. The small EVs captured by

MACSPlex Capture beads were then semi-quantified by fluorescent intensity following staining with anti-CD9, CD63 and CD81 tetraspanins detection antibodies; small EVs must express one of these tetraspanins due to their endosomal origin (140, 328). First we investigated which tetraspanins Treg-derived small EVs express by comparing the intensity of the detection antibody bonded to small EVs. CD9-expressing small EVs were neither detected in the control nor in the oligomycin-treated Treg culture supernatants, whilst expression of CD63 and CD81 was higher than isotype control capture beads. This indicates that both control and oligomycin-treated small EVs are $CD63^+$ and/or $CD81^+$ (***Figure 5.7.b***). Then we checked the quantity of both $CD63^+$ and $CD81^+$ small EVs produced by Tregs. Control Tregs produced a marginally (yet significantly) higher amount of both $CD63^+$ and $CD81^+$ small EVs compared with oligomycin-treated Tregs (***Figure 5.7. b and c***). To confirm this we semi-quantified the amount of small EVs using the Exosome-Human CD81 Flow Detection Reagent. Here, small EVs in culture supernatants are captured by anti-CD81 capture beads and then detected by anti-CD81 antibodies. Unlike the previous experiment utilising the MACSPlex kit, the Exosome-Human CD81 Flow detection regent demonstrated a similar quantity of $CD81^+$ small EVs between control

and oligomycin-treated Treg culture supernatants (***Figure 5.7.d***). This result was most likely due to the lower sensitivity of the kit compared with MACSPlex, and suggests that the amount of small EVs produced by control and oligomycin-treated Tregs does not differ significantly. Taken together, mitochondrial ATP synthase inhibited Tregs by oligomycin do not produce a higher quantity of small EVs. On the contrary, oligomycin-treated Tregs seem to produce slightly fewer small EVs, although the magnitude of the reduction is negligible.

Next, we further investigated the surface marker phenotype of small EVs produced by control and oligomycin-treated Tregs detected by the MACSPlex exosome kit. Both Tregs with and without oligomycin treatment produced small EVs expressing same types of surface markers with a high amount of $CD2^+$ and HLA-$DRDPDQ^+$ small EVs. The absolute production of all types of small EVs was generally lower in oligomycin-treated Tregs except for those expressing CD3 and CD25 (***Figure 5.8.a***). Because the MACSPlex exosome kit is highly sensitive and can quantitate even small differences in the production of small EVs between control and oligomycin-treated Treg culture

supernatants, the analysis is biased by the lower small EV production by oligomycin-treated Tregs. To analyse which small EVs oligomycin-treated Tregs preferentially produced, we therefore normalised the values of each EV to the mean value of CD63 and CD81 after exclusion of small EVs with values lower than isotype or medium control (a medium control was used to detect background noise and was generated by incubating medium at the same time as Tregs but without cells) (***Figure 5.8.b***). Small EVs derived from control Tregs highly expressed CD4 or CD24, whilst small EVs derived from oligomycin-treated Tregs expressed CD3, CD25, CD41b, CD45 or CD133/1 more highly than the small EVs produced by control Tregs. These data indicate that mitochondrial ATP synthase inhibition by oligomycin skews Treg small EV production from a $CD4^+$ and/or $CD24^+$ phenotype towards a $CD3^+$, $CD25^+$, $CD41b^+$, $CD45^+$ and/or $CD133/1^+$ phenotype

We conclude that mitochondrial ATP synthase inhibition by oligomycin does not enhance the quantity of small EV production from Tregs, indicating instead that the quality of the small EVs are dramatically changed by the treatment. Whilst we did not analyse the

components of small EVs directly, the skewed cell surface markers supports the idea that oligomycin-treated Tregs produce qualitatively different type of small EVs.

5.6 Mitochondrial ATP synthase inhibition induces the production of immunosuppressive small EVs by *in vitro*-expanded Tregs.

We showed that *ex vivo* human Tregs begin producing immunosuppressive small EVs after treatment with the irreversible mitochondrial ATP synthase inhibitor oligomycin. This result opens up a new therapeutic approach for Treg cellular therapy in patients requiring immunosuppression (9, 15, 16, 151). In Treg cellular therapy, Tregs are isolated from the patient, expanded *in vitro* and subsequently re-infused to the donor. One of main limitations to this method is that polyclonally expanded Tregs may be required at high doses to control aberrant immune responses. Because the Treg fold expansion varies between donors, Tregs from some patients may fail to expand sufficiently for therapeutic use (15, 16). Because oligomycin treatment dramatically increases the immunosuppressive properties of Tregs, pre-treatment of expanded Treg with

oligomycin prior to infusion may significantly reduce the required Treg dose (***Figure 5.9.a***). Moreover, as oligomycin-treated Tregs produce immunosuppressive small EVs, a second strategy may be to use the immunosuppressive small EVs (autologous or from a 3rd party person) instead of directly infusing Tregs (***Figure 5.9.b***).

Although oligomycin pre-treatment of expanded Tregs may deliver huge benefits in terms of the required Treg numbers, we did not directly prove that expanded Tregs also increase their suppressive function from oligomycin treatment in a similar manner to *ex vivo* Tregs. To investigate this, we assessed the suppressive function of oligomycin-treated expanded Tregs using an *in vitro* suppression assay. We pre-treated expanded Tregs in same way as before, washed the cells intensively, and then co-incubated either oligomycin-treated expanded Tregs or control expanded Tregs with VPD-stained CD4 T cells in the presence of anti-CD3/CD28 beads. Unlike *ex vivo* Tregs (***Figure 5.2.a***), expanded Tregs without treatment demonstrated a potent ability to prevent CD4 proliferation; however, oligomycin pre-treatment further enhanced Treg immunosuppressive function (***Figure 5.10.a and b***). Compared with *ex vivo* Tregs (***Figure***

5.2.b), the suppression of expanded Tregs demonstrated more donor-dependent variability. Our data did not therefore show significance at the ratio of 1:1 and 1:4 with the number of donors tested (***Figure 5.10.b Left***). However, comparing of Treg suppression within each donor revealed the robust tendency of expanded Tregs to display potentiated immunosuppressive function after oligomycin treatment (***Figure 5.10.b Right***).

Next, we investigated whether expanded Tregs also produced immunosuppressive small EVs after mitochondrial ATP synthase inhibition. We first investigated if oligomycin-treated expanded Tregs produced soluble immunosuppressive factors using Treg culture supernatants as previously described (***Figure 5.4.a***). In a similar manner to the *ex vivo* Treg culture supernatant (***Figure 5.4.b***), our control expanded Treg culture supernatant did not impact the CD4 T cell division index confirming that the enhanced immunosuppressive function of expanded Tregs is due to contact-dependent mechanisms (***Figure 5.11.a***). Importantly, culture supernatant derived from oligomycin-treated expanded Tregs revealed strong suppressive function. Therefore, mitochondrial

ATP synthase inhibition by oligomycin induces production of soluble immunosuppressive factors from expanded Tregs. Next, we again investigated if these suppressive soluble factors had a mass over 100 kDa using the Amicon ultra centrifugal filter. As expected, only the fraction containing molecules with a mass greater than 100 kDa from the oligomycin-treated Treg supernatant showed strong suppression of CD4 T cell proliferation (***Figure 5.11.b***). Lastly, we directly examined whether the immunosuppressive property of the supernatant was due to small EVs by depleting these with the Norgen exosome depletion kit before adding this to VPD-stained CD4 T cells in a proliferation assay. As we observed in our *ex vivo* Treg experiment (***Figure 5.6.a***), small EV depletion strongly reduced the immunosuppressive property of oligomycin-treated expanded Treg culture supernatant (***Figure 5.11.c***). To validate these findings we also used a second depletion method with the MACS exosome isolation kit. Here, we first applied immunomagnetic beads binding to CD9, CD63 and CD81 tetraspanins and then removed small EVs expressing $CD9^+$, $CD63^+$ and/or $CD81^+$ through passing the supernatant through a magnetic field/column. The immunosuppressive function of this depleted culture supernatant was assessed by mixing with VPD-stained CD4 T cells in a

proliferation assay. CD9, CD63 and CD81 small EVs removal strongly decreased the immunosuppressive function of oligomycin-treated expanded Treg culture supernatant (***Figure 5.11.d***) confirming that mitochondrial ATP synthase inhibition by oligomycin induces production of immunosuppressive small EVs from expanded Tregs.

We conclude that oligomycin treatment strongly increases *in vitro* expanded Treg suppressive function by inducing the production of immunosuppressive small EVs. These data support the viability of either using oligomycin to reduce the required dose of expanded Tregs in Treg cellular therapy or even exploring therapeutic use of the small EVs isolated from *in vitro* culture supernatant.

5.7 The immunosuppressive properties of small EVs derived from mitochondrial ATP synthase inhibited Treg are donor-independent and therefore may potentially be used 'off-the-shelf'.

We revealed that both *ex vivo* and *in vitro* expanded Tregs produce immunosuppressive small EVs when their mitochondrial ATP synthase is inhibited by oligomycin. The immunosuppressive properties of small EVs examined inhibited autologous CD4 T cell proliferation. We next explored whether small EVs are able to suppress T cells from a third-party donor, because donor independent suppression would allow us to use the therapy 'off-the-shelf' (***Figure 5.9.b***). To investigate this, we added oligomycin-treated Treg supernatant to VPD-stained CD4 T cells from either same (autologous) donor or different (allogeneic) donor in the presence of anti-CD3/CD28 beads. Surprisingly, the division indices of CD4 T cells of both autologous and allogeneic $CD4^+$ cells were equally suppressed by the small EVs produced by oligomycin-treated *ex vivo* Treg (***Figure 5.12.a***) and expanded Tregs (***Figure 5.12.b***). These data strongly suggest that small EVs derived from oligomycin-treated Tregs could be used 'off-the-shelf' to control aberrant immune reactions in autoimmunity and transplant rejection.

Lastly, we examined whether the donor-independent immunosuppressive properties of the small EVs derived from oligomycin-treated Tregs could be observed *in vivo* using a mouse peritoneal lavage model. VPD-stained human PBMC were injected into the peritoneal cavities of mice together with the 100 kDa fraction of culture medium either without cells (medium control), with culture supernatants from control (0.2% DMSO), or with oligomycin-treated expanded Tregs. Tregs were from different donor of PBMC. The VPD-stained human PBMC were harvested at day 5 by lavage of the peritoneal cavity and the proliferation rates of both CD4 and CD8 were examined by FACS. However, unfortunately the T cells in this preliminary experiment did not proliferate well compared with *in vitro* stimulation (***Figure 5.13.a and b***). Moreover, the proliferation of both CD4 and CD8 T cells varied substantially between mice (***Figure 5.13.a***). Therefore, it was hard to draw conclusions in this experiment. Further experiments investigating in vivo effectiveness of oligomycin-pretreated Tregs and small EVs are needed.

Taken together, small EVs derived from mitochondrial ATP synthase inhibited Tregs by oligomycin suppress T cell proliferation donor independently. This opens a potential new

therapy strategy by preparing and banking Treg-derived immunosuppressive small EVs to treat patients with acute immune overactivation. Although our *in vivo* study was inconclusive and did not show obvious immunosuppressive effects due to failed T cell proliferation in our positive control, we plan to explore this possibly in future experiments.

5.8 Discussion

Here we have demonstrated that OXPHOS perturbation with the mitochondrial ATP synthase inhibitor oligomycin enhances Treg suppressive function through the induction of immunosuppressive small EVs, opening up a potential new therapeutic avenue to translate Treg immunosuppressive capabilities into clinics (***Figure 5.9***). Whilst the main suppression of our mitochondrial ATP synthase inhibited Treg is caused by small EVs in the *in vitro* setting, oligomycin-treated Tregs also increase their IL-10 production (***Figure 5.4.c***). Thus, inhibition of mitochondrial ATP synthase enhances Treg suppressive function by multiple mechanisms. However, the expression of FOXP3 and CD25 together

with some contact-dependent immunosuppressive mechanisms including CTLA-4 and PD-1 were decreased when Tregs were treated with oligomycin (***Figure 5.3.b***). Together with direct suppression of immune cells, Tregs can also induce differentiation of Tconv into peripherally-derived Tregs (pTregs) via multiple mechanisms including IL-10, TGF-β, IL-35 and CTLA-4 (164, 329). Although our *in vitro* suppression assay data strongly indicates a generally potentiated immunosuppressive function of oligomycin-treated Tregs (***Figure 5.1., 5.2. and 5.10.***), whether mitochondrial ATP synthase inhibited Treg could induce long-term peripheral tolerance by induction of pTregs remains to be established. Achieving long-term peripheral tolerance through modulating systemic immune cells was well studied in transplantation model, termed 'infectious tolerance' (157, 158). This is the concept that tolerance of target tissues achieved by one cell population may transfer to another separate cell population, to establish the maintenance of durable peripheral tolerance. Studies subsequently demonstrated that induction of alloreactive pTreg is one of the key mechanisms of infectious tolerance (122, 162). The infusion of expanded Tregs following transplantation therefore not only boosts the number of alloreactive Tregs in patients, but also generates a tolerogenic

environment which may induce new alloreactive pTregs from Tconvs (163, 164). Because inhibition by oligomycin will not last long in expanded Tregs due to cellular proliferation and mitochondrial regeneration, oligomycin-treated Treg may not demonstrate an advantage in long-term graft acceptance compared with conventional Tregs therapy especially if infused in lower doses. As such, the potential for oligomycin-treated Tregs to induce Tregs from Tconvs must be assessed to further support the potential benefit of oligomycin pretreatment.

Whether pTregs are induced by oligomycin-treated Treg-derived small EVs is a crucial question. Small EVs derived from oligomycin-treated Tregs have the potential to be used as an off-the-shelf therapy given their ability to supress third party CD4 T cell proliferation (***Figure 5.12.b***). However, if small EVs do not induce alloreactive pTreg, repeated life-long infusions would be required. Other studies have demonstrated that Treg-derived EVs are immunosuppressive and prevent acute rejection of transplanted organs in mice and humanised mice models (146, 148-150). Importantly, some of these studies revealed induction of Treg and other regulatory-type T cells producing IL-10 by

the small EVs derived from Tregs (146, 148). Thus, using a single dose of Treg-derived small EVs would seem to have a huge potential as a new therapeutic strategy to prevent organ rejection. However, the doses of small EVs in published studies were extremely high. For example, Tung *et al* used small EVs extracted from between 5.0 and 50.0 million human expanded Tregs for *in vitro* experiments, suggesting that an unrealistic number small EVs would be required in human clinical settings (150). However in our hands oligomycin-treated Tregs produced strongly immunosuppressive small EVs from only 0.1 million human-expanded Tregs indicating that oligomycin treatment potentially overcome this limitation. Oligomycin treatment did not, however, induce larger quantity of small EVs production (***Figure 5.7.c and d***) and instead resulted in phenotypic skewing from $CD4^+$ and/or $CD24^+$ to $CD25^+$, $CD41b^+$, $CD45^+$ and/or $CD133/1^+$. This indicates that oligomycin treatment of Tregs induces production of a qualitatively different type of small EV (***Figure 5.8.b***). As such, it is not known whether these small EVs may also induce Tregs from Tconvs. Both the precise content of these small EVs and whether they induce Tregs are key outstanding questions before clinical translation may be pursued.

Although we revealed that mitochondrial ATP synthase inhibition by oligomycin renders Tregs more suppressive, it is still not clear whether this recapitulates specific physiological or pathological conditions. For example, the metabolically harsh conditions of tumour microenvironments have been demonstrated to increase Treg suppressive function (230, 325). Field *et al* suggested it is driven by a shortage of fatty acids which disrupts Treg mitochondrial integrity (230). Mitochondrial disruption releases mitochondrial DNA into the cytoplasm and induces Treg IL-10 production via IFN type 1 signalling pathway. Thus, mitochondrial integrity in Tregs is responsive to the extracellular environment and may result in modulation of their suppressive function. However, whether oligomycin causes mitochondrial disruption similarly to that induced by a shortage of fatty acids remains unknown. The ATPase Inhibitory Factor 1 (IF1) is a physiological inhibitor of mitochondrial ATP synthase (330, 331). IF1 activity depends on a mitochondrial acidic state. Under hypoxic conditions, the mitochondrial matrix acidifies due to lactate production which induces dimerisation and activation of IF1 (332, 333). Tumour microenvironments and inflammatory tissues are generally hypoxic and acidic in part due to high lactate production from cells. It is not clear how either the

extracellular acidic state and the extracellular hypoxic state effect Treg intracellular pH. Putatively, a low intracellular pH may be caused by either cellular lactate production or lactate import from extracellular environment under hypoxic and lactate-enriched conditions which may activate IF1 and inhibit mitochondrial ATP synthase leading to immunosuppressive small EV production in a similar fashion to oligomycin treatment. Thus, together with investigation of mitochondrial integrity after oligomycin treatment, it will be important to investigate if Tregs produce immunosuppressive small EVs under hypoxic and lactate-enriched microenvironments like in the oligomycin treated condition.

In *this chapter*, we reveal that mitochondrial ATP synthase inhibition by oligomycin directly enhances both *ex vivo* and *in vitro*-expanded human Treg suppressive function by inducing immunosuppressive small EVs production. We also explore potential clinical translation strategies to treat autoimmune diseases and prevent transplanted organ rejection by either pre-treating expanded Treg with oligomycin or by 'off-the-shelf' administration of small EVs derived from oligomycin-treated Treg. The enhanced Treg suppressive function we induce by mitochondrial inhibition sheds new light on Treg

immunometabolism: Tregs positively regulate their suppressive function via the limitation of mitochondrial energy metabolism, in contrast to Tconvs which negatively control their effector function through limiting glucose metabolism. However, we still do not understand the mechanism by which mitochondrial ATP synthase inhibition induces immunosuppressive small EV production by Tregs. This will be investigated in the *next chapter*.

5.9 Figures and legends

Figure 5.1

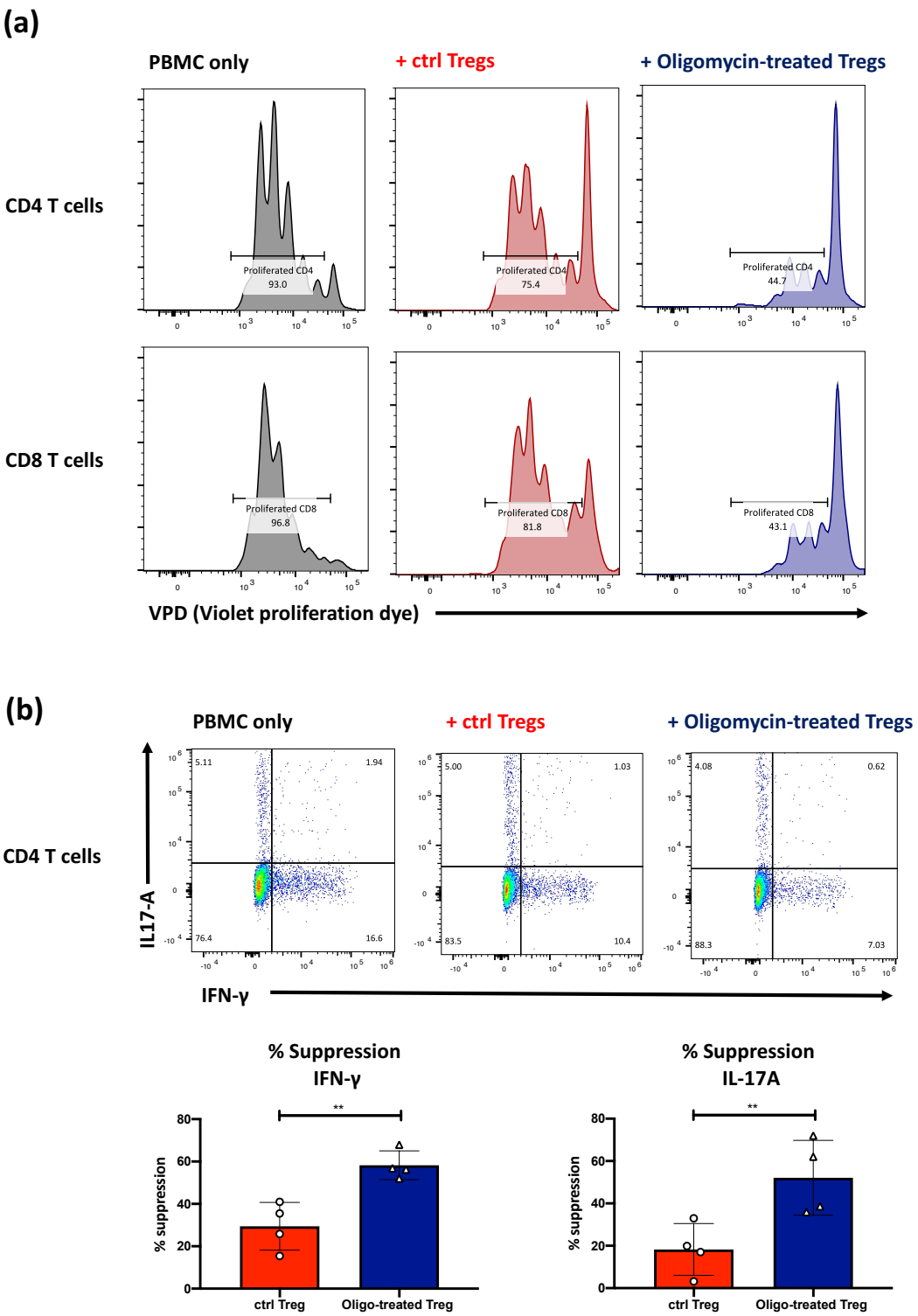

Figure 5.1 (cont.)

(c)

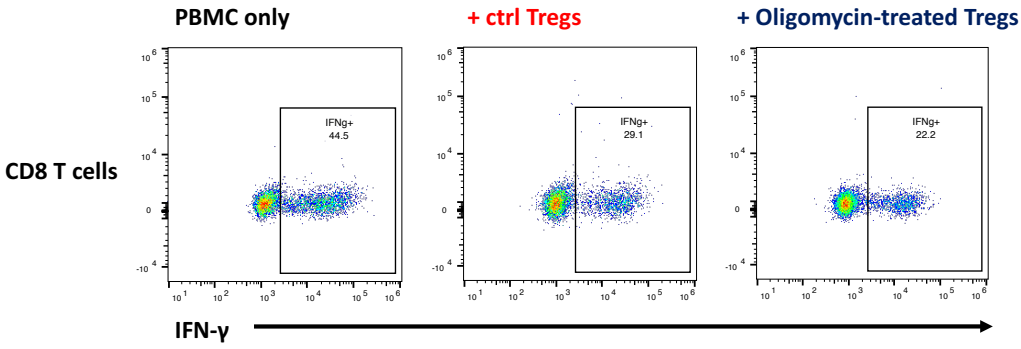

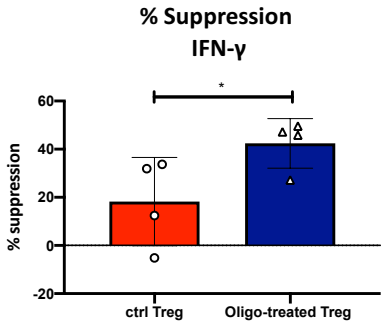

Figure 5.1. Mitochondrial ATP synthase inhibited human Tregs have superior immunosuppressive function.

Freshly isolated human Tregs were pre-treated with 2 μM oligomycin (Mitochondrial ATP synthase inhibitor) or 0.2% DMSO (control) for 2 hours, washed intensively, and then co-incubated with VPD-stained fresh PBMCs at a 1:1 (Tregs to PBMC) ratio. (a) Representative histograms from one of 3 independent donors revealing the percentage of proliferated CD4 T cells (top panel) and CD8 T cells (bottom panel). Tregs and PMBCs were co-incubated for 84 hours in the presence of anti-CD3/CD28 beads. (b-c) Tregs and PBMC were co-incubated with an anti-CD3/CD28 activating monoclonal antibodies for 33 hours, followed by PMA/ionomycin stimulation for 3h with monensin. (b) Investigation of Treg suppression of IFN-γ and IL-17A producing cells amongst CD4 T cells. Top, representative FACS plots from one of 4 independent donors. Bottom, graphs showing the quantification of the percentage suppression of IFN-γ (left panel) and IL-17A (right panel) producing cells by Tregs. (c) Investigation of Treg suppression of IFN-γ producing cells amongst CD8 T cells. Top, representative FACS plots from one of 4 independent donors. Bottom, graphs showing the quantification of the percentage

suppression of IFN-γ producing cells. Each dot represents an individual donor. Columns represent mean ± SD. *p<0.05, **p<0.01 by paired t test.

Figure 5.2

(a)

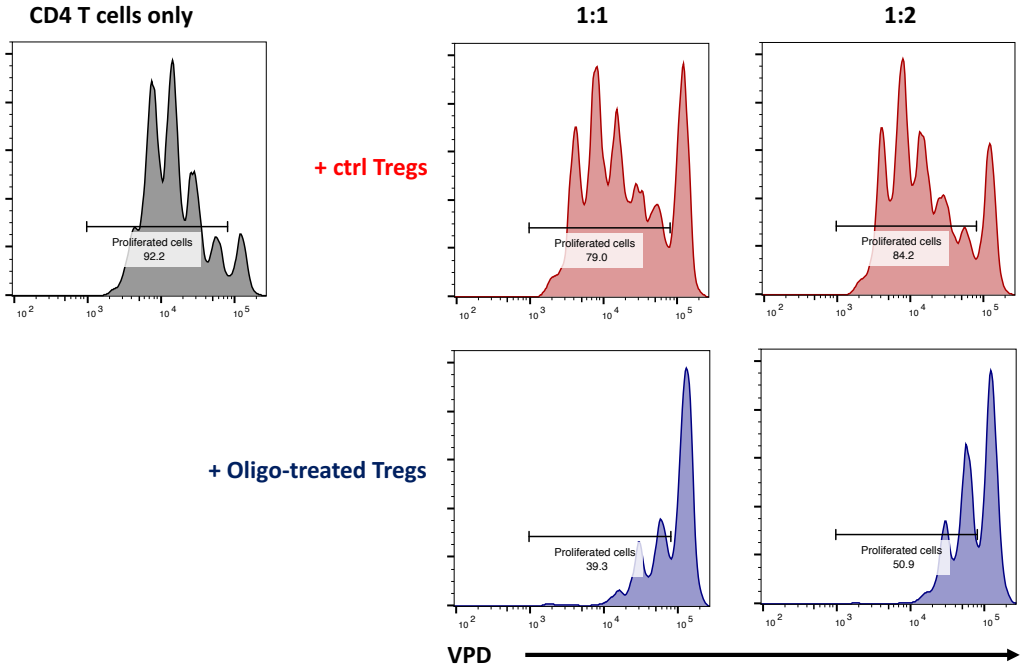
CD4 T cells only
1:1
1:2
+ ctrl Tregs
+ Oligo-treated Tregs
Proliferated cells
92.2
Proliferated cells
79.0
Proliferated cells
84.2
Proliferated cells
39.3
Proliferated cells
50.9
VPD

(b)

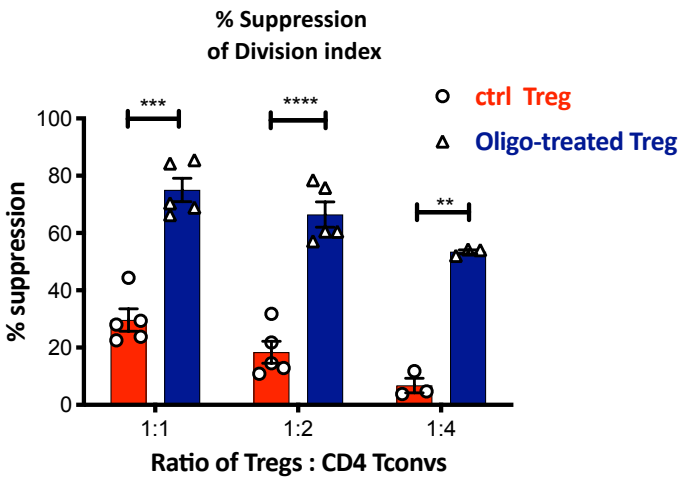
% Suppression
of Division index
ctrl Treg
Oligo-treated Treg
***
****
**
% suppression
100
80
60
40
20
0
1:1
1:2
1:4
Ratio of Tregs : CD4 Tconvs

Figure 5.2. Mitochondrial ATP synthase inhibited human Tregs directly suppress CD4 Tconvs.

Freshly isolated human Tregs were pre-treated with 2 μM oligomycin or 0.2% DMSO (control) for 2 hours, washed intensively, and then co-incubated with $CD4^+$ $CD25^-$ Tconvs at 1:1, 1:2, or 1:4 (Tregs to Tconvs) ratio in the presence of anti-CD3/CD28 beads for 84 hours. (a) Representative histograms from one of five independent donors. (b) A bar chart showing the percentage of suppression of CD4 Tconvs division index by the presence of Tregs at different ratios. The ratio of 1:4 was investigated in three independent donors. Columns represent mean ± SD. **p<0.01, ***p<0.001 ****p<0.0001 by paired t test.

Figure 5.3

(a)

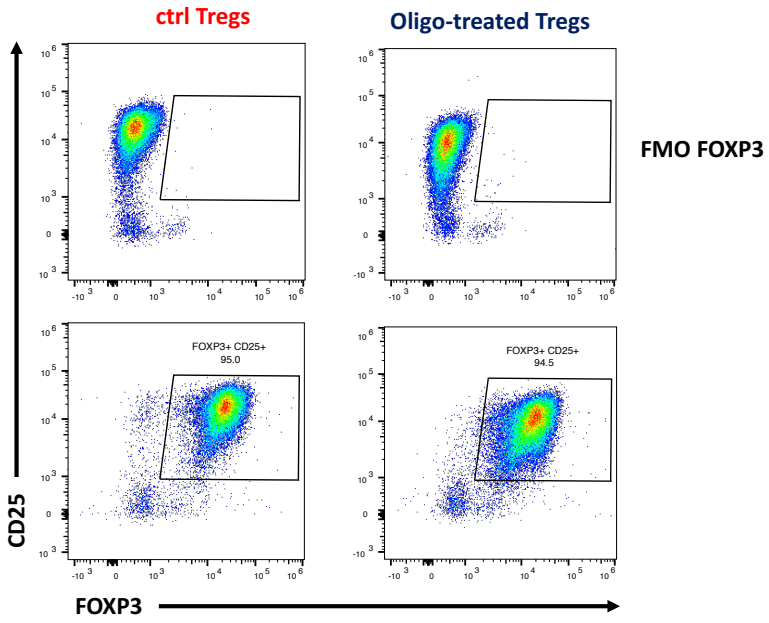
ctrl Tregs
Oligo-treated Tregs
FMO FOXP3
FOXP3+ CD25+
95.0
FOXP3+ CD25+
94.5
CD25
FOXP3

(b)

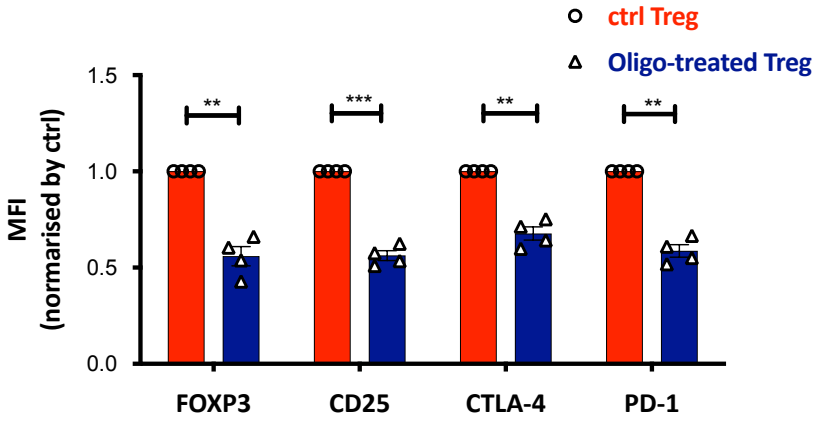
ctrl Treg
Oligo-treated Treg
MFI
(normarised by ctrl)
1.5
1.0
0.5
0.0
**
***
**
**
FOXP3
CD25
CTLA-4
PD-1

Figure 5.3. Phenotype of mitochondrial ATP synthase inhibited human Tregs.

Freshly isolated human Tregs were pre-treated with 2 μM oligomycin or 0.2% DMSO (control) for 2 hours, washed intensively, and then stimulated with anti-CD3/CD28 beads in fresh medium for 48h. (a) Representative FACS plots from one of four donors illustrating the percentage of $FOXP3^{+}$ $CD25^{+}$ cells. (b) A bar chart showing the MFI of Treg markers. The values were normalised to control Tregs from the same donor. Columns represent mean ± SD. **p<0.01, ***p<0.001 by paired t test.

Figure 5.4

(a)

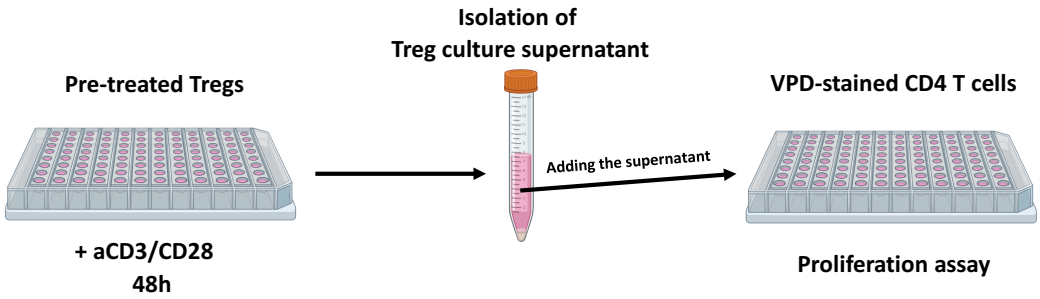

(b)

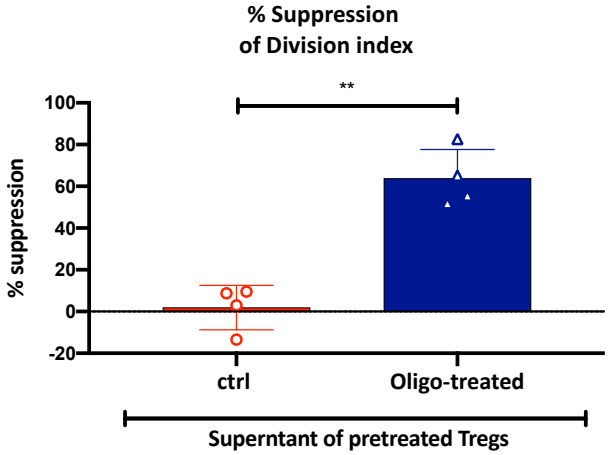

(c)

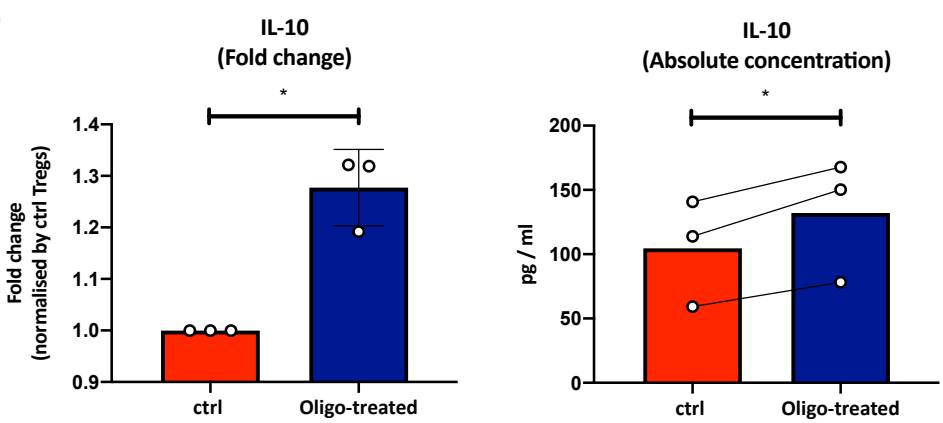

Figure 5.4 (cont.)

(d)

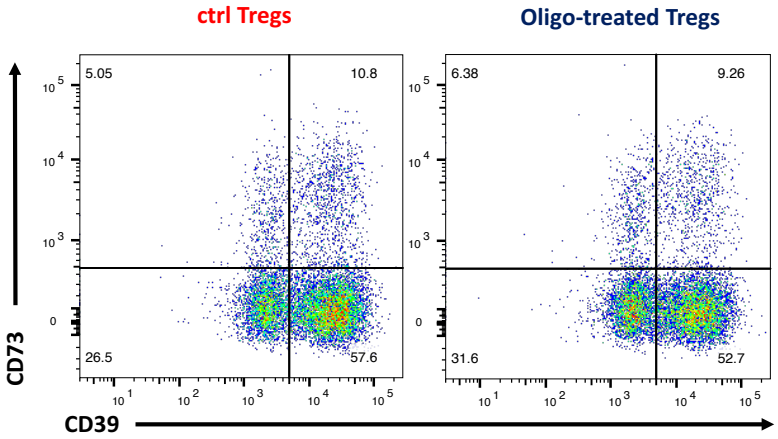

Figure 5.4. Mitochondrial ATP synthase inhibited human Tregs produce immunosuppressive soluble factor that is neither IL-10 nor adenosine.

Freshly isolated human Tregs were pre-treated with 2 μM oligomycin or 0.2% DMSO (control) for 2 hours, washed intensively, and then stimulated with anti-CD3/CD28 beads in fresh medium for 48h. (a and b) Treg culture supernatants were gently removed and then mixed with VPD-stained CD4 T cells suspended in the same volume of fresh RPMI along with anti-CD3/CD28 beads for 84h. (a) A schematic summarising the experimental design. (b) A graph showing the percentage of suppression of CD4 T cells division index by Tregs culture supernatants. (c) The concentration of IL-10 in the Treg culture supernatant was investigated by ELISA. Left, fold change of the IL-10 concentration normalised to control Treg supernatant. Right, absolute concentration of IL-10. Each dot represents an individual donor. Columns represent mean ± SD. *$p<0.05$, **$p<0.01$ by paired t test. (d) Representative FACS plot illustrating CD39 and CD73 expression on Tregs after 48h cultivation with anti-CD3/CD28 beads

Figure 5.5

(a)

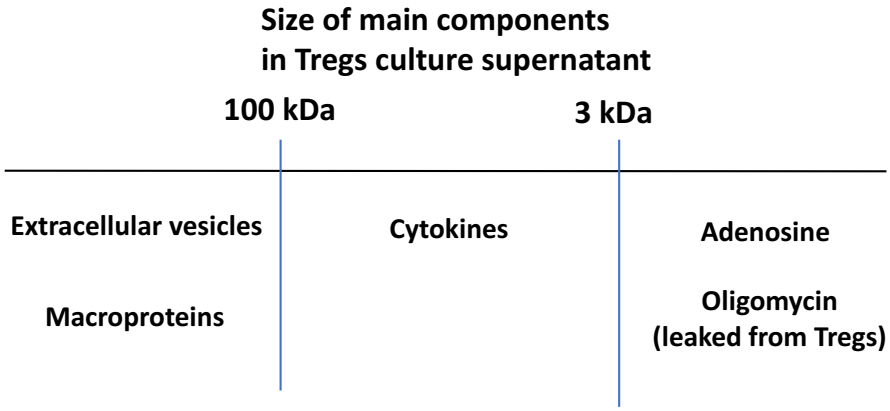

(b)

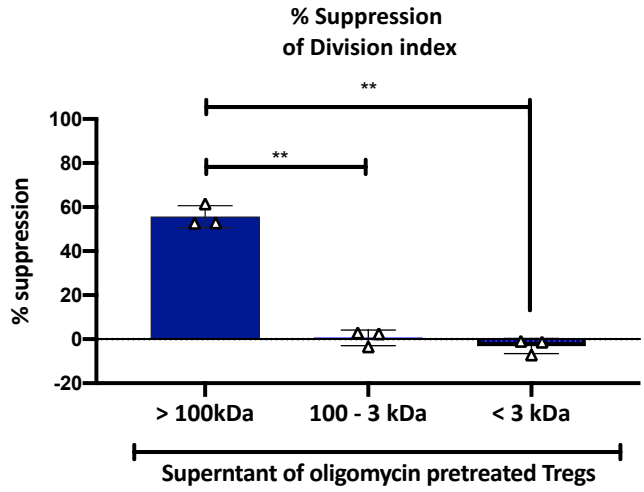

(c)

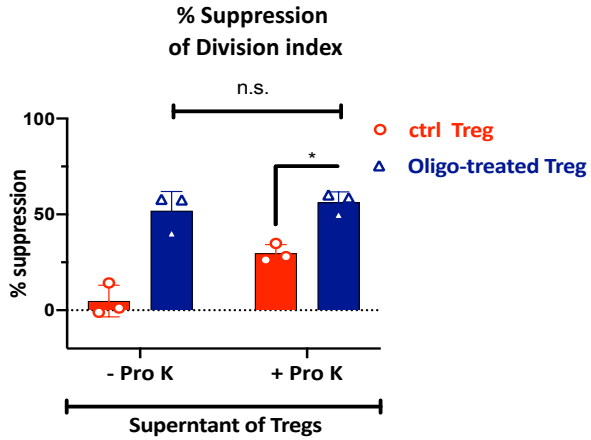

Figure 5.5 (cont.)

(d)

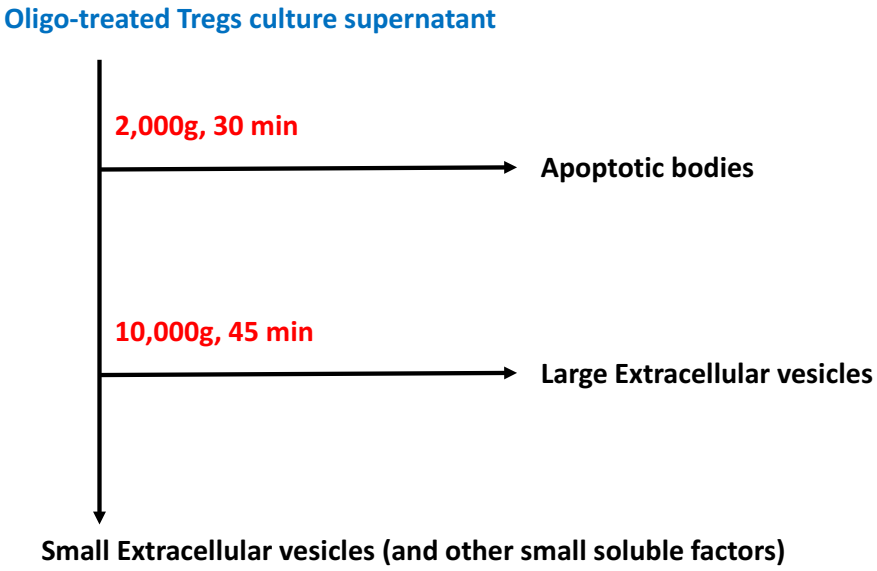

(e)

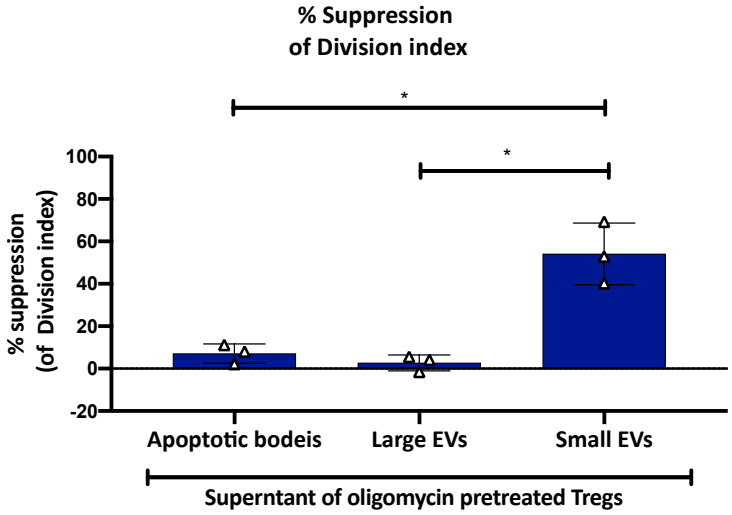

Figure 5.5. Mitochondrial ATP synthase inhibited human Tregs produce immunosuppressive extracellular vesicles.

Freshly isolated human Tregs were pre-treated with 2 μM oligomycin or 0.2% DMSO (control) for 2 hours, washed intensively, and then stimulated with anti-CD3/CD28 beads in fresh medium for 48h. The Treg culture supernatants were gently removed for assays. (a and b) Oligomycin pre-treated Treg supernatants were divided into three fractions based on their size: over 100 kDa, 3 to 100 kDa, and lower than 3 kDa using Amicon ultracentrifugation filters. In parallel, complete medium incubated without Tregs was also fractionated. Fractionated oligomycin pre-treated Treg supernatants were mixed with other fractions of complete medium up to the original volume. Each fraction of reconstituted supernatants was mixed with VPD-stained CD4 T cells in fresh RPMI in a ratio of one part supernatant to three parts cells along with anti-CD3/CD28 beads for 84h. (a) Schematic figure summarising the main components of possible suppressive substances in Tregs culture supernatants. (b) A bar chart showing the percentage suppression of CD4 T cells division index by fractionated oligomycin pre-treated Tregs supernatants. (c) A bar chart showing the percentage suppression of CD4 T cell division

index by proteinase K treated culture supernatants. Tregs culture supernatants were treated with proteinase K (+ Pro K) or without (- Pro K) for 1h at 37°C in a final concentration of 100μg/ml, followed by 95°C heat inactivation for 10 minutes. The supernatants were centrifuged at 10,000g for 10 minutes to remove debris and mixed with VPD-stained CD4 T cells in fresh RPMI in a ratio of one part supernatant to three parts cells along with anti-CD3/CD28 beads for 84h. (d and e) Oligomycin pre-treated Treg supernatant was fractionated into three fractions by differential centrifugation. The culture supernatants were first centrifuged at 2,000 g for 30 min to isolate apoptotic bodies as a pellet. The supernatants were then centrifuged at 10,000 g for 45 min to isolate large extracellular vesicles (large EVs) as a pellet and small extracellular vesicles (small EVs) as a supernatant. The pellets of apoptotic bodies and large EVs were reconstituted to the original volume by parallelly-centrifuged medium control. The fractionated supernatants were mixed with VPD-stained CD4 T cells in fresh RPMI in a ratio of one part supernatant to three parts cells along with anti-CD3/CD28 beads for 84h. (d) Schematic overview of differential centrifugation. (e) A bar chart showing the percentage suppression of CD4 T cell division index by fractionated supernatants. Each

dot represents an individual donor. Columns represent mean ± SD. *p<0.05, **p<0.01 by paired t test.

Figure 5.6

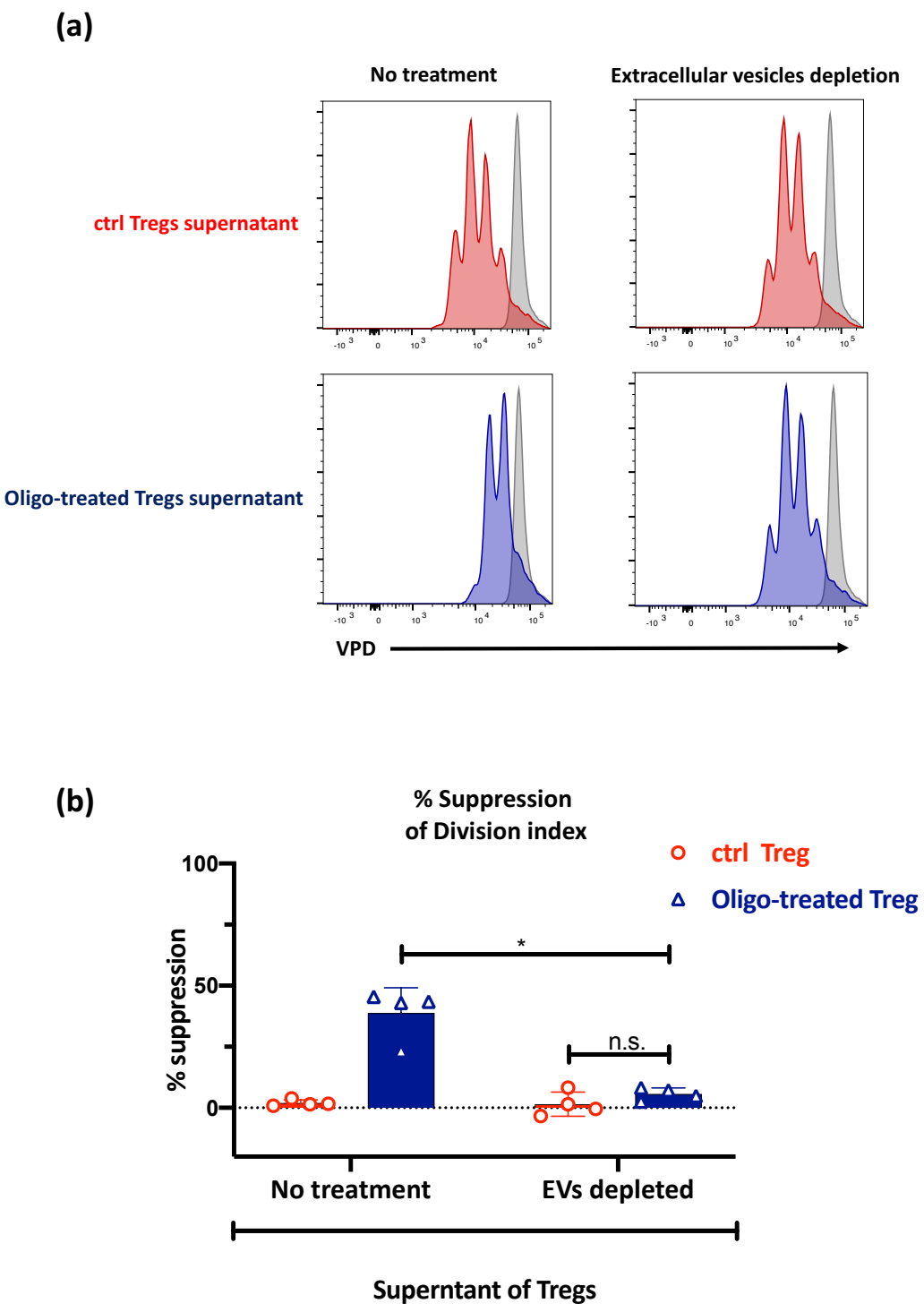
(a)
No treatment
Extracellular vesicles depletion
ctrl Tregs supernatant
Oligo-treated Tregs supernatant
VPD
(b)
% Suppression
of Division index
ctrl Treg
Oligo-treated Treg
100
50
0
% suppression
*
n.s.
No treatment
EVs depleted
Superntant of Tregs

Figure 5.6. Mitochondrial ATP synthase inhibited human Tregs produce immunosuppressive small extracellular vesicles (exsosomes).

Freshly isolated human Tregs were pre-treated with 2 μM oligomycin or 0.2% DMSO (control) for 2 hours, washed intensively, and then stimulated with anti-CD3/CD28 beads in fresh medium for 48h. The Treg culture supernatants were gently removed and small EVs (formally known as exosomes) contained in the culture supernatants were removed by Norgen's FBS Exosome Depletion kit before application into the VPD-stained CD4 T cell proliferation assay. (a) Representative histograms from one of 4 independent donors. (b) A bar chart showing the percentage suppression of CD4 T cell division index by small EV-depleted supernatants. Each dot represents an individual donor. Columns represent mean ± SD. *$p<0.05$ by paired t test.

Figure 5.7

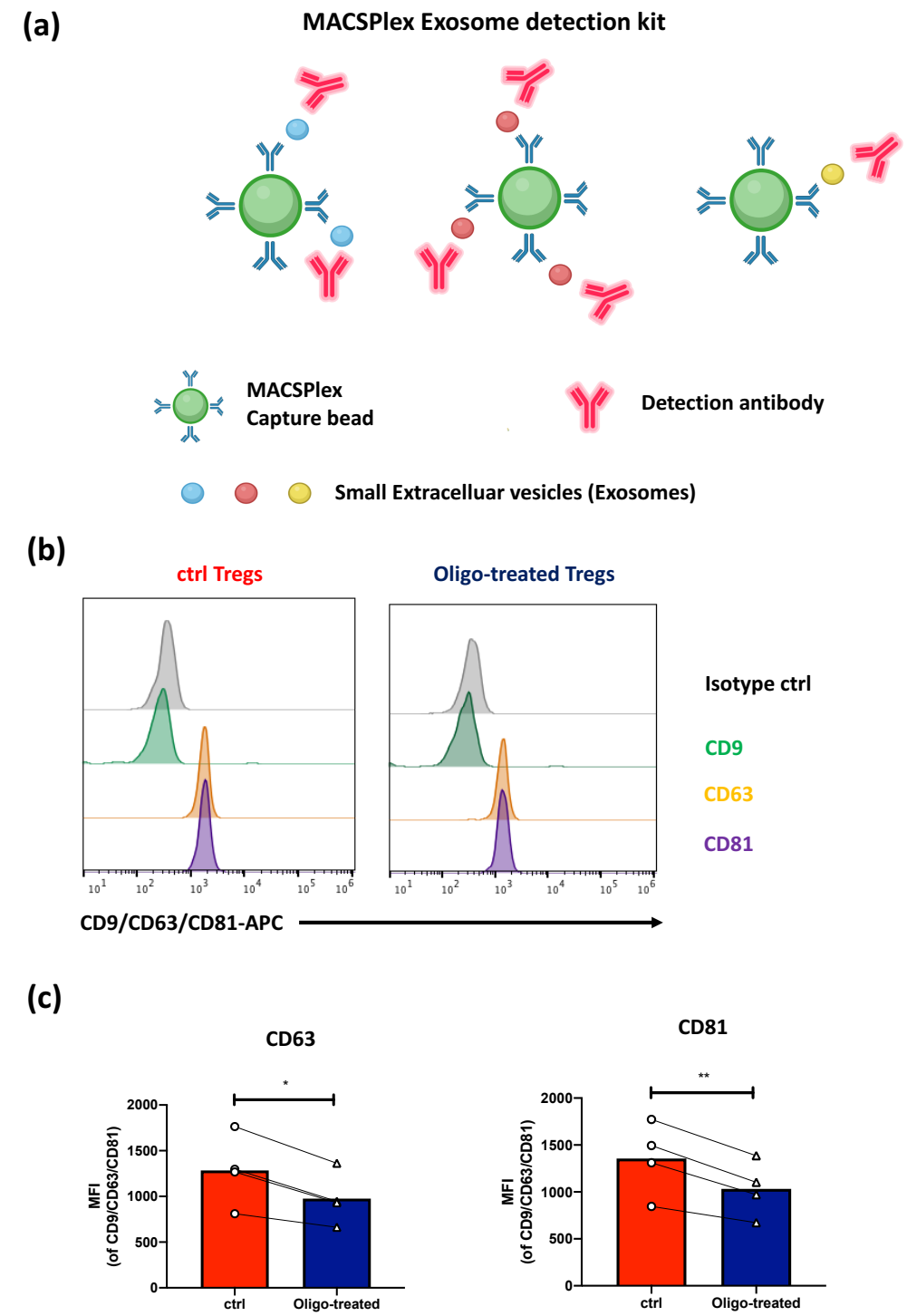
(a)
MACSPlex Exosome detection kit
MACSPlex
Capture bead
Detection antibody
Small Extracelluar vesicles (Exosomes)
(b)
ctrl Tregs
Oligo-treated Tregs
Isotype ctrl
CD9
CD63
CD81
CD9/CD63/CD81-APC
(c)
CD63
CD81
MFI
(of CD9/CD63/CD81)
2000
1500
1000
500
0
ctrl
Oligo-treated
*
**

Figure 5.7 (cont.)

(d)

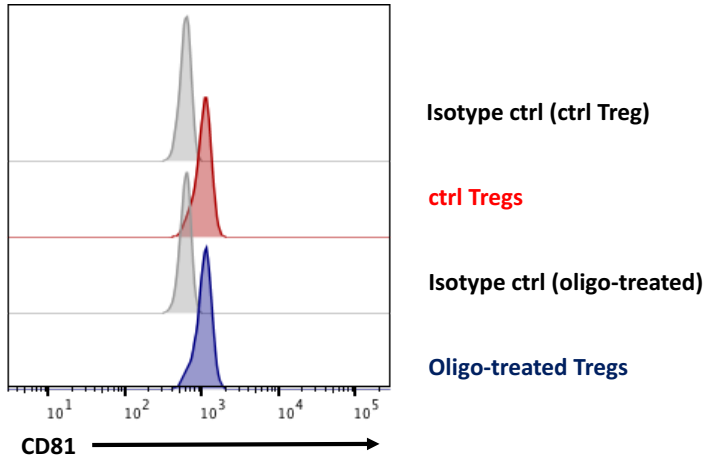

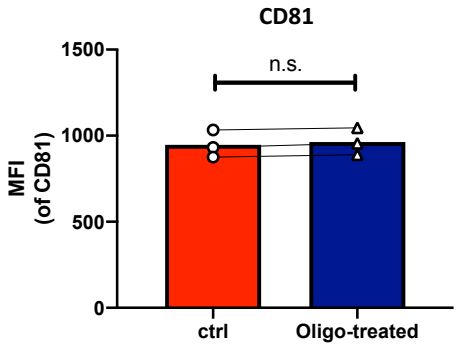

Figure 5.7. Mitochondrial ATP synthase inhibited human Tregs do not produce higher quantity of small extracellular vesicles (exosomes).

Freshly isolated human Tregs were pre-treated with 2 μM oligomycin or 0.2% DMSO (control) for 2 hours, washed intensively, and then stimulated with anti-CD3/CD28 beads in small EV-depleted medium for 48h. The gently removed Treg culture supernatants were first filtered through a 0.22μm membrane to remove large EVs, before concentration by ultracentrifugation through a 100 kDa Amicon filter. The concentrated >100 kDa fraction of supernatants were used in these assays. (a-c) Small EVs were detected using a MACSPlex Exosome kit. (a) Schematic summary of the MACSPlex Exosome kit. (b) Representative histograms showing the quantity of CD9, CD63 and CD81 small EVs as MFI of detection antibodies from one of four independent donors. (c) Bar charts showing the MFI of detection antibodies of $CD63^+$ small EVs (left panel) and $CD81^+$ small EVs (right panel). (d) $CD81^+$ small EVs in the supernatant were isolated with the Exosome-Human CD81 Flow Detection Reagent and quantified by a fluorescently-labelled anti-CD81 detection antibody. Top, representative histogram illustrating the quantities of $CD81^+$ small EVs from one of three independent donors. Bottom, a graph

showing the MFI of the anti-CD81 antibody representing the quantity of $CD81^+$ small EVs. Each dot represents an individual donor. Columns represent mean ± SD. *p<0.05, **p<0.01 by paired t test.

Figure 5.8

(a)

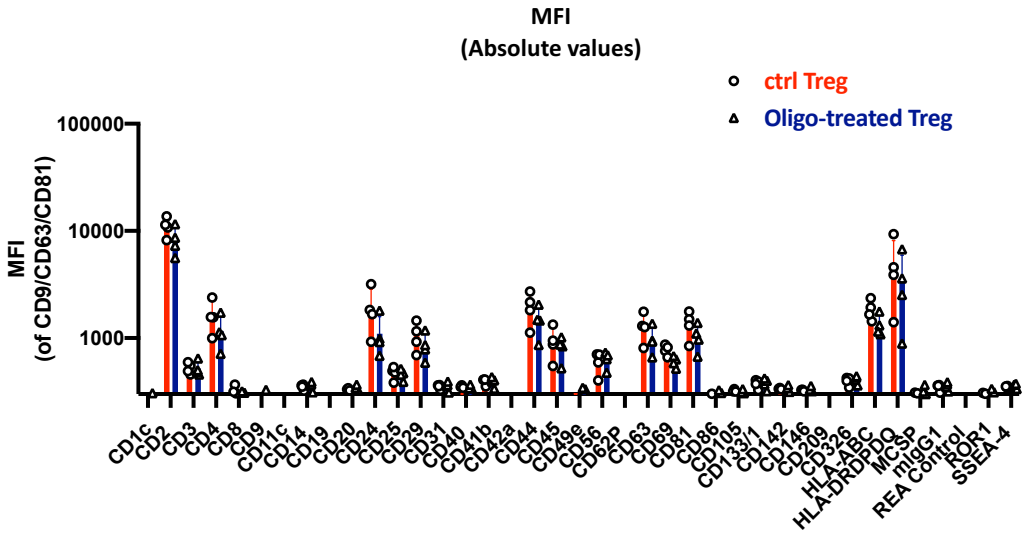
MFI
(Absolute values)
ctrl Treg
Oligo-treated Treg
MFI
(of CD9/CD63/CD81)
100000
10000
1000
CD1c
CD2
CD3
CD4
CD8
CD9
CD11c
CD14
CD19
CD20
CD24
CD25
CD29
CD31
CD40
CD41b
CD42a
CD44
CD45
CD49e
CD56
CD62P
CD63
CD69
CD81
CD86
CD105
CD133/1
CD142
CD146
CD309
CD326
HLA-ABC
HLA-DRDPDQ
MCSP
mIgG1
REA Control
ROR1
SSEA-4

(b)

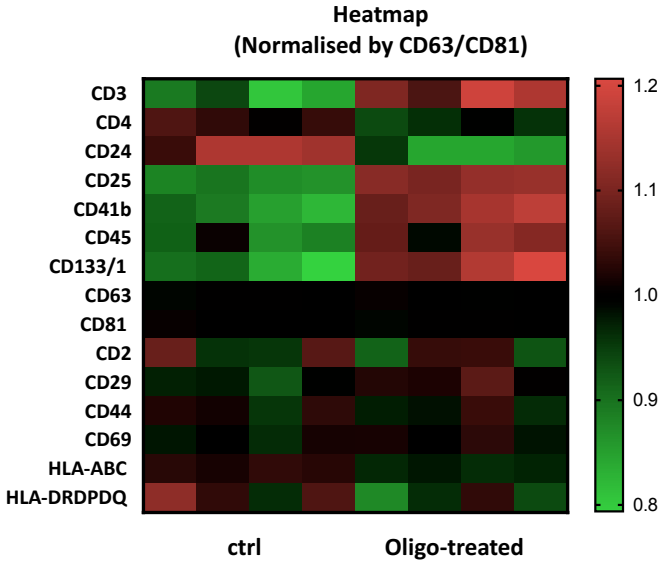
Heatmap
(Normalised by CD63/CD81)
CD3
CD4
CD24
CD25
CD41b
CD45
CD133/1
CD63
CD81
CD2
CD29
CD44
CD69
HLA-ABC
HLA-DRDPDQ
1.2
1.1
1.0
0.9
0.8
ctrl
Oligo-treated

Figure 5.8. Mitochondrial ATP synthase inhibited human Tregs produce different types of small extracellular vesicles.

Freshly isolated human Tregs were pre-treated with 2 μM oligomycin or 0.2% DMSO (control) for 2 hours, washed intensively, and then stimulated with anti-CD3/CD28 beads in small EV-depleted medium for 48h. The gently removed Treg culture supernatants were first filtered through a 0.22μm membrane to remove large EVs, before concentration by ultracentrifugation through a 100 kDa Amicon filter. The surface markers of small EVs were detected using MACSPlex Exosome kit. (a) Absolute MFIs of detection regents. Values below mIgG1 control are not shown. Each dot represents an individual donor. (b) A heatmap revealing the phenotype of produced small EVs. Values represent the relative level of small EVs produced between control and oligomycin pre-treated Tregs. Relative values were normalised to the mean of CD63 and CD81 MFI. Values lower than mIGg1 or REA control were excluded. Culture medium incubated without cells was also examined in parallel as another control. Values detected below the medium control were also excluded.

Figure 5.9

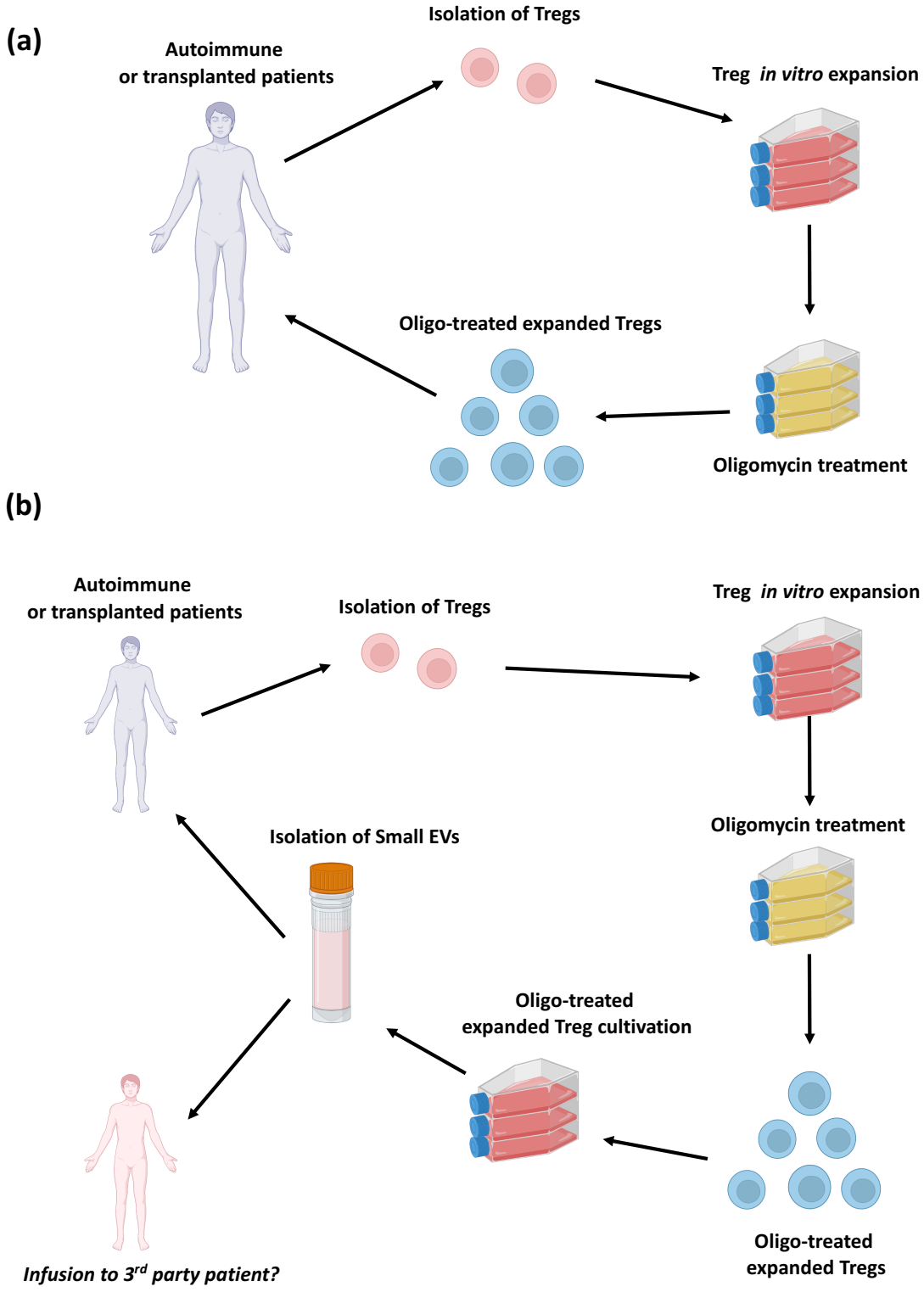
(a)
Autoimmune
or transplanted patients
Isolation of Tregs
Treg *in vitro* expansion
Oligomycin treatment
Oligo-treated expanded Tregs
(b)
Autoimmune
or transplanted patients
Isolation of Tregs
Treg *in vitro* expansion
Oligomycin treatment
Isolation of Small EVs
Oligo-treated
expanded Treg cultivation
Oligo-treated
expanded Tregs
Infusion to 3rd party patient?

Figure 5.9. Schematic overviews of Treg cellular therapy with oligomycin.

(a) Schematic overview of a potential strategy to incorporate oligomycin pre-treatment into adoptive Treg cellular therapy workflows. Human *ex vivo* Tregs would be isolated from patients, expanded *in vitro*, pre-treated with oligomycin and then be infused into patients. (b) Schematic overview of a potential strategy for small EV therapy. Human *ex vivo* Tregs would be isolated from patients, expanded *in vitro*, pre-treated with oligomycin, and then incubated in fresh medium. Expanded Treg culture supernatants would be removed, then small EVs would be isolated and infused into patients. It can be envisaged that small EVs could also be used from treatment of 3rd party patients as an off-the-shelf therapy.

Figure 5.10

(a)

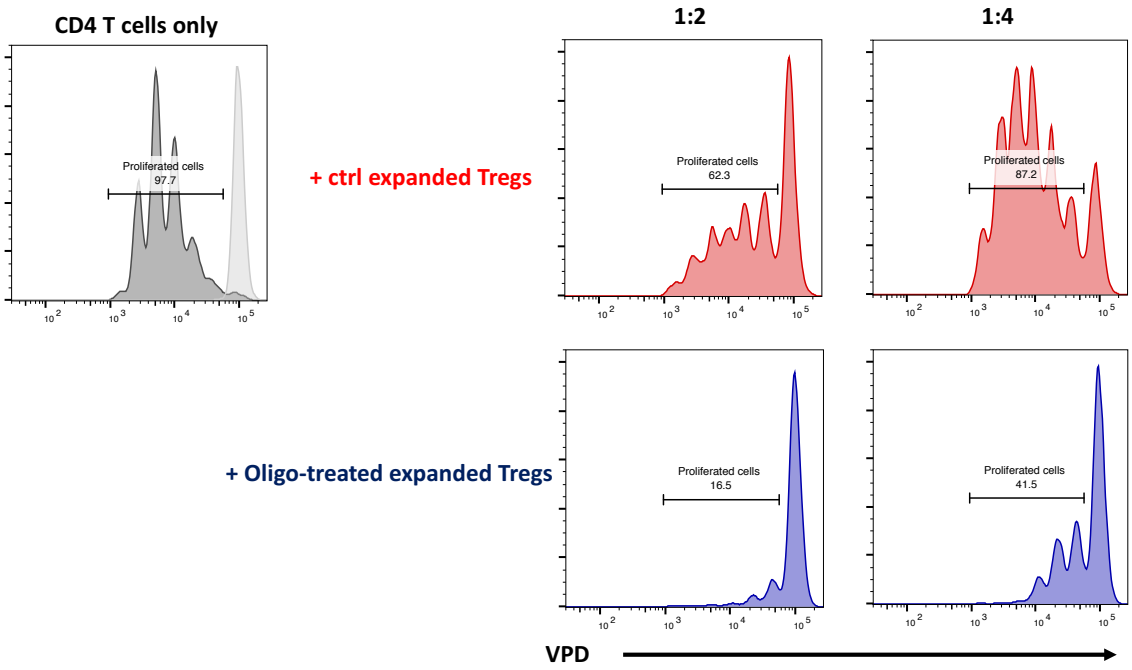

(b)

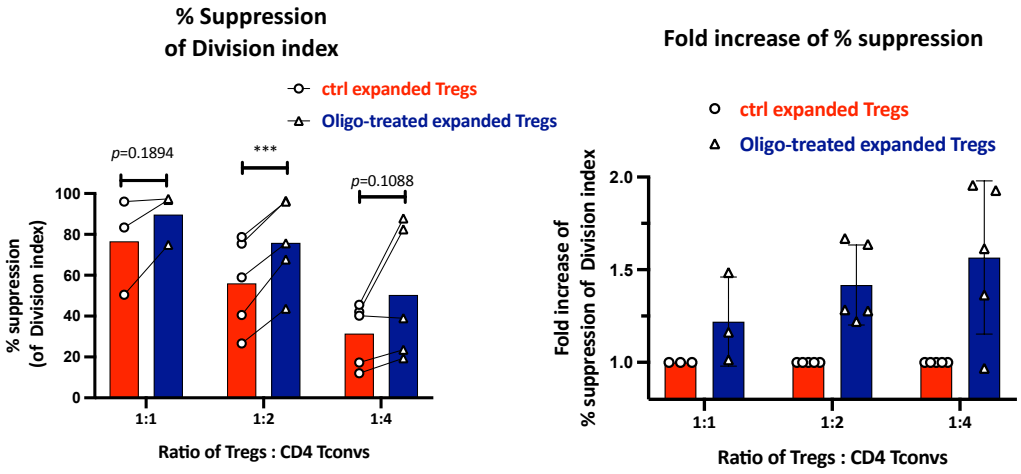

Figure 5.10. Mitochondrial ATP synthase inhibition also increases *in vitro* expanded human Tregs suppressive function.

Human *in vitro* expanded Tregs (expanded Tregs) were pre-treated with 2 μM oligomycin or 0.2% DMSO (control) for 2 hours, washed intensively, and then incubated with VPD-stained CD4 T cells at varying ratios in the presence of anti-CD3/CD28 beads for 84h. (a) Representative histograms from one of 5 independent donors. (b, left) A bar chart showing the percentage suppression of CD4 T cell division index by co-incubation with expanded Tregs. (b, right) A bar chart showing the fold increase in the percentage suppression of CD4 T cell division index based on control Treg values. The ratio of 1:1 (Tregs : CD4 Tcells) was examined in 3 donors and the ratio of 1:2 and 1:4 was examined in 5 donors. Each dot represents an individual donor. Columns represent mean ± SD. p values were calculated by paired t test.

Figure 5.11

(a)

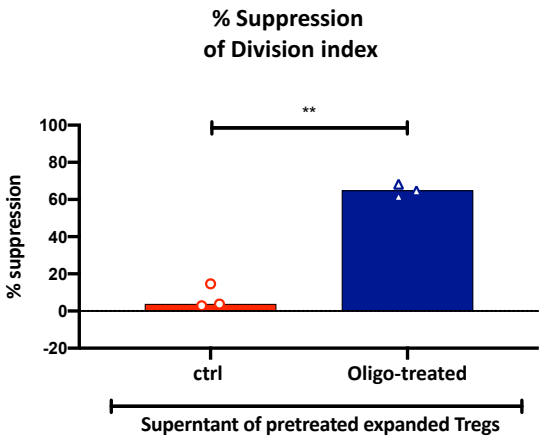

(b)

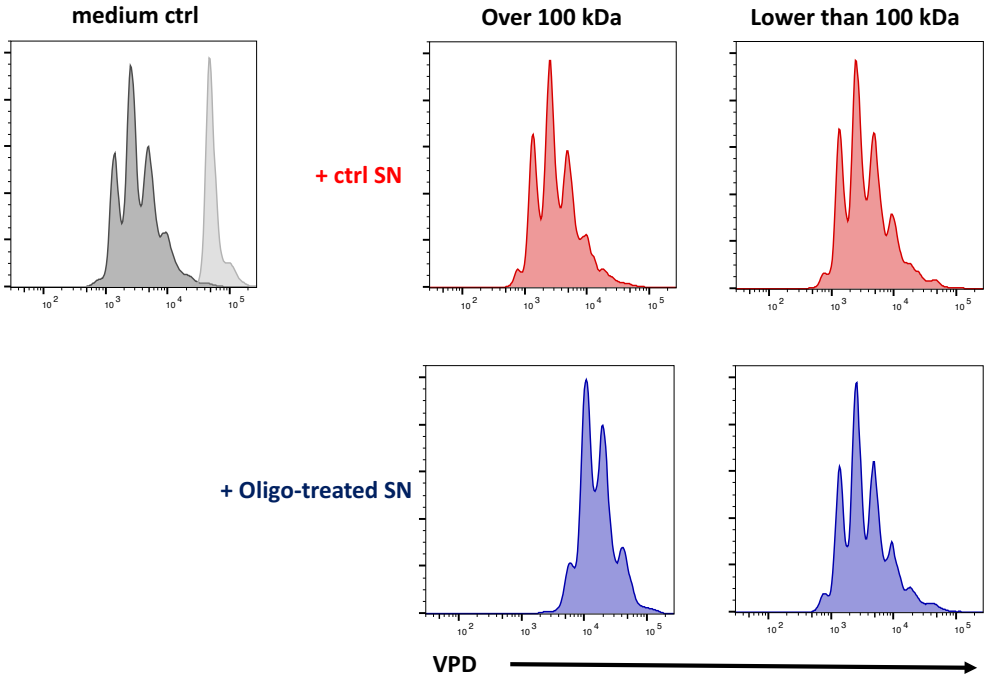

Figure 5.11 (cont.)

(c)

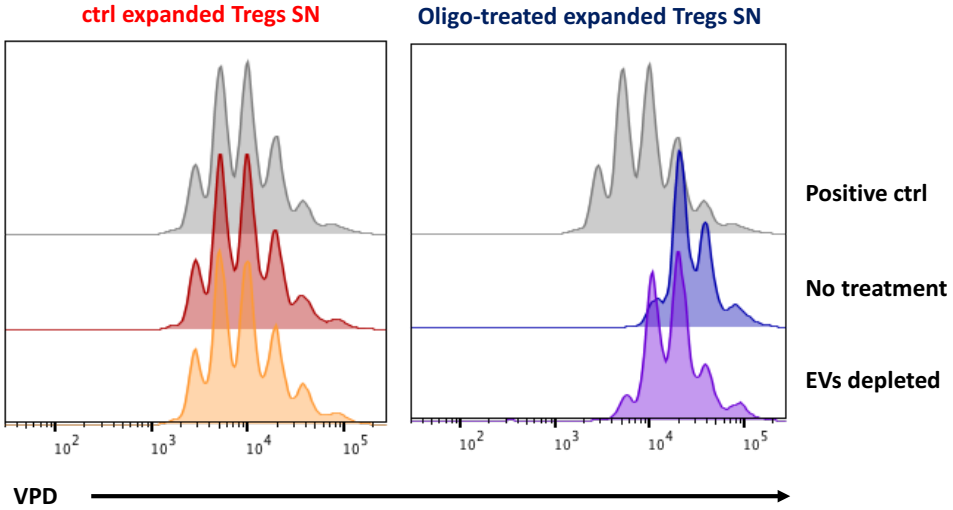

(d)

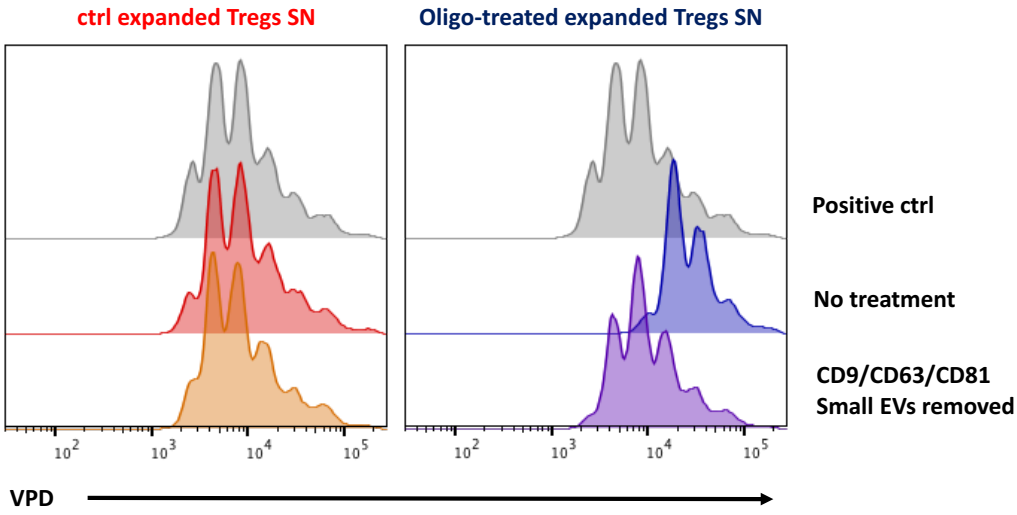

Figure 5.11. Mitochondrial ATP synthase inhibition also induces immunosuppressive small EV production from *in vitro* expanded human Tregs.

Human expanded Tregs were pre-treated with 2 μM oligomycin or 0.2% DMSO (control) for 2 hours, washed intensively, and then stimulated with anti-CD3/CD28 beads in fresh medium for 48h. The Treg culture supernatants (SN) were gently removed for the assays and then added into VPD-stained CD4 T cell proliferation assays. (a) A bar chart showing the percentage suppression of CD4 T cell division index by the expanded Treg culture supernatant. (b) Representative histograms illustrating the suppression of CD4 T cell proliferation by different fraction of Treg culture supernatant from one of two independent donors. Tregs culture supernatants were first separated into >100 kDa and <100 kDa fractions using 100 kDa Amicon ultracentrifugation filter prior to application to the VPD-stained CD4 T cell proliferation assay. (c,d) Representative histograms showing the suppression of CD4 T cell proliferation by Treg culture supernatant depleted of small EVs from 2 independent donors. (c) Small EVs were removed by Norgen's FBS exosome depletion kit. (d) Small EVs were removed by Miltenyi Exosome Isolation kit (pan-human) which depletes CD9, CD63 and CD81 small EVs. Each dot represents an

individual donor. Columns represent mean ± SD. **p<0.01 by paired t test.

Figure 5.12

(a)

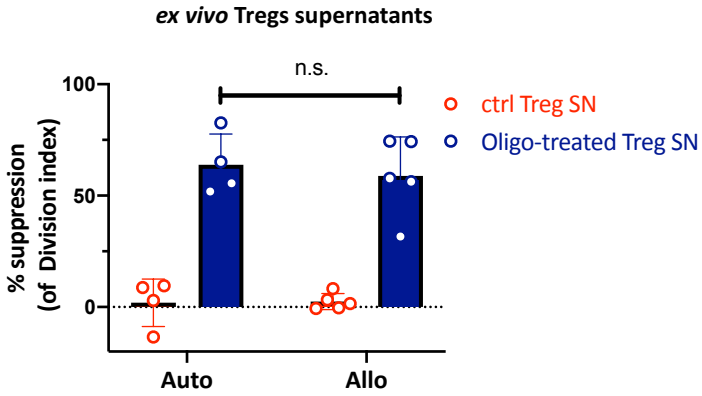

(b)

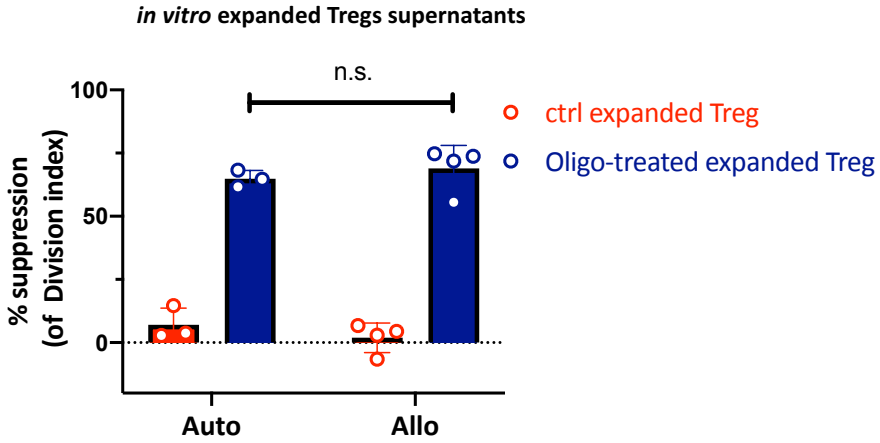

Figure 5.12. Immunosuppressive small EVs produced by mitochondrial ATP synthase inhibited Tregs suppress third party donor responses.

Human Tregs were pre-treated with 2 μM oligomycin or 0.2% DMSO (control) for 2 hours, washed intensively, and then stimulated with anti-CD3/CD28 beads in fresh medium for 48h. The Treg culture supernatants were added into VPD-stained CD4 T cells from same (autologous) or different (allogeneic) donor in the presence of anti-CD3/CD28 beads for 84h. (a) A bar chart showing the percentage suppression of CD4 T cell division index by freshly isolated human Treg culture supernatants. (b) A bar chart showing the percentage suppression of CD4 T cell division index by *in vitro* expanded human Treg culture supernatants. Each dot represents an individual donor. Columns represent mean ± SD. Significances were calculated by t test.

Figure 5.13

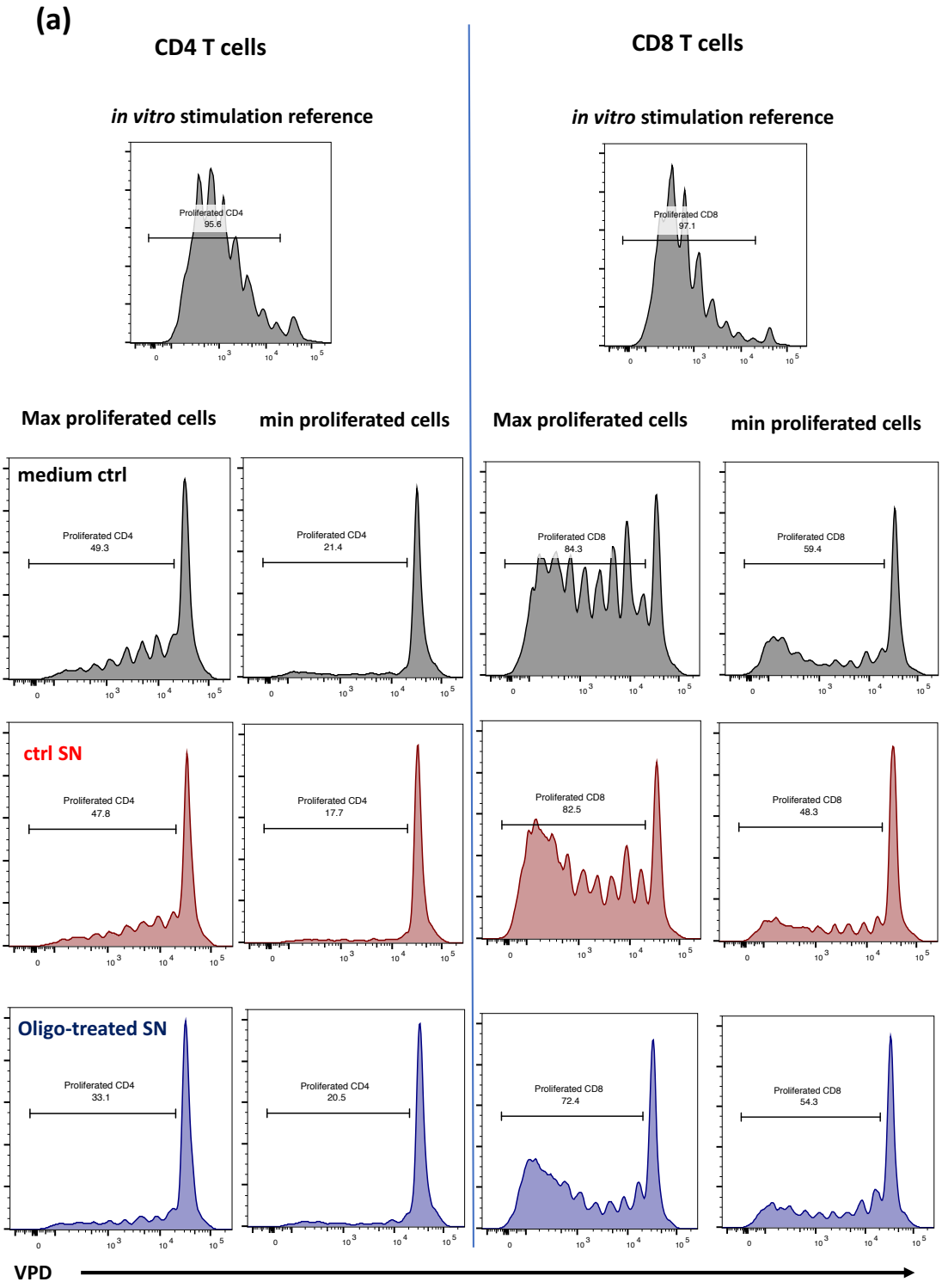
(a)
CD4 T cells
CD8 T cells
in vitro stimulation reference
in vitro stimulation reference
Proliferated CD4
95.6
Proliferated CD8
97.1
Max proliferated cells
min proliferated cells
Max proliferated cells
min proliferated cells
medium ctrl
Proliferated CD4
49.3
Proliferated CD4
21.4
Proliferated CD8
84.3
Proliferated CD8
59.4
ctrl SN
Proliferated CD4
47.8
Proliferated CD4
17.7
Proliferated CD8
82.5
Proliferated CD8
48.3
Oligo-treated SN
Proliferated CD4
33.1
Proliferated CD4
20.5
Proliferated CD8
72.4
Proliferated CD8
54.3
VPD

Figure 5.13 (cont.)

(b)

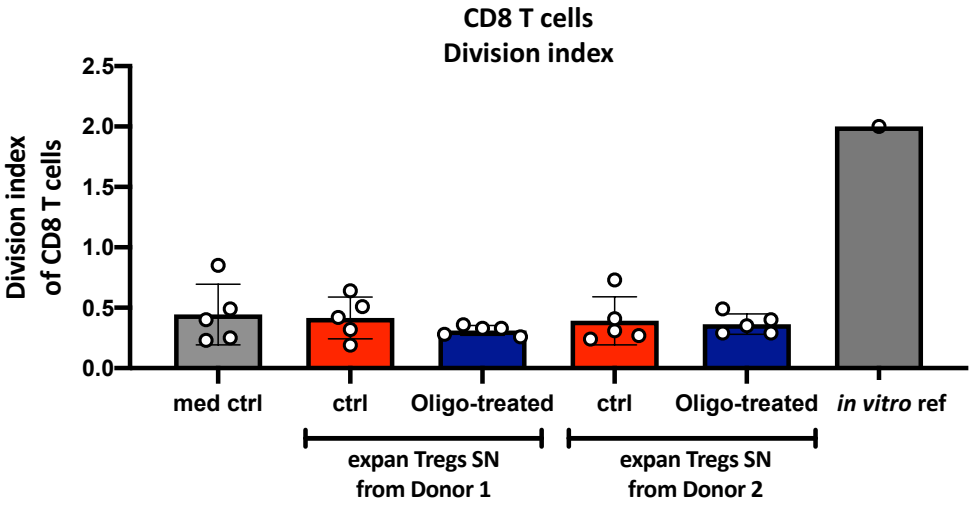

Figure 5.13. Immunosuppressive capacity of small EVs *in vivo* using a mouse peritoneal lavage model.

Human expanded Tregs were pre-treated with 2 µM oligomycin or 0.2% DMSO (control) for 2 hours, washed intensively, and then stimulated with anti-CD3/CD28 beads in fresh medium for 48h in a concentration of 1.0 x 10^6 cells/ml. 5 ml of expanded Treg culture supernatant was concentrated 20 times using a 100 kDa Amicon filter, and then the 250µl of concentrated culture supernatant containing the >100 kDa fraction was injected into the mouse peritoneal cavity together with VPD-stained 5.0 x 10^6 PBMC suspended in 250µl from a different donor. VPD-stained PBMCs harvested at day 5 by peritoneal lavage and the proliferation rates of human CD4 and CD8 T cells were examined by FACS. As a control, the same volume of medium was concentrated and injected into the mice (medium control). As a reference of human T cells gating and proliferation, VPD-stained PBMC were stimulated *in vitro* in the presence of anti-CD3/CD28 beads (*in vitro* ref). (a) Representative histograms illustrating CD4 (left panel) and CD8 (right panel) T cell proliferation either at maximum (Max proliferated cells) or minimum (min proliferated cells) rate in each condition. (b) A bar chart of the CD8 T cell division index. Each dot

represents an individual mouse. Columns represent mean ± SD.

Chapter 6: Investigating the mechanism by which immunosuppressive small EVs are produced by human Tregs following mitochondrial ATP synthase inhibition

6.1 Introduction

In *chapter 5*, we revealed that both *ex vivo* and expanded human Tregs produce immunosuppressive small EVs following mitochondrial ATP synthase inhibition by oligomycin, with a huge potential to translate this into clinical therapy. However, the molecular mechanisms by which mitochondrial ATP synthase inhibition induces the production of immunosuppressive small EVs in human Tregs remains unknown. Mitochondrial ATP synthase is also known as mitochondrial complex V which contributes to the terminal reaction of electron transport chain (ETC) to generate ATP in the mitochondria (307). Whilst mitochondria are important organelles required to maintain cellular energy homeostasis, recent studies have demonstrated that mitochondria also work as signalling organelles (225, 334). Therefore, the production of immunomodulatory small EVs following mitochondrial ATP synthase inhibition may not

simply result from suppression of ATP synthesis through OXPHOS inhibition, but instead may result from the modulation of mitochondrial signalling pathways. Because cellular proliferation requires a large quantity of ATP, Treg proliferation rate is reduced following oligomycin treatment (***Figure 3.9.c***). Moreover, despite of the production of immunosuppressive small EVs by Tregs, oligomycin slightly decreases the actual quantity of small EVs produced which may be caused by a lower energy metabolism of Tregs (***Figure 5.7.c***). Therefore, clarifying the molecular mechanism may reveal different targets to induce production of immunosuppressive small EVs by Treg without decreasing their energy metabolism. This may be advantageous for Treg cellular therapy compared with oligomycin administration by maintaining Treg proliferation and also by inducing higher production of immunosuppressive small EVs.

Mitochondrial stress can induce dysfunction or disruption of mitochondria leading to mitochondrial ROS production or mitochondrial DNA leakage, both of which initiate cellular signalling cascades (334, 335). Mitochondrial ROS are primarily generated by mitochondrial complexes I and III (201). As discussed in *Chapter 4*, mitochondrial ROS

directly modulate $CD4^+$ T cell effector function with high mitochondrial ROS production increasing production of Th-2 type cytokines and low mitochondrial ROS production increasing production of Th1- and Th17- type cytokines (313, 315-317). Tregs exhibit higher production of ROS compared with bulk CD4 Tconvs (336). However, the effect of ROS on Treg suppressive function is complicated. For example, Guo *et al* demonstrated that Tregs from aged mice produce an excess of ROS which was associated with impaired immunosuppressive function (337). Here, the reduction of ROS using N-acetyl cysteine recovered the suppressive function of aged Tregs illustrating the negative regulatory role of ROS in Treg suppression. However, others have demonstrated that reduced ROS production impairs Treg suppression (229, 338). Mechanistically, ROS is required for the accumulation of SUMO-specific protease 3 in Tregs following stimulation, which maintains stable FOXP3 expression. ROS in Tregs are therefore likely to be tightly regulated for optimal Treg suppressive function. Oligomycin treatment blocks only the last reaction of the ETC, with the result that other mitochondrial complexes maintain the intracellular proton gradient causing hyperpolarisation of the mitochondrial membrane potential. This in turn causes reverse electron transport (RET) and eventually results in

the production of ROS (339, 340). ROS generated by oligomycin treatment may induce mitochondrial damage releasing mitochondrial DNA into the cytosol resulting in the initiation of intracellular signalling cascades (341). Mitochondrial DNA in Tregs is known to induce production of the immunosuppressive cytokine IL-10 via the IFN type 1 signalling pathway (230). Thus, oligomycin treatment may alter Treg behaviour via ROS and possible mitochondrial DNA leakage. However, whilst there have been some studies examining the relationship between ROS, mitochondrial DNA and Treg suppressive function, the relationship between ROS, mitochondrial DNA and small EV production remains unknown.

Oligomycin treatment blocks Treg respiratory energy production resulting in enhanced glycolysis to compensate for reduced ATP synthesis. Blocking a part of the ETC by oligomycin may also modify the composition of TCA cycle intermediates. Metabolic intermediates and metabolic pathway enzymes may regulate cellular function (185, 186). For example, glucose deprivation decreases the usage of glycolysis enzymes in the glycolysis pathway, which increases non-canonical functions of glycolytic enzymes in

Tconvs including negative regulation of cytokine synthesis (27, 342). We have demonstrated that engaging glycolysis is key to maintaining human CD4 Tconv effector function (***Figure 4.12***). Metabolites of the TCA cycle may also regulate T cell function. For example, a secondary function of acetyl-CoA is to acetylate histones which promotes transcription of DNA (227). Glucose-derived acetyl-CoA is required for CD4 T cell expression of IFN-γ by histone modification (198). Extracellular fatty acids also provide a source of acetyl-CoA, but short-chain fatty acids such as butyrate and propionate directly increase histone acetylation by inhibiting histone deacetylases (HDACs) (227, 343). Inhibition of HDACs by short chain fatty acid enhances *foxp3* expression by histone acetylation in Tregs (344, 345). Indeed, pharmacological inhibition of HDAC 11 increases Treg suppressive function with increased *foxp3* expression (346). DNA demethylation may also be mediated by α-ketoglutarate which modulates epigenetic marks through acting as a cofactor of ten-eleven translocation (TET) or the Jumonji C domain-containing histone demethylase (JHDMs) (225-227). Succinate, fumarate and 2-hydroxyglutarate have homologous structures to α-ketoglutarate, and so competitively inhibit TET and JHDMs. Thus, the balance between α-ketoglutarate and succinate, fumarate and 2-

hydroxyglutarate regulates DNA and histone methylation. Mouse Tregs with mitochondrial complex III deletion exhibit significantly impaired suppressive function independent of their *foxp3* expression (228). Importantly, this is associated with both hypermethylation of DNA coding neuropilin-1, PD-1, CD73 and TIGIT, and with accumulation of succinate and 2-hydroxyglutarate (228). Whilst this study did not directly prove that the accumulation of succinate and 2-hydroxyglutarate was responsible for impaired Treg suppressive function, it clearly illustrates that modulation of mitochondrial respiration at least changes DNA methylation status in mouse Tregs.

Methionine is an essential amino acid that is catabolised to succinyl-CoA in order to enter the TCA cycle; its intermediate, S-adenosyl methionine (SAM), methylates both DNA and histones by transfer of a methyl group (227, 347). Mouse CD4 T cells uptake methionine on activation whilst methionine restriction reduces intracellular SAM (348). Methionine restriction reduces CD4 T cell histone H3K4 methylation which decreases expression of certain genes including IFN-γ and IL-17A. SAM is also important for human Treg *FOXP3* expression through histone methylation by the protein arginine

methyltransferase 5 (PRMT5) (349). Pharmacological SAM-competitive PRMT5 inhibitors reduce human Treg suppressive function by inhibiting histone methylation. An interaction between TCA intermediates and components of small EVs has not been reported in any cell types. However, because TCA intermediates may modify DNA epigenetics, microRNAs (miRNAs) in Treg-derived small EVs play a key role their immunosuppressive properties (144, 147, 148), and miRNAs are influenced by DNA epigenetic modification (350), it is plausible that alteration of TCA intermediates enhances the immunosuppressive function of Treg-derived small EVs through modification of their genetic payload.

In addition to induction of HIF, hypoxia also induces mitochondrial ROS production through mitochondrial complex III and alters both glycolysis and TCA cycle intracellular metabolic signatures (351-353). Moreover, oxygen is a substrate for the DNA-demethylating TET enzyme; hypoxia therefore directly controls epigenetics by suppressing DNA demethylation (354). Although the mechanism remains unclear, hypoxia is known to alter the content of small EVs produced by certain cell types (334,

355). For example, human mesenchymal stem cells produce distinct small EVs that induce anti-inflammatory macrophage polarisation and increase environmental IL-10 concentration under hypoxic conditions (356, 357). Similarly, hypoxia induces the production of immunosuppressive small EVs from certain human cancer cells (358-360). Whether this pattern equally applies to small EV production by human Tregs remains to be seen, but plausibly Tregs may also modulate the contents of their small EVs under hypoxic conditions via mitochondrial signalling pathway and epigenetic alterations.

To summarise, oligomycin treatment alters Tregs by three possible mechanisms:

1. Low energy production,
2. High ROS production and mitochondrial DNA leakage, and
3. Altered metabolite profile.

Whilst EM human Tregs exhibit a lower OXPHOS rate compared to $CD4^+$ EM Tconvs (***Figure 4.7.d***), they nevertheless highly express pyruvate-acetyl CoA metabolism regulatory genes (***Figure 4.9.e***). As TCR intermediates are known to modulate DNA

epigenetics and miRNA plays a key role in Treg-derived small EV immunosuppression, we hypothesised that oligomycin treatment modifies the composition of Treg intracellular metabolites which alter Treg epigenetics and the miRNA composition of Treg small EVs.

6.1.1 Chapter aim

The aim of this chapter is to investigate the mechanisms by which oligomycin induces Treg production of immunosuppressive small EVs.

6.2 Mitochondrial complex I and III inhibitors do not induce production of Treg immunosuppressive small EVs.

Oligomycin treatment completely blocks ATP-linked OXPHOS and dramatically reduces Treg energy production, which in turn induces the AMP-activated protein kinase (AMPK) signalling pathway to adopt a low energy status (361). Moreover, oligomycin treatment induces RET and generates mitochondrial ROS (339, 340). To investigate if oligomycin treatment induces production of immunosuppressive EVs from Tregs via either low

energy production or mitochondrial ROS generation, we used different mitochondrial inhibitors targeting mitochondrial complex I (rotenone) and III (antimycin A). First, we confirmed that rotenone and antimycin A inhibit human Treg respiration using the Seahorse XF. As expected, injections of rotenone or antimycin A dramatically reduced oxygen consumption rate (OCR) akin to oligomycin demonstrating that both rotenone and antimycin A block mitochondrial energy production (***Figure 6.1.a***). Importantly, injection of FCCP, which uncouples transporting protons across the mitochondrial inner membrane, did not increase OCR in rotenone- or antimycin A-treated Tregs unlike oligomycin. This indicates that the decrease in OCR observed following rotenone and antimycin A administration results from specific inhibition of complex I or III disrupting the generation of the mitochondrial intermembrane proton gradient. However, the low OCR we observed in Tregs following rotenone or antimycin A injections could simply be caused by cell death as both rotenone and antimycin A are known to induce excess ROS production (362, 363). To check that these agents did not induce Treg death we analysed Treg ECAR which, if strongly cytotoxic, would dramatically reduce. Injections of rotenone and antimycin A, however, increased Treg ECAR in a manner similar to that observed

following oligomycin administration. This indicates that rotenone and antimycin A did not induce cell death, but instead induced a higher rate of aerobic glycolysis to compensate for a lack of energy production in a similar manner to oligomycin (***Figure 6.1.b***). Thus, rotenone and antimycin A can modify Treg energy metabolism in a similar manner to oligomycin.

Next, we investigated if rotenone and antimycin A can enhance Treg suppressive function by inducing production of immunomodulatory small EVs. To examine this, we pre-treated Tregs with either rotenone, antimycin A, or oligomycin for 2 hours and then co-incubated these with VPD-stained $CD4^+$ T cells in the presence of anti-CD3/CD28 beads. Surprisingly, neither rotenone nor antimycin A pre-treated Tregs enhanced Treg suppressive function despite effective OXPHOS inhibition. This indicates that OXPHOS inhibition itself does not induce production of immunosuppressive small EVs from Tregs (***Figure 6.2.a***). However, this result may possibly be because the effect of rotenone and antimycin A is not irreversible unlike oligomycin. To confirm that complex I and III inhibitors do not induce immunosuppressive small EVs, we first incubated Tregs with

these inhibitors for 48 hours in the presence of anti-CD3/CD28 beads. The Treg culture supernatants were removed and filtered using 100 kDa filters to separate small EVs, which are over 100 kDa, from the remaining mitochondrial inhibitors. The isolated small EVs were repeatedly washed by PBS using a 100 kDa filter to remove the inhibitors prior to addition into a $CD4^+$ T cell proliferation assay. Molecules over 100 kDa isolated from rotenone- and antimycin A- treated Tregs did not suppress $CD4^+$ T cells proliferation unlike oligomycin treated Tregs confirming that only inhibition of mitochondrial complex V, but not I and III, induces production of immunosuppressive small EVs from human Tregs (***Figure 3.2.b***).

Rotenone and antimycin A completely block Treg OXPHOS by inhibiting mitochondrial complex I and complex III, respectively. However, these drugs did not induce the production of immunosuppressive small EVs from Tregs. Therefore, the production of immunosuppressive small EVs is not induced by low energy metabolism. Moreover, rotenone and antimycin A are known to induce high ROS production. Thus, both ROS and possible leakage of mitochondrial DNA also are unlikely to modify the contents of

Treg small EVs. Others have reported that targeting different mitochondrial complexes induces distinct metabolomic signatures (228, 364). Therefore, we hypothesised that oligomycin induces Treg immunosuppressive small EV production via changing Treg metabolic signature.

6.3 Tconvs do not produce immunosuppressive small EVs from Tconvs. Distinct metabolic responses of Tregs and Tconvs induced by oligomycin correlate with the ability to produce immunosuppressive small EVs.

We hypothesised that mitochondrial complex V inhibition by oligomycin induces Treg to produce immunosuppressive small EVs via modulating Treg metabolism intermediates. However, whether this applies solely to Tregs or also to Tconvs remains to be established. To investigate this, we first expanded Tconvs *in vitro* by the same expansion method. Unlike mouse Tconvs, human CD4 Tconvs begin expressing FOXP3 after stimulation and can obtain contact-dependent immunosuppressive function (79, 80). In agreement with

this, our *in vitro* expanded CD4 Tconvs (expanded Tconvs) also started expressing FOXP3 (***Figure 6.3.a***). However, expanded Tconvs completely lacked the capacity to produce immunosuppressive small EVs revealing that induced production following mitochondrial complex V inhibition occurs only in Tregs, and importantly is not driven by FOXP3 expression (***Figure 6.3.b***).

As expanded Tconvs completely lack the ability to produce immunosuppressive small EVs despite FOXP3 expression, we next hypothesised that this observation is correlated to distinct metabolic responses of Tconvs and Tregs to oligomycin treatment. To investigate this directly, we used mass-spectrometry based metabolomics. Expanded Tregs and expanded Tconvs were pre-treated with DMSO (ctrl) or oligomycin (oligo) for 2 hours, washed intensively, and stimulated for 48 hours prior to extraction of metabolites. As expected, the metabolomics profile of expanded Tregs and Tconvs was differentially altered by oligomycin treatment (***Figure 6.4***). Within Tconvs, oligomycin treatment generally reduced the amount of metabolites except for glycolysis intermediates including glucose 6-phosphate. This indicates that oligomycin-treated Tconvs have a

generally lower metabolism except for enhanced glycolysis which compensates for reduced energy production. On the other hand, within Tregs, approximately half of detected metabolites were increased. This reveals that Tregs do not simply suppress their metabolism after oligomycin treatment but instead enhance certain pathways, suggesting that only human Tregs and not human Tconvs have a specific metabolic mechanism to modulate the components of their small EVs after oligomycin treatment.

Taken together, immunosuppressive small EV production after mitochondrial complex V inhibition is only observed in Tregs, and not in CD4 Tconvs. Because expanded CD4 Tconvs inducibly express FOXP3, the mechanism of EV production is unlikely to be directly dependent on FOXP3 expression. We hypothesised that intracellular metabolites trigger the production of immunosuppressive small EVs from Tregs. As expected, oligomycin treatment dramatically changes the Treg metabolic profile, whilst Tconvs generally supress their metabolism as they reduce their energy production. Thus, the ability to produce immunosuppressive small EVs after oligomycin treatment seems to be correlated with differential metabolic responses to oligomycin treatment.

6.4 Mitochondrial complex V inhibition appears to induce high lipid synthesis and epigenetic change in Tregs.

We showed that oligomycin treatment dramatically alters the metabolic profile of Tregs. Next, we deeply analysed which metabolites or metabolic pathways play a key role in inducing production of immunosuppressive small EVs. As oligomycin targets mitochondrial ATP synthase, which is involved in the TCA cycle metabolism, we focused on branches of the TCA cycle and glycolysis which are enhanced by respiratory inhibition (***Figure 6.5.a and b***). As expected, metabolites in the glycolysis pathway were generally increased in oligomycin-treated Tregs. Interestingly, whilst metabolites in the pentose phosphate pathway (PPP) increased, another glycolysis branch, the hexosamine pathway, decreased in oligomycin-treated Tregs. The PPP is an important mechanism to reduce $NADP^+$ into NADPH and produce ribose 5-phosphate which is subsequently used for purine and pyrimidine synthesis (***Figure 6.6.a***). NADPH is a key substance required to maintain cellular redox balance by reducing oxidised glutathione. Although oligomycin-treated Tregs demonstrated a high PPP flow inducing high NADPH production, the amount of oxidised glutathione remained unchanged. This indicates that the ROS

produced by oligomycin treatment is reduced by this system and that Treg redox balance is highly regulated. Notably, one metabolite in the PPP called ribulose 5-phosphate was increased only in Tregs and was decreased in Tconvs (***Figure 6.6.b***). The PPP is divided into two pathways: an irreversible pathway derived from the upper stream of glycolysis which generates NADPH, and a reversible pathway derived from the lower stream of glycolysis which does not generate NADPH. The last step of the irreversible PPP is to produce ribulose 5-phosphate. Therefore, we assume that Tconvs do not increase NADPH production after oligomycin treatment. This assumption is supported by our observation that the amount of oxidised glutathione is slightly reduced in Tconvs. Thus, Tconvs are more susceptible to damage by ROS induced by oligomycin compared to Tregs. When it comes to aerobic glycolysis, oligomycin-treated Tconvs increase glucose 6-phosphate but maintain the same level of intracellular lactate production. This indicates that the increased lactate export rate does not limit the rate of increased aerobic glycolysis in Tconvs. On the other hand, oligomycin-treated Tregs significantly increase all detected aerobic glycolysis metabolites except for pyruvate, indicating that the rate of lactate export capacity is not high enough to maintain the amount of intracellular

lactate in Tregs following oligomycin treatment. Despite high glycolysis intermediates and lactate (the end-product of glycolysis), the amount of intracellular pyruvate was unchanged in Tregs suggesting that the higher amount of pyruvate generated by enhanced glycolysis is consumed by the TCA cycle. Taken together, Tregs enhance aerobic glycolysis and the irreversible PPP. The enhanced irreversible PPP indicates that Tregs have a higher resistance to ROS-induced damage compared with Tconvs after mitochondrial ATP synthase inhibition. Moreover, oligomycin-treated Tregs accumulate glycolysis intermediates intracellularly which allows Tregs to use pyruvate in the TCA cycle.

Next, we investigated specific branches of TCA cycle (***Figure 6.7.a***). After entering mitochondria, pyruvate is catalysed into acetyl-CoA and then enters the TCA cycle. Although analysis of oligomycin-treated Treg glycolysis suggested a high flow of pyruvate into the TCA cycle, the amount of citrate and cis-aconitate were lower in treated compared with control Tregs (***Figure 6.7.a and b***). The metabolite α-ketoglutarate is produced downstream of the TCA cycle, and was more accumulated in oligomycin-

treated Tregs. This indicates that pyruvate-derived mitochondrial acetyl-CoA seems to be consumed by a different pathway. Instead of catalysing into cis-aconitate, citrate can be exported from mitochondria via the mitochondrial citrate carrier and converted into cytosolic acetyl-CoA, which has an important role in protein acetylation including histone acetylation and lipid synthesis. Thus, oligomycin-treated Tregs consume glucose-derived pyruvate to increase cytosolic acetyl-CoA by bypassing citrate, which increases protein acetylation and lipid synthesis. Despite low cis-aconitate accumulation, intracellular α-ketoglutarate is increased in oligomycin-treated Tregs indicating that Tregs exhibit high glutamine consumption when mitochondrial ATP synthase is inhibited. This was interestingly contrasted with oligomycin-treated Tconvs which showed a significant reduction of TCA cycle intermediates including α-ketoglutarate and fumarate. The high glutamine metabolism in oligomycin-treated Tregs was correlated with accumulation of 2-hydroxyglutarate and fumarate (an intermediate downstream of the TCA cycle). Unfortunately, we could not detect succinate in our mass spectrometry experiment despite accumulation of the succinate downstream metabolites, fumarate and succinic semialdehyde, which suggests higher intracellular succinate in oligomycin-treated Tregs.

In addition to glutamine, catabolism of other amino acids was also enhanced by oligomycin treatment in Tregs. Isoleucine, methionine, threonine, and valine entered the TCA cycle via succinyl-CoA. The intermediate of isoleucine catabolism, 3-methyl-2-oxovalerate was increased in oligomycin-treated Tregs. Similarly, α-ketobutyrate, an intermediate of methionine and threonine metabolism, also accumulated. The accumulation of metabolic intermediates suggests a high rate of metabolism of these amino acids. Interestingly, this was a general characteristic of Tregs whilst oligomycin treatment of Tconvs did not increase intermediates of amino acids metabolism. Thus, the TCA cycle in oligomycin-treated Tregs is characterised by two distinct features: reduction of upper intermediates (citrate and cis-aconitate) due to high flow of cytosolic acetyl CoA production; and accumulation of lower intermediates (α-ketoglutarate and fumarate) due to high glutamine and other amino acid metabolism. The enhanced glutamine metabolism after oligomycin treatment is a characteristic feature of Tregs, since Tconvs instead reduce intracellular α-ketoglutarate and fumarate when mitochondrial ATP synthase is inhibited.

High glutamine metabolism is a characteristic of oligomycin-treated Tregs. α-ketoglutarate works as a cofactor of TET and JHDM for DNA and histone demethylation, whilst 2-hydroxyglutarate, succinate, and fumarate competitively inhibit α-ketoglutarate (225-227). Thus, the balance of α-ketoglutarate to α-ketoglutarate analogues (2-hydroxyglutarate, succinate, and fumarate) impacts the methylation status of DNA and histones. To investigate how mitochondrial ATP synthase inhibition changes the balance of α-ketoglutarate and its analogues, we calculated how the ratio of these metabolites changed after inhibition. Whilst both α-ketoglutarate and 2-hydroxyglutarate increased in oligomycin-treated Tregs, the increase of 2-hydroxyglutarate was higher (***Figure 6.7.c***). The ratio of fumarate to α-ketoglutarate did not change by mitochondrial ATP synthase inhibition (***Figure 6.7.d***). Although we could not calculate the ratio of succinate to α-ketoglutarate, oligomycin-treated Tregs may have more methylated DNA and histones due to higher expression of 2-hydroxyglutarate compared with α-ketoglutarate which inhibits demethylation enzymes. The high methylation status after oligomycin treatment is not a Treg-specific phenomenon as Tconvs also increased the ratio of 2-hydroxyglutarate to α-ketoglutarate. However, unlike Tregs which increase 2-

hydroxyglutarate after oligomycin treatment, an elevated 2-hydroxyglutarate to α-ketoglutarate ratio in Tconvs was driven by a reduction in intracellular α-ketoglutarate. The ratio of fumarate to α-ketoglutarate was also increased in oligomycin-treated Tconvs. Therefore, oligomycin likely inhibits DNA and histone demethylation in both Tregs and Tconvs by changing the balance of α-ketoglutarate to its analogues.

Lastly we analysed methionine metabolism (***Figure 6.8.a***). Methionine is first catabolised into SAM, which acts as a methyl donor to other biological substrates including DNA and histones. SAM also donates a methyl group to phospholipid to produce phosphatidylcholine (PtdCho) from phosphatidylethanolamine (PtdEtn), both of which are abundant phospholipids in biological membranes including exosomes (365). Both PtdCho and PtdEtn can be generated from diacylglycerol (DAG) which is synthesised from glycolysis-derived glycerol 3-phosphate and citrate-derived acetyl CoA. The formation of PtdCho and PtdEtn from DAG require CDP-ethanolamine and citicholine which are derived from ethanolamine and choline, respectively. Although the level of CDP-ethanolamine was unchanged between control and oligomycin-treated Tregs, citicholine

accumulated more in oligomycin-treated Tregs (***Figure 6.8.b***). This indicates that oligomycin-treated Tregs have either an enhanced choline uptake, an enhanced PtdEtn methylation which generates more PtdCho than required, or a lower consumption rate of PtdCho. SAM forms S-adenosyl-L-homocysteine (SAH) after demethylation which it further converts into homocysteine and adenosine. Adenosine is a purine nucleoside that is converted into either a purine nucleotide or urate during elimination. Accumulation of purine nucleotides and urate indicates high SAH metabolism in oligomycin-treated Tregs. Homocysteine is then either recycled into methionine by accepting a methyl group from 5-methyl tetrahydrofolate or choline-derived betaine, or is catabolised into α-ketobutyrate and cysteine. Although intracellular taurine (a cysteine metabolite) remained unchanged, α-ketobutyrate was accumulated in oligomycin-treated Tregs indicating high homocysteine production from SAH. α-ketobutyrate then enters into the TCA cycle via succinyl CoA. This metabolic pathway requires vitamin B12 as a coenzyme; vitamin B12 deficiency causes the accumulation of a side product, methylmalonate (366). Vitamin B12 is also required for homocysteine methylation from 5-methyl tetrahydrofolate. Importantly, intracellular methylmalonate was decreased in

oligomycin-treated Tregs despite α-ketobutyrate accumulation indicating that oligomycin-treated Tregs have sufficient intracellular vitamin B12 for their biological processes. Therefore, recycling of homocysteine into methionine was not inhibited by vitamin B12 deficiency. Taken together, oligomycin-treated Tregs accumulated citicholine but not CDP-ethanolamine, purine metabolites, and catabolites of homocysteine. This indicates that oligomycin-treated Tregs enhance their methionine metabolism cycle and their methylation processes including DNA and histone methylation. Interestingly, citicholine, purine metabolites, and α-ketobutyrate were not increased in oligomycin-treated Tconvs. Therefore, the enhanced methionine cycle after mitochondrial ATP synthase inhibition occurs only in Tregs.

We conclude that oligomycin-treated Tregs enhance the irreversible PPP to increase NADPH which maintains redox balance and causes accumulation of aerobic glycolysis intermediates to provide pyruvate to the TCA cycle. Pyruvate is then converted into cytosolic acetyl CoA via citrate which is used for protein acetylation or lipid synthesis. Glutamine metabolism is also enhanced in oligomycin-treated Tregs, resulting in the

maintenance of high amounts of TCA cycle intermediates after α-ketoglutarate despite low cis-aconitate. Although oligomycin-treated Tregs accumulate α-ketoglutarate compared to control, accumulation of 2-hydroxyglutarate occurs to a greater degree. Therefore, DNA and histone demethylation is disturbed by 2-hydroxyglutarate antagonising α-ketoglutarate in oligomycin-treated Tregs. At the same time, DNA and histone methylation is enhanced in oligomycin-treated Tregs due to high methionine metabolism. Thus, mitochondrial ATP synthase inhibition induces lipid synthesis and epigenetic changes in Tregs due to enhanced acetylation and methylation process via a modulated metabolic profile.

6.5. Mitochondrial ATP synthase inhibited Tregs require glucose to produce immunosuppressive small EVs.

Our metabolomics study revealed that oligomycin-treated Tregs enhance both aerobic glycolysis to compensate for energy deprivation, and PPP to maintain redox balance. Accumulation of lactate but not pyruvate indicates that high glycolytic flow is also

required to supply the TCA cycle from glucose. Because oligomycin blocks mitochondrial ATP synthesis, the high flow observed to the glucose-acetyl CoA pathway is not for ATP synthesis. Indeed, the TCA cycle intermediates citrate and cis-aconitate were decreased in oligomycin-treated Tregs, indicating that glycolysis-derived pyruvate is used for cytosolic acetyl-CoA synthesis leading to protein acetylation and lipid synthesis. This suggests that glucose metabolism plays an important role in immunosuppressive small EV synthesis from oligomycin-treated Tregs not only for generating ATP. We therefore hypothesised that mitochondrial ATP synthase inhibition in a glucose limited environment does not induce Tregs to produce immunosuppressive small EVs. To investigate this, we incubated oligomycin-treated Tregs under glucose limiting conditions in the presence of anti-CD3/CD28 beads for 48h. We first investigated the viability of Tregs, because in a glucose-deprived condition Tregs do not generate energy. As expected, when glucose was entirely absent from the culture medium (*RPMI 1640, no glucose*, no human serum) Tregs did not survive (***Figure 6.9.a***). To investigate Treg survival in a glucose restricted environment we used culture medium comprising *RPMI 1640 without glucose* supplemented with 10% human serum (which contains less than

1 mM glucose). In this condition, although viability is notably lower than control medium condition, more than 60% of oligomycin-treated Tregs survived.

We then investigated if the oligomycin-treated Tregs cultivated under very low glucose medium produced immunosuppressive small EVs. To examine this, the supernatants of oligomycin-treated Tregs cultured in medium containing differing quantities of glucose were added to a VPD-stained $CD4^+$ T cell proliferation assay. Surprisingly, incubation in very low glucose medium completely abolished the production of immunosuppressive small EVs by oligomycin-treated Tregs (***Figure 6.9.b***).

We conclude that mitochondrial ATP synthase inhibited Tregs completely lose the ability to produce immunosuppressive small EVs under a low glucose condition. This is not simply due to cell death from lack of ATP synthesis because mitochondrial ATP synthase inhibited Tregs still survive. Instead, this finding likely arises from the inhibition of other pathways that require either ATP or are derived from glucose metabolism including lipid synthesis and protein acetylation from cytosolic acetyl-CoA.

6.6 Discussion

Here we showed that rotenone and antimycin A induce similar but not indentical metabolic changes in Tregs compared with those treated with oligomycin, as demonstrated by Seahorse XF. However, neither rotenone nor antimycin A induced immunosuppressive small EV production (***Figure 6.2***). Moreover, both inhibitors are known to induce excess production of ROS (362, 363). Thus, immunosuppressive small EV production from oligomycin-treated Tregs does not result from OXPHOS inhibition or ROS production. On the contrary, it has been reported that targeting different mitochondrial complexes induces distinct metabolic signatures (228, 364). Therefore, we conclude that mitochondrial complex V inhibition by oligomycin induces Tregs to produce immunosuppressive small EVs via changing their metabolomics profile. However, it is not yet clear what key metabolic changes are induced by mitochondrial complex V inhibition compared with complex I and III inhibition. Given that the metabolic profile induced by oligomycin was completely different between Tregs and Tconvs (***Figure 6.4***), extrapolating oligomycin specific changes to Tregs from studies of other cell types has clear limitations. Additional metabolomics studies to compare

oligomycin treated Tregs with rotenone or antimycin A treated Tregs may narrow down the metabolic pathways responsible for immunosuppressive small EV induction.

We demonstrate that Tconvs completely lack the ability to produce immunosuppressive small EVs after oligomycin treatment which was correlated with a distinct metabolomic signature after inhibition compared with Tregs (***Figure 6.3.b and 6.4***). However, this does not necessarily mean that Tconvs would produce immunosuppressive small EVs if a similar metabolomics signature was somehow induced. Although Tregs were originally defined as T cells expressing FOXP3, Tregs and Tconvs also display distinct epigenetic signatures (72, 367). Even when FOXP3 is overexpressed in Tconvs, approximately 70% of genes remain differentially expressed (368). Moreover, a Treg-specific gene expression pattern and epigenetic signature can be observed in Tregs from *foxp3* mutated mice (72, 369, 370). Therefore, it is reasonable to assume that the Treg epigenetic signature controls their specific phenotype to some degree independently of FOXP3 expression. However, despite a demonstrable Treg epigenetic signature in *foxp3* mutated Tregs, these mice still exhibit a catastrophic autoimmune phenotype (12, 44). Thus, expression

of FOXP3 is still key to maintain Treg immunosuppressive function. At least some Treg suppressive mechanisms are directly controlled by FOXP3 illustrated by the acquisition of contact-dependent immunosuppressive function in human Tconvs expressing FOXP3 (80). Here, we demonstrated that the lack of immunosuppressive small EV production by human expanded Tconvs was associated with a completely distinct metabolomics signature despite stimulation-induced FOXP3 expression compared with oligomycin-treated Tregs. Therefore, both the metabolic changes and production of immunosuppressive small EVs are not dependent on FOXP3, and instead are most probably under epigenetic control in human Tregs.

We also showed that oligomycin-treated Tregs completely cease production of immunosuppressive small EVs when cultured in a glucose limited condition, despite maintaining their viability (***Figure 6.9.***). However, this does not necessarily mean that Tregs require glucose-derived metabolites such as cytosolic acetyl-CoA to induce immunosuppressive small EV production. For example, methionine metabolism may instead be a key factor for the induction of immunosuppressive small EV production

(***Figure 6.8***). Although this step appears to be independent of glycolysis, conversion of methionine into SAM requires ATP. Therefore, limitation of available energy due to limitation of glucose can leads to low methionine metabolism. Therefore, even though the results of our glucose deprivation experiment demonstrates that induction of immunosuppressive small EV production requires at least some ATP production and/or glucose-derived metabolites, it cannot exclude the involvement of other metabolic pathways. Nevertheless, the physiological relevance of this experiment valuably demonstrates that the metabolic harshness in peripheral tissues (OXPHOS inhibition together with glucose deprivation) does not induce Treg production of immunosuppressive small EVs which instead are probably generated in the more metabolically-permissive systemic circulation. Thus, the metabolic harshness of peripheral tissues may limit inflammation by either 1) glucose deprivation alone negatively regulating local Tconv effector function, 2) OXPHOS limitation alone (mitochondrial complex V inhibition) leading to production of immunosuppressive small EVs by Tregs which modulate local and systemic responses, or 3) both glucose and OXPHOS limitation negatively regulating local Tconv effector function but not inducing

small EVs from Tregs. However, as discussed in last chapter, it remains to be determined which physiological or pathological factors may limit Treg mitochondrial complex V.

In this chapter, we revealed that mitochondrial complex V inhibition by oligomycin induces production of immunosuppressive small EVs by Tregs through altering their metabolomics signature (***Figure 6.4***). In summary, oligomycin-treated Tregs:

1) Increase aerobic glycolysis intermediates except for pyruvate,
2) Increase PPP intermediates with unchanged oxidised glutathione,
3) Decrease citrate and cis-aconitate (despite high glucose-derived acetyl-CoA flow),
4) Increase α-ketoglutarate, fumarate, and 2-hydroxyglutarate with a higher 2-hydroxyglutarate to α-ketoglutarate ratio, and
5) Increase products of methionine metabolism.

This metabolic profile suggests that oligomycin-treated Tregs may have:

1. Higher aerobic glycolysis and PPP rates,
2. A higher resistance to ROS-induced damage,

3. Increased lipid synthesis,
4. Increased protein acetylation including histone acetylation, and
5. Increased methylation including of histone and DNA.

However, importantly we still do not know which combination of characteristics induce the production of immunosuppressive small EVs. We hypothesise that modifying intracellular metabolites by oligomycin causes epigenetic changes in Tregs leading to a modified small EV payload including miRNA. Our next steps will be to employ epigenetic techniques to investigate this hypothesis. For example, ATACseq (assay for transposase-accessible chromatin with high-throughput sequencing) may be used to assess chromatin accessibility, bisulfite sequencing to identify DNA methylation regions, and NanoString miRNA expression panel to identify miRNA contained in small EVs produced by oligomycin-treated Tregs. With these techniques we will begin to identify which regions and pathways are of importance in inducting epigenetic changes. These results may allow us to narrow the specific metabolic or epigenetic targets for pharmacological modulation of Tregs without mitochondrial ATP synthesis inhibition.

6.7 Figures and legends

Figure 6.1

(a)

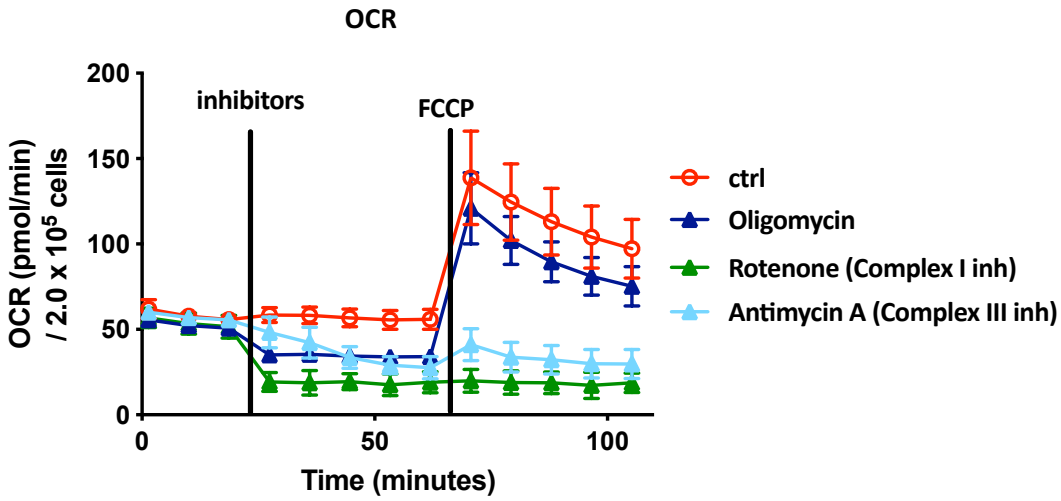

(b)

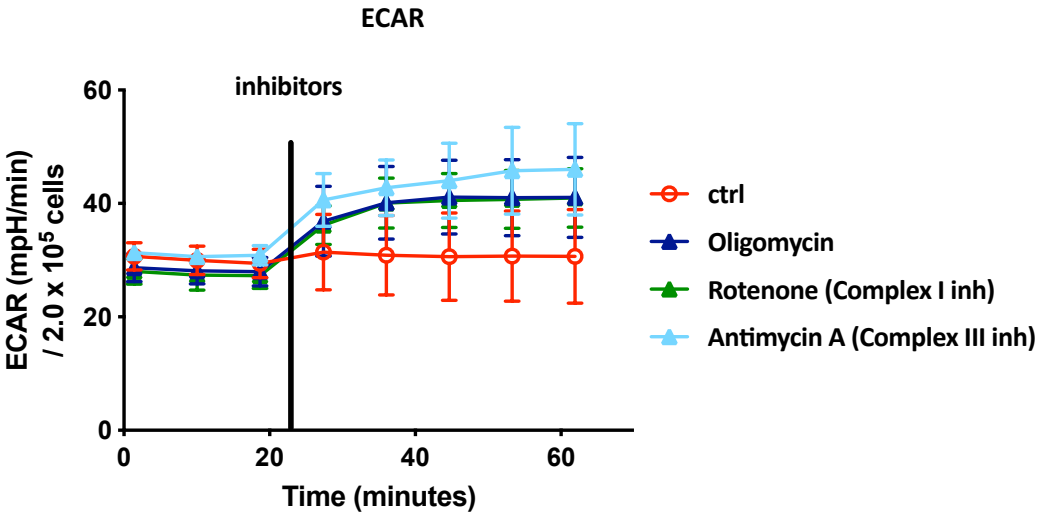

Figure 6.1. Both mitochondrial complex I and III inhibitors supress OXPHOS and increase aerobic glycolysis akin to the mitochondrial complex V (ATP synthase) inhibitor oligomycin.

Human expanded Tregs were applied to the Seahorse XF to investigate the effects of metabolic inhibitors. Mitochondrial complex inhibitors of complex V (oligomycin, 2 uM in final concentration), I (rotenone, 1uM in final concentration), or III (antimycin A , 4 uM in final concentration), or vehicle control (0.2% DMSO in final concentration) were injected during the experiment followed by FCCP injection. (a) A representative OCR plot from one of two independent donors. (b) A representative ECAR plot from one of two independent donors.

Figure 6.2

(a)

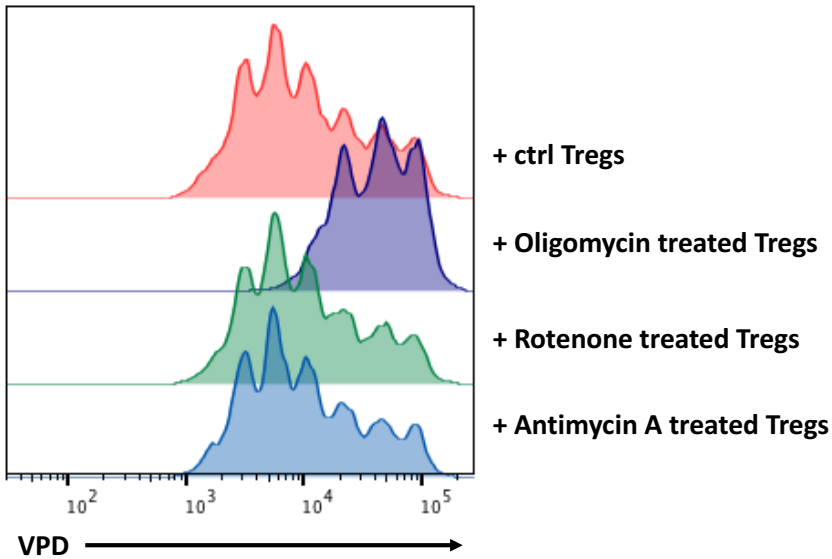
+ ctrl Tregs
+ Oligomycin treated Tregs
+ Rotenone treated Tregs
+ Antimycin A treated Tregs
10^2
10^3
10^4
10^5
VPD

(b)

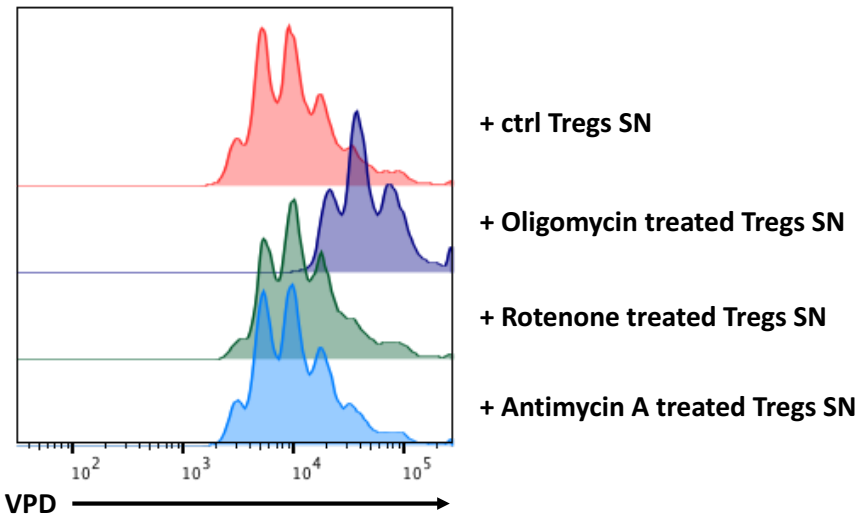
+ ctrl Tregs SN
+ Oligomycin treated Tregs SN
+ Rotenone treated Tregs SN
+ Antimycin A treated Tregs SN
10^2
10^3
10^4
10^5
VPD

Figure 6.2. Mitochondrial complex I and III inhibitions do not enhance Treg suppressive function.

Representative histograms from two independent donors revealing how the proliferation of CD4 T cells is suppressed by Tregs treated with different mitochondrial inhibitors. (a) Freshly isolated human Tregs were pre-treated with 2 uM oligomycin (mitochondrial complex V inhibitor), 1 uM rotenone (mitochondrial complex I inhibitor), 4 uM antimycin A (mitochondrial complex III inhibitor) or 0.2% DMSO (control) for 2 hours, washed intensively, and then co-incubated with VPD-stained CD4 T cells at a 1:1 (Tregs to CD4 T cells) ratio in the presence of anti-CD3/CD28 beads. (b) expanded Tregs were incubated for 48 hours with anti-CD3/CD28 beads in the presence of 2 uM oligomycin (mitochondrial complex V inhibitor), 1 uM rotenone (mitochondrial complex I inhibitor), 4 uM antimycin A (mitochondrial complex III inhibitor) or 0.2% DMSO (control). The supernatants of Treg cell cultures were gently removed and filtered by 100 kDa amicon ultracentrifugal filter to isolate EVs. PBS was added into over 100 kDa and fractionated again using 100 kDa amicon filter to remove mitochondrial inhibitors. The

washing step was repeated and the washed >100 kDa fractions of culture supernatants were added into a CD4 T cell proliferation assay. A representative histogram from one of two donors.

Figure 6.3

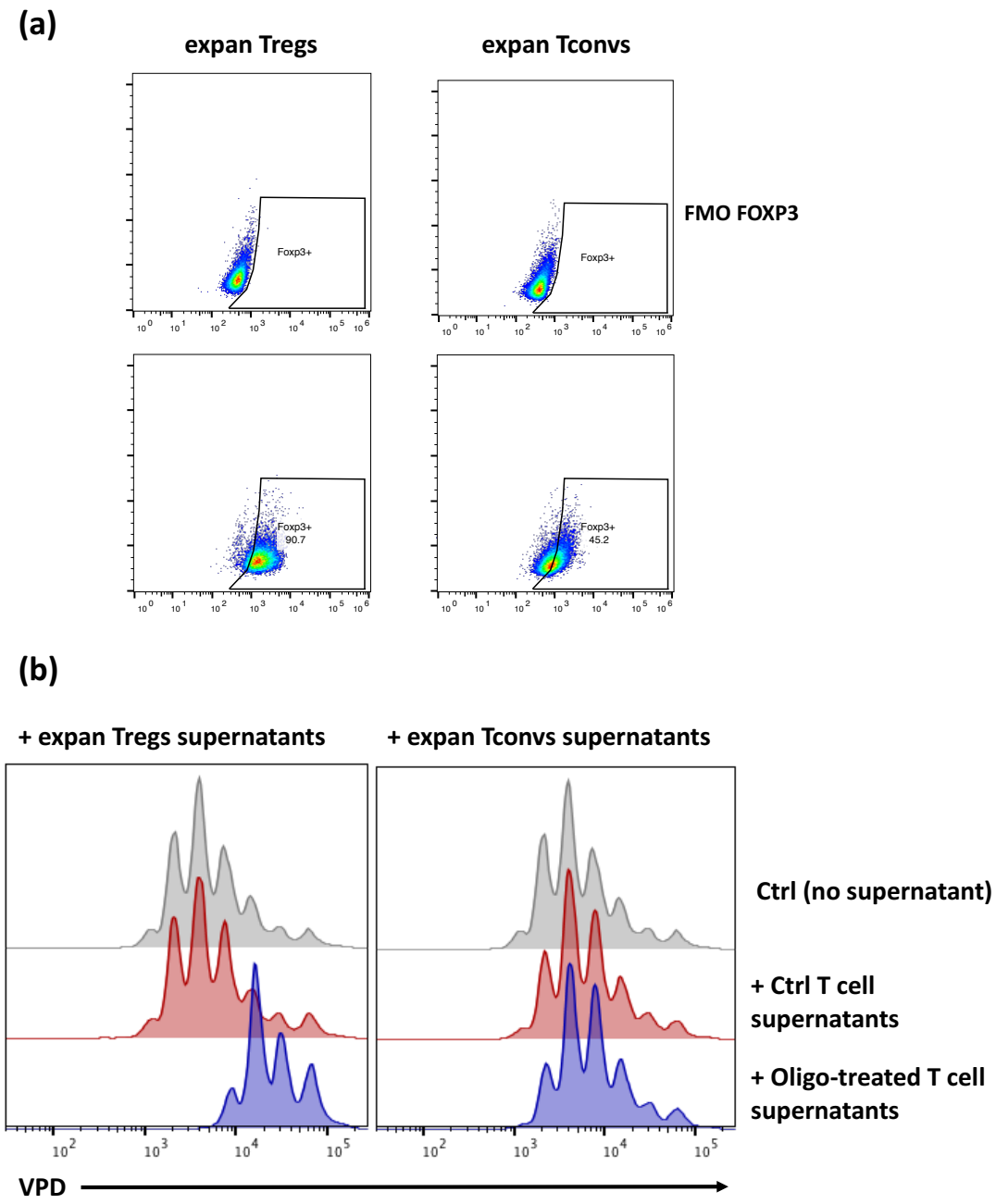
(a)
expan Tregs
expan Tconvs
Foxp3+
FMO FOXP3
Foxp3+
90.7
Foxp3+
45.2
(b)
+ expan Tregs supernatants
+ expan Tconvs supernatants
Ctrl (no supernatant)
+ Ctrl T cell supernatants
+ Oligo-treated T cell supernatants
VPD

Figure 6.3. Mitochondrial ATP synthase inhibition does not induce immunosuppressive small EVs from CD4 Tconvs.

Freshly isolated human CD4 Tconvs were expanded *in vitro* for 2 weeks by the same protocol as Treg expansion. (a) Representative FACS plots from two independent donors showing FOXP3 expression of expanded Tregs and *in vitro* expanded CD4 Tconvs (expanded Tconvs). (b) Representative histograms from two independent donors revealing the suppression of CD4 T cell proliferation by expanded Treg or Tconv culture supernatants. Both expanded Tregs and expanded Tconvs were pre-treated with 2uM oligomycin or 0.2% DMSO for 2 hours, washed intensively and then stimulated with anti-CD3/CD28 beads in fresh medium for 48h. The culture supernatants were gently removed and added into a VPD-stained CD4 T cell proliferation assay in a final concentration of one part of supernatant to three parts cells

Figure 6.4

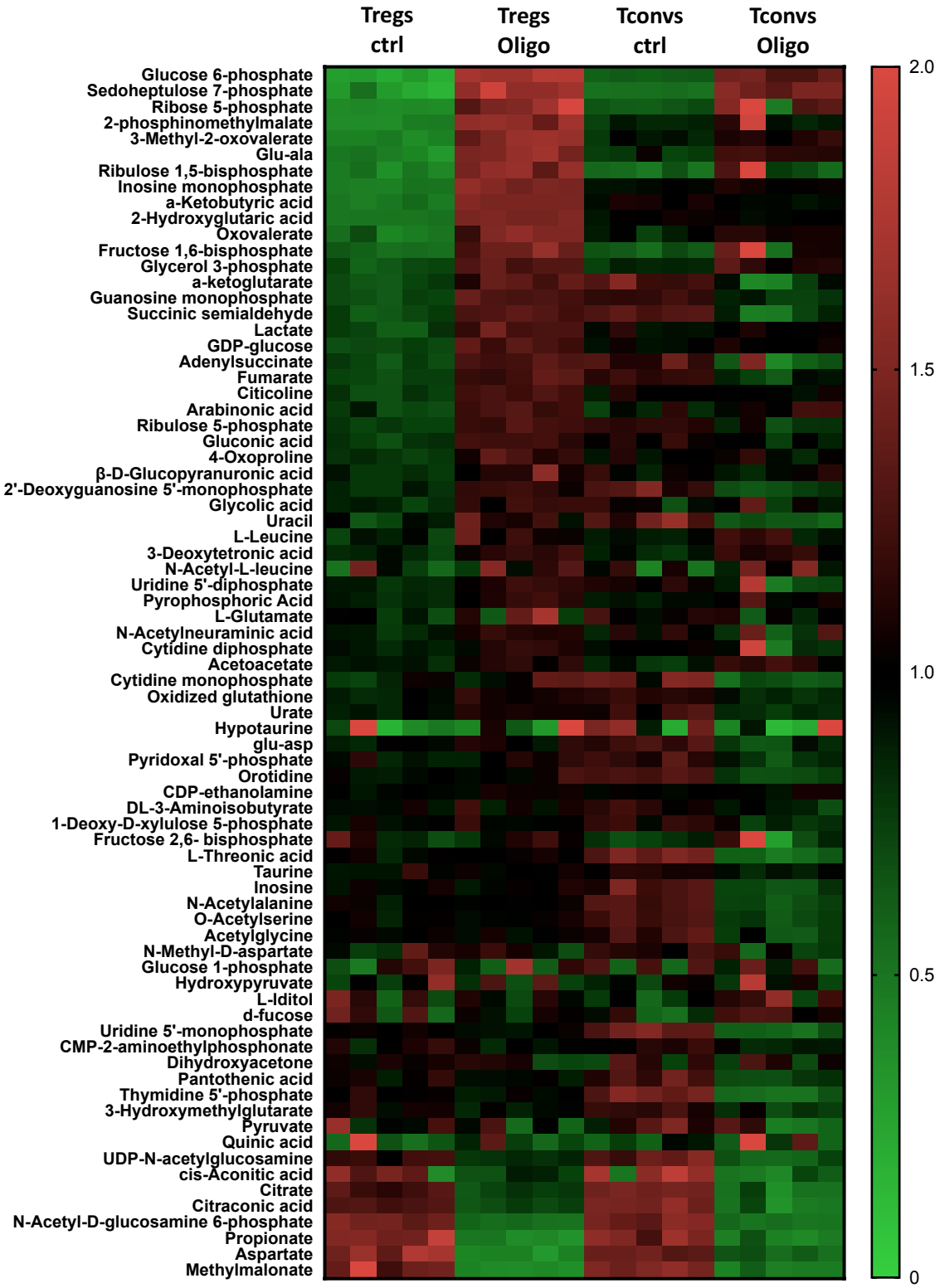
Tregs ctrl
Tregs Oligo
Tconvs ctrl
Tconvs Oligo
Glucose 6-phosphate
Sedoheptulose 7-phosphate
Ribose 5-phosphate
2-phosphinomethylmalate
3-Methyl-2-oxovalerate
Glu-ala
Ribulose 1,5-bisphosphate
Inosine monophosphate
a-Ketobutyric acid
2-Hydroxyglutaric acid
Oxovalerate
Fructose 1,6-bisphosphate
Glycerol 3-phosphate
a-ketoglutarate
Guanosine monophosphate
Succinic semialdehyde
Lactate
GDP-glucose
Adenylsuccinate
Fumarate
Citicoline
Arabinonic acid
Ribulose 5-phosphate
Gluconic acid
4-Oxoproline
β-D-Glucopyranuronic acid
2'-Deoxyguanosine 5'-monophosphate
Glycolic acid
Uracil
L-Leucine
3-Deoxytetronic acid
N-Acetyl-L-leucine
Uridine 5'-diphosphate
Pyrophosphoric Acid
L-Glutamate
N-Acetylneuraminic acid
Cytidine diphosphate
Acetoacetate
Cytidine monophosphate
Oxidized glutathione
Urate
Hypotaurine
glu-asp
Pyridoxal 5'-phosphate
Orotidine
CDP-ethanolamine
DL-3-Aminoisobutyrate
1-Deoxy-D-xylulose 5-phosphate
Fructose 2,6- bisphosphate
L-Threonic acid
Taurine
Inosine
N-Acetylalanine
O-Acetylserine
Acetylglycine
N-Methyl-D-aspartate
Glucose 1-phosphate
Hydroxypyruvate
L-Iditol
d-fucose
Uridine 5'-monophosphate
CMP-2-aminoethylphosphonate
Dihydroxyacetone
Pantothenic acid
Thymidine 5'-phosphate
3-Hydroxymethylglutarate
Pyruvate
Quinic acid
UDP-N-acetylglucosamine
cis-Aconitic acid
Citrate
Citraconic acid
N-Acetyl-D-glucosamine 6-phosphate
Propionate
Aspartate
Methylmalonate
2.0
1.5
1.0
0.5
0

Figure 6.4. Mitochondrial ATP synthase inhibition changes metabolomics profiling of human Tregs differently to Tconvs.

Mass spectrometry-based metabolomics. Human expanded Tregs and expanded Tconvs were pre-treated with 2 uM oligomycin or 0.2% DMSO (control) for 2 hours, washed intensively, and then stimulated by anti-CD3/CD28 beads for 48 hours. Stimulated cells were harvested, washed by PBS, and kept in 80% methanol to extract intracellular metabolites. The extracted metabolites were first centrifuged and filtered through a 10 kDa filter to remove cell debris, and then standardised by NanoDrop based on DNA concentration prior to mass spectrometry assay. A heat map with all detected 76 intracellular metabolites revealing the relative levels of metabolites between the control (ctrl) and oligomycin-treated (Oligo) conditions indicating how oligomycin changes the quantity of intracellular metabolites in Tregs and Tconvs. Each column represents a technical replicate, five of which were prepared separately in culture plates.

Figure 6.5

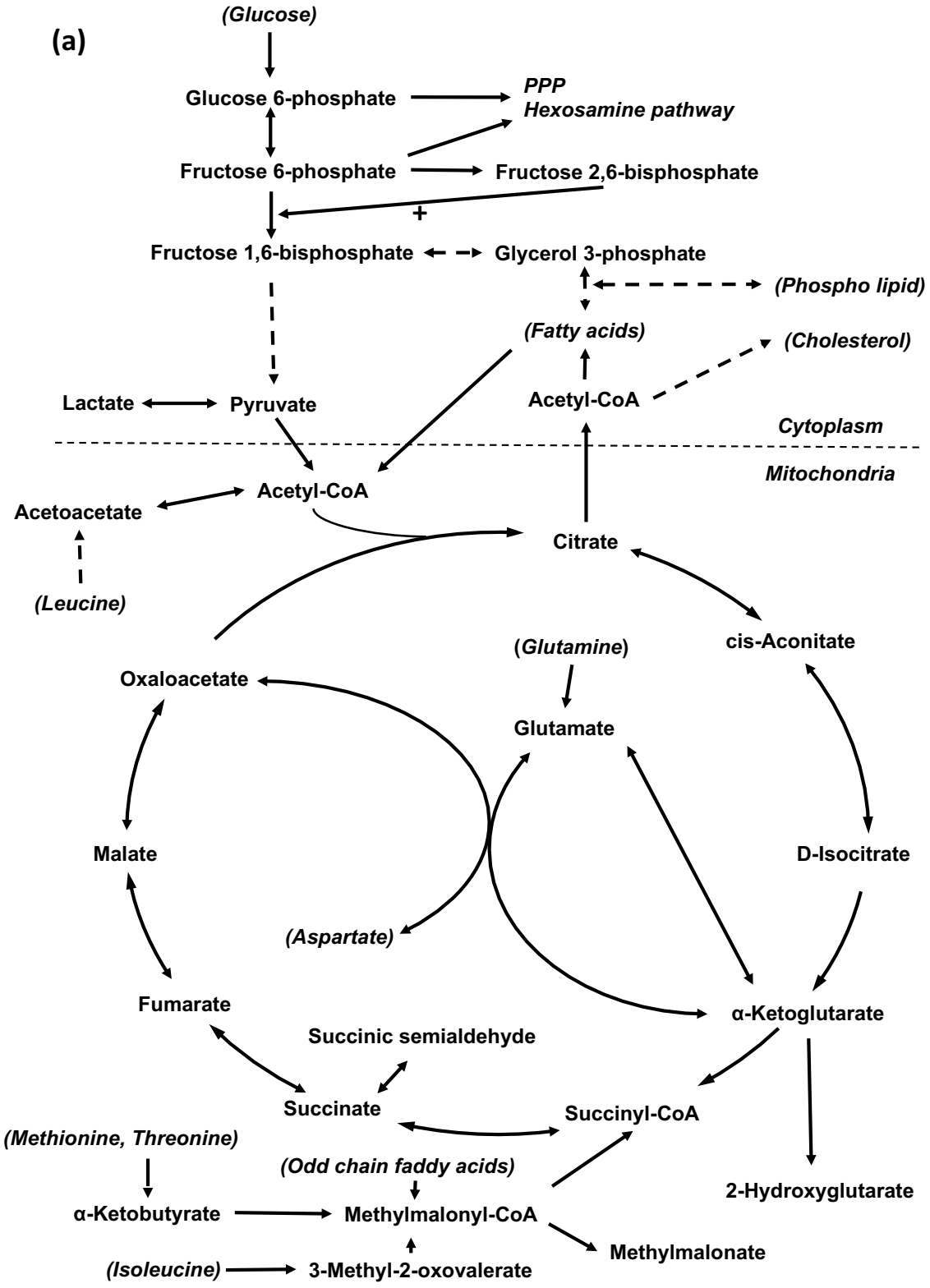
(a)
(Glucose)
Glucose 6-phosphate
PPP
Hexosamine pathway
Fructose 6-phosphate
Fructose 2,6-bisphosphate
+
Fructose 1,6-bisphosphate
Glycerol 3-phosphate
(Phospho lipid)
(Fatty acids)
(Cholesterol)
Lactate
Pyruvate
Acetyl-CoA
Cytoplasm
Mitochondria
Acetyl-CoA
Acetoacetate
(Leucine)
Citrate
cis-Aconitate
(Glutamine)
Oxaloacetate
Glutamate
Malate
D-Isocitrate
(Aspartate)
Fumarate
α-Ketoglutarate
Succinic semialdehyde
Succinate
Succinyl-CoA
(Methionine, Threonine)
(Odd chain faddy acids)
2-Hydroxyglutarate
α-Ketobutyrate
Methylmalonyl-CoA
Methylmalonate
(Isoleucine)
3-Methyl-2-oxovalerate

Figure 6.5 (cont.)

(b)

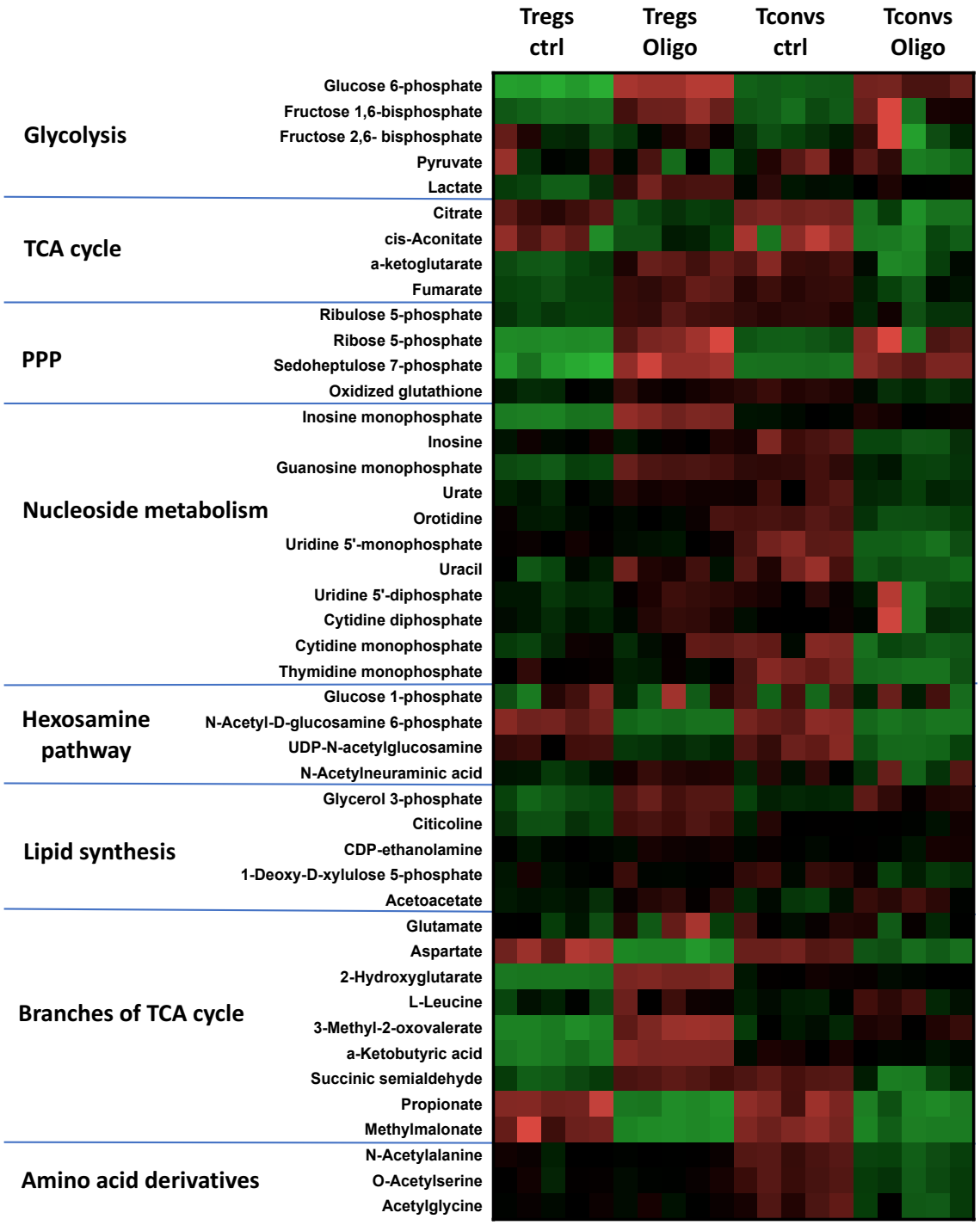

Figure 6.5. Mitochondrial ATP synthase inhibition alters the composition of glycolysis and TCA cycle intermediates and the metabolites of their branches in human Tregs.

Mass spectrometry-based metabolomics. Analysis of the data from *Figure 6.4* focussing on branches of the glycolysis pathway and the TCA cycle. (a) A schematic summarising the branches of the glycolysis pathway and the TCA cycle. Dotted arrows indicate reactions with more than one step between the metabolites. (b) A heat map showing 45 metabolites relating to the glycolysis and TCA cycle branches.

Figure 6.6

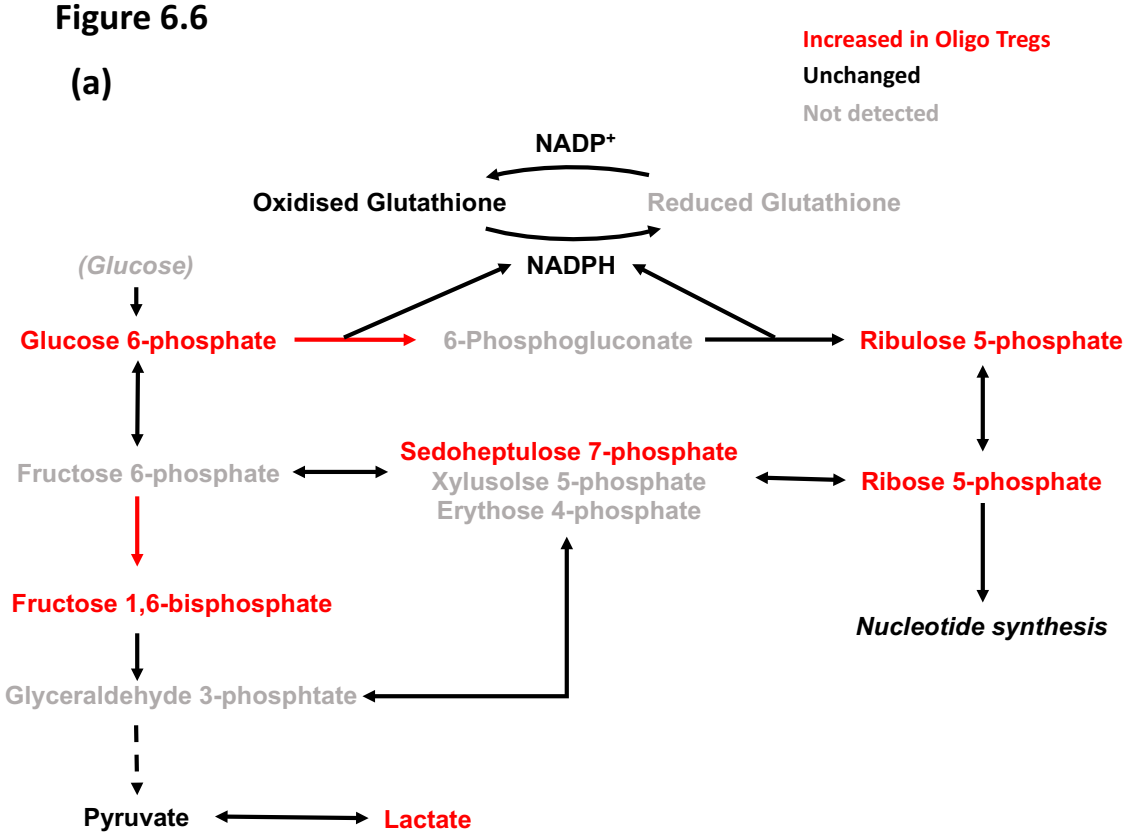
(a)
Increased in Oligo Tregs
Unchanged
Not detected
NADP+
Oxidised Glutathione
Reduced Glutathione
NADPH
(Glucose)
Glucose 6-phosphate
6-Phosphogluconate
Ribulose 5-phosphate
Fructose 6-phosphate
Sedoheptulose 7-phosphate
Xylusolse 5-phosphate
Erythose 4-phosphate
Ribose 5-phosphate
Fructose 1,6-bisphosphate
Nucleotide synthesis
Glyceraldehyde 3-phosphtate
Pyruvate
Lactate

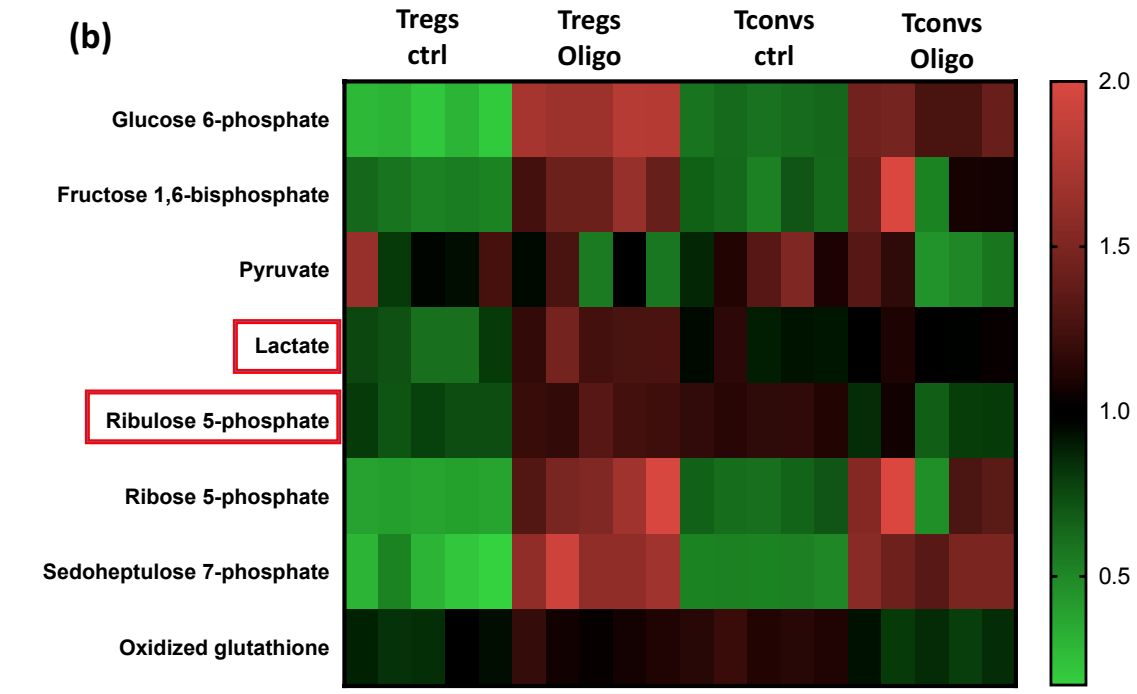
(b)
Tregs ctrl
Tregs Oligo
Tconvs ctrl
Tconvs Oligo
Glucose 6-phosphate
Fructose 1,6-bisphosphate
Pyruvate
Lactate
Ribulose 5-phosphate
Ribose 5-phosphate
Sedoheptulose 7-phosphate
Oxidized glutathione
2.0
1.5
1.0
0.5

Figure 6.6. Mitochondrial ATP synthase inhibition increases metabolites of both irreversible and reversible pentose phosphate pathways and aerobic glycolysis intermediates, except for pyruvate, in Tregs.

Mass spectrometry-based metabolomics. Analysis of the data from *Figure 6.5* focussing on the pentose phosphate pathway (PPP). (a) A schematic summarising the PPP. Red arrows indicate rate limiting steps of the PPP and glycolysis. Metabolites increased in oligomycin-treated Tregs compared to control Tregs are highlighted in red, unchanged are in black, whilst undetected metabolites are shaded in grey. (b) A heat map revealing relative levels of metabolites between control (ctrl) and oligomycin-treated (Oligo) conditions in Tregs and Tconvs.

Figure 6.7

(a)

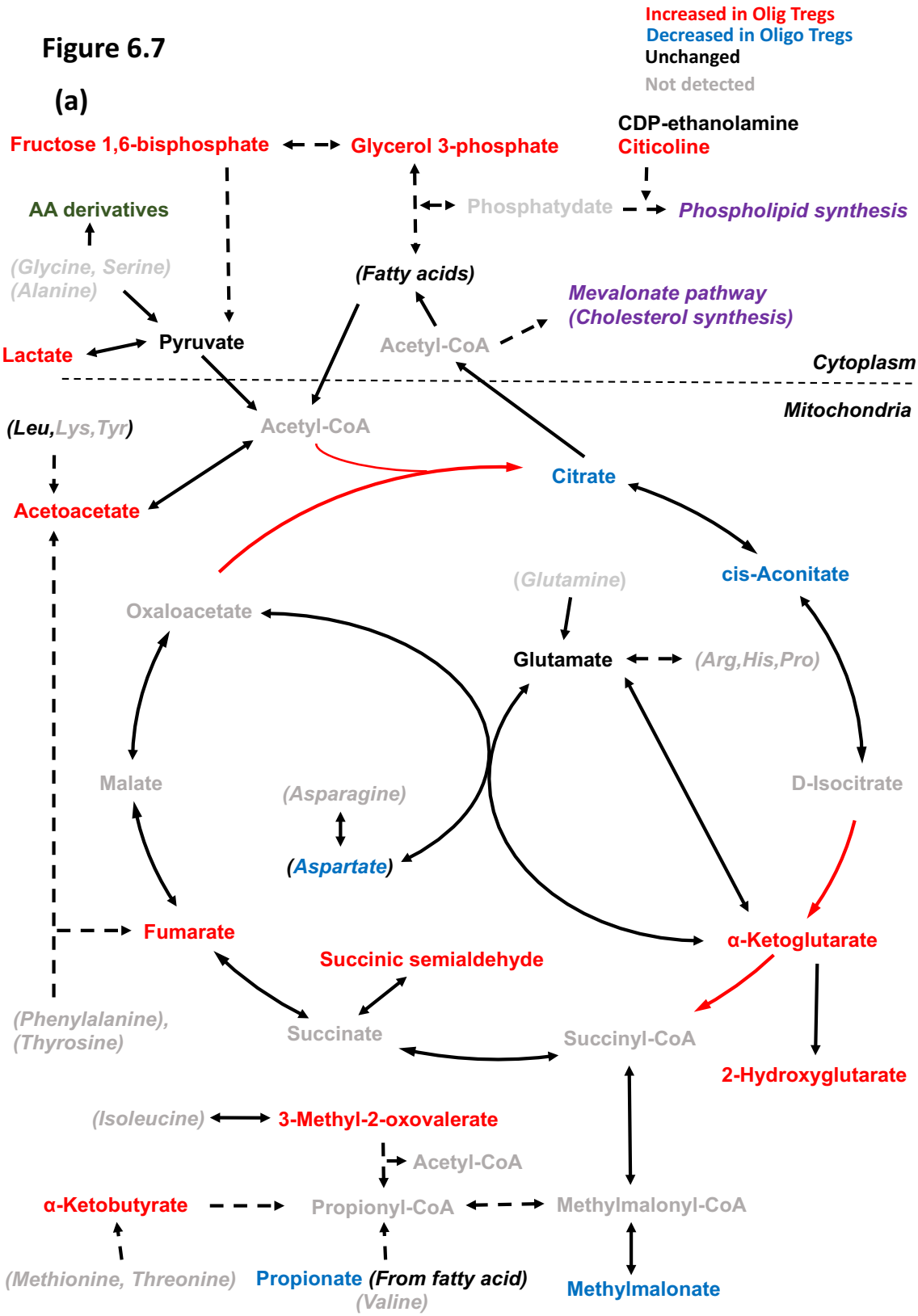
Increased in Olig Tregs
Decreased in Oligo Tregs
Unchanged
Not detected
CDP-ethanolamine
Citicoline
Fructose 1,6-bisphosphate
Glycerol 3-phosphate
AA derivatives
Phosphatydate
Phospholipid synthesis
(Glycine, Serine)
(Alanine)
(Fatty acids)
Mevalonate pathway
(Cholesterol synthesis)
Lactate
Pyruvate
Acetyl-CoA
Cytoplasm
Mitochondria
(Leu,Lys,Tyr)
Acetyl-CoA
Citrate
Acetoacetate
(Glutamine)
cis-Aconitate
Oxaloacetate
Glutamate
(Arg,His,Pro)
Malate
(Asparagine)
D-Isocitrate
(Aspartate)
Fumarate
α-Ketoglutarate
Succinic semialdehyde
(Phenylalanine),
(Thyrosine)
Succinate
Succinyl-CoA
2-Hydroxyglutarate
(Isoleucine)
3-Methyl-2-oxovalerate
Acetyl-CoA
α-Ketobutyrate
Propionyl-CoA
Methylmalonyl-CoA
(Methionine, Threonine)
Propionate (From fatty acid)
(Valine)
Methylmalonate

Figure 6.7 (cont.)

(b)

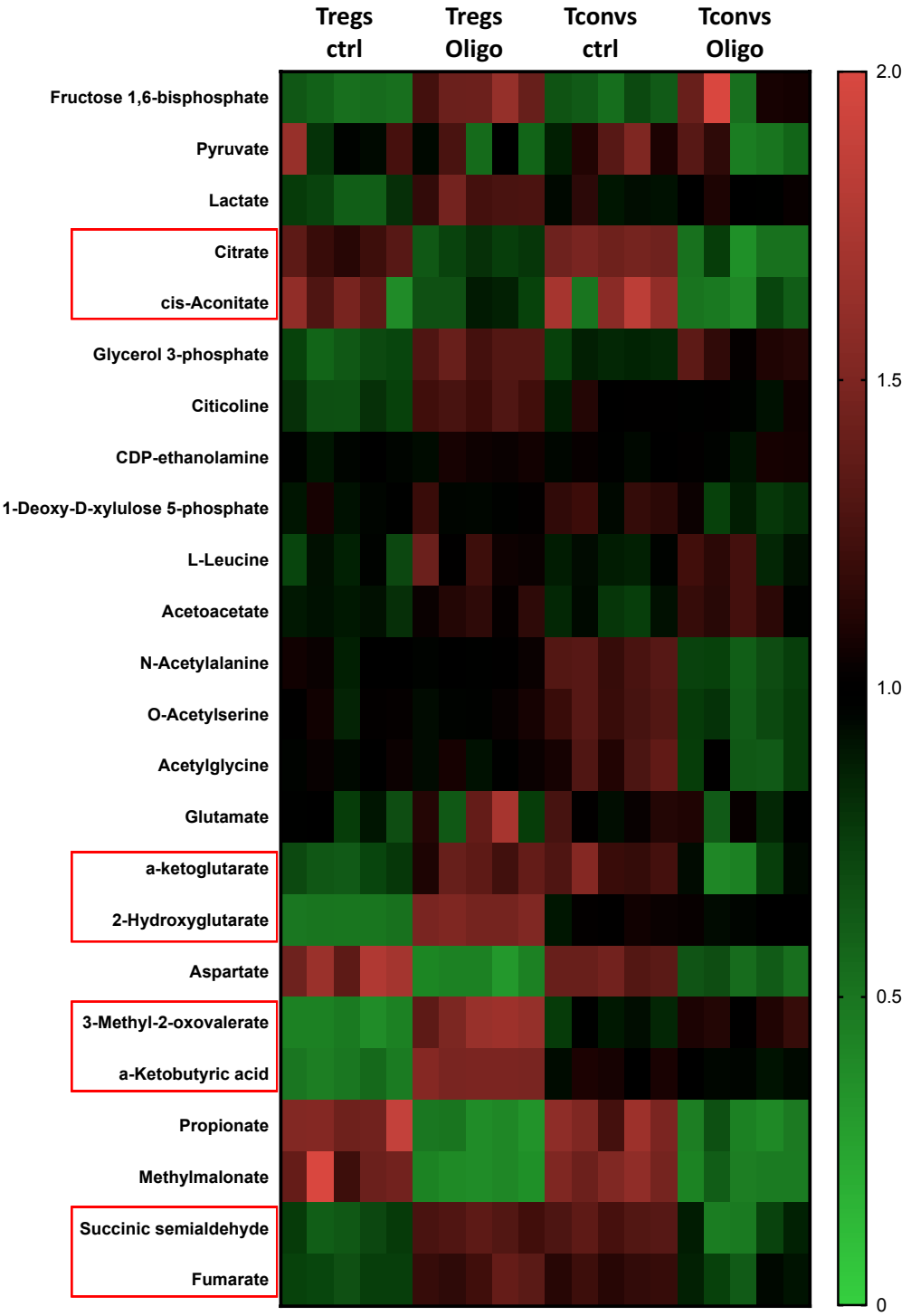

Figure 6.7 (cont.)

(c)

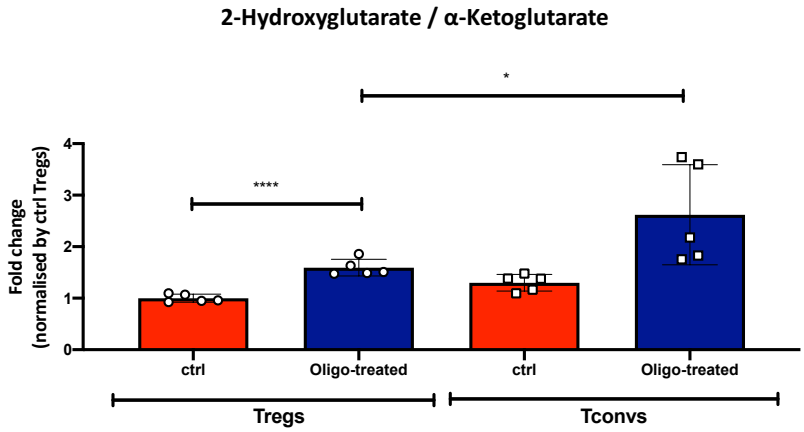

(d)

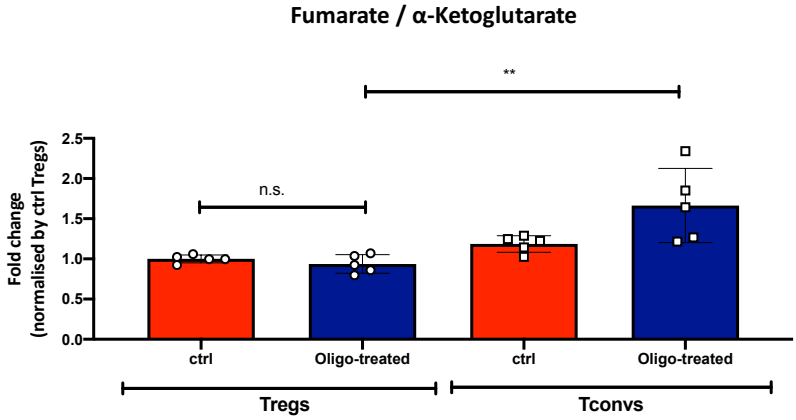

Figure 6.7. Mitochondrial ATP synthase inhibition in Tregs decreases citrate and cis-aconitate but increases α-ketoglutarate, fumarate, and 2-hydroxyglutarate with a high 2-hydroxyglutarte to α-ketoglutarate ratio.

Mass spectrometry-based metabolomics. Analysis of the data from *Figure 6.5* focussing on the TCA cycle. (a) A schematic summarising the TCA cycle. Red arrows indicate irreversible steps of the TCA cycle. Metabolites increased in oligomycin-treated Tregs compared to control Tregs are highlighted in red, decreased are highlighted in blue, unchanged are black, whilst undetected metabolites are shaded by grey. (b) A heatmap revealing relative levels of metabolites between control (ctrl) and oligomycin-treated (Oligo) conditions in Tregs and Tconvs. (c and d) Bar charts showing the ratio of 2-hydroxybutyrate (c) and fumarate (d) to α-ketoglutarate. The absolute values of metabolites (2-hydroxybutyrate or fumarate) were first divided by the value of α-ketoglutarate from the same samples. The calculated values were then normalised by the mean value of control Tregs. Each dot represents a technical replicate. Columns represent mean ± SD. *p<0.05, **p<0.01 ****p<0.0001 by unpaired t test.

Figure 6.8

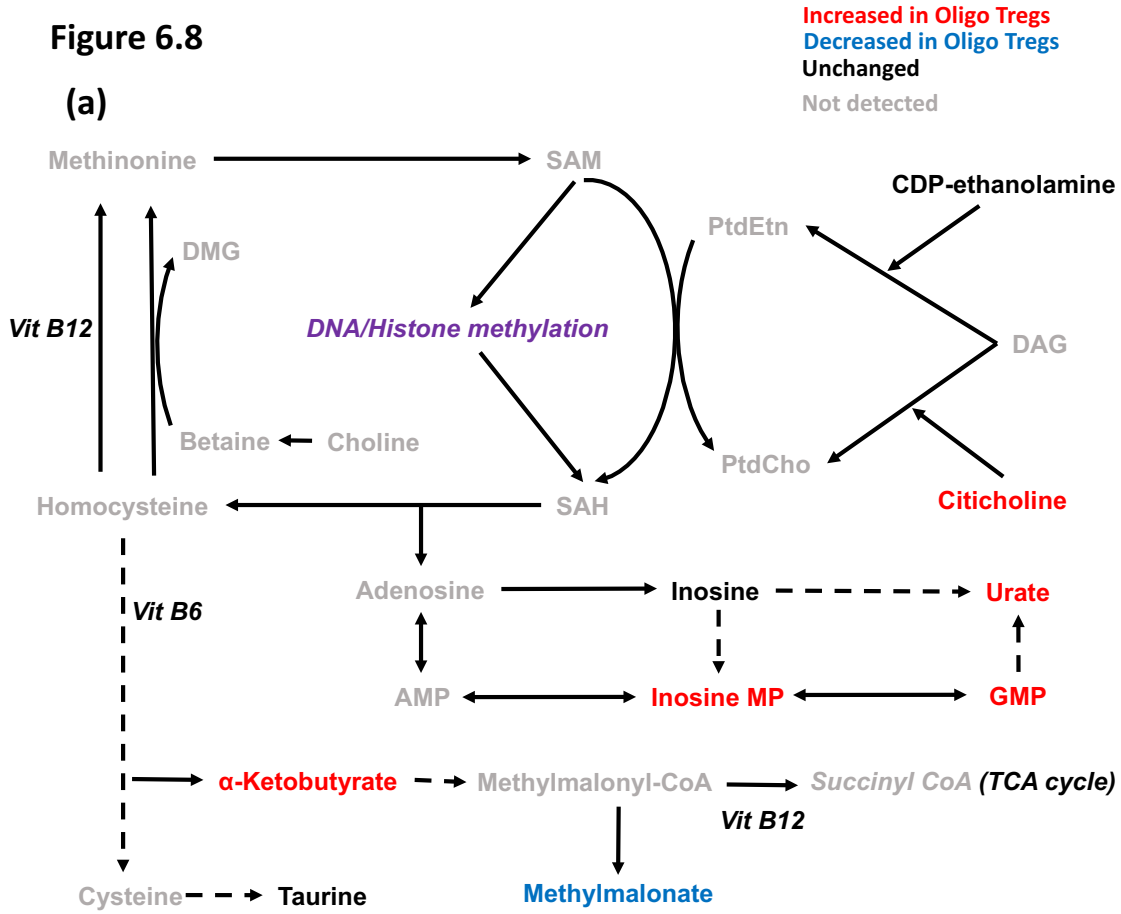
Increased in Oligo Tregs
Decreased in Oligo Tregs
Unchanged
Not detected
(a)
Methinonine
SAM
CDP-ethanolamine
PtdEtn
DMG
Vit B12
DNA/Histone methylation
DAG
Betaine
Choline
PtdCho
Citicholine
Homocysteine
SAH
Adenosine
Inosine
Urate
Vit B6
AMP
Inosine MP
GMP
α-Ketobutyrate
Methylmalonyl-CoA
Succinyl CoA (TCA cycle)
Vit B12
Cysteine
Taurine
Methylmalonate

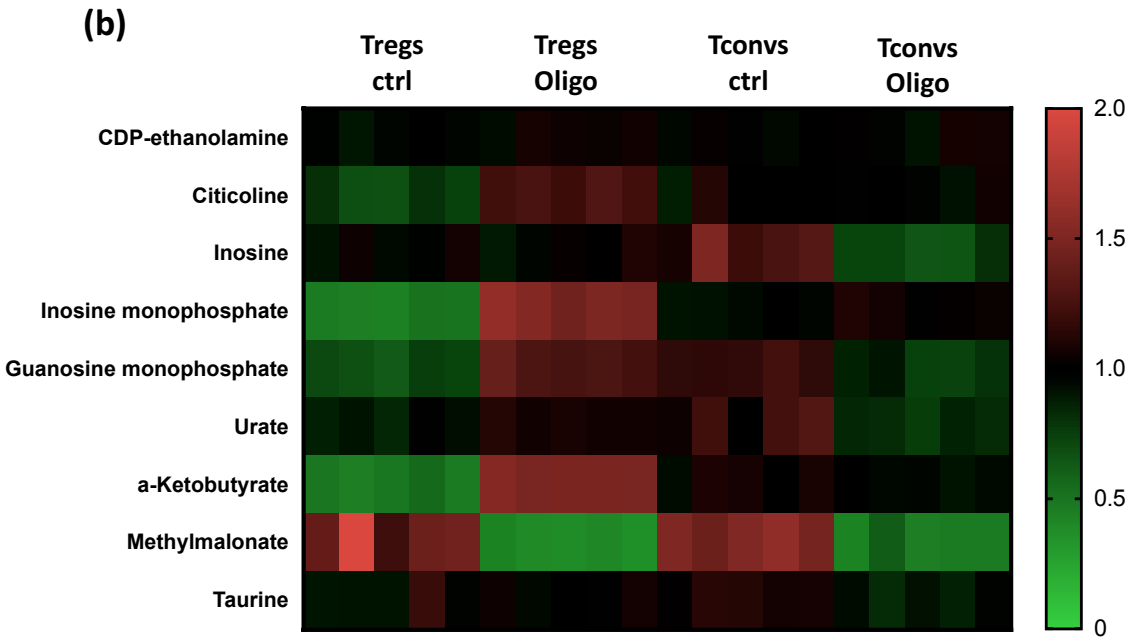
(b)
Tregs ctrl
Tregs Oligo
Tconvs ctrl
Tconvs Oligo
CDP-ethanolamine
Citicoline
Inosine
Inosine monophosphate
Guanosine monophosphate
Urate
a-Ketobutyrate
Methylmalonate
Taurine
2.0
1.5
1.0
0.5
0

Figure 6.8. Mitochondrial ATP synthase inhibition increases metabolites of methionine metabolism in Tregs.

Mass spectrometry-based metabolomics. Analysis of the data from *Figure 6.5* focussing on methionine metabolism. (a) A schematic summarising the methionine metabolic pathway. Metabolites increased in oligomycin-treated Tregs compared to control Tregs are highlighted in red, decreased are highlighted in blue, unchanged are black, whilst undetected metabolites are shaded grey. (b) A heatmap revealing relative levels of metabolites between control (ctrl) and oligomycin-treated (Oligo) conditions in Tregs and Tconvs.

Figure 6.9

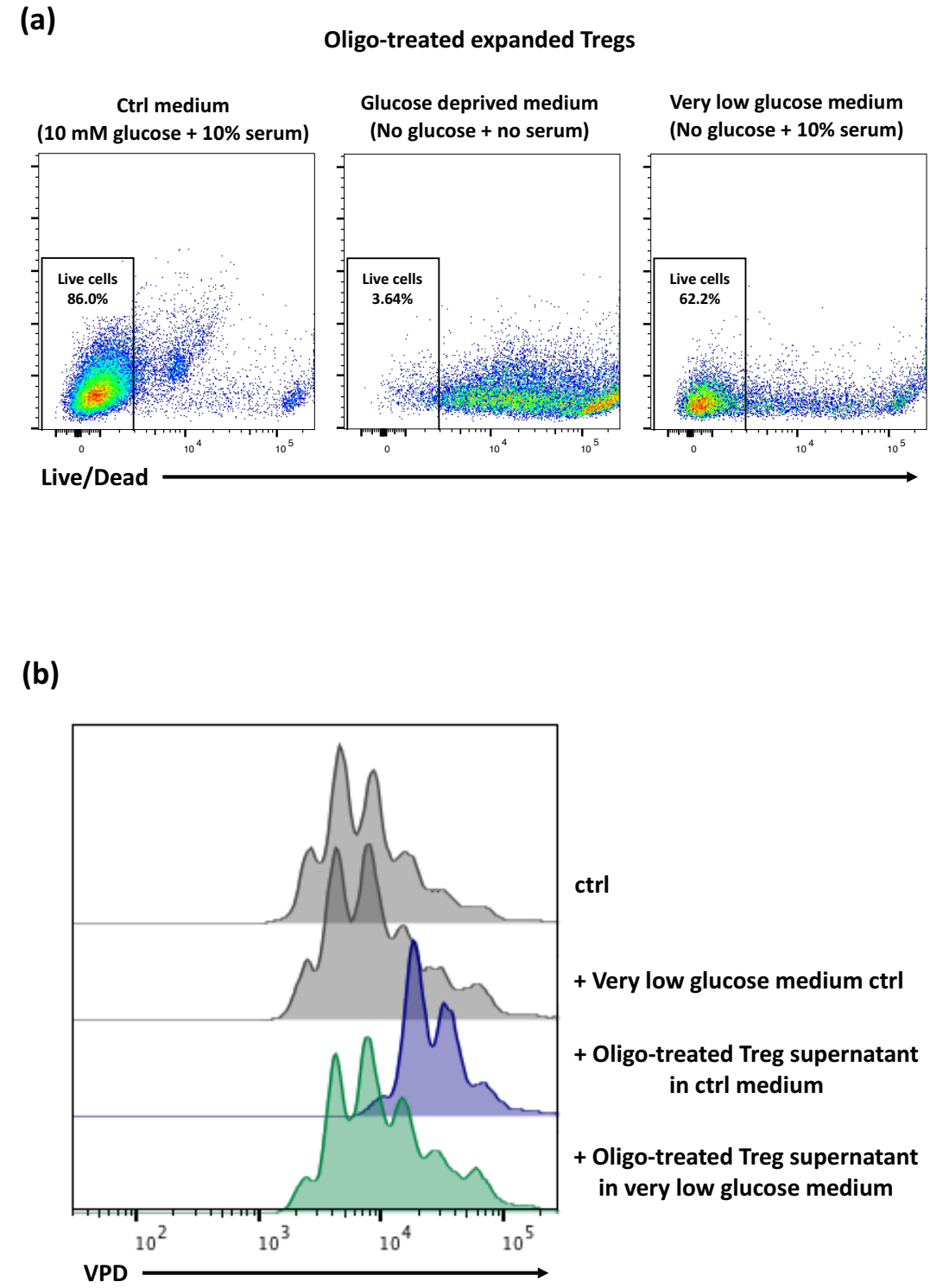
(a)
Oligo-treated expanded Tregs
Ctrl medium
(10 mM glucose + 10% serum)
Glucose deprived medium
(No glucose + no serum)
Very low glucose medium
(No glucose + 10% serum)
Live cells
86.0%
Live cells
3.64%
Live cells
62.2%
0
10 4
10 5
Live/Dead
(b)
ctrl
+ Very low glucose medium ctrl
+ Oligo-treated Treg supernatant
in ctrl medium
+ Oligo-treated Treg supernatant
in very low glucose medium
10 2
10 3
10 4
10 5
VPD

Figure 6.9. Mitochondrial ATP synthase inhibited Tregs require glucose to produce immunosuppressive small EVs.

Expanded human Tregs were pre-treated with 2 uM oligomycin for 2 hours, washed intensively and incubated in fresh glucose-deprived medium with either 10 mM glucose and 10 % human serum (control), 0 mM glucose and 0 % human serum (glucose deprived medium) or 0 mM glucose and 10 % human serum (very low glucose medium) added in the presence of anti-CD3/CD28 beads. (a) Representative FACS plots from two independent donors revealing the viabilities of oligomycin-treated expanded Tregs in different medium after 48h cultivation. (b) Representative histograms from two independent donors revealing the suppression of CD4 T cell proliferation by oligomycin-treated Treg culture supernatants. The supernatants of oligomycin-treated Treg cultures were gently removed, and added into VPD-stained CD4 T cell proliferation assays in a final concentration of 25%. Very low glucose medium and control medium were incubated in parallel with Tregs, and added into the proliferation assays at the same ratio as controls.

Chapter 7: Results summary and general discussion

7.1 Introduction

Regulatory T cells are essential to homeostatic immune tolerance. Their antigen non-specific manner of immunosuppression (bystander suppression) and their potential to induce infectious tolerance renders them attractive therapeutic targets to treat autoimmune diseases and prevent transplantation rejection. Clinical trials of autologous Treg therapy have showed promising results, but there are issues to overcome for further improvements: 1) recipient-dependent expansion variability, 2) the duration required to expand Treg, 3) the manufacturing costs, and 4) the risk of non-specific suppression by polyclonal Tregs. Generation of Tregs from third-party donors by genetic modification may be a solution, but is far from use. Enhancing expanded Treg suppressive function may be a more straight-forward strategy to reduce the dose of Treg therapy required to overcome the issue of recipient-dependent expansion variability.

Cellular metabolism regulates immune cells through two interacting aspects: bioenergic

and biosynthetic activities, and non-canonical activities of metabolic enzymes and intermediates. In terms of energy metabolism, iTregs and Tconvs have distinct characteristics, with iTregs favouring OXPHOS and Tconvs favouring aerobic glycolysis (28, 29, 188, 189). However, given that natural Tregs (tTregs and pTregs) and iTregs are epigenetically different, the energy metabolism of natural Tregs may also be different from iTregs. Nevertheless, the relationship between their metabolism and function is clearly different between natural Tregs (tTregs and pTregs) and Tconvs: Tconvs are dependent on glycolysis (27, 196, 198), whilst glycolysis impairs Treg suppressive function (206, 207, 210). Despite this, glycolysis is still necessary for Treg tissue migration highlighting the context dependence of immunometabolic effects (215, 217). Mitochondria also play several important roles outside of their primary metabolic function including as a signalling organelle including reactive oxygen species (ROS) production and synthesiser of cellular lipid in both Tconvs and Tregs. However, the precise differences remain unclear and require further investigation.

Understanding the contrasting metabolic demands and regulation of function between

Tconvs and Tregs raises the possibility of targeting metabolic pathways to modulate human immune responses and to enhance Treg cellular therapy. In this thesis, we revealed how human Treg change their metabolism upon activation and how the metabolism regulates Treg function. These results provide a new therapeutic strategy using Tregs from third-party donors to overcome current limitations of Treg cellular therapy.

7.2 Summary of experimental results

7.2.1 Chapter 3

In *chapter 3*, we investigate how human *ex vivo* Tregs change their metabolism upon activation in comparison to Tconvs. This is the first human Treg metabolism data revealing an aerobic switch in human Treg and its importance in human Treg clonal expansion.

Human *ex vivo* Tregs dramatically increase their glucose uptake, aerobic glycolysis and

OXPHOS rates upon TCR (CD3) signalling alongside CD28 co-stimulation; revealing that stimulation induces a high catabolic rate in Tregs (***Figure 3.1 and Figure 3.2.a and b***). However, their energy metabolism dependence extensively shifts from OXPHOS into aerobic glycolysis (***Figure 3.2.c***). This dependence can also be seen at the transcriptional level in the upregulation of glycolysis genes and the down-regulation of mitochondrial respiration genes (***Figure 3.3***). Thus, human Tregs demonstrate the 'Warburg effect' on stimulation. Although the metabolic rate of activated Tregs is lower than Tconvs (***Figure 3.4 and 3.5.a and b***), the catabolic dependency on aerobic glycolysis is comparable between Tregs and Tconvs (***Figure 3.5.f***). Despite their dependency on aerobic glycolysis, both Tregs and Tconvs reach close to their maximum glycolytic capacity on stimulation and maintain high spare respiratory capacity indicating that both cells use OXPHOS to meet acute increases in energy requirement (***Figure 3.5.c-e***). Interestingly, the metabolic gene signatures are similar between Tregs and Tconvs revealing that the low Treg metabolic rate is regulated post-transcriptionally (***Figure 3.6***).

The mTOR inhibitor rapamycin does not induce Treg cell death (***Figure 3.7.a***), but does

dramatically block enhancement of Treg metabolic rate on activation (***Figure 3.7.b and c***). Moreover, it significantly reduces (although not completely) their proliferation rate (***Figure 3.7.d***). Therefore, mTOR signalling is central to the regulation of Treg metabolism and the increase in metabolic rate mediated by TCR-mTOR signalling is necessary for Treg clonal expansion.

Proliferating Tregs show a high glucose uptake rate and Glut1 expression, which is not distinguishable from their proliferating Tconvs counterpart (***Figure 3.8.a-c***). This suggests that Treg and Tconv glycolysis rates are similarly high during proliferation. ATP-linked OXPHOS inhibition by the mitochondrial ATP synthase inhibitor oligomycin reduces Treg proliferation rate probably due to the limitation of energy compensation mechanism through aerobic glycolysis, whilst glycolysis inhibition by the structural glucose analogue 2-DG completely abolishes Treg proliferation despite their high spare respiratory capacity (***Figure 3.9.a-c***). Inhibition of glycolysis catabolic pathways by the lactate dehydrogenase inhibitors (which inhibits energy production without oxygen consumption) and the mitochondrial pyruvate carrier inhibitor (which inhibits aerobic

glycolysis) does not reduce Treg proliferation rate, whilst inhibition of the pentose phosphate pathway (one of the glycolysis anabolic pathways) dramatically inhibits Treg proliferation ***(Figure 3.9.d-f***). Therefore, stimulated Tregs require glucose for biosynthetic, but not bioenergic, reasons.

These data show that human *ex vivo* Tregs increase their metabolism upon TCR stimulation alongside CD28 co-stimulation via the mTOR signalling pathway. Treg metabolism shifts to be more dependent on aerobic glycolysis in the same manner as Tconvs. Glucose is an absolute requirement for Treg proliferation, but this is for biosynthetic and not bioenergetic reasons. In conclusion, human *ex vivo* Tregs change their metabolism upon stimulation to be dependent on aerobic glycolysis to support glycolysis anabolic pathways and maintain their clonal expansion.

7.2.2 Chapter 4

In *chapter 4*, we examined the different subsets (naïve, central memory and effector memory) of human Tregs metabolism in comparison with their Tconv counterparts. This is the first reported data suggesting that naïve and CM subsets have similar metabolic signatures in Tregs and Tconvs, whilst EM Tregs and Tconvs have distinct metabolic characteristics with contrasting metabolic regulation of their functions.

CD45RA and CCR7 divide human *ex vivo* Tregs into three subsets: $CD45RA^{+}$ $CCR7^{+}$, $CD45RA^{-}$ $CCR7^{+}$, and $CD45RA^{-}$ $CCR7^{-}$ Tregs (***Figure 4.1***). Lack of CCR7 expression suggests a lost migratory capacity to secondary lymphoid organ (SLO) and $CD45RA^{-}$ $CCR7^{-}$ Tregs have a higher suppressive and lower proliferative capacity (effector memory-like property) compared with $CD45RA^{-}$ $CCR7^{+}$ Tregs (***Figure 4.2***). Therefore, we conclude that CCR7 can divide Tregs into central memory (CM) and effector memory (EM) subsets like CD4 Tconvs. Metabolically, EM Tregs show a significantly lower glucose uptake rate compared with naïve and CM Tregs upon activation (***Figure 4.3***). Although naïve and EM Tregs have different metabolic gene signatures (***Figure 4.4***) CM and EM Tregs do not

except for cell cycle genes (***Figure 4.5***). The high glucose consumption rate of naïve and CM Tregs is the same level as their Tconv counterparts, whilst Tregs and Tconvs show interesting differences between EM compartments: for example, EM Tregs have a low glucose uptake rate whilst this is high in EM Tconv (***Figure 4.6***). However, the majority of metabolic genes, including glycolysis genes, were similar between EM Tregs and Tconvs (***Figure 4.7***). Therefore, the low glucose metabolism rate observed in EM Tregs is regulated post-transcriptionally. Interestingly, genes regulating pyruvate dehydrogenase complex (PDC) and lactate transporters were highly expressed in EM Tregs revealing that pyruvate and acetyl-CoA are more tightly regulated in EM Tregs (***Figure 4.7 c***).

Whilst EM Tregs maintain a high mitochondrial mass, EM Tconvs have two distinct populations: high mitochondrial mass Tconvs ($Mito^{hi}$ EM Tconvs) and low mitochondrial mass Tconvs ($Mito^{lo}$ EM Tconvs) (***Figure 4.8***). However, despite low mitochondrial mass $Mito^{lo}$ EM Tconvs possess the highest OXPHOS rates together with the highest aerobic glycolysis rate (***Figure 4.9***). In comparison, EM Tregs are metabolically quiescent with remarkably lower OXPHOS and aerobic glycolysis rates and a missing aerobic switch

upon activation. Transcriptomic (***Figure 4.10***) and functional (***Figure 4.11***) assays reveal that Mito^{hi} EM Tconvs are more Th2-type CD4 T cells, whilst Mito^{lo} EM Tconvs are more Th1- and 17-type CD4 T cells. Although Mito^{hi} and Mito^{lo} EM Tconvs are metabolically distinct, they both require glycolysis for their effector function and OXPHOS inhibition influences this to a markedly lesser degree than glycolysis inhibition (***Figure 4.12***). Another important aspect of Mito^{hi} and Mito^{lo} EM Tconvs is their differential susceptibility to Treg-mediated suppression. Mito^{hi} EM Tconvs are sensitive to EM Treg suppression both in proliferation and cytokine production whilst Mito^{lo} EM Tconvs are resistant (***Figure 4.13***). Interestingly, this differential susceptibility is not due to the distribution of different Th subsets as IFN-γ and IL-17A production from Mito^{hi} EM Tconvs is also remarkably suppressed (***Figure 4.13.d and h***). However, EM Tregs strongly gain the ability to supress Mito^{lo} EM Tconvs under the ATP-linked OXPHOS inhibited condition introduced by oligomycin (***Figure 4.14***).

These data reveal that human Tregs and Tconvs demonstrate similar metabolic characteristics with a high glucose consumption rate amongst naïve and CM

compartments, whilst EM subsets demonstrate differences: EM Tregs are metabolically quiescent whilst EM Tconvs are metabolically active. This indicates that Tregs and Tconvs show the same metabolic signature in SLO, but a different signature in peripheral tissues. These data are the first to describe two functionally distinct subsets having different susceptibilities to Treg-mediate suppression amongst EM Tconvs based on mitochondrial mass: Treg-sensitive $Mito^{hi}$ and Treg-resistant $Mito^{lo}$ EM Tconvs. Both EM Tconv subsets require glucose for their effector function, whilst EM Tregs exhibit enhanced suppressive function against Treg-resistant $Mito^{lo}$ EM Tconvs under OXPHOS-inhibited conditions. These data shed new light on Treg immunometabolism: Tregs positively regulate their suppressive function via limiting mitochondrial energy metabolism, in contrast to Tconvs which negatively control their effector function through limiting glucose metabolism.

7.2.3 Chapter 5

In *chapter 5*, we investigated by which mechanism Tregs gain enhanced immunosuppressive function after mitochondrial ATP synthase inhibition, and explored the possible strategies for clinical translation. Here, we describe a method to enhance the suppressive capacity of expanded Treg to reduce the required dose for adoptive Treg therapy in addition to describing a novel 'off-the-shelf' therapeutic strategy using Treg-derived small extracellular vesicles (EVs).

Human *ex vivo* Tregs treated by the mitochondrial ATP synthase inhibitor oligomycin strongly gain suppressive potency against proliferation and cytokine production of both $CD4^+$ and $CD8^+$ T cells (***Figure 5.1 and Figure 5.2***). Although oligomycin-treated Tregs reveal linage stability with a high percentage of $FOXP3^+$ $CD25^+$ (***Figure 5.3.a***), the expression level of FOXP3, CD25, CTLA-4 and PD-1 is decreased (***Figure 5.3.b***). Instead, oligomycin-treated Tregs produce immunosuppressive soluble factors (***Figure 5.4***). Although oligomycin-treated Tregs secrete a higher amount of IL-10 (***Figure 5.4.c***), their potent immunosuppression *in vitro* is maintained by molecules over 100 kDa (***Figure***

5.5.a and b) and not by proteins (***Figure 5.5.c***) suggesting that EVs are responsible for this effect. Our differential centrifugation experiments exclude apoptotic bodies and large EVs as causative (***Figure 5.5.d and e***). Instead, depletion of small EVs (formerly known as exosomes) completely abolishes their immunosuppressive function (***Figure 5.6***). Therefore, we conclude that human *ex vivo* Tregs start producing immunosuppressive small EVs when their mitochondrial ATP synthase is inhibited. Mitochondrial ATP synthase inhibition by oligomycin does not increase the quantity of small EV production from Tregs (***Figure 5.7***). Instead, the phenotype of Treg-derived small EVs skews from expression of CD4 and/or CD24 towards expression of CD3, CD25, CD41b, CD45 and/or CD133/1 (***Figure 5.8***). This suggests that oligomycin-treated Tregs produce qualitatively different type of small EVs.

Enhancement of human *ex vivo* Tregs suppressive function by oligomycin opens up a potential new therapeutic avenue in Treg cellular therapy. Pre-treatment of *in vitro* expanded Tregs with oligomycin prior to infusion may significantly reduce the required Treg dose (***Figure 5.9.a***). Moreover, immunosuppressive small EVs produced by

expanded Tregs from a third-party donor may be used instead of infusion of autologous Tregs (***Figure 5.9.b***) as an 'off-the-shelf' therapy. In the same manner as *ex vivo* Tregs, oligomycin treatment strongly increases expanded Treg suppressive function (***Figure 5.10***), and oligomycin-treated expanded Tregs produce immunosuppressive small EVs (***Figure 5.11***). Importantly, the immunosuppressive small EVs work donor-independently (***Figure 5.12***) further supporting their use 'off-the-shelf'. We investigated donor-independent immunosuppressive properties *in vivo* using a mouse peritoneal lavage model (***Figure 5.13***). However, because of the low level of T cell proliferation in our positive controls, the result was inconclusive. Thus, further experiments investigating *in vivo* efficacy are needed.

These data reveal that mitochondrial ATP synthase inhibition by oligomycin enhances both *ex vivo* and *in vitro* expanded human Treg suppressive function by inducing production of immunosuppressive small EVs. These data also indicate potential clinical translation strategies to treat autoimmune diseases and prevent transplantation rejection by either pre-treating expanded Treg with oligomycin or by 'off-the-shelf'

administration of small EVs derived from oligomycin-treated Treg.

7.2.4 Chapter 6

In *chapter 6*, we explored by which mechanism mitochondrial ATP synthase inhibition induces immunosuppressive small EV production from human Tregs.

Oligomycin treatment alters Tregs by three mechanisms: 1) inducing low energy production, 2) inducing high ROS production and mitochondrial DNA leakage, and 3) altering cells metabolite profile. Although inhibitors of mitochondrial complex I (rotenone) and III (antimycin A) completely block OXPHOS in Tregs (***Figure 6.1***), these inhibitors do not induce production of immunosuppressive small EVs from Tregs (***Figure 6.2***) revealing that the mechanism of production is not due to low energy availability. Because rotenone and antimycin A are known to induce high ROS production, we ruled out ROS and potential ROS damage inducing leakage of mitochondrial DNA as causative. Therefore, we hypothesised that oligomycin induces Tregs to produce

immunosuppressive small EVs via changing their metabolic signature.

In vitro expanded Tconvs inducibly express FOXP3 ***(Figure 6.3.a***), but expanded Tconvs do not produce immunosuppressive small EVs after oligomycin treatment (***Figure 6.3.b***). Therefore, the mechanism of EV production is probably not driven by FOXP3 expression. Oligomycin treatment dramatically changes the Treg metabolic profile, whilst causing Tconvs to generally supress their metabolism (***Figure 6.4***). Thus, the ability to produce immunosuppressive small EVs after oligomycin treatment seems to be correlated with differential metabolic responses to oligomycin treatment.

Oligomycin-treated Tregs generally increase their glycolysis pathway including the irreversible pentose phosphate pathway (PPP) to increase NADPH. This maintains their intracellular redox balance and causes accumulation of aerobic glycolysis intermediates to provide pyruvate to the TCA cycle (***Figure 6.5 and 6***). Despite high aerobic glycolysis (importing pyruvate into the TCA cycle), citrate and cis-aconitate (intermediates immediately downstream of the TCA cycle after mitochondrial acetyl-CoA) were reduced

indicating that oligomycin-treated Tregs use pyruvate for protein acetylation and lipid synthesis (***Figure 6.7 a and b***). Despite low cis-aconitate accumulation, intracellular α-ketoglutarate (an intermediate immediately downstream of the TCA cycle intermediate after cis-aconitate) is increased in oligomycin-treated Tregs indicating that Tregs exhibit high glutamine metabolism (***Figure 6.7 a and b***). Although oligomycin-treated Tregs accumulate α-ketoglutarate compared to control cells, accumulation of 2-hydroxyglutarate occurred to a greater degree (***Figure 6.7.c***). Therefore, both DNA and histone demethylation were likely disturbed by 2-hydroxyglutarate antagonising α-ketoglutarate in oligomycin-treated Tregs. At the same time, accumulation of by-products of methionine one-carbon metabolism (***Figure 6.8***) indicates that DNA and histone methylation are enhanced in oligomycin-treated Tregs. Thus, mitochondrial ATP synthase inhibition seems to induce lipid synthesis and epigenetic changes in Tregs due to enhanced acetylation and methylation process via a modulated metabolic profile. Lastly, we revealed that oligomycin-treated Tregs completely lose their ability to produce immunosuppressive small EVs under a low glucose condition (***Figure 6.9***). This indicates that systemic immunosuppression by small EVs derived from Tregs in OXPHOS inhibited

peripheral tissue is abolished when the peripheral tissue starts to face glucose limitation.

These data indicate that Tregs exhibit FOXP3-independent specific metabolic changes after mitochondrial ATP synthase inhibition. Mechanistically, Tregs enhance the irreversible PPP to protect themselves from ROS-induced damage, accumulate pyruvate to supply lipid synthesis and protein acetylation including histone acetylation, and increases 2-hydroxyglutarate and methionine metabolism for methylation including histone and DNA. Thus, mitochondrial ATP synthase inhibition induces changes that likely result in enhanced lipid synthesis and epigenetic changes in Tregs. ***Figure 7.1*** summarises Tregs and Tconvs metabolism and the metabolic regulation of their function.

7.3 Discussion

The data in this thesis have three principal implications. First, human Tregs have different metabolic signatures in different anatomical locations due to differential demands for clonal expansion and function. Second, cellular metabolism controls Tregs and Tconv functions differently. Third, targeting Treg metabolism may facilitate 'off-the-shelf' Treg therapy.

Here we report that human Tregs switch their metabolism toward aerobic glycolysis to support their proliferation. Because naïve and CM Tregs have significantly higher glucose consumption compared with EM Tregs and EM Tregs do not switch their metabolism after stimulation, aerobic glycolysis is the metabolic feature of naïve and CM compartments. Given that naïve and CM Tregs encounter antigens (stimulation) in SLOs whilst EM Tregs do so in peripheral tissues, Tregs have different metabolic signatures in different locations. A recent study has revealed that Tregs require glycolysis for tissue migration (215, 217). Thus, naïve and CM Tregs require glycolysis for their proliferation and migration. Because glycolysis is also required for Tconv proliferation and migration

(243, 371), the metabolic requirements of Tregs and Tconvs are the same in SLOs. However, the process to induce glycolysis may have interesting contrasts between Tregs and Tconvs. Treg migration is mediated by the mTORC2 signalling pathway which is initiated by glucokinase (hexokinase isozyme) activity (217), whilst Tconvs migration is mediated by the mTORC1 signalling pathway initiated by hexokinase 1 (243). We showed that low-dose rapamycin (which preferentially inhibits mTORC1) decreases Treg metabolism and reduces proliferation rate. However, rapamycin does not completely block their proliferation unlike 2-DG (a glycolysis inhibitor). Importantly, low-dose rapamycin selectively inhibits Tconv proliferation (165, 166). Interestingly, different sensitivities to low-dose rapamycin is observed in the migration of Tregs and Tconvs with low-dose rapamycin inhibiting Tconv, but not Treg migration (217, 243). Thus, glycolysis in naïve and CM Treg metabolism is supported by mTORC2 signalling, whilst glycolysis in naïve and CM Tconvs is mTORC1 dependent. This indicates that Treg and Tconv proliferation and migration may be regulated by external mTORC1-specific or mTORC2-specific inhibitory stimuli. For example, mTORC1 requires essential amino acids such as leucine for activation (372, 373). Thus, the deprivation of some essential amino acids

may selectively inhibit Tconv proliferation and migration. However, Treg and Tconv regulation in terms of glycolysis induction by different mTOR complexes does not modulate their functions in the same way. Whilst we showed that glycolysis is absolutely required for Tconv effector function, glycolysis induced by both mTORC1 and mTORC2 negatively regulates Treg suppressive function (374).

We shed new light on Treg immunometabolism: Tregs positively regulate their suppressive function via mitochondrial ATP synthase inhibition, in contrast to Tconvs which negatively control their effector function through limiting glucose metabolism. However, we do not know the physiological or pathological conditions that induce mitochondrial ATP synthase inhibition. We demonstrate that EM Tregs highly express lactate transporter genes including extracellular lactate importer *MCT1*, unlike other metabolic pathways which are post-transcriptionally regulated. We hypothesised that lactate may inhibit mitochondrial ATP synthase through the activation of ATPase inhibitory factor 1 (IF1) in *chapter5* (332, 333). However, IF1 function in Tregs has not been reported yet. Moreover, the fundamental problem of this hypothesis is how Tregs

can maintain energy homeostasis in high lactate environment, as importing lactate blocks glycolysis-dependent energy production. Whilst, lactate may induce immunosuppressive small EVs without mitochondrial ATP synthase inhibition. Our metabolomics study reveals that oligomycin-treated Tregs have a characteristic metabolic signature showing higher lipid synthesis via glucose-pyruvate derived cytosolic acetyl-CoA together with high glutamine metabolism. The cytosolic acetyl-CoA may be an important metabolic intermediate to maintain the production of immunosuppressive small EVs as mitochondrial ATP synthase inhibited Tregs stop producing EVs under conditions of low glucose. However, low glucose and high lactate environment allows Tregs to generate cytosolic acetyl-CoA through importing lactate. Furthermore, under this condition, Tregs increase glutamine metabolism even if Tregs are not treated by oligomycin, to compensate for low energy production through glycolysis. Therefore, as long as TCA cycle metabolic intermediates are considered, Tregs in high lactate environment may show similar metabolic signature (high lipid synthesis with high glutamine metabolism) to mitochondrial ATP synthase inhibited Tregs. Moreover, lactate itself can function as a histone deacetylase (HDAC) inhibitor (375). A

recent study revealed that lactate transported through MCT1 increases mouse Treg suppressive function (224). Taken together, we hypothesised that excess inflammation in tissue enriches lactate by inducing a high rate of aerobic glycolysis in immune cells. Lactate is imported by Tregs via MCT1 and can be used as a substrate for cytosolic acetyl-CoA with high glutamine metabolism, which induces epigenetic changes in Tregs. Epigenetically changed Treg then start producing immunosuppressive EVs which work antigen non-specifically and systemically.

Autologous Treg therapy in clinical trials has demonstrated early successes (15, 16), but improvements will be required to overcome several key issues including recipient-dependent expansion variability, the time required to expand Tregs, and the manufacturing costs (153, 175). Using immunosuppressive EVs produced by oligomycin-treated third-party expanded Tregs could be a future approach to overcome these issues. However, we have not yet clearly demonstrated immunosuppressive function *in vivo*. Nevertheless, others have shown that human *in vitro* expanded Treg-derived small EVs are sufficient to prevent allograft rejection in a humanised skin graft model (150). Given

that our *in vitro* suppression model does not show clear suppressive function by small EVs produced by expanded Tregs without oligomycin pre-treatment, and that the prevention of organ rejection in this humanised skin graft model required EVs isolated from ten times the number of Tregs required for adoptive transfer (small EVs from 50 million Tregs to 5 million Tconvs per mouse), without modification this strategy has limited translational potential. In this thesis we have shown that oligomycin treatment clearly enhances the immunosuppressive properties of Treg-derived small EVs, increasing the translational potential of this strategy.

Beyond using expanded Tregs, pharmacological induction of small EV production *in vivo* could be another approach. However, direct administration of oligomycin directly to patients is patently of limited therapeutic value given its non-specific action in other organs including the brain. However, we may use other pharmacological drugs. For example, our metabolomics study indicated that oligomycin-induced Treg epigenetic changes may induce immunosuppressive small EV production. HDAC inhibitors can be tolerated *in vivo* and have immunosuppressive properties (346, 376, 377). Further

defining the molecular mechanisms by which oligomycin induces the production of immunosuppressive small EVs may reveal druggable metabolic targets to induce clinical tolerance.

7.4 Future investigations

As discussed in the *previous section* (discussion), we hypothesise that naïve and CM Tregs and Tconvs have differential reliance on mTORC1 and mTORC2 for proliferation. We could confirm this by investigating the phosphorylation of mTORC2 in activated Tregs and Tconvs by FACS, and Treg and Tconv proliferation assay in the presence of selective mTOR inhibitors or under one of nonessential amino acid deprived medium.

We revealed that EM Tconvs have two distinct populations based on their mitochondrial mass: Mito^{hi} and Mito^{lo} EM Tconvs. Although we showed that they are functionally different and have different susceptibilities to Treg-mediated suppression, understanding their phenotypical differences is still limited. Although Mito^{lo} EM Tconvs

have a lower mitochondrial mass, they also have a higher OXPHOS rate compared with Mito^{hi} EM Tconvs indicating more effective mitochondrial activity in Mito^{lo} EM Tconvs compared with Mito^{hi} EM Tconvs. Morphological studies of mitochondria using electron microscopy may be an option to reveal deep mitochondrial differences. Moreover, mitochondria alter cellular function through ROS production and metabolic intermediates which modulate epigenetic signatures. Therefore, investigation of intracellular ROS level and epigenetics may be options to understand the origin of this difference.

We clearly proved that oligomycin-treated Tregs produce immunosuppressive small EVs using several methods; however, we did not yet isolate these small EVs directly. Ultracentrifugation is a classic method to isolate untouched small EVs as no artificial contaminants such as magnetic beads are required (378). Following isolation of small EVs we can directly examine their immunosuppressive properties. Moreover, although we suggest qualitative alterations of small EVs after oligomycin treatment based on their surface markers, we did not yet directly show different EV contents. We suggest that

oligomycin induces epigenetic changes in Tregs, and others have reported both that miRNA is influenced by DNA epigenetic modification and that miRNA in Treg-derived small EVs plays a key role their immunosuppressive properties (144, 147, 148, 350). Therefore, we will investigate the qualitative difference of Treg-derived small EVs after oligomycin treatment using nanoString miRNA expression panel after success isolation of small EVs.

As discussed in the *previous section* (discussion), we do not yet know the physiological or pathological conditions inducing mitochondrial ATP synthase inhibition or resembling metabolomic signature to mitochondrial ATP synthase inhibited Tregs. Lactate is a primary candidate to induce similar metabolic change. Thus, we could apply lactate instead of oligomycin to Treg culture in order to investigate whether extracellular lactate can induce production of immunosuppressive small EVs from Tregs.

We suggest that oligomycin induces Treg epigenetic change. However, we have not directly investigated epigenetic changes in Tregs after oligomycin treatment. Therefore,

employing epigenetic techniques such as ATACseq to assess chromatin accessibility and bisulfite sequencing to identify DNA methylation regions will be required to confirm this hypothesis.

Lastly, but importantly, we could not successfully observe clear immunosuppression *in vivo* using a mouse peritoneal lavage model, because of low levels of T cell proliferation in our positive control. However, this technique is a well-established model in our lab (379), and therefore the failure was most likely due to the effector cells donor used not being well adapted to a mouse environment. Repeated experiments are required to confirm that immunosuppressive small EVs function *in vivo*, followed by humanised skin graft model to confirm that the small EVs can prevent graft rejection. Moreover, immunosuppressive small EVs treatment must induce regulatory cells to maintain clinical tolerance to avoid repeated infusion and we will therefore investigate whether EVs can induce Tregs from naïve Tconvs *in vitro*.

Investigation of Treg immunometabolism in this thesis definitised human Treg metabolic

nature and the differential metabolic regulation of human Tregs and Tconvs, and revealed the novel and potent Treg-mediated immunosuppression through metabolism. We, therefore, shed new light on immunometabolism in terms of immunotolerance, which opens up new therapeutic strategies to achieve clinical tolerance.

7.5 Figures and legend

Figure 7.1

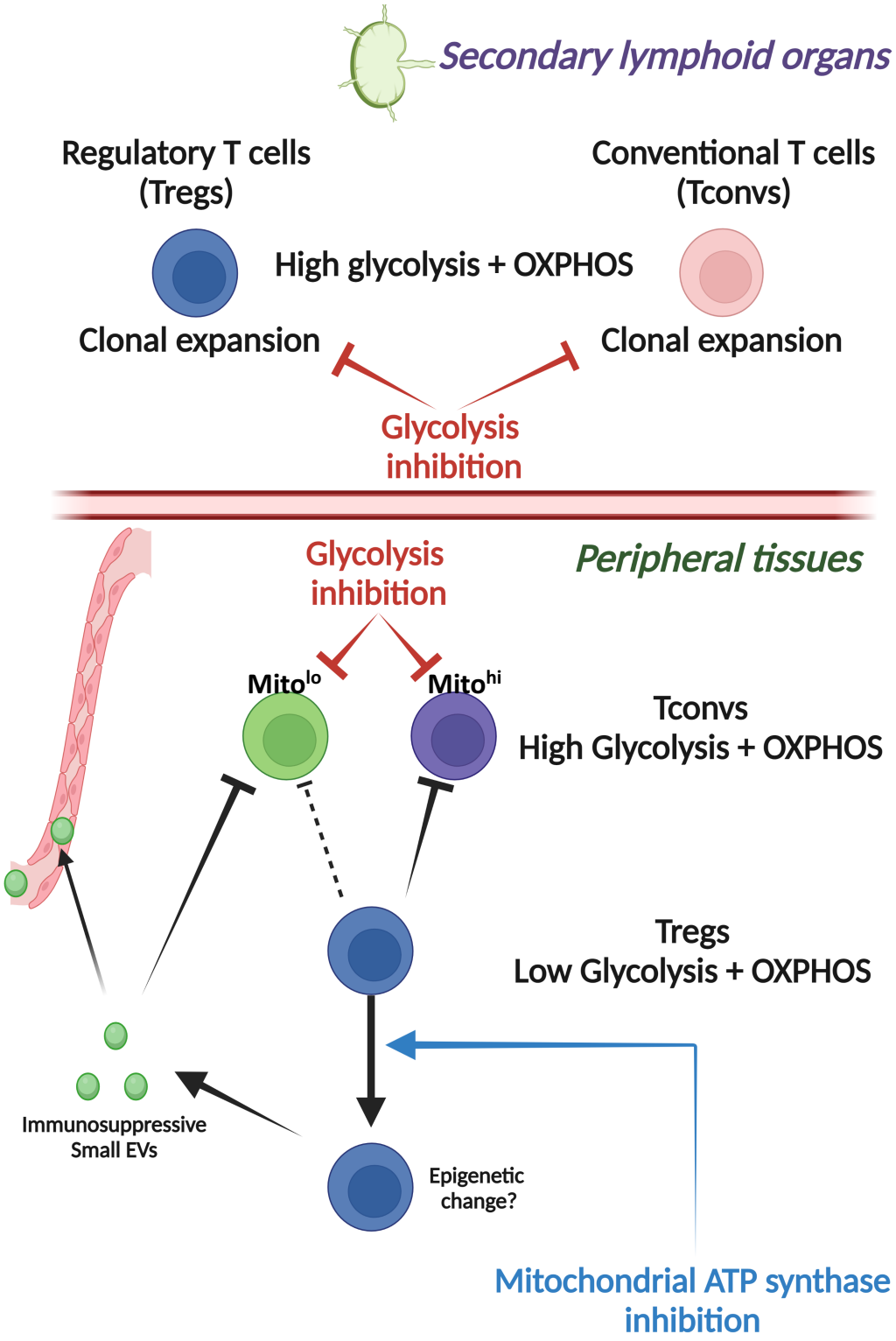

Figure 7.1. Summary of human Treg and Tconv immunometabolism.

Both naïve and CM Tregs and Tconvs, residing mostly in secondary lymphoid organs, have high rates of glycolysis and OXPHOS for their clonal expansion, with glycolysis specifically required for their proliferation. In peripheral tissues Mito^{hi} and Mito^{lo} EM Tconvs have higher rates of glycolysis and OXPHOS compared with EM Tregs. Glycolysis inhibition negatively regulates both Mito^{hi} and Mito^{lo} EM Tconv effector function, but Mito^{lo} EM Tconvs are resistant to EM Treg-mediated suppression. EM Tregs increase their immunosuppressive function when mitochondrial ATP synthase is inhibited which likely causes epigenetic changes in Tregs. Mitochondrial ATP synthase-inhibited Tregs start producing immunosuppressive small EVs which can suppress Mito^{lo} EM Tconvs and most likely exert a systemic effect.

References

1. Pancer Z, Cooper MD. The evolution of adaptive immunity. Annu Rev Immunol. 2006;24:497-518.
2. Flajnik MF, Kasahara M. Origin and evolution of the adaptive immune system: genetic events and selective pressures. Nat Rev Genet. 2010;11(1):47-59.
3. Waldmann H. Tolerance: an overview and perspectives. Nat Rev Nephrol. 2010;6(10):569-76.
4. Cheng M, Anderson MS. Thymic tolerance as a key brake on autoimmunity. Nature immunology. 2018;19(7):659-64.
5. Sakaguchi S, Yamaguchi T, Nomura T, Ono M. Regulatory T cells and immune tolerance. Cell. 2008;133(5):775-87.
6. Nemazee D. Mechanisms of central tolerance for B cells. Nat Rev Immunol. 2017;17(5):281-94.
7. Schwartz RH. T cell anergy. Annu Rev Immunol. 2003;21:305-34.
8. Cambier JC, Gauld SB, Merrell KT, Vilen BJ. B-cell anergy: from transgenic models to naturally occurring anergic B cells? Nat Rev Immunol. 2007;7(8):633-43.
9. Wood KJ, Bushell A, Hester J. Regulatory immune cells in transplantation. Nat Rev Immunol. 2012;12(6):417-30.
10. Peng B, Ming Y, Yang C. Regulatory B cells: the cutting edge of immune tolerance in kidney transplantation. Cell Death Dis. 2018;9(2):109.
11. Sakaguchi S, Sakaguchi N, Asano M, Itoh M, Toda M. Immunologic self-tolerance maintained by activated T cells expressing IL-2 receptor alpha-chains (CD25). Breakdown of a single mechanism of self-tolerance causes various autoimmune diseases. J Immunol. 1995;155(3):1151-64.
12. Fontenot JD, Gavin MA, Rudensky AY. Foxp3 programs the development and function of CD4+CD25+ regulatory T cells. Nature immunology. 2003;4(4):330-6.
13. Hori S, Nomura T, Sakaguchi S. Control of regulatory T cell development by the transcription factor Foxp3. Science. 2003;299(5609):1057-61.

14. Raffin C, Vo LT, Bluestone JA. T(reg) cell-based therapies: challenges and perspectives. Nat Rev Immunol. 2020;20(3):158-72.
15. Sawitzki B, Harden PN, Reinke P, Moreau A, Hutchinson JA, Game DS, et al. Regulatory cell therapy in kidney transplantation (The ONE Study): a harmonised design and analysis of seven non-randomised, single-arm, phase 1/2A trials. Lancet. 2020;395(10237):1627-39.
16. Romano M, Fanelli G, Albany CJ, Giganti G, Lombardi G. Past, Present, and Future of Regulatory T Cell Therapy in Transplantation and Autoimmunity. Front Immunol. 2019;10:43.
17. Clayton PA, McDonald SP, Russ GR, Chadban SJ. Long-Term Outcomes after Acute Rejection in Kidney Transplant Recipients: An ANZDATA Analysis. Journal of the American Society of Nephrology : JASN. 2019;30(9):1697-707.
18. Choudhary NS, Saigal S, Bansal RK, Saraf N, Gautam D, Soin AS. Acute and Chronic Rejection After Liver Transplantation: What A Clinician Needs to Know. Journal of clinical and experimental hepatology. 2017;7(4):358-66.
19. Wilhelm MJ. Long-term outcome following heart transplantation: current perspective. Journal of thoracic disease. 2015;7(3):549-51.
20. Hariharan S, Israni AK, Danovitch G. Long-Term Survival after Kidney Transplantation. N Engl J Med. 2021;385(8):729-43.
21. de Fijter JW. Rejection and function and chronic allograft dysfunction. Kidney international Supplement. 2010(119):S38-41.
22. Mathis D, Shoelson SE. Immunometabolism: an emerging frontier. Nat Rev Immunol. 2011;11(2):81.
23. O'Neill LA, Kishton RJ, Rathmell J. A guide to immunometabolism for immunologists. Nat Rev Immunol. 2016;16(9):553-65.
24. Yang K, Shrestha S, Zeng H, Karmaus PW, Neale G, Vogel P, et al. T cell exit from quiescence and differentiation into Th2 cells depend on Raptor-mTORC1-mediated metabolic reprogramming. Immunity. 2013;39(6):1043-56.
25. Frauwirth KA, Riley JL, Harris MH, Parry RV, Rathmell JC, Plas DR, et al. The CD28 signaling pathway regulates glucose metabolism. Immunity. 2002;16(6):769-77.

26. Wang R, Dillon CP, Shi LZ, Milasta S, Carter R, Finkelstein D, et al. The transcription factor Myc controls metabolic reprogramming upon T lymphocyte activation. Immunity. 2011;35(6):871-82.
27. Chang CH, Curtis JD, Maggi LB, Faubert B, Villarino AV, O'Sullivan D, et al. Posttranscriptional Control of T Cell Effector Function by Aerobic Glycolysis. Cell. 2013;153(6):1239-51.
28. Michalek RD, Gerriets VA, Jacobs SR, Macintyre AN, MacIver NJ, Mason EF, et al. Cutting Edge: Distinct Glycolytic and Lipid Oxidative Metabolic Programs Are Essential for Effector and Regulatory CD4(+) T Cell Subsets. Journal of Immunology. 2011;186(6):3299-303.
29. Gerriets VA, Kishton RJ, Nichols AG, Macintyre AN, Inoue M, Ilkayeva O, et al. Metabolic programming and PDHK1 control CD4+ T cell subsets and inflammation. J Clin Invest. 2015;125(1):194-207.
30. Brent L. The discovery of immunologic tolerance. Human immunology. 1997;52(2):75-81.
31. Hogquist KA, Baldwin TA, Jameson SC. Central tolerance: learning self-control in the thymus. Nat Rev Immunol. 2005;5(10):772-82.
32. Ignatowicz L, Kappler J, Marrack P. The repertoire of T cells shaped by a single MHC/peptide ligand. Cell. 1996;84(4):521-9.
33. Burkly LC, Degermann S, Longley J, Hagman J, Brinster RL, Lo D, et al. Clonal deletion of V beta 5+ T cells by transgenic I-E restricted to thymic medullary epithelium. J Immunol. 1993;151(8):3954-60.
34. Anderson MS, Venanzi ES, Klein L, Chen Z, Berzins SP, Turley SJ, et al. Projection of an immunological self shadow within the thymus by the aire protein. Science. 2002;298(5597):1395-401.
35. Anderson G, Partington KM, Jenkinson EJ. Differential effects of peptide diversity and stromal cell type in positive and negative selection in the thymus. J Immunol. 1998;161(12):6599-603.
36. Takaba H, Morishita Y, Tomofuji Y, Danks L, Nitta T, Komatsu N, et al. Fezf2 Orchestrates a Thymic Program of Self-Antigen Expression for Immune Tolerance. Cell. 2015;163(4):975-87.
37. Villaseñor J, Benoist C, Mathis D. AIRE and APECED: molecular

insights into an autoimmune disease. Immunol Rev. 2005;204:156-64.
38. Itoh M, Takahashi T, Sakaguchi N, Kuniyasu Y, Shimizu J, Otsuka F, et al. Thymus and autoimmunity: production of CD25+CD4+ naturally anergic and suppressive T cells as a key function of the thymus in maintaining immunologic self-tolerance. J Immunol. 1999;162(9):5317-26.
39. Jordan MS, Boesteanu A, Reed AJ, Petrone AL, Holenbeck AE, Lerman MA, et al. Thymic selection of CD4+CD25+ regulatory T cells induced by an agonist self-peptide. Nature immunology. 2001;2(4):301-6.
40. Nishizuka Y, Sakakura T. Thymus and reproduction: sex-linked dysgenesia of the gonad after neonatal thymectomy in mice. Science. 1969;166(3906):753-5.
41. Kojima A, Tanaka-Kojima Y, Sakakura T, Nishizuka Y. Spontaneous development of autoimmune thyroiditis in neonatally thymectomized mice. Lab Invest. 1976;34(6):550-7.
42. Sakaguchi S, Takahashi T, Nishizuka Y. Study on cellular events in post-thymectomy autoimmune oophoritis in mice. II. Requirement of Lyt-1 cells in normal female mice for the prevention of oophoritis. J Exp Med. 1982;156(6):1577-86.
43. Asano M, Toda M, Sakaguchi N, Sakaguchi S. Autoimmune disease as a consequence of developmental abnormality of a T cell subpopulation. J Exp Med. 1996;184(2):387-96.
44. Bennett CL, Christie J, Ramsdell F, Brunkow ME, Ferguson PJ, Whitesell L, et al. The immune dysregulation, polyendocrinopathy, enteropathy, X-linked syndrome (IPEX) is caused by mutations of FOXP3. Nat Genet. 2001;27(1):20-1.
45. Brunkow ME, Jeffery EW, Hjerrild KA, Paeper B, Clark LB, Yasayko SA, et al. Disruption of a new forkhead/winged-helix protein, scurfin, results in the fatal lymphoproliferative disorder of the scurfy mouse. Nat Genet. 2001;27(1):68-73.
46. Legoux FP, Lim JB, Cauley AW, Dikiy S, Ertelt J, Mariani TJ, et al. CD4+ T Cell Tolerance to Tissue-Restricted Self Antigens Is Mediated by Antigen-Specific Regulatory T Cells Rather Than Deletion. Immunity.

2015;43(5):896-908.
47. Haftmann C, Zwicky P, Ingelfinger F, Mair F, Floess S, Riedel R, et al. Protection against autoimmunity is driven by thymic epithelial cell-mediated regulation of T(reg) development. Sci Immunol. 2021;6(65):eabf3111.
48. Issa F, Hester J, Goto R, Nadig SN, Goodacre TE, Wood K. Ex vivo-expanded human regulatory T cells prevent the rejection of skin allografts in a humanized mouse model. Transplantation. 2010;90(12):1321-7.
49. Xia G, He J, Leventhal JR. Ex vivo-expanded natural CD4+CD25+ regulatory T cells synergize with host T-cell depletion to promote long-term survival of allografts. Am J Transplant. 2008;8(2):298-306.
50. Gershon RK, Kondo K. Cell interactions in the induction of tolerance: the role of thymic lymphocytes. Immunology. 1970;18(5):723-37.
51. Hall BM, Jelbart ME, Gurley KE, Dorsch SE. Specific unresponsiveness in rats with prolonged cardiac allograft survival after treatment with cyclosporine. Mediation of specific suppression by T helper/inducer cells. J Exp Med. 1985;162(5):1683-94.
52. Hall BM, Pearce NW, Gurley KE, Dorsch SE. Specific unresponsiveness in rats with prolonged cardiac allograft survival after treatment with cyclosporine. III. Further characterization of the CD4+ suppressor cell and its mechanisms of action. J Exp Med. 1990;171(1):141-57.
53. Powrie F, Mason D. OX-22high CD4+ T cells induce wasting disease with multiple organ pathology: prevention by the OX-22low subset. J Exp Med. 1990;172(6):1701-8.
54. Sakaguchi S, Fukuma K, Kuribayashi K, Masuda T. Organ-specific autoimmune diseases induced in mice by elimination of T cell subset. I. Evidence for the active participation of T cells in natural self-tolerance; deficit of a T cell subset as a possible cause of autoimmune disease. J Exp Med. 1985;161(1):72-87.
55. Powrie F, Leach MW, Mauze S, Caddle LB, Coffman RL. Phenotypically distinct subsets of CD4+ T cells induce or protect from chronic intestinal inflammation in C. B-17 scid mice. Int Immunol. 1993;5(11):1461-71.
56. Khattri R, Cox T, Yasayko SA, Ramsdell F. An essential role for Scurfin in CD4+CD25+ T regulatory cells. Nature immunology. 2003;4(4):337-42.

57. Chen W, Jin W, Hardegen N, Lei KJ, Li L, Marinos N, et al. Conversion of peripheral CD4+CD25- naive T cells to CD4+CD25+ regulatory T cells by TGF-beta induction of transcription factor Foxp3. J Exp Med. 2003;198(12):1875-86.
58. Davidson TS, DiPaolo RJ, Andersson J, Shevach EM. Cutting Edge: IL-2 is essential for TGF-beta-mediated induction of Foxp3+ T regulatory cells. J Immunol. 2007;178(7):4022-6.
59. Karim M, Kingsley CI, Bushell AR, Sawitzki BS, Wood KJ. Alloantigen-induced CD25+CD4+ regulatory T cells can develop in vivo from CD25-CD4+ precursors in a thymus-independent process. J Immunol. 2004;172(2):923-8.
60. Karim M, Feng G, Wood KJ, Bushell AR. CD25+CD4+ regulatory T cells generated by exposure to a model protein antigen prevent allograft rejection: antigen-specific reactivation in vivo is critical for bystander regulation. Blood. 2005;105(12):4871-7.
61. Abbas AK, Benoist C, Bluestone JA, Campbell DJ, Ghosh S, Hori S, et al. Regulatory T cells: recommendations to simplify the nomenclature. Nature immunology. 2013;14(4):307-8.
62. Pacholczyk R, Ignatowicz H, Kraj P, Ignatowicz L. Origin and T cell receptor diversity of Foxp3+CD4+CD25+ T cells. Immunity. 2006;25(2):249-59.
63. Fazilleau N, Bachelez H, Gougeon ML, Viguier M. Cutting edge: size and diversity of CD4+CD25high Foxp3+ regulatory T cell repertoire in humans: evidence for similarities and partial overlapping with CD4+CD25- T cells. J Immunol. 2007;179(6):3412-6.
64. Lathrop SK, Bloom SM, Rao SM, Nutsch K, Lio CW, Santacruz N, et al. Peripheral education of the immune system by colonic commensal microbiota. Nature. 2011;478(7368):250-4.
65. Zhou X, Bailey-Bucktrout S, Jeker LT, Bluestone JA. Plasticity of CD4(+) FoxP3(+) T cells. Curr Opin Immunol. 2009;21(3):281-5.
66. Shevach EM, Thornton AM. tTregs, pTregs, and iTregs: similarities and differences. Immunol Rev. 2014;259(1):88-102.
67. Rubtsov YP, Niec RE, Josefowicz S, Li L, Darce J, Mathis D, et al. Stability of the regulatory T cell lineage in vivo. Science. 2010;329(5999):1667-

71.
68. Xu L, Kitani A, Fuss I, Strober W. Cutting edge: regulatory T cells induce CD4+CD25-Foxp3- T cells or are self-induced to become Th17 cells in the absence of exogenous TGF-beta. J Immunol. 2007;178(11):6725-9.
69. Hoechst B, Gamrekelashvili J, Manns MP, Greten TF, Korangy F. Plasticity of human Th17 cells and iTregs is orchestrated by different subsets of myeloid cells. Blood. 2011;117(24):6532-41.
70. Koenecke C, Czeloth N, Bubke A, Schmitz S, Kissenpfennig A, Malissen B, et al. Alloantigen-specific de novo-induced Foxp3+ Treg revert in vivo and do not protect from experimental GVHD. Eur J Immunol. 2009;39(11):3091-6.
71. Polansky JK, Kretschmer K, Freyer J, Floess S, Garbe A, Baron U, et al. DNA methylation controls Foxp3 gene expression. Eur J Immunol. 2008;38(6):1654-63.
72. Ohkura N, Hamaguchi M, Morikawa H, Sugimura K, Tanaka A, Ito Y, et al. T cell receptor stimulation-induced epigenetic changes and Foxp3 expression are independent and complementary events required for Treg cell development. Immunity. 2012;37(5):785-99.
73. Ohkura N, Sakaguchi S. Transcriptional and epigenetic basis of Treg cell development and function: its genetic anomalies or variations in autoimmune diseases. Cell Res. 2020;30(6):465-74.
74. Floess S, Freyer J, Siewert C, Baron U, Olek S, Polansky J, et al. Epigenetic control of the foxp3 locus in regulatory T cells. PLoS Biol. 2007;5(2):e38.
75. Samstein RM, Arvey A, Josefowicz SZ, Peng X, Reynolds A, Sandstrom R, et al. Foxp3 exploits a pre-existent enhancer landscape for regulatory T cell lineage specification. Cell. 2012;151(1):153-66.
76. Morikawa H, Ohkura N, Vandenbon A, Itoh M, Nagao-Sato S, Kawaji H, et al. Differential roles of epigenetic changes and Foxp3 expression in regulatory T cell-specific transcriptional regulation. Proc Natl Acad Sci U S A. 2014;111(14):5289-94.
77. Miyao T, Floess S, Setoguchi R, Luche H, Fehling HJ, Waldmann H, et al. Plasticity of Foxp3(+) T cells reflects promiscuous Foxp3 expression in

conventional T cells but not reprogramming of regulatory T cells. Immunity. 2012;36(2):262-75.
78. Komatsu N, Okamoto K, Sawa S, Nakashima T, Oh-hora M, Kodama T, et al. Pathogenic conversion of Foxp3+ T cells into TH17 cells in autoimmune arthritis. Nat Med. 2014;20(1):62-8.
79. Miyara M, Yoshioka Y, Kitoh A, Shima T, Wing K, Niwa A, et al. Functional delineation and differentiation dynamics of human CD4+ T cells expressing the FoxP3 transcription factor. Immunity. 2009;30(6):899-911.
80. Walker MR, Kasprowicz DJ, Gersuk VH, Benard A, Van Landeghen M, Buckner JH, et al. Induction of FoxP3 and acquisition of T regulatory activity by stimulated human CD4+CD25- T cells. J Clin Invest. 2003;112(9):1437-43.
81. Wang J, Ioan-Facsinay A, van der Voort EI, Huizinga TW, Toes RE. Transient expression of FOXP3 in human activated nonregulatory CD4+ T cells. Eur J Immunol. 2007;37(1):129-38.
82. Liu W, Putnam AL, Xu-Yu Z, Szot GL, Lee MR, Zhu S, et al. CD127 expression inversely correlates with FoxP3 and suppressive function of human CD4+ T reg cells. J Exp Med. 2006;203(7):1701-11.
83. Nadig SN, Wieckiewicz J, Wu DC, Warnecke G, Zhang W, Luo S, et al. In vivo prevention of transplant arteriosclerosis by ex vivo-expanded human regulatory T cells. Nat Med. 2010;16(7):809-13.
84. Barzaghi F, Passerini L, Gambineri E, Ciullini Mannurita S, Cornu T, Kang ES, et al. Demethylation analysis of the FOXP3 locus shows quantitative defects of regulatory T cells in IPEX-like syndrome. J Autoimmun. 2012;38(1):49-58.
85. Josefowicz SZ, Lu LF, Rudensky AY. Regulatory T cells: mechanisms of differentiation and function. Annu Rev Immunol. 2012;30:531-64.
86. Wing JB, Tanaka A, Sakaguchi S. Human FOXP3(+) Regulatory T Cell Heterogeneity and Function in Autoimmunity and Cancer. Immunity. 2019;50(2):302-16.
87. Shevyrev D, Tereshchenko V. Treg Heterogeneity, Function, and Homeostasis. Front Immunol. 2019;10:3100.
88. Onishi Y, Fehervari Z, Yamaguchi T, Sakaguchi S. Foxp3+ natural

regulatory T cells preferentially form aggregates on dendritic cells in vitro and actively inhibit their maturation. Proc Natl Acad Sci U S A. 2008;105(29):10113-8.
89. Sage PT, Paterson AM, Lovitch SB, Sharpe AH. The coinhibitory receptor CTLA-4 controls B cell responses by modulating T follicular helper, T follicular regulatory, and T regulatory cells. Immunity. 2014;41(6):1026-39.
90. Qureshi OS, Zheng Y, Nakamura K, Attridge K, Manzotti C, Schmidt EM, et al. Trans-endocytosis of CD80 and CD86: a molecular basis for the cell-extrinsic function of CTLA-4. Science. 2011;332(6029):600-3.
91. Maeda Y, Nishikawa H, Sugiyama D, Ha D, Hamaguchi M, Saito T, et al. Detection of self-reactive CD8(+) T cells with an anergic phenotype in healthy individuals. Science. 2014;346(6216):1536-40.
92. Fallarino F, Grohmann U, Hwang KW, Orabona C, Vacca C, Bianchi R, et al. Modulation of tryptophan catabolism by regulatory T cells. Nature immunology. 2003;4(12):1206-12.
93. Wing K, Onishi Y, Prieto-Martin P, Yamaguchi T, Miyara M, Fehervari Z, et al. CTLA-4 control over Foxp3+ regulatory T cell function. Science. 2008;322(5899):271-5.
94. Klocke K, Sakaguchi S, Holmdahl R, Wing K. Induction of autoimmune disease by deletion of CTLA-4 in mice in adulthood. Proc Natl Acad Sci U S A. 2016;113(17):E2383-92.
95. Paterson AM, Lovitch SB, Sage PT, Juneja VR, Lee Y, Trombley JD, et al. Deletion of CTLA-4 on regulatory T cells during adulthood leads to resistance to autoimmunity. J Exp Med. 2015;212(10):1603-21.
96. Schubert D, Bode C, Kenefeck R, Hou TZ, Wing JB, Kennedy A, et al. Autosomal dominant immune dysregulation syndrome in humans with CTLA4 mutations. Nat Med. 2014;20(12):1410-6.
97. Kuehn HS, Ouyang W, Lo B, Deenick EK, Niemela JE, Avery DT, et al. Immune dysregulation in human subjects with heterozygous germline mutations in CTLA4. Science. 2014;345(6204):1623-7.
98. Waterhouse P, Penninger JM, Timms E, Wakeham A, Shahinian A, Lee KP, et al. Lymphoproliferative disorders with early lethality in mice deficient in

Ctla-4. Science. 1995;270(5238):985-8.
99. Chambers CA, Sullivan TJ, Allison JP. Lymphoproliferation in CTLA-4-deficient mice is mediated by costimulation-dependent activation of CD4+ T cells. Immunity. 1997;7(6):885-95.
100. Ishida Y, Agata Y, Shibahara K, Honjo T. Induced expression of PD-1, a novel member of the immunoglobulin gene superfamily, upon programmed cell death. Embo j. 1992;11(11):3887-95.
101. Simon S, Labarriere N. PD-1 expression on tumor-specific T cells: Friend or foe for immunotherapy? Oncoimmunology. 2017;7(1):e1364828.
102. Nishimura H, Nose M, Hiai H, Minato N, Honjo T. Development of lupus-like autoimmune diseases by disruption of the PD-1 gene encoding an ITIM motif-carrying immunoreceptor. Immunity. 1999;11(2):141-51.
103. Gong J, Chehrazi-Raffle A, Reddi S, Salgia R. Development of PD-1 and PD-L1 inhibitors as a form of cancer immunotherapy: a comprehensive review of registration trials and future considerations. Journal for immunotherapy of cancer. 2018;6(1):8.
104. Kumagai S, Togashi Y, Kamada T, Sugiyama E, Nishinakamura H, Takeuchi Y, et al. The PD-1 expression balance between effector and regulatory T cells predicts the clinical efficacy of PD-1 blockade therapies. Nature immunology. 2020;21(11):1346-58.
105. Sage PT, Francisco LM, Carman CV, Sharpe AH. The receptor PD-1 controls follicular regulatory T cells in the lymph nodes and blood. Nature immunology. 2013;14(2):152-61.
106. Hartley GP, Chow L, Ammons DT, Wheat WH, Dow SW. Programmed Cell Death Ligand 1 (PD-L1) Signaling Regulates Macrophage Proliferation and Activation. Cancer Immunol Res. 2018;6(10):1260-73.
107. Koch MA, Tucker-Heard G, Perdue NR, Killebrew JR, Urdahl KB, Campbell DJ. The transcription factor T-bet controls regulatory T cell homeostasis and function during type 1 inflammation. Nature immunology. 2009;10(6):595-602.
108. Levine AG, Mendoza A, Hemmers S, Moltedo B, Niec RE, Schizas M, et al. Stability and function of regulatory T cells expressing the transcription factor

T-bet. Nature. 2017;546(7658):421-5.
109. Wohlfert EA, Grainger JR, Bouladoux N, Konkel JE, Oldenhove G, Ribeiro CH, et al. GATA3 controls Foxp3$^+$ regulatory T cell fate during inflammation in mice. J Clin Invest. 2011;121(11):4503-15.
110. Zheng Y, Chaudhry A, Kas A, deRoos P, Kim JM, Chu TT, et al. Regulatory T-cell suppressor program co-opts transcription factor IRF4 to control T(H)2 responses. Nature. 2009;458(7236):351-6.
111. Yang BH, Hagemann S, Mamareli P, Lauer U, Hoffmann U, Beckstette M, et al. Foxp3(+) T cells expressing RORγt represent a stable regulatory T-cell effector lineage with enhanced suppressive capacity during intestinal inflammation. Mucosal Immunol. 2016;9(2):444-57.
112. Sefik E, Geva-Zatorsky N, Oh S, Konnikova L, Zemmour D, McGuire AM, et al. MUCOSAL IMMUNOLOGY. Individual intestinal symbionts induce a distinct population of RORγ^+ regulatory T cells. Science. 2015;349(6251):993-7.
113. Yu X, Harden K, Gonzalez LC, Francesco M, Chiang E, Irving B, et al. The surface protein TIGIT suppresses T cell activation by promoting the generation of mature immunoregulatory dendritic cells. Nature immunology. 2009;10(1):48-57.
114. Joller N, Lozano E, Burkett PR, Patel B, Xiao S, Zhu C, et al. Treg cells expressing the coinhibitory molecule TIGIT selectively inhibit proinflammatory Th1 and Th17 cell responses. Immunity. 2014;40(4):569-81.
115. Setoguchi R, Hori S, Takahashi T, Sakaguchi S. Homeostatic maintenance of natural Foxp3(+) CD25(+) CD4(+) regulatory T cells by interleukin (IL)-2 and induction of autoimmune disease by IL-2 neutralization. J Exp Med. 2005;201(5):723-35.
116. Fontenot JD, Rasmussen JP, Gavin MA, Rudensky AY. A function for interleukin 2 in Foxp3-expressing regulatory T cells. Nature immunology. 2005;6(11):1142-51.
117. Ross SH, Cantrell DA. Signaling and Function of Interleukin-2 in T Lymphocytes. Annu Rev Immunol. 2018;36:411-33.
118. Pandiyan P, Zheng L, Ishihara S, Reed J, Lenardo MJ.

CD4+CD25+Foxp3+ regulatory T cells induce cytokine deprivation-mediated apoptosis of effector CD4+ T cells. Nature immunology. 2007;8(12):1353-62.
119. Chinen T, Kannan AK, Levine AG, Fan X, Klein U, Zheng Y, et al. An essential role for the IL-2 receptor in T(reg) cell function. Nature immunology. 2016;17(11):1322-33.
120. Verbsky JW, Chatila TA. Immune dysregulation, polyendocrinopathy, enteropathy, X-linked (IPEX) and IPEX-related disorders: an evolving web of heritable autoimmune diseases. Current opinion in pediatrics. 2013;25(6):708-14.
121. Kretschmer K, Apostolou I, Hawiger D, Khazaie K, Nussenzweig MC, von Boehmer H. Inducing and expanding regulatory T cell populations by foreign antigen. Nature immunology. 2005;6(12):1219-27.
122. Cobbold SP, Castejon R, Adams E, Zelenika D, Graca L, Humm S, et al. Induction of foxP3+ regulatory T cells in the periphery of T cell receptor transgenic mice tolerized to transplants. J Immunol. 2004;172(10):6003-10.
123. Tone Y, Furuuchi K, Kojima Y, Tykocinski ML, Greene MI, Tone M. Smad3 and NFAT cooperate to induce Foxp3 expression through its enhancer. Nature immunology. 2008;9(2):194-202.
124. Xu L, Kitani A, Strober W. Molecular mechanisms regulating TGF-beta-induced Foxp3 expression. Mucosal Immunol. 2010;3(3):230-8.
125. Stockis J, Colau D, Coulie PG, Lucas S. Membrane protein GARP is a receptor for latent TGF-beta on the surface of activated human Treg. Eur J Immunol. 2009;39(12):3315-22.
126. Edwards JP, Hand TW, Morais da Fonseca D, Glass DD, Belkaid Y, Shevach EM. The GARP/Latent TGF-β1 complex on Treg cells modulates the induction of peripherally derived Treg cells during oral tolerance. Eur J Immunol. 2016;46(6):1480-9.
127. Edwards JP, Thornton AM, Shevach EM. Release of active TGF-β1 from the latent TGF-β1/GARP complex on T regulatory cells is mediated by integrin β8. J Immunol. 2014;193(6):2843-9.
128. Stockis J, Liénart S, Colau D, Collignon A, Nishimura SL, Sheppard D, et al. Blocking immunosuppression by human Tregs in vivo with antibodies targeting integrin αVβ8. Proc Natl Acad Sci U S A. 2017;114(47):E10161-e8.

129. Saraiva M, O'Garra A. The regulation of IL-10 production by immune cells. Nat Rev Immunol. 2010;10(3):170-81.
130. Rubtsov YP, Rasmussen JP, Chi EY, Fontenot J, Castelli L, Ye X, et al. Regulatory T cell-derived interleukin-10 limits inflammation at environmental interfaces. Immunity. 2008;28(4):546-58.
131. Glocker EO, Kotlarz D, Klein C, Shah N, Grimbacher B. IL-10 and IL-10 receptor defects in humans. Ann N Y Acad Sci. 2011;1246:102-7.
132. Collison LW, Workman CJ, Kuo TT, Boyd K, Wang Y, Vignali KM, et al. The inhibitory cytokine IL-35 contributes to regulatory T-cell function. Nature. 2007;450(7169):566-9.
133. Collison LW, Chaturvedi V, Henderson AL, Giacomin PR, Guy C, Bankoti J, et al. IL-35-mediated induction of a potent regulatory T cell population. Nature immunology. 2010;11(12):1093-101.
134. Shen P, Roch T, Lampropoulou V, O'Connor RA, Stervbo U, Hilgenberg E, et al. IL-35-producing B cells are critical regulators of immunity during autoimmune and infectious diseases. Nature. 2014;507(7492):366-70.
135. Bastid J, Cottalorda-Regairaz A, Alberici G, Bonnefoy N, Eliaou JF, Bensussan A. ENTPD1/CD39 is a promising therapeutic target in oncology. Oncogene. 2013;32(14):1743-51.
136. Jarvis LB, Rainbow DB, Coppard V, Howlett SK, Georgieva Z, Davies JL, et al. Therapeutically expanded human regulatory T-cells are super-suppressive due to HIF1A induced expression of CD73. Communications biology. 2021;4(1):1186.
137. Roh M, Wainwright DA, Wu JD, Wan Y, Zhang B. Targeting CD73 to augment cancer immunotherapy. Current opinion in pharmacology. 2020;53:66-76.
138. Agarwal A, Fanelli G, Letizia M, Tung SL, Boardman D, Lechler R, et al. Regulatory T cell-derived exosomes: possible therapeutic and diagnostic tools in transplantation. Front Immunol. 2014;5:555.
139. Li P, Liu C, Yu Z, Wu M. New Insights into Regulatory T Cells: Exosome- and Non-Coding RNA-Mediated Regulation of Homeostasis and Resident Treg Cells. Front Immunol. 2016;7:574.

140. Théry C, Witwer KW, Aikawa E, Alcaraz MJ, Anderson JD, Andriantsitohaina R, et al. Minimal information for studies of extracellular vesicles 2018 (MISEV2018): a position statement of the International Society for Extracellular Vesicles and update of the MISEV2014 guidelines. Journal of extracellular vesicles. 2018;7(1):1535750.
141. O'Brien K, Breyne K, Ughetto S, Laurent LC, Breakefield XO. RNA delivery by extracellular vesicles in mammalian cells and its applications. Nat Rev Mol Cell Biol. 2020;21(10):585-606.
142. Théry C, Amigorena S, Raposo G, Clayton A. Isolation and characterization of exosomes from cell culture supernatants and biological fluids. Current protocols in cell biology. 2006;Chapter 3:Unit 3.22.
143. Kalluri R, LeBleu VS. The biology, function, and biomedical applications of exosomes. Science. 2020;367(6478).
144. Okoye IS, Coomes SM, Pelly VS, Czieso S, Papayannopoulos V, Tolmachova T, et al. MicroRNA-containing T-regulatory-cell-derived exosomes suppress pathogenic T helper 1 cells. Immunity. 2014;41(1):89-103.
145. Smyth LA, Ratnasothy K, Tsang JY, Boardman D, Warley A, Lechler R, et al. CD73 expression on extracellular vesicles derived from CD4+ CD25+ Foxp3+ T cells contributes to their regulatory function. Eur J Immunol. 2013;43(9):2430-40.
146. Sullivan JA, Tomita Y, Jankowska-Gan E, Lema DA, Arvedson MP, Nair A, et al. Treg-Cell-Derived IL-35-Coated Extracellular Vesicles Promote Infectious Tolerance. Cell Rep. 2020;30(4):1039-51.e5.
147. Tung SL, Boardman DA, Sen M, Letizia M, Peng Q, Cianci N, et al. Regulatory T cell-derived extracellular vesicles modify dendritic cell function. Sci Rep. 2018;8(1):6065.
148. Aiello S, Rocchetta F, Longaretti L, Faravelli S, Todeschini M, Cassis L, et al. Extracellular vesicles derived from T regulatory cells suppress T cell proliferation and prolong allograft survival. Sci Rep. 2017;7(1):11518.
149. Chen L, Huang H, Zhang W, Ding F, Fan Z, Zeng Z. Exosomes Derived From T Regulatory Cells Suppress CD8+ Cytotoxic T Lymphocyte Proliferation and Prolong Liver Allograft Survival. Medical science monitor : international

medical journal of experimental and clinical research. 2019;25:4877-84.
150. Tung SL, Fanelli G, Matthews RI, Bazoer J, Letizia M, Vizcay-Barrena G, et al. Regulatory T Cell Extracellular Vesicles Modify T-Effector Cell Cytokine Production and Protect Against Human Skin Allograft Damage. Frontiers in cell and developmental biology. 2020;8:317.
151. Kawai K, Uchiyama M, Hester J, Wood K, Issa F. Regulatory T cells for tolerance. Human immunology. 2018;79(5):294-303.
152. Sakaguchi S, Wing K, Onishi Y, Prieto-Martin P, Yamaguchi T. Regulatory T cells: how do they suppress immune responses? Int Immunol. 2009;21(10):1105-11.
153. Rana J, Biswas M. Regulatory T cell therapy: Current and future design perspectives. Cell Immunol. 2020;356:104193.
154. Neefjes J, Jongsma ML, Paul P, Bakke O. Towards a systems understanding of MHC class I and MHC class II antigen presentation. Nat Rev Immunol. 2011;11(12):823-36.
155. Nierkens S, Tel J, Janssen E, Adema GJ. Antigen cross-presentation by dendritic cell subsets: one general or all sergeants? Trends Immunol. 2013;34(8):361-70.
156. Grossman WJ, Verbsky JW, Barchet W, Colonna M, Atkinson JP, Ley TJ. Human T regulatory cells can use the perforin pathway to cause autologous target cell death. Immunity. 2004;21(4):589-601.
157. Gershon RK, Kondo K. Infectious immunological tolerance. Immunology. 1971;21(6):903-14.
158. Qin SX, Cobbold SP, Pope H, Elliott J, Kioussis D, Davies J, et al. Infectious Transplantation Tolerance. Science. 1993;259(5097):974-7.
159. Dieckmann D, Bruett CH, Ploettner H, Lutz MB, Schuler G. Human CD4(+)CD25(+) regulatory, contact-dependent T cells induce interleukin 10-producing, contact-independent type 1-like regulatory T cells [corrected]. J Exp Med. 2002;196(2):247-53.
160. Jonuleit H, Schmitt E, Kakirman H, Stassen M, Knop J, Enk AH. Infectious tolerance: human CD25(+) regulatory T cells convey suppressor activity to conventional CD4(+) T helper cells. J Exp Med. 2002;196(2):255-60.

161. Lan Q, Zhou X, Fan H, Chen M, Wang J, Ryffel B, et al. Polyclonal CD4+Foxp3+ Treg cells induce TGFβ-dependent tolerogenic dendritic cells that suppress the murine lupus-like syndrome. J Mol Cell Biol. 2012;4(6):409-19.
162. Kendal AR, Waldmann H. Infectious tolerance: therapeutic potential. Current Opinion in Immunology. 2010;22(5):560-5.
163. Issa F, Wood KJ. Translating tolerogenic therapies to the clinic - where do we stand? Front Immunol. 2012;3:254.
164. Gravano DM, Vignali DA. The battle against immunopathology: infectious tolerance mediated by regulatory T cells. Cell Mol Life Sci. 2012;69(12):1997-2008.
165. Strauss L, Whiteside TL, Knights A, Bergmann C, Knuth A, Zippelius A. Selective survival of naturally occurring human CD4+CD25+Foxp3+ regulatory T cells cultured with rapamycin. J Immunol. 2007;178(1):320-9.
166. Fraser H, Safinia N, Grageda N, Thirkell S, Lowe K, Fry LJ, et al. A Rapamycin-Based GMP-Compatible Process for the Isolation and Expansion of Regulatory T Cells for Clinical Trials. Mol Ther-Meth Clin D. 2018;8:198-209.
167. Hester J, Schiopu A, Nadig SN, Wood KJ. Low-dose rapamycin treatment increases the ability of human regulatory T cells to inhibit transplant arteriosclerosis in vivo. Am J Transplant. 2012;12(8):2008-16.
168. Issa F, Milward K, Goto R, Betts G, Wood KJ, Hester J. Transiently Activated Human Regulatory T Cells Upregulate BCL-XL Expression and Acquire a Functional Advantage in vivo. Front Immunol. 2019;10:889.
169. Tang Q, Henriksen KJ, Bi M, Finger EB, Szot G, Ye J, et al. In vitro-expanded antigen-specific regulatory T cells suppress autoimmune diabetes. J Exp Med. 2004;199(11):1455-65.
170. Golshayan D, Jiang S, Tsang J, Garin MI, Mottet C, Lechler RI. In vitro-expanded donor alloantigen-specific CD4+CD25+ regulatory T cells promote experimental transplantation tolerance. Blood. 2007;109(2):827-35.
171. Sagoo P, Ali N, Garg G, Nestle FO, Lechler RI, Lombardi G. Human regulatory T cells with alloantigen specificity are more potent inhibitors of alloimmune skin graft damage than polyclonal regulatory T cells. Sci Transl Med. 2011;3(83):83ra42.

172. Putnam AL, Safinia N, Medvec A, Laszkowska M, Wray M, Mintz MA, et al. Clinical grade manufacturing of human alloantigen-reactive regulatory T cells for use in transplantation. Am J Transplant. 2013;13(11):3010-20.
173. Mederacke YS, Vondran FW, Kollrich S, Schulde E, Schmitt R, Manns MP, et al. Transient increase of activated regulatory T cells early after kidney transplantation. Sci Rep. 2019;9(1):1021.
174. Veerapathran A, Pidala J, Beato F, Yu XZ, Anasetti C. Ex vivo expansion of human Tregs specific for alloantigens presented directly or indirectly. Blood. 2011;118(20):5671-80.
175. Fritsche E, Volk HD, Reinke P, Abou-El-Enein M. Toward an Optimized Process for Clinical Manufacturing of CAR-Treg Cell Therapy. Trends in biotechnology. 2020;38(10):1099-112.
176. MacDonald KG, Hoeppli RE, Huang Q, Gillies J, Luciani DS, Orban PC, et al. Alloantigen-specific regulatory T cells generated with a chimeric antigen receptor. J Clin Invest. 2016;126(4):1413-24.
177. Boardman DA, Philippeos C, Fruhwirth GO, Ibrahim MA, Hannen RF, Cooper D, et al. Expression of a Chimeric Antigen Receptor Specific for Donor HLA Class I Enhances the Potency of Human Regulatory T Cells in Preventing Human Skin Transplant Rejection. Am J Transplant. 2017;17(4):931-43.
178. Poorebrahim M, Melief J, Pico de Coaña Y, S LW, Cid-Arregui A, Kiessling R. Counteracting CAR T cell dysfunction. Oncogene. 2021;40(2):421-35.
179. Gornalusse GG, Hirata RK, Funk SE, Riolobos L, Lopes VS, Manske G, et al. HLA-E-expressing pluripotent stem cells escape allogeneic responses and lysis by NK cells. Nat Biotechnol. 2017;35(8):765-72.
180. Warburg O. On the origin of cancer cells. Science. 1956;123(3191):309-14.
181. Krawczyk CM, Holowka T, Sun J, Blagih J, Amiel E, DeBerardinis RJ, et al. Toll-like receptor-induced changes in glycolytic metabolism regulate dendritic cell activation. Blood. 2010;115(23):4742-9.
182. Rodríguez-Prados JC, Través PG, Cuenca J, Rico D, Aragonés J, Martín-Sanz P, et al. Substrate fate in activated macrophages: a comparison between

innate, classic, and alternative activation. J Immunol. 2010;185(1):605-14.
183. Vander Heiden MG, Cantley LC, Thompson CB. Understanding the Warburg effect: the metabolic requirements of cell proliferation. Science. 2009;324(5930):1029-33.
184. Jones W, Bianchi K. Aerobic glycolysis: beyond proliferation. Front Immunol. 2015;6:227.
185. Nowicki S, Gottlieb E. Oncometabolites: tailoring our genes. Febs J. 2015;282(15):2796-805.
186. Snaebjornsson MT, Schulze A. Non-canonical functions of enzymes facilitate cross-talk between cell metabolic and regulatory pathways. Exp Mol Med. 2018;50(4):1-16.
187. Tannahill GM, Curtis AM, Adamik J, Palsson-McDermott EM, McGettrick AF, Goel G, et al. Succinate is an inflammatory signal that induces IL-1β through HIF-1α. Nature. 2013;496(7444):238-42.
188. Berod L, Friedrich C, Nandan A, Freitag J, Hagemann S, Harmrolfs K, et al. De novo fatty acid synthesis controls the fate between regulatory T and T helper 17 cells. Nat Med. 2014;20(11):1327-33.
189. Newton R, Priyadharshini B, Turka LA. Immunometabolism of regulatory T cells. Nature immunology. 2016;17(6):618-25.
190. Macintyre AN, Gerriets VA, Nichols AG, Michalek RD, Rudolph MC, Deoliveira D, et al. The glucose transporter Glut1 is selectively essential for CD4 T cell activation and effector function. Cell Metab. 2014;20(1):61-72.
191. Düvel K, Yecies JL, Menon S, Raman P, Lipovsky AI, Souza AL, et al. Activation of a metabolic gene regulatory network downstream of mTOR complex 1. Mol Cell. 2010;39(2):171-83.
192. Shi LZ, Wang R, Huang G, Vogel P, Neale G, Green DR, et al. HIF1alpha-dependent glycolytic pathway orchestrates a metabolic checkpoint for the differentiation of TH17 and Treg cells. J Exp Med. 2011;208(7):1367-76.
193. Dang EV, Barbi J, Yang HY, Jinasena D, Yu H, Zheng Y, et al. Control of T(H)17/T-reg Balance by Hypoxia-Inducible Factor 1. Cell. 2011;146(5):772-84.
194. Jacobs SR, Herman CE, Maciver NJ, Wofford JA, Wieman HL, Hammen

JJ, et al. Glucose uptake is limiting in T cell activation and requires CD28-mediated Akt-dependent and independent pathways. J Immunol. 2008;180(7):4476-86.
195. Villarino AV, Katzman SD, Gallo E, Miller O, Jiang S, McManus MT, et al. Posttranscriptional silencing of effector cytokine mRNA underlies the anergic phenotype of self-reactive T cells. Immunity. 2011;34(1):50-60.
196. Ho PC, Bihuniak JD, Macintyre AN, Staron M, Liu XJ, Amezquita R, et al. Phosphoenolpyruvate Is a Metabolic Checkpoint of Anti-tumor T Cell Responses. Cell. 2015;162(6):1217-28.
197. Hermann-Kleiter N, Baier G. NFAT pulls the strings during CD4+ T helper cell effector functions. Blood. 2010;115(15):2989-97.
198. Peng M, Yin N, Chhangawala S, Xu K, Leslie CS, Li MO. Aerobic glycolysis promotes T helper 1 cell differentiation through an epigenetic mechanism. Science. 2016;354(6311):481-4.
199. Bailis W, Shyer JA, Zhao J, Canaveras JCG, Al Khazal FJ, Qu R, et al. Distinct modes of mitochondrial metabolism uncouple T cell differentiation and function. Nature. 2019;571(7765):403-7.
200. Jones N, Cronin JG, Dolton G, Panetti S, Schauenburg AJ, Galloway SAE, et al. Metabolic Adaptation of Human CD4(+) and CD8(+) T-Cells to T-Cell Receptor-Mediated Stimulation. Front Immunol. 2017;8:1516.
201. Paul BT, Manz DH, Torti SV. Mitochondria and iron: current questions (vol 10, pg 65, 2017). Expert Rev Hematol. 2017;10(3):275-.
202. Sena LA, Li S, Jairaman A, Prakriya M, Ezponda T, Hildeman DA, et al. Mitochondria are required for antigen-specific T cell activation through reactive oxygen species signaling. Immunity. 2013;38(2):225-36.
203. Piganelli JD, Flores SC, Cruz C, Koepp J, Batinic-Haberle I, Crapo J, et al. A metalloporphyrin-based superoxide dismutase mimic inhibits adoptive transfer of autoimmune diabetes by a diabetogenic T-cell clone. Diabetes. 2002;51(2):347-55.
204. Angelin A, Gil-de-Gomez L, Dahiya S, Jiao J, Guo L, Levine MH, et al. Foxp3 Reprograms T Cell Metabolism to Function in Low-Glucose, High-Lactate Environments. Cell Metab. 2017;25(6):1282-93 e7.

205. Howie D, Cobbold SP, Adams E, Ten Bokum A, Necula AS, Zhang W, et al. Foxp3 drives oxidative phosphorylation and protection from lipotoxicity. Jci Insight. 2017;2(3):e89160.
206. Gerriets VA, Kishton RJ, Johnson MO, Cohen S, Siska PJ, Nichols AG, et al. Foxp3 and Toll-like receptor signaling balance Treg cell anabolic metabolism for suppression. Nature immunology. 2016;17(12):1459-66.
207. Yu XY, Teng XL, Wang FX, Zheng YH, Qu GJ, Zhou Y, et al. Metabolic control of regulatory T cell stability and function by TRAF3IP3 at the lysosome. Journal of Experimental Medicine. 2018;215(9):2463-76.
208. Lee JH, Elly C, Park Y, Liu YC. E3 Ubiquitin Ligase VHL Regulates Hypoxia-Inducible Factor-1alpha to Maintain Regulatory T Cell Stability and Suppressive Capacity. Immunity. 2015;42(6):1062-74.
209. Hsiao HW, Hsu TS, Liu WH, Hsieh WC, Chou TF, Wu YJ, et al. Deltex1 antagonizes HIF-1alpha and sustains the stability of regulatory T cells in vivo. Nat Commun. 2015;6:6353.
210. Charbonnier LM, Cui Y, Stephen-Victor E, Harb H, Lopez D, Bleesing JJ, et al. Functional reprogramming of regulatory T cells in the absence of Foxp3. Nature immunology. 2019;20(9):1208-19.
211. Huynh A, DuPage M, Priyadharshini B, Sage PT, Quiros J, Borges CM, et al. Control of PI(3) kinase in Treg cells maintains homeostasis and lineage stability. Nature immunology. 2015;16(2):188-96.
212. Kerdiles YM, Stone EL, Beisner DR, McGargill MA, Ch'en IL, Stockmann C, et al. Foxo transcription factors control regulatory T cell development and function. Immunity. 2010;33(6):890-904.
213. Ouyang W, Liao W, Luo CT, Yin N, Huse M, Kim MV, et al. Novel Foxo1-dependent transcriptional programs control T(reg) cell function. Nature. 2012;491(7425):554-9.
214. Clambey ET, McNamee EN, Westrich JA, Glover LE, Campbell EL, Jedlicka P, et al. Hypoxia-inducible factor-1 alpha-dependent induction of FoxP3 drives regulatory T-cell abundance and function during inflammatory hypoxia of the mucosa. Proc Natl Acad Sci U S A. 2012;109(41):E2784-93.
215. Miska J, Lee-Chang C, Rashidi A, Muroski ME, Chang AL, Lopez-Rosas

A, et al. HIF-1 alpha Is a Metabolic Switch between Glycolytic-Driven Migration and Oxidative Phosphorylation-Driven Immunosuppression of Tregs in Glioblastoma. Cell Reports. 2019;27(1):226-+.
216. Luo CT, Liao W, Dadi S, Toure A, Li MO. Graded Foxo1 activity in Treg cells differentiates tumour immunity from spontaneous autoimmunity. Nature. 2016;529(7587):532-6.
217. Kishore M, Cheung KCP, Fu H, Bonacina F, Wang G, Coe D, et al. Regulatory T Cell Migration Is Dependent on Glucokinase-Mediated Glycolysis. Immunity. 2017;47(5):875-89 e10.
218. Shi L, Tu BP. Acetyl-CoA and the regulation of metabolism: mechanisms and consequences. Current opinion in cell biology. 2015;33:125-31.
219. Zeng H, Yang K, Cloer C, Neale G, Vogel P, Chi H. mTORC1 couples immune signals and metabolic programming to establish T(reg)-cell function. Nature. 2013;499(7459):485-90.
220. He N, Fan W, Henriquez B, Yu RT, Atkins AR, Liddle C, et al. Metabolic control of regulatory T cell (Treg) survival and function by Lkb1. Proc Natl Acad Sci U S A. 2017;114(47):12542-7.
221. Yang K, Blanco DB, Neale G, Vogel P, Avila J, Clish CB, et al. Homeostatic control of metabolic and functional fitness of Treg cells by LKB1 signalling. Nature. 2017;548(7669):602-6.
222. Timilshina M, You Z, Lacher SM, Acharya S, Jiang L, Kang Y, et al. Activation of Mevalonate Pathway via LKB1 Is Essential for Stability of Treg Cells. Cell Rep. 2019;27(10):2948-61 e7.
223. Lacher SM, Bruttger J, Kalt B, Berthelet J, Rajalingam K, Wortge S, et al. HMG-CoA reductase promotes protein prenylation and therefore is indispensible for T-cell survival. Cell Death Dis. 2017;8(5):e2824.
224. Watson MJ, Vignali PDA, Mullett SJ, Overacre-Delgoffe AE, Peralta RM, Grebinoski S, et al. Metabolic support of tumour-infiltrating regulatory T cells by lactic acid. Nature. 2021;591(7851):645-51.
225. Chakrabarty RP, Chandel NS. Mitochondria as Signaling Organelles Control Mammalian Stem Cell Fate. Cell stem cell. 2021;28(3):394-408.
226. Lu C, Thompson CB. Metabolic regulation of epigenetics. Cell Metab.

2012;16(1):9-17.
227. Dai Z, Ramesh V, Locasale JW. The evolving metabolic landscape of chromatin biology and epigenetics. Nat Rev Genet. 2020;21(12):737-53.
228. Weinberg SE, Singer BD, Steinert EM, Martinez CA, Mehta MM, Martínez-Reyes I, et al. Mitochondrial complex III is essential for suppressive function of regulatory T cells. Nature. 2019;565(7740):495-9.
229. Yu X, Lao Y, Teng XL, Li S, Zhou Y, Wang F, et al. SENP3 maintains the stability and function of regulatory T cells via BACH2 deSUMOylation. Nat Commun. 2018;9(1):3157.
230. Field CS, Baixauli F, Kyle RL, Puleston DJ, Cameron AM, Sanin DE, et al. Mitochondrial Integrity Regulated by Lipid Metabolism Is a Cell-Intrinsic Checkpoint for Treg Suppressive Function. Cell Metabolism. 2020;31(2):422-+.
231. Wang H, Franco F, Tsui YC, Xie X, Trefny MP, Zappasodi R, et al. CD36-mediated metabolic adaptation supports regulatory T cell survival and function in tumors. Nature immunology. 2020;21(3):298-308.
232. Newsholme EA, Crabtree B, Ardawi MSM. The Role of High-Rates of Glycolysis and Glutamine Utilization in Rapidly Dividing Cells. Bioscience Rep. 1985;5(5):393-400.
233. Priyadharshini B, Loschi M, Newton RH, Zhang JW, Finn KK, Gerriets VA, et al. Cutting Edge: TGF-beta and Phosphatidylinositol 3-Kinase Signals Modulate Distinct Metabolism of Regulatory T Cell Subsets. J Immunol. 2018;201(8):2215-9.
234. Heiden MGV, Cantley LC, Thompson CB. Understanding the Warburg Effect: The Metabolic Requirements of Cell Proliferation. Science. 2009;324(5930):1029-33.
235. Nakamura H, Makino Y, Okamoto K, Poellinger L, Ohnuma K, Morimoto C, et al. TCR engagement increases hypoxia-inducible factor-1 alpha protein synthesis via rapamycin-sensitive pathway under hypoxic conditions in human peripheral T cells. J Immunol. 2005;174(12):7592-9.
236. Shyer JA, Flavell RA, Bailis W. Metabolic signaling in T cells. Cell Res. 2020;30(8):649-59.
237. Chapman NM, Zeng H, Nguyen TM, Wang Y, Vogel P, Dhungana Y, et

al. mTOR coordinates transcriptional programs and mitochondrial metabolism of activated Treg subsets to protect tissue homeostasis. Nat Commun. 2018;9(1):2095.
238. Shi H, Chapman NM, Wen J, Guy C, Long L, Dhungana Y, et al. Amino Acids License Kinase mTORC1 Activity and Treg Cell Function via Small G Proteins Rag and Rheb. Immunity. 2019.
239. Gabriel SS, Tsui C, Chisanga D, Weber F, Llano-León M, Gubser PM, et al. Transforming growth factor-β-regulated mTOR activity preserves cellular metabolism to maintain long-term T cell responses in chronic infection. Immunity. 2021;54(8):1698-714.e5.
240. Wang RN, Dillon CP, Shi LZ, Milasta S, Carter R, Finkelstein D, et al. The Transcription Factor Myc Controls Metabolic Reprogramming upon T Lymphocyte Activation. Immunity. 2011;35(6):871-82.
241. Vardhana SA, Hwee MA, Berisa M, Wells DK, Yost KE, King B, et al. Impaired mitochondrial oxidative phosphorylation limits the self-renewal of T cells exposed to persistent antigen. Nature immunology. 2020;21(9):1022-33.
242. Scharping NE, Rivadeneira DB, Menk AV, Vignali PDA, Ford BR, Rittenhouse NL, et al. Mitochondrial stress induced by continuous stimulation under hypoxia rapidly drives T cell exhaustion. Nature immunology. 2021;22(2):205-15.
243. Haas R, Smith J, Rocher-Ros V, Nadkarni S, Montero-Melendez T, D'Acquisto F, et al. Lactate Regulates Metabolic and Pro-inflammatory Circuits in Control of T Cell Migration and Effector Functions. PLoS Biol. 2015;13(7):e1002202.
244. Mukhopadhyay S, Frias MA, Chatterjee A, Yellen P, Foster DA. The Enigma of Rapamycin Dosage. Molecular Cancer Therapeutics. 2016;15(3):347-53.
245. Foster DA, Toschi A. Targeting mTOR with rapamycin One dose does not fit all. Cell Cycle. 2009;8(7):1026-9.
246. Farber DL, Yudanin NA, Restifo NP. Human memory T cells: generation, compartmentalization and homeostasis. Nat Rev Immunol. 2014;14(1):24-35.

247. Pepper M, Jenkins MK. Origins of CD4(+) effector and central memory T cells. Nature immunology. 2011;12(6):467-71.
248. Chang JT, Palanivel VR, Kinjyo I, Schambach F, Intlekofer AM, Banerjee A, et al. Asymmetric T lymphocyte division in the initiation of adaptive immune responses. Science. 2007;315(5819):1687-91.
249. Verbist KC, Guy CS, Milasta S, Liedmann S, Kaminski MM, Wang RN, et al. Metabolic maintenance of cell asymmetry following division in activated T lymphocytes. Nature. 2016;532(7599):389-+.
250. Pollizzi KN, Sun IH, Patel CH, Lo YC, Oh MH, Waickman AT, et al. Asymmetric inheritance of mTORC1 kinase activity during division dictates CD8(+) T cell differentiation. Nature immunology. 2016;17(6):704-+.
251. Pearce EL, Walsh MC, Cejas PJ, Harms GM, Shen H, Wang LS, et al. Enhancing CD8 T-cell memory by modulating fatty acid metabolism. Nature. 2009;460(7251):103-U18.
252. Araki K, Turner AP, Shaffer VO, Gangappa S, Keller SA, Bachmann MF, et al. mTOR regulates memory CD8 T-cell differentiation. Nature. 2009;460(7251):108-U24.
253. Sukumar M, Liu J, Ji Y, Subramanian M, Crompton JG, Yu ZY, et al. Inhibiting glycolytic metabolism enhances CD8(+) T cell memory and antitumor function. Journal of Clinical Investigation. 2013;123(10):4479-88.
254. van der Windt GJW, Everts B, Chang CH, Curtis JD, Freitas TC, Amiel E, et al. Mitochondrial Respiratory Capacity Is a Critical Regulator of CD8(+) T Cell Memory Development. Immunity. 2012;36(1):68-78.
255. Raud B, Roy DG, Divakaruni AS, Tarasenko TN, Franke R, Ma EH, et al. Etomoxir Actions on Regulatory and Memory T Cells Are Independent of Cpt1a-Mediated Fatty Acid Oxidation. Cell Metabolism. 2018;28(3):504-+.
256. Buck MD, O'Sullivan D, Geltink RIK, Curtis JD, Chang CH, Sanin DE, et al. Mitochondrial Dynamics Controls T Cell Fate through Metabolic Programming. Cell. 2016;166(1):63-76.
257. Kawalekar OU, Connor RSO, Fraietta JA, Guo LL, McGettigan SE, Posey AD, et al. Distinct Signaling of Coreceptors Regulates Specific Metabolism Pathways and Impacts Memory Development in CAR T Cells (vol 44, pg 380,

2016). Immunity. 2016;44(3):712-.
258. Phan AT, Doedens AL, Palazon A, Tyrakis PA, Cheung KP, Johnson RS, et al. Constitutive Glycolytic Metabolism Supports CD8(+) T Cell Effector Memory Differentiation during Viral Infection. Immunity. 2016;45(5):1024-37.
259. Taguchi N, Ishihara N, Jofuku A, Oka T, Mihara K. Mitotic phosphorylation of dynamin-related GTPase Drp1 participates in mitochondrial fission. Journal of Biological Chemistry. 2007;282(15):11521-9.
260. Gubser PM, Bantug GR, Razik L, Fischer M, Dimeloe S, Hoenger G, et al. Rapid effector function of memory CD8(+) T cells requires an immediate-early glycolytic switch. Nature immunology. 2013;14(10):1064-+.
261. Foulds KE, Zenewicz LA, Shedlock DJ, Jiang J, Troy AE, Shen H. Cutting edge: CD4 and CD8 T cells are intrinsically different in their proliferative responses. J Immunol. 2002;168(4):1528-32.
262. Gomez-Rodriguez J, Wohlfert EA, Handon R, Meylan F, Wu JZ, Anderson SM, et al. Itk-mediated integration of T cell receptor and cytokine signaling regulates the balance between Th17 and regulatory T cells. J Exp Med. 2014;211(3):529-43.
263. Gottschalk RA, Corse E, Allison JP. TCR ligand density and affinity determine peripheral induction of Foxp3 in vivo. J Exp Med. 2010;207(8):1701-11.
264. Delgoffe GM, Kole TP, Zheng Y, Zarek PE, Matthews KL, Xiao B, et al. The mTOR Kinase Differentially Regulates Effector and Regulatory T Cell Lineage Commitment. Immunity. 2009;30(6):832-44.
265. Xu Y, Chaudhury A, Zhang M, Savoldo B, Metelitsa LS, Rodgers J, et al. Glycolysis determines dichotomous regulation of T cell subsets in hypoxia. J Clin Invest. 2016;126(7):2678-88.
266. Dimeloe S, Mehling M, Frick C, Loeliger J, Bantug GR, Sauder U, et al. The Immune-Metabolic Basis of Effector Memory CD4+ T Cell Function under Hypoxic Conditions. J Immunol. 2016;196(1):106-14.
267. Rosenblum MD, Way SS, Abbas AK. Regulatory T cell memory. Nat Rev Immunol. 2016;16(2):90-101.
268. Rosenblum MD, Gratz IK, Paw JS, Lee K, Marshak-Rothstein A, Abbas

AK. Response to self antigen imprints regulatory memory in tissues. Nature. 2011;480(7378):538-42.
269. Rowe JH, Ertelt JM, Xin L, Way SS. Pregnancy imprints regulatory memory that sustains anergy to fetal antigen. Nature. 2012;490(7418):102-6.
270. Booth NJ, McQuaid AJ, Sobande T, Kissane S, Agius E, Jackson SE, et al. Different proliferative potential and migratory characteristics of human CD4+ regulatory T cells that express either CD45RA or CD45RO. J Immunol. 2010;184(8):4317-26.
271. Seddiki N, Santner-Nanan B, Tangye SG, Alexander SI, Solomon M, Lee S, et al. Persistence of naive CD45RA+ regulatory T cells in adult life. Blood. 2006;107(7):2830-8.
272. Schneider MA, Meingassner JG, Lipp M, Moore HD, Rot A. CCR7 is required for the in vivo function of CD4+ CD25+ regulatory T cells. J Exp Med. 2007;204(4):735-45.
273. Zhang N, Schröppel B, Lal G, Jakubzick C, Mao X, Chen D, et al. Regulatory T cells sequentially migrate from inflamed tissues to draining lymph nodes to suppress the alloimmune response. Immunity. 2009;30(3):458-69.
274. Weninger W, Crowley MA, Manjunath N, von Andrian UH. Migratory properties of naive, effector, and memory CD8(+) T cells. J Exp Med. 2001;194(7):953-66.
275. Sallusto F, Lenig D, Förster R, Lipp M, Lanzavecchia A. Two subsets of memory T lymphocytes with distinct homing potentials and effector functions. Nature. 1999;401(6754):708-12.
276. Gavin MA, Rasmussen JP, Fontenot JD, Vasta V, Manganiello VC, Beavo JA, et al. Foxp3-dependent programme of regulatory T-cell differentiation. Nature. 2007;445(7129):771-5.
277. Sallusto F, Geginat J, Lanzavecchia A. Central memory and effector memory T cell subsets: Function, generation, and maintenance. Annual Review of Immunology. 2004;22:745-63.
278. Sato T, Thorlacius H, Johnston B, Staton TL, Xiang W, Littman DR, et al. Role for CXCR6 in recruitment of activated CD8+ lymphocytes to inflamed liver. J Immunol. 2005;174(1):277-83.

279. Morgan AJ, Guillen C, Symon FA, Huynh TT, Berry MA, Entwisle JJ, et al. Expression of CXCR6 and its ligand CXCL16 in the lung in health and disease. Clinical and experimental allergy : journal of the British Society for Allergy and Clinical Immunology. 2005;35(12):1572-80.
280. Kim MJ, Sun HJ, Song YS, Yoo SK, Kim YA, Seo JS, et al. CXCL16 positively correlated with M2-macrophage infiltration, enhanced angiogenesis, and poor prognosis in thyroid cancer. Sci Rep. 2019;9(1):13288.
281. Jin JJ, Dai FX, Long ZW, Cai H, Liu XW, Zhou Y, et al. CXCR6 predicts poor prognosis in gastric cancer and promotes tumor metastasis through epithelial-mesenchymal transition. Oncology reports. 2017;37(6):3279-86.
282. Mayer AL, Higgins CB, Heitmeier MR, Kraft TE, Qian X, Crowley JR, et al. SLC2A8 (GLUT8) is a mammalian trehalose transporter required for trehalose-induced autophagy. Sci Rep. 2016;6:38586.
283. Payen VL, Mina E, Van Hée VF, Porporato PE, Sonveaux P. Monocarboxylate transporters in cancer. Mol Metab. 2020;33:48-66.
284. Picard F, Géhin M, Annicotte J, Rocchi S, Champy MF, O'Malley BW, et al. SRC-1 and TIF2 control energy balance between white and brown adipose tissues. Cell. 2002;111(7):931-41.
285. Duteil D, Chambon C, Ali F, Malivindi R, Zoll J, Kato S, et al. The transcriptional coregulators TIF2 and SRC-1 regulate energy homeostasis by modulating mitochondrial respiration in skeletal muscles. Cell Metab. 2010;12(5):496-508.
286. Zhou RB, Yazdi AS, Menu P, Tschopp J. A role for mitochondria in NLRP3 inflammasome activation (vol 469, pg 221, 2011). Nature. 2011;475(7354).
287. Xiao B, Deng X, Zhou W, Tan EK. FlowCytometry-Based Assessment of Mitophagy Using MitoTracker. Front Cell Neurosci. 2016;10.
288. Panduro M, Benoist C, Mathis D. Tissue Tregs. Annu Rev Immunol. 2016;34:609-33.
289. Miragaia RJ, Gomes T, Chomka A, Jardine L, Riedel A, Hegazy AN, et al. Single-Cell Transcriptomics of Regulatory T Cells Reveals Trajectories of Tissue Adaptation. Immunity. 2019;50(2):493-+.

290. Ager A. High Endothelial Venules and Other Blood Vessels: Critical Regulators of Lymphoid Organ Development and Function. Frontiers in Immunology. 2017;8.
291. Munoz-Erazo L, Rhodes JL, Marion VC, Kemp RA. Tertiary lymphoid structures in cancer - considerations for patient prognosis. Cellular & Molecular Immunology. 2020;17(6):570-5.
292. Forster R, Davalos-Misslitz AC, Rot A. CCR7 and its ligands: balancing immunity and tolerance. Nature Reviews Immunology. 2008;8(5):362-71.
293. Kocks JR, Davalos-Misslitz ACM, Hintzen G, Ohl L, Forster R. Regulatory T cells interfere with the development of bronchus-associated lymphoid tissue. Journal of Experimental Medicine. 2007;204(4):723-34.
294. Hopken UE, Wengner AM, Loddenkemper C, Stein H, Heimesaat MM, Rehm A, et al. CCR7 deficiency causes ectopic lymphoid neogenesis and disturbed mucosal tissue integrity. Blood. 2007;109(3):886-95.
295. Milutinovic S, Abe J, Godkin A, Stein JV, Gallimore A. The Dual Role of High Endothelial Venules in Cancer Progression versus Immunity. Trends Cancer. 2021;7(3):214-25.
296. Joshi NS, Akama-Garren EH, Lu YS, Lee DY, Chang GP, Li A, et al. Regulatory T Cells in Tumor-Associated Tertiary Lymphoid Structures Suppress Anti-tumor T Cell Responses. Immunity. 2015;43(3):579-90.
297. Li W, Bribriesco AC, Nava RG, Brescia AA, Ibricevic A, Spahn JH, et al. Lung transplant acceptance is facilitated by early events in the graft and is associated with lymphoid neogenesis. Mucosal Immunology. 2012;5(5):544-54.
298. Li WJ, Gauthier JM, Higashikubo R, Hsiao HM, Tanaka S, Vuong L, et al. Bronchus-associated lymphoid tissue-resident Foxp3(+) T lymphocytes prevent antibody-mediated lung rejection. Journal of Clinical Investigation. 2019;129(2):556-68.
299. Brown K, Sacks SH, Wong W. Tertiary lymphoid organs in renal allografts can be associated with donor-specific tolerance rather than rejection. European Journal of Immunology. 2011;41(1):89-96.
300. Ricciardi S, Manfrini N, Alfieri R, Calamita P, Crosti MC, Gallo S, et al. The Translational Machinery of Human CD4(+) T Cells Is Poised for Activation

and Controls the Switch from Quiescence to Metabolic Remodeling. Cell Metab. 2018;28(6):961.
301. Rego AC, Vesce S, Nicholls DG. The mechanism of mitochondrial membrane potential retention following release of cytochrome c in apoptotic GT1-7 neural cells. Cell Death Differ. 2001;8(10):995-1003.
302. Legros F, Lombes A, Frachon P, Rojo M. Mitochondrial fusion in human cells is efficient, requires the inner membrane potential, and is mediated by mitofusins. Mol Biol Cell. 2002;13(12):4343-54.
303. Westermann B. Bioenergetic role of mitochondrial fusion and fission. Bba-Bioenergetics. 2012;1817(10):1833-8.
304. Baixauli F, Acin-Perez R, Villarroya-Beltri C, Mazzeo C, Nunez-Andrade N, Gabande-Rodriguez E, et al. Mitochondrial Respiration Controls Lysosomal Function during Inflammatory T Cell Responses. Cell Metabolism. 2015;22(3):485-98.
305. Desdin-Mico G, Soto-Heredero G, Aranda JF, Oller J, Carrasco E, Gabande-Rodriguez E, et al. T cells with dysfunctional mitochondria induce multimorbidity and premature senescence. Science. 2020;368(6497):1371-+.
306. Bailis W, Shyer JA, Zhao J, Canaveras JCG, Al Khazal FJ, Qu RH, et al. Distinct modes of mitochondrial metabolism uncouple T cell differentiation and function (vol 571, pg 403, 2019). Nature. 2019;573(7773):E2-E.
307. Zhao RZ, Jiang S, Zhang L, Yu ZB. Mitochondrial electron transport chain, ROS generation and uncoupling (Review). International Journal of Molecular Medicine. 2019;44(1):3-15.
308. Jarvis JH, Jacobs A. Morphological Abnormalities in Lymphocyte Mitochondria Associated with Iron-Deficiency Anemia. J Clin Pathol. 1974;27(12):973-9.
309. Roth-Walter F, Pacios LF, Bianchini R, Jensen-Jarolim E. Linking iron-deficiency with allergy: role of molecular allergens and the microbiome. Metallomics. 2017;9(12):1676-92.
310. Oppenheimer SJ. Iron and its relation to immunity and infectious disease. J Nutr. 2001;131(2):616s-33s.
311. Thorson JA, Smith KM, Gomez F, Naumann PW, Kemp JD. Role of Iron

in T-Cell Activation - Th1 Clones Differ from Th2 Clones in Their Sensitivity to Inhibition of DNA-Synthesis Caused by Igg Mabs against the Transferrin Receptor and the Iron Chelator Deferoxamine. Cell Immunol. 1991;134(1):126-37.
312. Leung S, Holbrook A, King B, Lu HT, Evans V, Miyamoto N, et al. Differential inhibition of inducible T cell cytokine secretion by potent iron chelators. J Biomol Screen. 2005;10(2):157-67.
313. Frossi B, De Carli M, Piemonte M, Pucillo C. Oxidative microenvironment exerts an opposite regulatory effect on cytokine production by Th1 and Th2 cells. Molecular immunology. 2008;45(1):58-64.
314. Kaminski MM, Sauer SW, Klemke CD, Suss D, Okun JG, Krammer PH, et al. Mitochondrial Reactive Oxygen Species Control T Cell Activation by Regulating IL-2 and IL-4 Expression: Mechanism of Ciprofloxacin-Mediated Immunosuppression. Journal of Immunology. 2010;184(9):4827-41.
315. Jackson SH, Devadas S, Kwon J, Pinto LA, Williams MS. T cells express a phagocyte-type NADPH oxidase that is activated after T cell receptor stimulation. Nature immunology. 2004;5(8):818-27.
316. Fu GT, Xu Q, Qiu YJ, Jin XX, Xu T, Dong SL, et al. Suppression of Th17 cell differentiation by misshapen/NIK-related kinase MINK1. Journal of Experimental Medicine. 2017;214(5):1453-69.
317. Abimannan T, Peroumal D, Parida JR, Barik PK, Padhan P, Devadas S. Oxidative stress modulates the cytokine response of differentiated Th17 and Th1 cells. Free Radical Bio Med. 2016;99:352-63.
318. Schodel J, Ratcliffe PJ. Mechanisms of hypoxia signalling: new implications for nephrology. Nat Rev Nephrol. 2019;15(10):641-59.
319. Westendorf AM, Skibbe K, Adamczyk A, Buer J, Geffers R, Hansen W, et al. Hypoxia Enhances Immunosuppression by Inhibiting CD4+ Effector T Cell Function and Promoting Treg Activity. Cell Physiol Biochem. 2017;41(4):1271-84.
320. De Rosa V, Galgani M, Porcellini A, Colamatteo A, Santopaolo M, Zuchegna C, et al. Glycolysis controls the induction of human regulatory T cells by modulating the expression of FOXP3 exon 2 splicing variants. Nature

immunology. 2015;16(11):1174-84.
321. Newton RH, Shrestha S, Sullivan JM, Yates KB, Compeer EB, Ron-Harel N, et al. Maintenance of CD4 T cell fitness through regulation of Foxo1. Nature immunology. 2018;19(8):838-48.
322. Lee CF, Lo YC, Cheng CH, Furtmuller GJ, Oh B, Andrade-Oliveira V, et al. Preventing Allograft Rejection by Targeting Immune Metabolism. Cell Rep. 2015;13(4):760-70.
323. Villa G, Zaragoza JJ, Sharma A, Neri M, De Gaudio AR, Ronco C. Cytokine removal with high cut-off membrane: review of literature. Blood purification. 2014;38(3-4):167-73.
324. Corso G, Mäger I, Lee Y, Görgens A, Bultema J, Giebel B, et al. Reproducible and scalable purification of extracellular vesicles using combined bind-elute and size exclusion chromatography. Sci Rep. 2017;7(1):11561.
325. Maj T, Wang W, Crespo J, Zhang H, Wang W, Wei S, et al. Oxidative stress controls regulatory T cell apoptosis and suppressor activity and PD-L1-blockade resistance in tumor. Nature immunology. 2017;18(12):1332-41.
326. Beechey RB, Williams V, Holloway CT, Knight IG, Roberton AM. Estimation of the molecular weights and molecular formulae of oligomycin-A, rutamycin & aurovertin by mass spectrometry. Biochemical and biophysical research communications. 1967;26(3):339-41.
327. Livshits MA, Khomyakova E, Evtushenko EG, Lazarev VN, Kulemin NA, Semina SE, et al. Isolation of exosomes by differential centrifugation: Theoretical analysis of a commonly used protocol. Sci Rep. 2015;5:17319.
328. Andreu Z, Yáñez-Mó M. Tetraspanins in extracellular vesicle formation and function. Front Immunol. 2014;5:442.
329. Barnes MJ, Griseri T, Johnson AM, Young W, Powrie F, Izcue A. CTLA-4 promotes Foxp3 induction and regulatory T cell accumulation in the intestinal lamina propria. Mucosal Immunol. 2013;6(2):324-34.
330. García-Aguilar A, Cuezva JM. A Review of the Inhibition of the Mitochondrial ATP Synthase by IF1 in vivo: Reprogramming Energy Metabolism and Inducing Mitohormesis. Front Physiol. 2018;9:1322.
331. Esparza-Moltó PB, Nuevo-Tapioles C, Cuezva JM. Regulation of the

H(+)-ATP synthase by IF1: a role in mitohormesis. Cell Mol Life Sci. 2017;74(12):2151-66.
332. Cabezon E, Butler PJ, Runswick MJ, Walker JE. Modulation of the oligomerization state of the bovine F1-ATPase inhibitor protein, IF1, by pH. J Biol Chem. 2000;275(33):25460-4.
333. Rouslin W. Protonic inhibition of the mitochondrial oligomycin-sensitive adenosine 5'-triphosphatase in ischemic and autolyzing cardiac muscle. Possible mechanism for the mitigation of ATP hydrolysis under nonenergizing conditions. J Biol Chem. 1983;258(16):9657-61.
334. Zhang Y, Tan J, Miao Y, Zhang Q. The effect of extracellular vesicles on the regulation of mitochondria under hypoxia. Cell Death Dis. 2021;12(4):358.
335. Picca A, Guerra F, Calvani R, Coelho-Junior HJ, Bossola M, Landi F, et al. Generation and Release of Mitochondrial-Derived Vesicles in Health, Aging and Disease. Journal of clinical medicine. 2020;9(5).
336. Beier UH, Angelin A, Akimova T, Wang L, Liu Y, Xiao H, et al. Essential role of mitochondrial energy metabolism in Foxp3^{+} T-regulatory cell function and allograft survival. Faseb J. 2015;29(6):2315-26.
337. Guo Z, Wang G, Wu B, Chou WC, Cheng L, Zhou C, et al. DCAF1 regulates Treg senescence via the ROS axis during immunological aging. J Clin Invest. 2020;130(11):5893-908.
338. Kim HR, Lee A, Choi EJ, Hong MP, Kie JH, Lim W, et al. Reactive oxygen species prevent imiquimod-induced psoriatic dermatitis through enhancing regulatory T cell function. PLoS One. 2014;9(3):e91146.
339. Perry SW, Norman JP, Barbieri J, Brown EB, Gelbard HA. Mitochondrial membrane potential probes and the proton gradient: a practical usage guide. BioTechniques. 2011;50(2):98-115.
340. Scialò F, Fernández-Ayala DJ, Sanz A. Role of Mitochondrial Reverse Electron Transport in ROS Signaling: Potential Roles in Health and Disease. Front Physiol. 2017;8:428.
341. West AP, Shadel GS. Mitochondrial DNA in innate immune responses and inflammatory pathology. Nat Rev Immunol. 2017;17(6):363-75.
342. Menk AV, Scharping NE, Moreci RS, Zeng X, Guy C, Salvatore S, et al.

Early TCR Signaling Induces Rapid Aerobic Glycolysis Enabling Distinct Acute T Cell Effector Functions. Cell Rep. 2018;22(6):1509-21.
343. Chen JS, Faller DV, Spanjaard RA. Short-chain fatty acid inhibitors of histone deacetylases: promising anticancer therapeutics? Current cancer drug targets. 2003;3(3):219-36.
344. Arpaia N, Campbell C, Fan X, Dikiy S, van der Veeken J, deRoos P, et al. Metabolites produced by commensal bacteria promote peripheral regulatory T-cell generation. Nature. 2013;504(7480):451-5.
345. Furusawa Y, Obata Y, Fukuda S, Endo TA, Nakato G, Takahashi D, et al. Commensal microbe-derived butyrate induces the differentiation of colonic regulatory T cells. Nature. 2013;504(7480):446-50.
346. Huang J, Wang L, Dahiya S, Beier UH, Han R, Samanta A, et al. Histone/protein deacetylase 11 targeting promotes Foxp3+ Treg function. Sci Rep. 2017;7(1):8626.
347. Cheng Y, He C, Wang M, Ma X, Mo F, Yang S, et al. Targeting epigenetic regulators for cancer therapy: mechanisms and advances in clinical trials. Signal transduction and targeted therapy. 2019;4:62.
348. Roy DG, Chen J, Mamane V, Ma EH, Muhire BM, Sheldon RD, et al. Methionine Metabolism Shapes T Helper Cell Responses through Regulation of Epigenetic Reprogramming. Cell Metab. 2020;31(2):250-66.e9.
349. Nagai Y, Ji MQ, Zhu F, Xiao Y, Tanaka Y, Kambayashi T, et al. PRMT5 Associates With the FOXP3 Homomer and When Disabled Enhances Targeted p185(erbB2/neu) Tumor Immunotherapy. Front Immunol. 2019;10:174.
350. Glaich O, Parikh S, Bell RE, Mekahel K, Donyo M, Leader Y, et al. DNA methylation directs microRNA biogenesis in mammalian cells. Nat Commun. 2019;10(1):5657.
351. Bell EL, Klimova TA, Eisenbart J, Moraes CT, Murphy MP, Budinger GR, et al. The Qo site of the mitochondrial complex III is required for the transduction of hypoxic signaling via reactive oxygen species production. The Journal of cell biology. 2007;177(6):1029-36.
352. Chandel NS, McClintock DS, Feliciano CE, Wood TM, Melendez JA, Rodriguez AM, et al. Reactive oxygen species generated at mitochondrial complex

III stabilize hypoxia-inducible factor-1alpha during hypoxia: a mechanism of O2 sensing. J Biol Chem. 2000;275(33):25130-8.
353. Tang K, Yu Y, Zhu L, Xu P, Chen J, Ma J, et al. Hypoxia-reprogrammed tricarboxylic acid cycle promotes the growth of human breast tumorigenic cells. Oncogene. 2019;38(44):6970-84.
354. Thienpont B, Steinbacher J, Zhao H, D'Anna F, Kuchnio A, Ploumakis A, et al. Tumour hypoxia causes DNA hypermethylation by reducing TET activity. Nature. 2016;537(7618):63-8.
355. Bister N, Pistono C, Huremagic B, Jolkkonen J, Giugno R, Malm T. Hypoxia and extracellular vesicles: A review on methods, vesicular cargo and functions. Journal of extracellular vesicles. 2020;10(1):e12002.
356. Ren W, Hou J, Yang C, Wang H, Wu S, Wu Y, et al. Extracellular vesicles secreted by hypoxia pre-challenged mesenchymal stem cells promote non-small cell lung cancer cell growth and mobility as well as macrophage M2 polarization via miR-21-5p delivery. Journal of experimental & clinical cancer research : CR. 2019;38(1):62.
357. Li L, Jin S, Zhang Y. Ischemic preconditioning potentiates the protective effect of mesenchymal stem cells on endotoxin-induced acute lung injury in mice through secretion of exosome. International journal of clinical and experimental medicine. 2015;8(3):3825-32.
358. Chen X, Zhou J, Li X, Wang X, Lin Y, Wang X. Exosomes derived from hypoxic epithelial ovarian cancer cells deliver microRNAs to macrophages and elicit a tumor-promoted phenotype. Cancer Lett. 2018;435:80-91.
359. Guo X, Qiu W, Liu Q, Qian M, Wang S, Zhang Z, et al. Immunosuppressive effects of hypoxia-induced glioma exosomes through myeloid-derived suppressor cells via the miR-10a/Rora and miR-21/Pten Pathways. Oncogene. 2018;37(31):4239-59.
360. Hsu YL, Hung JY, Chang WA, Lin YS, Pan YC, Tsai PH, et al. Hypoxic lung cancer-secreted exosomal miR-23a increased angiogenesis and vascular permeability by targeting prolyl hydroxylase and tight junction protein ZO-1. Oncogene. 2017;36(34):4929-42.
361. Lin SC, Hardie DG. AMPK: Sensing Glucose as well as Cellular Energy

Status. Cell Metab. 2018;27(2):299-313.
362. Lambert AJ, Brand MD. Reactive oxygen species production by mitochondria. Methods Mol Biol. 2009;554:165-81.
363. Li NY, Ragheb K, Lawler G, Sturgist J, Rajwa B, Melendez JA, et al. Mitochondrial complex I inhibitor rotenone induces apoptosis through enhancing mitochondrial reactive oxygen species production. Journal of Biological Chemistry. 2003;278(10):8516-25.
364. Chen WW, Freinkman E, Wang T, Birsoy K, Sabatini DM. Absolute Quantification of Matrix Metabolites Reveals the Dynamics of Mitochondrial Metabolism. Cell. 2016;166(5):1324-37.e11.
365. Skotland T, Sandvig K, Llorente A. Lipids in exosomes: Current knowledge and the way forward. Progress in lipid research. 2017;66:30-41.
366. Savage DG, Lindenbaum J, Stabler SP, Allen RH. Sensitivity of serum methylmalonic acid and total homocysteine determinations for diagnosing cobalamin and folate deficiencies. The American journal of medicine. 1994;96(3):239-46.
367. Wei G, Wei L, Zhu J, Zang C, Hu-Li J, Yao Z, et al. Global mapping of H3K4me3 and H3K27me3 reveals specificity and plasticity in lineage fate determination of differentiating CD4+ T cells. Immunity. 2009;30(1):155-67.
368. Sugimoto N, Oida T, Hirota K, Nakamura K, Nomura T, Uchiyama T, et al. Foxp3-dependent and -independent molecules specific for CD25+CD4+ natural regulatory T cells revealed by DNA microarray analysis. Int Immunol. 2006;18(8):1197-209.
369. Hill JA, Feuerer M, Tash K, Haxhinasto S, Perez J, Melamed R, et al. Foxp3 transcription-factor-dependent and -independent regulation of the regulatory T cell transcriptional signature. Immunity. 2007;27(5):786-800.
370. Zheng Y, Josefowicz SZ, Kas A, Chu TT, Gavin MA, Rudensky AY. Genome-wide analysis of Foxp3 target genes in developing and mature regulatory T cells. Nature. 2007;445(7130):936-40.
371. Dumitru C, Kabat AM, Maloy KJ. Metabolic Adaptations of CD4(+) T Cells in Inflammatory Disease. Front Immunol. 2018;9:540.
372. Goberdhan DC, Wilson C, Harris AL. Amino Acid Sensing by mTORC1:

Intracellular Transporters Mark the Spot. Cell Metab. 2016;23(4):580-9.
373. Shi H, Chapman NM, Wen J, Guy C, Long L, Dhungana Y, et al. Amino Acids License Kinase mTORC1 Activity and Treg Cell Function via Small G Proteins Rag and Rheb. Immunity. 2019;51(6):1012-27.e7.
374. Hashimoto H, McCallion O, Kempkes RWM, Hester J, Issa F. Distinct metabolic pathways mediate regulatory T cell differentiation and function. Immunol Lett. 2020;223:53-61.
375. Latham T, Mackay L, Sproul D, Karim M, Culley J, Harrison DJ, et al. Lactate, a product of glycolytic metabolism, inhibits histone deacetylase activity and promotes changes in gene expression. Nucleic Acids Res. 2012;40(11):4794-803.
376. Choi SW, Braun T, Chang L, Ferrara JL, Pawarode A, Magenau JM, et al. Vorinostat plus tacrolimus and mycophenolate to prevent graft-versus-host disease after related-donor reduced-intensity conditioning allogeneic haemopoietic stem-cell transplantation: a phase 1/2 trial. The Lancet Oncology. 2014;15(1):87-95.
377. Ellis JD, Neil DA, Inston NG, Jenkinson E, Drayson MT, Hampson P, et al. Inhibition of Histone Deacetylase 6 Reveals a Potent Immunosuppressant Effect in Models of Transplantation. Transplantation. 2016;100(8):1667-74.
378. Patel GK, Khan MA, Zubair H, Srivastava SK, Khushman M, Singh S, et al. Comparative analysis of exosome isolation methods using culture supernatant for optimum yield, purity and downstream applications. Sci Rep-Uk. 2019;9.
379. Zaitsu M, Issa F, Hester J, Vanhove B, Wood KJ. Selective blockade of CD28 on human T cells facilitates regulation of alloimmune responses. Jci Insight. 2017;2(19).